Emerging Trends in Semiconductor Photochemistry: Graphene-Based Heterojunction Photocatalysts for Antibiotic Degradation

Asghar Taghiloo[a], Milad Aalipour[b], Seyed Mohammad Matin Ahmadi[b], Ali Akbar Asgharinezhad*[,c], Rui Tan [d], Afsanehsadat Larimi*[, d]

[a] School of Chemical Engineering, University of Tehran, Tehran, Iran

[b] Department of Chemical and Petroleum Engineering, Sharif University of Technology, Tehran, Iran

[c] Chemistry and Process Research Department, Niroo Research Institute, Tehran, Iran

[d] School of Engineering and Applied Sciences, Department of Chemical Engineering, Swansea University, Wales, UK

ABSTRACT

The increasing occurrence of antibiotic residues in aquatic environments has become a significant environmental concern due to their persistence and their role in promoting antibiotic resistance. Among advanced oxidation technologies, photocatalysis has attracted considerable attention because it enables the mineralization of organic contaminants into harmless products without generating secondary pollution. In recent years, the incorporation of graphene-based materials and the design of semiconductor heterojunctions have emerged as effective strategies for improving photocatalytic efficiency. Unlike previous overviews that focus primarily on photocatalytic efficiency, this review integrates mechanistic insights, heterojunction engineering strategies, and practical considerations such as real-wastewater performance, catalyst stability, and toxicity evolution. Particular emphasis is placed on the roles of graphene oxide and reduced graphene oxide in promoting charge separation, facilitating electron transport, and enhancing the activity of conventional semiconductor photocatalysts. Different

*Corresponding authors. Tel: +44-01792-606115. Email: a.larimi@swansea.ac.uk (A. Larimi) and Tel: +98-021-88079400. Email: aasgharinezhad@nri.ac.ir (A. A. Asgharinezhad)

heterojunction architectures, including Type-II and Z-scheme systems, are comparatively discussed to clarify their charge-transfer pathways and their influence on photocatalytic performance under UV, visible, and solar irradiation. Furthermore, this review synthesizes current knowledge on the key factors governing photocatalytic antibiotic degradation, including operational parameters, reactive species generation, catalyst stability, and reusability. Special attention is also given to studies conducted in real wastewater matrices and to issues related to mineralization efficiency, toxicity evolution, and the mitigation of antibiotic resistance during photocatalytic treatment. Finally, current challenges and future research directions are highlighted, including the application of advanced characterization techniques and the emerging role of artificial intelligence and machine learning in optimizing photocatalyst design. These perspectives provide a clearer understanding of the potential of graphene-based heterojunction photocatalysts for sustainable antibiotic removal in water treatment applications.

Keywords: Photocatalysis; Antibiotics; Graphene; Photoreactor; Degradation; Semiconductor Heterojunctions

1-INTRODUCTION

With the development of urbanization, the main problem of mankind in the 21st century is the lack of energy and the problem of global warming[1,2]. However, water resources are essential for survival [3]. Urbanization and industrialization are important factors of modern civilization that underlie many advances in improving living standards, economic growth, and technological innovations[4,5]. Water pollution is becoming a global threat due to urbanization, industrialization and human activities. Any change in the physical, chemical, and biological properties of groundwater, oceans, lakes, and rivers is

called water pollution[6]. With the increase in the world's population and the shortage of water resources on the one hand, and environmental pollution issues on the other, water resources for humans have been severely reduced[7]. A large portion of industrial wastewater is discharged into the environment without treatment[8]. Industrial operations are an important part of industrial wastewater, which are by-products of various industrial processes and include a wide range of substances such as Organic pollutants (pharmaceuticals, antibiotics, organic dyes, nitrobenzene, cyclohexane, phenols, toluene, biphenyls, pesticides, plasticizers, detergents, oils, greases, proteins and carbohydrates, fertilizers, hydrocarbons)[9,10]. Inorganic pollutants (such as heavy metals), and biological pollutants (such as microorganisms) are the three common groups of pollutants in wastewater[11]. Antibiotics have been widely used in the treatment and prevention of microbial infections in humans and animals since their introduction in the 1930s[12]. With the rapid development of pharmaceutical and medical industries, the use of antibiotics has expanded greatly among animals and humans. The use of antibiotics is actually to prevent the occurrence of diseases by treating infections quickly, also prevents the spread of bacterial infections in humans and animals and thus saves many lives[13]. Most antibiotics used in animals are excreted in the environment as metabolites through urine or feces due to the low capacity of absorption of antibiotics by the animal intestine (about 30 to 90%). Antibiotics have a toxic effect on some organisms in the aquatic environment[14]. Although the discovery of antibiotics has played an important role in maintaining human health and saving lives, their excessive use has led to environmental pollution of antibiotics in the environment[15]. The long-term presence of antibiotics in water makes it easier for bacteria to develop resistance, posing a serious risk to humans and the effectiveness of antibiotic drugs[16]. Antibiotics, even at very low concentrations, can be hazardous to the environment because[15], Excessive use of antibiotics has led to the accumulation of antibiotic-resistant bacteria (ARB) and antibiotic-resistant genes (ARGs) in the environment, which is a serious threat to the ecosystem and human health[14]. The overuse of antibiotics has led to their rapid entry into the environment, entering the food chain, disrupting ecosystems, and threatening the health of

living organisms[14,17]. The amount of antibiotic consumption in 2016 was 40.8 billion doses per day and is expected to reach 49.3 billion doses in 2023. This amount is expected to reach 75.1 billion doses by 2030[18]. Wastewater treatment can be carried out by various physical or chemical methods, including filtration, adsorption, boiling, distillation, chlorination, electromagnetic radiation, etc. These methods have several problems. For example, the chlorination method produces carcinogenic substances during the process, and the hypochlorite in the treated water has a high corrosive power, which leads to increased treatment costs[7]. Although conventional methods are effective in removing many pollutants, they do not perform well in removing antibiotics. Therefore, the development of pollutant removal technologies is essential[19]. Biological treatment methods are not effective in the degradation of these pollutants due to their toxicity and chemical stability. Advanced oxidation processes (AOPs) have been considered in the degradation of these pollutants[9]. Among the effective AOP methods, photocatalytic degradation is an effective method that uses semiconductor materials as catalysts to accelerate chemical reactions under sunlight exposure[9]. Photocatalytic degradation is initiated when semiconductor materials absorb photons with energies equal to or greater than their band gap, promoting electrons from the valence band to the conduction band and leaving positively charged holes behind [20,21]. These photogenerated charge carriers drive the redox reactions responsible for pollutant degradation. Electrons in the conduction band can react with dissolved oxygen to generate superoxide radicals ($\cdot O_2^-$), while holes in the valence band oxidize water or hydroxide ions to produce highly reactive hydroxyl radicals (·OH), which are capable of attacking and decomposing organic contaminants such as antibiotics [22,23]. However, rapid recombination of electron–hole pairs significantly limit photocatalytic efficiency because the absorbed light energy is dissipated as heat rather than being used in surface reactions [21,24]. Once formed, these reactive oxygen species initiate a sequence of oxidation reactions that break chemical bonds in antibiotic molecules, producing smaller intermediates that are gradually mineralized into harmless products such as CO_2 and H_2O [20,22]. Improving photocatalytic activity therefore requires strategies that enhance light absorption and

suppress electron–hole recombination. Various studies show that constructing heterojunction systems or incorporating conductive materials such as graphene can facilitate charge separation and directional electron transfer, thereby prolonging carrier lifetimes and increasing reactive species generation [22–25]. These improvements in charge-transfer dynamics are considered a key factor in enhancing the degradation efficiency of semiconductor photocatalysts for antibiotic removal [26]. Recent studies have shown that constructing more advanced heterojunction configurations can further improve photocatalytic efficiency by simultaneously enhancing charge separation, increasing visible-light absorption, and maintaining strong redox capability. In particular, S-scheme and dual Z-scheme heterojunctions have received significant attention because they enable the migration of photogenerated electrons and holes along an energetically favorable pathway that reduces carrier recombination and preserves the high oxidation and reduction potentials required for efficient pollutant degradation [27,28]. For example, a dual S-scheme g-C_3N_4/ZnO/TiO_2 photocatalyst supported on cork exhibited 98.25% degradation of methyl orange under visible light, while a dual Z-scheme GCN/CdO/$CaFe_2O_4$ composite achieved 88% Congo red removal within 60 min [27,28]. Likewise, the Bi_2O_3/g-C_3N_4/ZnO ternary heterojunction showed 92% degradation of methylene blue due to its effective dual Z-scheme charge-transfer pathway and enhanced carrier migration confirmed by photocurrent analysis [29]. A similar improvement was observed for Ag_3PO_4/g-C_3N_4/Bi_2MoO_6, where a dual Z-scheme mechanism led to approximately 94% degradation of methylene blue and improved catalyst stability through efficient generation of $\cdot O_2^-$ and ·OH radicals [30,31]. These findings confirm that heterojunction engineering, particularly in S-scheme and Z-scheme forms, is a promising approach for achieving higher photocatalytic activity by prolonging charge-carrier lifetime and promoting the formation of reactive oxygen species essential for the degradation of persistent organic contaminants. Although adsorption, flocculation/coagulation ion exchange membranes and Fenton-like catalysts are widely used in the removal of pollutants from water, their use is limited due to the complex process, high energy requirements and the production of by-products such as sludge and sediment. Which is not environmentally friendly. Photocatalyst is an environmentally friendly method that reacts with the

pollutant electrons and holes and converts them into simpler substances[32]. Photocatalysts are an effective method for removing antibiotics, due to their lack of secondary pollution, simple operation, and low energy consumption[15]. However, complete removal of antibiotics requires a long time, so the development of photocatalysts using metal-organic frameworks (MOFs) is necessary due to their semiconductor-like behavior under light irradiation. The porous MOF structures can provide more active sites for the photocatalyst and have more surface contact with the pollutant[33]. Graphene-based materials (GBMs) are an effective method for the removal of various pollutants due to their properties such as specific adsorption capacity, high surface area and excellent chemical stability [34,35]. Graphene and its derivatives such as GO and rGO have been extensively studied and investigated in wastewater treatment. The use of graphene has received serious attention due to its performance in the adsorption of antibiotics and its large-scale efficiency[19]. Heterojunction structure is the interface between two different photocatalysts with different electronic properties. A suitable heterojunction structure leads to effective separation of electron-hole pairs in the presence of light, and consequently leads to improved photocatalyst performance. Different types of heterojunction structures are S-type, p-n-type, Schottky-type, surface heterojunctions, traditional heterojunctions (such as type I, type II, and type III), and Z-type[36]. Most photocatalysts suffer from electron-hole recombination, which leads to a decrease in the performance of the photocatalysts. Therefore, it is important to use visible light efficiently [37–39]. The use of heterojunction structure leads to a decrease in the band gap of the photocatalyst, an increase in the specific surface area of the photocatalyst, and electrons and holes must be separated, and their lifetime is extended[40].

In this review, we first provide a brief overview of the major methods used for antibiotic removal and then examine how graphene-based materials—particularly GO and rGO—enhance the photocatalytic degradation of antibiotics. A structured classification of heterojunction architectures relevant to antibiotic removal is presented, covering p–n, non-p–n, Z-scheme, and Schottky junction systems. In addition, the key environmental variables and operational parameters influencing photocatalytic

efficiency are discussed, followed by a comparison of photocatalysts that exhibit superior performance for different antibiotic classes. Although several previous reviews have addressed graphene-based photocatalysts or focused on isolated heterojunction types, a comprehensive synthesis that integrates graphene chemistry, heterojunction engineering, charge-transfer mechanisms, and antibiotic-specific degradation pathways has been lacking. The present article fills this gap by combining mechanistic insights with a unified heterojunction classification and a critical evaluation of photocatalytic performance under both laboratory and real-wastewater conditions. By also considering catalyst stability, mineralization, and toxicity evolution—factors often overlooked in earlier literature—this review offers a more application-oriented perspective. These elements collectively establish the novelty and contribution of this work.

1-1-Methodology

The articles reviewed in this study were mainly identified from Google Scholar and Scopus using keywords such as “photocatalyst”, “graphene”, “heterojunction structure”, and combinations such as “photocatalyst + graphene” or “photocatalyst + heterojunction structure”. Only peer-reviewed articles and books published between 2011 and 2025 were included in this study. Studies were selected if they investigated antibiotic removal from a photocatalytic perspective and involved both graphene-based materials and heterojunction structures. Fig. 1 presents the PRISMA flow diagram illustrating the selection process and the number of articles included in this review.

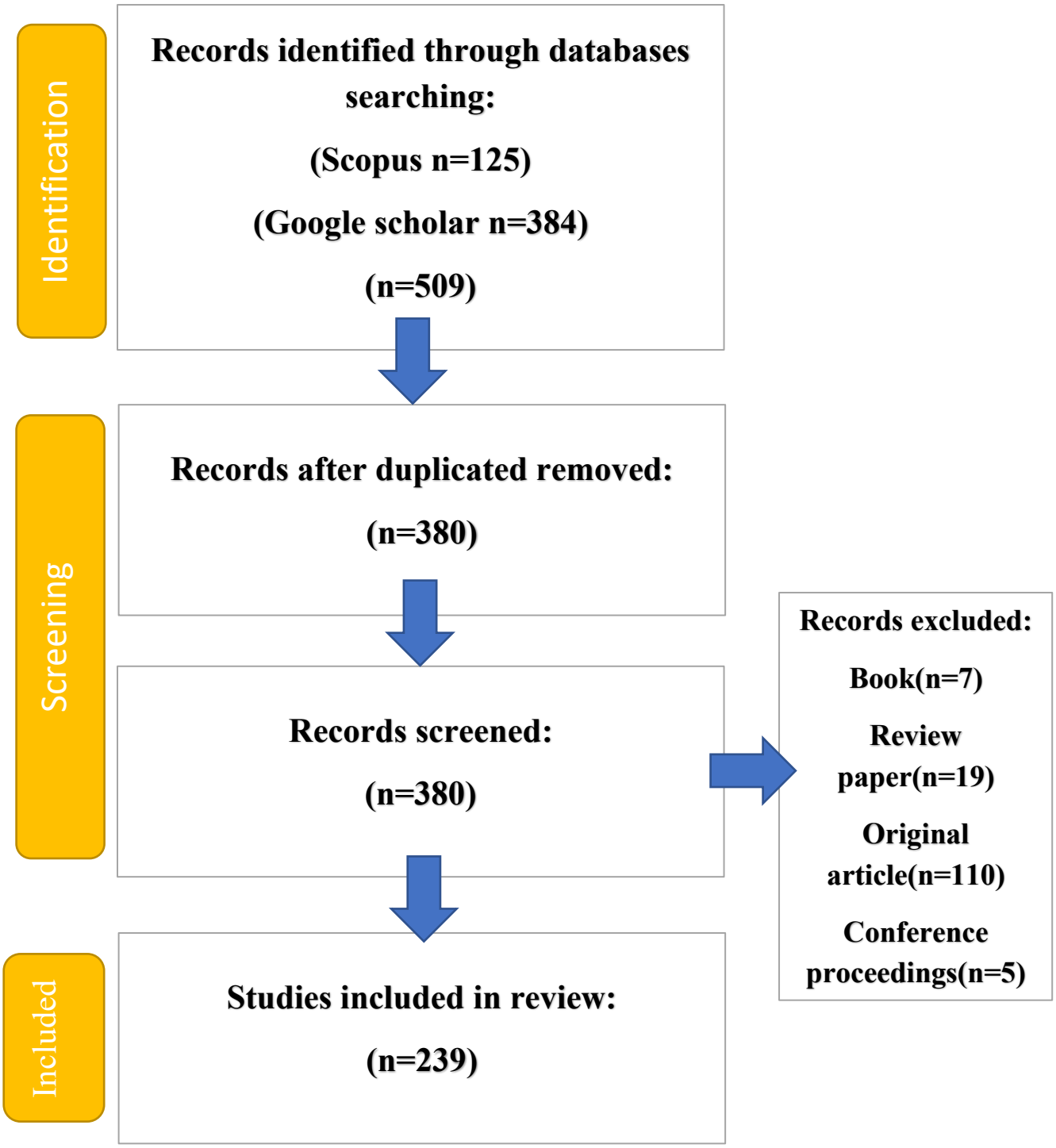

Fig.1- PRISMA Flowchart for selection of literature.

2- ANTIBIOTICS: CLASSIFICATION, OCCURRENCE, AND ENVIRONMENTAL IMPACTS

The extensive and often uncontrolled use of antibiotics in human therapy, veterinary medicine, aquaculture, and agriculture has led to their widespread occurrence in aquatic environments. A significant proportion of administered antibiotics is not fully metabolized and is consequently excreted into sewage systems, eventually reaching wastewater treatment plants and natural water bodies [41,42]. Conventional treatment processes are frequently inefficient in completely removing these biologically active compounds, allowing them to persist and accumulate in the environment. The presence of antibiotics in water systems has raised serious concerns due to their potential ecological toxicity and their role in promoting antimicrobial resistance among microbial communities. Therefore, a clear understanding of the major classes of antibiotics, their environmental occurrence, and their associated impacts is essential for evaluating the challenges they pose and for guiding the development of effective remediation technologies [43–45].

2-1- CLASSIFICATION AND EXAMPLES OF ANTIBIOTICS

Antibiotics are a structurally diverse group of bioactive molecules used extensively in human and veterinary medicine, aquaculture, and agriculture. They can be broadly categorized into several major classes based on their core chemical scaffolds and modes of action, including tetracyclines, β-lactams, fluoroquinolones/quinolones, sulfonamides, macrolides, and others. In environmental studies, these compounds are often selected as model pollutants because they are frequently detected in surface waters, groundwaters, and wastewater effluents [46,47]. Among these, tetracyclines constitute one of the most widely studied families. Tetracycline (TC) and its hydrochloride salt (TC-HCl), as well as oxytetracycline (OTC), are commonly used broad-spectrum antibiotics that have been extensively investigated as target contaminants in adsorption and photocatalytic degradation studies using graphene-based materials. These compounds are often used to simulate “tetracycline antibiotic wastewater” due to their frequent detection and relatively high persistence in aquatic environments [43,47]. β-Lactam antibiotics, such as amoxicillin (AMOX), are another important group. They are

widely prescribed in clinical practice and are frequently found in municipal and hospital effluents, where they can be removed using graphene oxide (GO) and reduced graphene oxide (rGO)–based adsorbents and photocatalysts [45,48]. Fluoroquinolones and quinolones, including norfloxacin and flumequine, are synthetic broad-spectrum antibiotics that exhibit high activity at low concentrations and are often reported in wastewater and surface water monitoring campaigns. Their removal via advanced oxidation processes and graphene-based composites has been reported in several studies, underscoring their environmental relevance [45,49]. In addition, sulfonamides represent a historically important and still widely used class of synthetic antibiotics. Trace-level occurrence of multiple sulfonamides has been documented in environmental wastewater, with low detection limits and high analytical recoveries, indicating that they can persist in treated effluents at $ng \cdot L^{-1}$ levels [41,46,47].

Taken together, tetracyclines, β-lactams, fluoroquinolones/quinolones, and sulfonamides are frequently selected as representative antibiotic pollutants in graphene-based adsorption and photocatalytic studies [45,47].

2-2- OCCURRENCE AND PATHWAYS INTO THE AQUATIC ENVIRONMENT

The continuous detection of antibiotics in environmental waters is largely attributed to their incomplete metabolism in humans and animals, followed by excretion as parent compounds and active metabolites into sewage systems. Municipal wastewater treatment plants (WWTPs), hospital effluents, pharmaceutical manufacturing discharges, and effluents from livestock and aquaculture facilities therefore act as key point sources of antibiotic residues [41,43]. Conventional WWTPs are generally not designed to efficiently remove trace organic micropollutants such as antibiotics. As a result, these compounds can pass through treatment barriers and be discharged into receiving surface waters or infiltrate into groundwater. The presence of “antibiotic wastewater” and “tetracycline antibiotic wastewater” specifically highlights the role of pharmaceutical and related industrial effluents as concentrated sources [44,47,50]. Monitoring studies have reported antibiotics at concentrations ranging from $ng \cdot L^{-1}$ to $\mu g \cdot L^{-1}$ in environmental wastewater samples, including sulfonamides and various

tetracycline- and β-lactam-type compounds [44,51]. These findings indicate that antibiotics are not only episodic pollutants but can behave as pseudo-persistent contaminants due to their continuous input and limited removal in conventional treatment systems [43,49].

2-3- ENVIRONMENTAL AND BIOLOGICAL IMPACTS

The occurrence of antibiotics in wastewater and natural waters raises serious concerns regarding both ecological integrity and public health. A key issue is the promotion of antibiotic resistance: long-term exposure of environmental microbial communities to sub-inhibitory concentrations of antibiotics can contribute to the selection and propagation of antibiotic-resistant bacteria (ARB) and the dissemination of antibiotic resistance genes (ARGs) [49,50]. Several studies have emphasized that antibiotics in wastewater create selective pressure that worsens the emergence of antimicrobial-resistant pathogens, thereby compounding global water quality challenges [44,52,53]. Beyond resistance development, antibiotics can directly disrupt aquatic ecosystems. Even at low concentrations, they may alter the composition and function of microbial communities, affect primary productivity, and impact higher trophic levels. Persistent antibiotic residues can enter the food chain, eventually posing risks to human health through bioaccumulation or chronic exposure to mixtures of antibiotics and their transformation products [54–56]. The ecotoxicological consequences are not limited to microbial endpoints. Antibiotics and their degradation products may exhibit biological toxicity towards a range of aquatic organisms, including algae, invertebrates, and fish. Therefore, the removal of both antibiotic molecules and their associated biological toxicity has been highlighted as a critical objective for advanced water treatment technologies [57,58]. From a human health perspective, the co-occurrence of antibiotics and antibiotic-resistant bacteria in wastewater and receiving waters represents a dual threat, potentially facilitating the spread of resistance determinants and increasing the difficulty of treating bacterial infections. These combined environmental and public-health concerns underscore the urgent need for effective treatment strategies capable of degrading antibiotics, mitigating their toxicity, and limiting the propagation of antimicrobial resistance [42,46,56]. A summary of the major antibiotic classes,

representative compounds, common environmental sources, and their associated ecological concerns is presented in Table 1.

Table1- Representative antibiotic classes commonly investigated in graphene-based photocatalytic studies and their environmental relevance.

Antibiotic class	Representative examples	Typical use	Key environmental and biological concerns	Reference
Tetracyclines	Tetracycline (TC), TC-HCl, Oxytetracycline (OTC)	Broad-spectrum, widely used in medicine & livestock	1-frequent detection in "tetracycline antibiotic wastewater" 2- persistent in aquatic systems 3- contribute to antibiotic resistance 4- ecotoxicity to algae, microbes, fish	[45,46,49]
β-Lactam	Amoxicillin (AMOX)	Common in clinical medicine, enters municipal & hospital effluents	1-passes through conventional WWTPs 2-affects microbial communities 3-contributes to resistance gene propagation	[45,49,56]
Fluoroquinolones / Quinolones	Norfloxacin, Flumequine, Ciprofloxacin	Synthetic broad-spectrum, human & veterinary use	1-detected in surface waters & wastewater 2-difficult to remove by conventional treatment 3-disrupt aquatic ecosystems	[45,56,59]

Sulfonamides	Sulfadiazine, sulfanilamide, sulfamethoxazole	Widely used historically & currently	1-persistent at very low concentrations 2-chronic exposure risks 3-contributes to resistance selection	[45,46,56,59]
Mixed Antibiotic Systems	General "antibiotics" used in photocatalysis tests	Model mixed pollutants representing real wastewater matrices	1-biological toxicity of antibiotics in water 2-interplay with pathogenic bacteria 3-combined ecotoxicity of antibiotic mixtures	[43,44,47]

3-METHODS OF REMOVING ANTIBIOTIC POLLUTANTS FROM WASTEWATER

There are various methods for removing antibiotics, including biological, adsorption, and advanced oxidation methods.

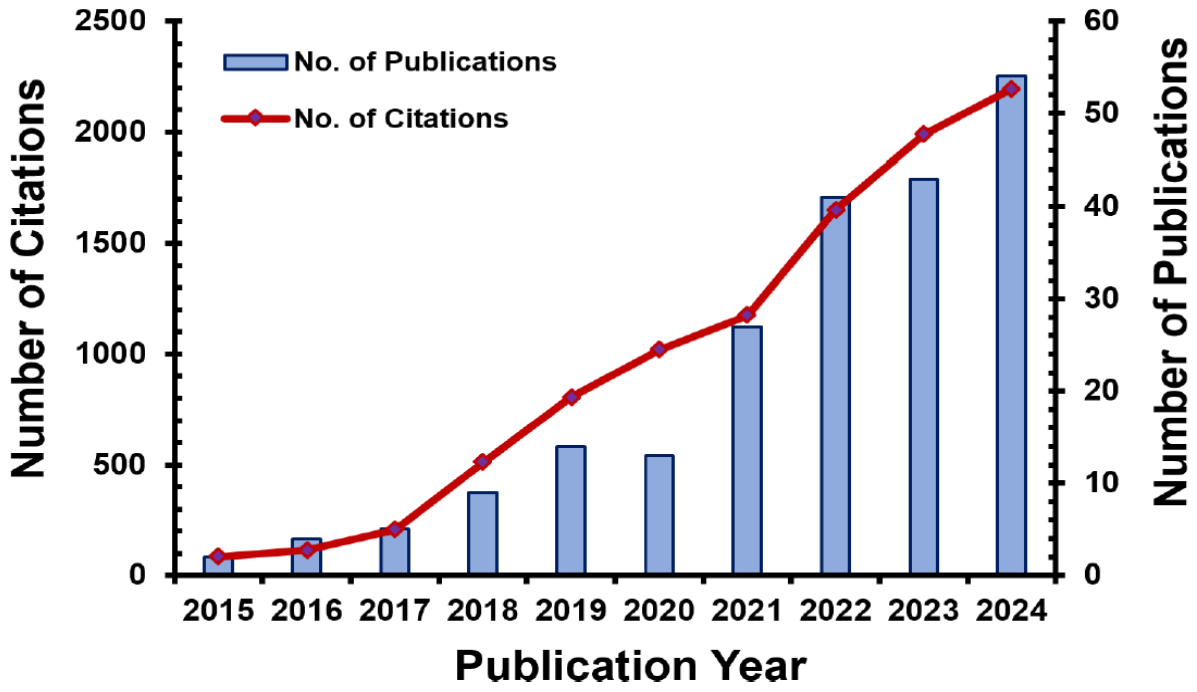

Fig.2- number of articles and citations on the use of photocatalysts in the removal of antibiotics[60].

Fig.2 shows that published articles and citations using photocatalysts for antibiotic removal have increased from 2015 to 2024, indicating that the use of this method in antibiotic removal is increasing day by day.

3-1- BIOLOGICAL METHOD

In this method, bacteria and fungi are used to remove pollutants and both aerobic and anaerobic processes can be used in wastewater treatment. In the aerobic process, free or dissolved oxygen is used together with microorganisms. In the anaerobic process, organic compounds convert into methane, carbon dioxide and water in the absence of oxygen[61].

Tylosin, Sulfamethoxazole, Sulfamethazine, sulfachloropyridazine, sulfadiazine, chlorotetracycline, tetracycline,

Chloramphenicol, thiamphenicol, levofloxacin, minocycline, amoxicillin, Oxytetracycline and Ciprofloxacin antibiotics are removed using biological methods [62–65].

3-2- ADSORPTION METHOD

Adsorption is one of the uncomplicated methods to remove organic pollutants, including antibiotics, due to its simplicity in design and operations, easy regeneration of the adsorbent, low energy consumption, no by-product generation and relatively low operating cost[66]. However, this method only leads to the change of the antibiotic phase, not the destruction of the antibiotic. The influencing factors in the amount of absorption are: initial concentration of adsorbate, solution pH, temperature and physical properties of adsorbent[67,68]. Activated carbon has a porous structure and has been used to remove many organic compounds from water. Activated carbon has a high absorption surface (500-1500 m^2/g) and pore volume of 0.7-1.8 cm^3/g[69]. Chlortetracycline, Tetracycline, Ciprofloxacin, norfloxacin, Sulfamethazine,

Amoxicillin, erythromycin, clarithromycin, ampicillin, ofloxacin, sulfamethoxazole, trimethoprim antibiotics that have been removed using the absorption method[70–72].

3-3- ADVANCED OXIDATION PROCESS (AOP)

The advanced oxidation method is an effective and promising method for removing emerging contaminants, including antibiotics[73,74]. The basis of this method is the production of highly oxidative free radicals (mainly hydroxyl radicals) in a very short time. Hydroxyl radicals can be produced in AOPs in different ways[75]. Hydroxyl radicals (OH•), with strong oxidation capacity (2.8 V oxidation potential) is the most common reactive oxygen species (ROS) and is commonly used for conventional AOPs. Hydroxyl radicals produced from the reaction with water, react with the pharmaceutical pollutants and after the formation of intermediates, carbon dioxide and water are produced. The basis of this method is the production of hydroxyl radicals[76–78]. Fig.3 shows different methods of the advanced oxidation process, which is divided into three categories: photochemical processes, non-photochemical processes, and hybrid processes. Equation 1 shows the reaction in the advanced oxidation process.

$$\mathbf{OH^{\cdot} + antibiotics \rightarrow Intermediates \longrightarrow CO_2 + H_2O} \quad (1)$$

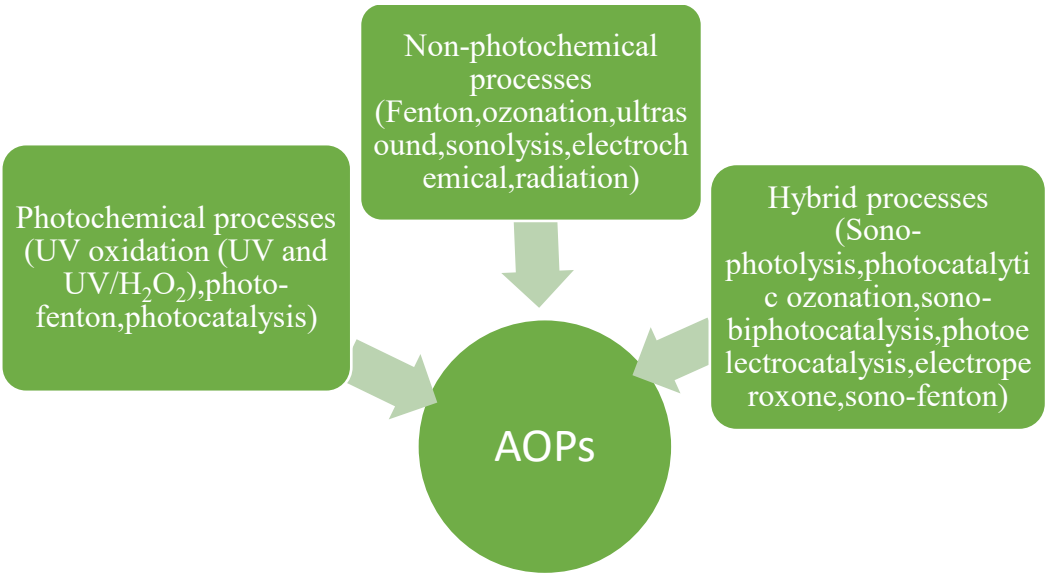

Fig.3- Types of AOPs for Antibiotics wastewater treatment (adopted from [76]).

3-3-1-TYPES OF METHODS

The most common wastewater treatment methods with advanced oxidation methods are shown in the Table 2 below. Methods such as the combination of O_3, H_2O_2 and UV, Fenton's method, supercritical oxidation and ionizing radiation are used in all scales, such as laboratory and industrial. But the ultrasonic and photocatalyst methods are only used on a laboratory scale[79].

Table2-Most used AOPs for water and wastewater treatments (adopted from [80]).

Photochemical processes	**Non- photochemical processes**
UV oxidation processes	Ozonation
UV/H_2O_2	Fenton
UV/O_3	Ultrasound(us)
UV/H_2O_2/O_3	Us/H_2O_2,Us/O_3, Us/Fenton
UV/ultrasound	Electrochemical water oxidation
Photo-Fenton	supercritical water oxidation
photocatalysis	Ionizing radiation
sonophotocatalysis	Electron-beam irradiation
Vacuum UV(VUV)	wet-air oxidation
Microwave	pulsed plasma

3-3-1-1-OZONATION

The use of ozone for wastewater treatment dates back to the early 20th century. For the first time, ozone was used to disinfect drinking water in 1906. Ozone has been used for several purposes, including disinfection, minimizing taste and smell, reducing the formation of secondary disinfectants, and oxidizing organic pollutants[81]. The use of ozone in aqueous reactions produces various unwanted side products due to its high redox potential. Usually, ozone is used to break C=C bonds in organic compounds. Ozone/hydrogen peroxide is used in the removal of drugs, especially antibiotics. One of the limitations of ozone is its low solubility in water[82].

In surface water as well as wastewater, ozone decomposition is done through active organic compounds in water (dissolved organic matter (DOM)). Ozone has a high reactivity with some of the DOM, such as second and third-type amines and phenols. In 2 reaction, ozone reduced the ozonide radical by donating an electron.

$$DOM + O_3 \rightarrow DOM^{\cdot+} + O_3^{\cdot-} \quad (2)$$

Then the ozonide radical decomposes according to the 3 and 4 reactions and provides $OH^{\cdot}$ [83].

$$O_3^{\cdot-} \rightarrow O_2 + O^{\cdot-} \quad (3)$$

$$O^{\cdot-} + H_2O \rightarrow OH^{\cdot} + OH^{-} \quad (4)$$

Florfenicol, oxytetracycline, sulfadimethoxine, sulfamethoxazole, trimethoprim, mpicillin, azithromycin, erythromycin, clarithromycin, ofloxacin, and tetracycline antibiotics that have been removed using the absorption method[84,85].

3-3-1-2-FENTON METHOD

Adding aqueous solutions of Fe^{2+}ions and hydrogen peroxide (H_2O_2) to produce hydroxyl radicals is called Fenton's process. Fenton process is a good method to remove organic pollutants, including antibiotics,

and its basis is the production of hydroxyl radical from Fe-catalyzed decomposition of H_2O_2. This method has limitations, including continuous production of iron sludge, a narrow pH range, high chemical involvement, and high costs attributed to chemicals, namely H_2O_2[86–88]. Fenton method is divided into four categories: Homogeneous Fenton process, Heterogeneous Fenton process, Homogeneous photo Fenton process and Heterogeneous photo Fenton process. In Homogeneous Fenton process, all reactions take place in the aqueous phase and the catalysts Fe_{eq}^{2+} and Fe_{eq}^{3+} have been used. In the heterogeneous photon process, Fe_s^{2+} and Fe_s^{3+} are used as catalysts. The use of iron, which is initially solid, can reduce the amount of sludge formed. The difference between Homogeneous Fenton process and Heterogeneous Fenton is that in a homogeneous process, chemicals react throughout the solution. In a heterogeneous way, chemical reactions are carried out on the surface of catalyst adsorption and mass transfer limit of reactants[83]. In homogeneous photo Fenton process according to reactions 5 to 7, $Fe_{(aq)}^{3+}/H_2O_2$ photolysis $Fe^{3+}$to Fe^{2+} in the presence of UV light, also along with the direct production of $OH^{\cdot}$. The reactivity of $Fe(OH)^{2+}$ is extremely high, which leads to a clear effect of pH in the process[83].

$$Fe^{3+} \rightarrow Fe^{2+} + OH^{\cdot} \quad (5)$$

$$Fe(OH)^{2+} \rightarrow Fe^{2+} + OH^{\cdot} \quad (6)$$

$$H_2O_2 \rightarrow 2OH^{\cdot} \quad (7)$$

The heterogeneous photo-Fenton process is usually done using the iron catalyst in the presence of light [83]. The disadvantages of the photo-Fenton method include the need for an acidic environment and the need to remove the iron catalyst at the end of the process[89]. Tylosin, Chloramphenicol, Amoxicillin, Cloxacillin,

Tetracycline, Sulfamethoxazole, and ofloxacin are antibiotics that have been removed using the Fenton method[90,91].

3-3-1-3-PHOTOCATALYST METHOD

Choosing the right photocatalyst is the most important step in any process[92]. Photocatalysis is one of the advanced oxidation processes that is known as an efficient method for breaking down toxic and harmful pollutants[93]. The chemical reaction resulting from the absorption of photons by a photocatalyst is called photocatalysis. Photocatalysis is an effective method for removing veterinary antibiotics from wastewater[94]. Photocatalytic degradation, or simply photodegradation, is a process that uses infrared (IR), ultraviolet (UV), and visible (Vis) light to convert an environmental pollutant into an environmentally harmless product that occurs on the solid surface of a photocatalyst[95]. Recently, research into efficient and active photocatalysts with the ability to be activated in the visible light range has gained particular importance[96]. When the photocatalyst is activated by absorbing light, it leads to the excitation of electrons, which are transferred from the valence band (VB) to the conduction band (CB). The holes in the VB react with water molecules on the surface of the photocatalyst and produce hydroxyl radicals. At the same time, the charge separation between the two bands increases the electrons in the conduction band to carry out reduction reactions on the surface. The performance of a photocatalyst requires a narrow band gap energy, enhanced charge separation and charge transport, suitable band edge location, reasonable surface active sites, and a low charge recombination rate[97]. Fig.4 shows the photocatalytic method of antibiotic removal. After the photocatalyst is activated by light, electrons and holes react with oxygen and water molecules to produce hydroxide radicals and superoxide radicals, which react with the antibiotic and convert the antibiotic into lighter substances, water, and carbon dioxide. The chemical reaction resulting from the absorption of photons by a photocatalyst is called photocatalysis. Photocatalysis is an effective method for removing veterinary antibiotics from wastewater[98]. The photocatalyst process consists of several steps, which are:

1-Transfer of pollutants to the surface of the photocatalyst

2-Adsorption of pollutants on the surface of the photocatalyst

3-Degradation of molecules activated by photons begins

4-Removal of reaction products

5-Removal of reaction products from the surface of the photocatalyst[98].

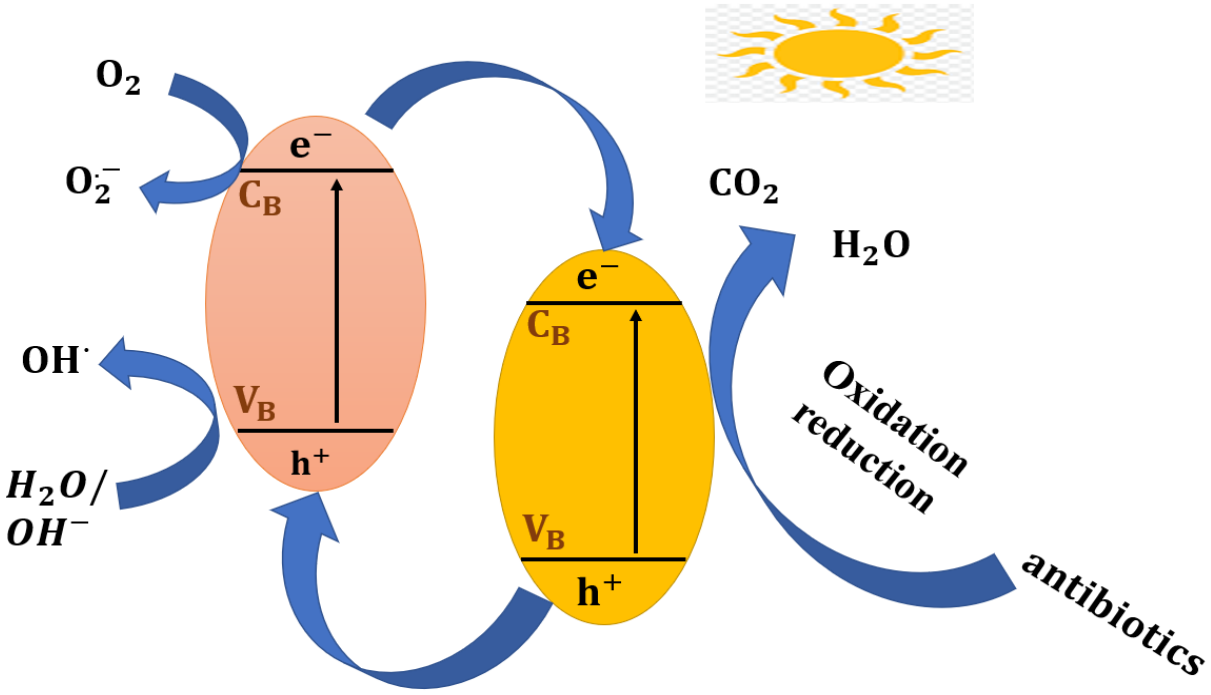

Fig.4-Schematic diagram of the photocatalytic removal process of antibiotics in the presence of sunlight(adopted from[99]).

3-3-1-3-1-PHOTOCATALYTIC DEGRADATION OF ANTIBIOTICS

In general, it can be said that the photocatalytic reactions in antibiotics are as follows: after reacting with a hole, hydroxyl radical, and superoxide, the antibiotic finally turns into water and carbon dioxide. Equations 8-12 show how the photocatalytic reaction for antibiotics occurs[100].

$$\text{Photocatalyst} + h\nu \rightarrow \text{Photocatalyst} + h^+ + e^- \quad (8)$$

$$h^+ + \text{antibiotics} \rightarrow CO_2 + H_2O + \text{Degradation products} \quad (9)$$

$$O_2 + e^- \rightarrow O_2^{-\cdot} \quad (10)$$

$$H_2O/OH^- + h^+ \rightarrow OH^{\cdot} + H^+ \quad (11)$$

$$\text{antibiotics} + O_2^{-\cdot}/OH^{\cdot} \rightarrow CO_2 + H_2O + \text{Degradation products} \quad (12)$$

4- GRAPHENE

Graphene is an allotropic form of graphite in which carbon atoms are arranged in a single layer. Carbon atoms are hybridized in a two-dimensional arrangement with a honeycomb or hexagonal structure, consisting of a monoatomic layer of SP^2 carbon atoms[101], which has a large specific surface area (2630 m^2/g), zero band gap (band gap of 0-0.25 eV), Hall effect at room temperature, adjustable band gap, high electron mobility, optical transparency, good chemical stability, excellent electrical, thermal conductivity and hydrophilic properties, low production cost on a large production scale, unexpected high absorption of white light, high elasticity, unusual magnetic properties[102–107], gas absorption and charge- transfer interactions with molecules[108] and has different functional groups (epoxy, carbonyl, hydroxyl) that enable graphene-based catalysts to adsorb pollutants on their surface and effectively scavenge through adsorbed reactive oxygen species (ROS) decompose[109]. Graphene has a high capacity to absorb antibiotic pollutants through van der Waals interactions. Antibiotic compounds mainly include aminoglycosides, β-lactams, glycopeptides, macrolides, quinolone, and sulfonamides. This structure of antibiotics suggests that graphene may be an ideal adsorbent for the removal of antibiotics using π-π interactions, however, graphene easily aggregates in solution and is a challenge for adsorption, separation and recovery capacity. Therefore, is necessary to overcome these limitations. As a co-catalyst, in addition to the fact that

graphene as an electron acceptor prevents electron-hole recombination, the high absorption activity of molecules leads to the extension of the light range[110]. Also, graphene can be combined with other semiconductor photocatalysts in the removal of antibiotics. The combination of graphene with metal oxide photocatalysts leads to the improvement of the performance of the catalysts by helping to overcome the inherent problems of ultraviolet light activity and fast electron-hole recombination rates[111]. Graphene consists of a single-layer structure, and all atoms are exposed to the environment from all sides, and their contact with antibiotics easy compared to conventional adsorbents. The porous structure and high surface area of graphene adsorbents make it an ideal option for faster diffusion or surface reactions of antibiotics, leading to effective and faster adsorption[110]. The large-scale production cost of graphene adsorbents is lower than that of other high-performance adsorbents (carbon nanotubes), but the antibiotic adsorption capacity is comparable[110]. The main limitation of graphene is its hydrophobicity, which leads to its accumulation in aqueous solutions, greatly reducing the adsorption capacity of graphene[110]. To improve the dispersion of graphene, modified graphene which have oxygen-containing groups attached to carbon can be used, thus forming a homogeneous aqueous suspension[110]. Graphene oxide (GO) and Reduced graphene oxide (RGO) are among the most important graphene-based nanocomposites. The use of oxygen in the graphene network leads to the distribution of carboxyl, hydroxyl, and epoxy groups in the carbon network[110]. GO is a compound of carbon, oxygen, and hydrogen whose relative ratios can be modified mainly through synthesis conditions. GO acts as a stable suspension and provides the possibility of antibiotic adsorption due to its high dispersion. GO surface has a good adsorption for organic and inorganic pollutants due to its carboxyl(-COOH), carbonyl (C=O), and hydroxyl(-OH) functional groups[111]. Most of the graphene-based composites that are used to remove antibiotics have functional groups such as oxygen, carbonyl, epoxy,carboxyl, and hydroxyl compounds[110,111]. Some molecules such as nitrilotriacetic acid and polymers such as chitosan have more adsorption sites for antibiotics due to having rich hydrophilic groups, and as a result, their binding to graphene is easy. Therefore, modification of GO with hydrophilic compounds leads to the binding of antibiotics in the graphene oxide surface and accelerates the removal of antibiotics[110]. Due to the expensive and toxic nature of some organic molecules, in terms of cost and environmental considerations, polymers are a

good option for modifying GO, which can be easily mixed with many polymers [110,112]. Nanoparticles such as magnetic nanoparticles, metal oxides, etc, are easily placed on the surface of graphene and it leads to an increase in the absorption capacity of antibiotics[110]. Modification of GO/graphene with metal oxides leads to increased adsorption capacity and separation efficiency[111]. GO has good dispersion and adsorbs antibiotics quickly, while graphene and RGO adsorption rate is low and due to poor dispersion require higher time to reach adsorption equilibrium. For example, the adsorption of tetracycline by GO takes 15 minutes, while for RGO this time is 6 hours[110]. When the pH is low, most functional groups of graphene are protonated and therefore have a positive charge. At pH lower than the PZC level, graphene is fully positively charged and binding of anions occurs due to electrostatic interactions. Most of the studies based on graphene nanoparticles show that the adsorption rate is low at low pH. As the pH increases, the graphene surface becomes deprotonated which results in the antibiotic cation ions are easily adsorbed by graphene. The optimal pH is around 4-9[110]. Fig.5 shows the antibiotic removal mechanism with graphene. Fig.5 shows the different methods of adsorption mechanism of antibiotics on graphene/ graphene-based nanocomposites (GBNP), which are: hydrogen bonding, π-π interaction, cation-π bonding, amidation bonding, electrostatic attraction, hydrophobic interaction and others (pore-filling and ion exchange). The study of the adsorption mechanism of antibiotics on the graphene/GBNP surface has been considered in order to improve the adsorption capacity. The adsorption mechanism depends on the surface properties of graphene/GBNP, especially the surface area and pore structure which play an important role in the absorption of antibiotics. However, the properties of antibiotics and surface functional groups may affect the adsorption mechanism. When the surface area becomes larger, more active sites are exposed to antibiotics, and as a result, the adsorption rate increases. Therefore, to maximize the surface area and achieve higher adsorption, the adsorbent should have high porosity and smaller particle size distribution. Graphene has a high specific surface area, but it does not have porosity, so to solve the lack of porosity, the solution is to combine it with other porous materials. Different adsorption interactions between antibiotics and graphene/GBNP include Physical forces and chemical interactions. The main interactions of graphene/GBNP with antibiotics are hydrogen bonding

interactions, electrostatic interactions, and π-π interactions. However, other mechanisms such as cation-π bonding, hydrophobic interaction, and amidation reaction are also used between antibiotics and Graphene/GBNPs, which are less important. Graphene/GBNP structure, due to being rich in π electrons, actively establishes π-π interaction with antibiotics that have an aromatic ring and plays an important role in the absorption of antibiotics on graphene/GBNP. Different functional groups involved in antibiotics and graphene/GBNP due to the creation of specific bonds with antibiotics may be another way to improve the adsorption performance of graphene/GBNP. Oxygenated functional groups such as hydroxyl (-OH), carboxyl (-COOH) and carbonyl (-CO-), amino ($-NH_2$) lead to more hydrophilic GBNPs and easily antibiotics react with containing -OH, -COOH, $-NH_2$ through hydrogen bonding. Another main mechanism of antibiotic absorption with graphene/GBNP is electrostatic interaction, which includes two driving forces of electrostatic attraction and electrostatic repulsion, which are related to the surface charge of adsorbents and adsorbates. Mechanisms that are less important: Graphene/GBNPs, which have π electrons, can easily protonate amino groups to form cation-π bonds. Hydrophobic interaction, which occurs between the hydrophobic part of the antibiotic and graphene. The amidation reaction, which is less useful, occurs between the amino and carboxyl groups of antibiotics and GBNPs through the amide bond (-CO-NH-)[110]. MOFs, which are porous materials composed of organic ligands and inorganic clusters, have been considered to have properties such as high specific surface area, tunable porosity, high thermal stability, high mechanical stability, uniform pore structure, and low density in various fields such as storage, membranes, pharmaceuticals, catalysis, separation, and photocatalysis. The use of MOFs in graphene structures has attracted attention[113].

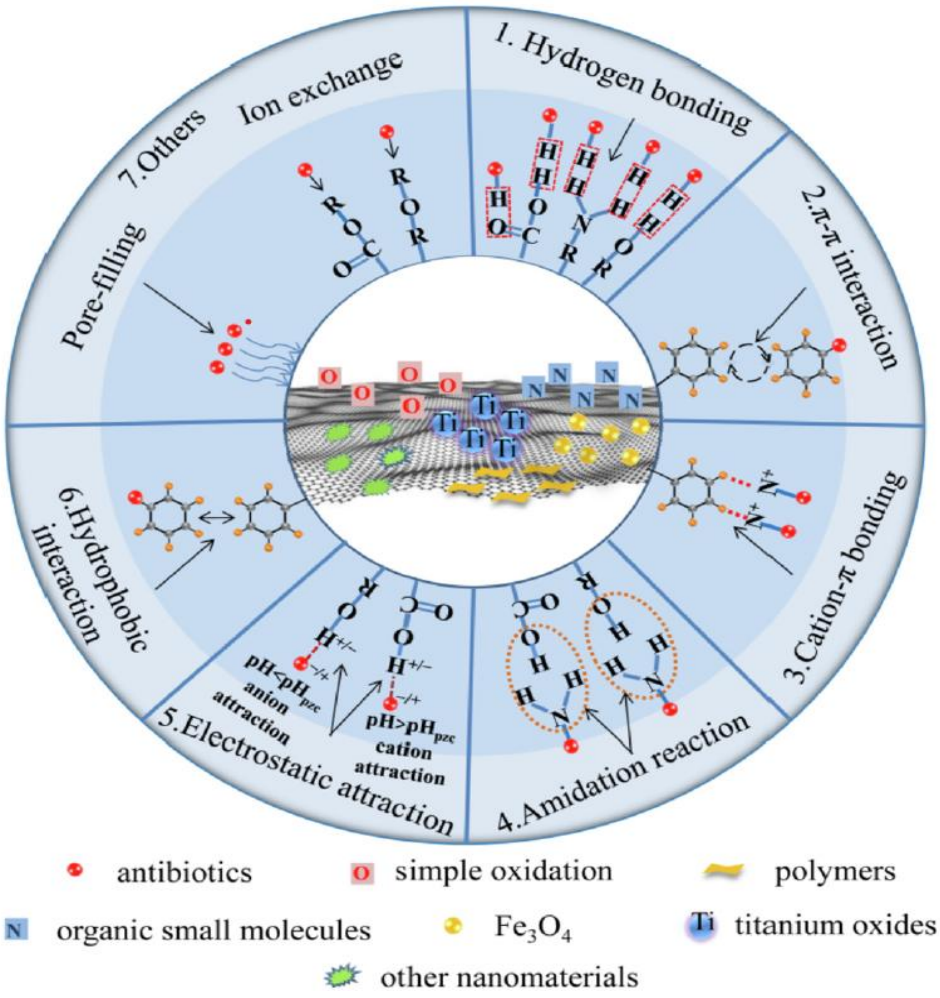

Fig.5-The proposed mechanism for the removal of antibiotics using graphene-based nanoparticles[110].

4-1- PHOTOCATALYTIC REACTION OF GRAPHENE WITH ANTIBIOTICS

The photocatalytic removal of antibiotics with graphene has two mechanisms[110,114].

In the first mechanism in equations 13-15, after GBPs are activated by light, electrons and holes are produced. The electrons react with oxygen and produce superoxide radicals. In the second mechanism in equations 16-24, after GBPs are activated by light, electrons and holes are produced. The electrons react with oxygen and produce the superoxide radical. The holes react with water and produce OH and H^+ radicals. Hydroxyl radical, superoxide radical, and antibiotic react to produce intermediates and finally water and carbon dioxide. Superoxide radical and H^+react together to produce $HOO^{\cdot}$. $HOO^{\cdot}$ is converted into hydrogen peroxide and oxygen. Hydrogen peroxide and electrons react to produce

hydroxide ion and hydroxide radical. Holes react with hydroxide ions and hydroxide radicals are produced. Holes react with hydroxide radical, superoxide radical, and antibiotic react to produce intermediates and finally water and carbon dioxide.

The first mechanism:

$$\text{Graphene based photocatalysts(GBPs)} + h\upsilon \rightarrow \text{GBPs}(e_{CB}^{-} + h_{VB}^{+}) \quad (13)$$

$$\text{GBPs}(e_{CB}^{-}) + O_2 \rightarrow \text{GBPs} + O_2^{-\cdot} \quad (14)$$

$$O_2^{-\cdot} + \text{GBPs}(h_{VB}^{+}) + \text{antibiotic} \rightarrow \text{intermediate products} \rightarrow CO_2 + H_2O \quad (15)$$

The second mechanism:

$$\text{GBPs} + h\upsilon \rightarrow \text{GBPs}(e_{CB}^{-} + h_{VB}^{+}) \quad (16)$$

$$\text{GBPs}(e_{CB}^{-}) + O_2 \rightarrow \text{GBPs} + O_2^{-\cdot} \quad (17)$$

$$\text{GBPs}(h_{VB}^{+}) + H_2O \rightarrow \text{GBPs} + H^{+} + OH^{\cdot} \quad (18)$$

$$O_2^{-\cdot} + OH^{\cdot} + \text{antibiotic} \rightarrow \text{intermediate products} \rightarrow CO_2 + H_2O \quad (19)$$

$$O_2^{-\cdot} + H^{+} \rightarrow HOO^{\cdot} \quad (20)$$

$$2HOO^{\cdot} \rightarrow H_2O_2 + O_2 \quad (21)$$

$$H_2O_2 + e^- \rightarrow OH^- + OH^{\cdot} \quad (22)$$

$$GBPs(h^+_{VB}) + OH^- \rightarrow GBPs + OH^{\cdot} \quad (23)$$

$$GBPs(h^+_{VB}) + OH^{\cdot} + O_2^{-\cdot} + \text{antibiotic} \rightarrow \text{intermediate products} \rightarrow CO_2 + H_2O \quad (24)$$

Table 3 summarizes the removal rate in the optimal state. Raja et al. [115] used RGO- $BiVO_4$-ZnO photocatalyst to remove the antibiotic ciprofloxacin. The synthesis method plays an important role in the morphology of the photocatalyst for photocatalytic reactions, and the synthesis method of the photocatalyst is hydrothermal. The cubic structure of pure ZnO leads to the creation of a significant number of cavities on the surface. The use of $BiVO_4$ due to its low band gap (2.4ev), good stability and excellent efficiency for the decomposition of ciprofloxacin. $BiVO_4$ conduction band potential (+0.32ev) is more positive than ZnO conduction band potential (-0.38ev), Also, the valence bands are 2.78ev and 2.85ev respectively. Therefore, electrons are transferred from ZnO to $BiVO_4$and lead to effective charge separation. Doping RGO to ZnO and $BiVO_4$ photocatalysts lead to a decrease in electron-hole recombination . The higher efficiency of rGO-$BiVO_4$-ZnO compared to other catalysts is due to the cooperative effect of rGO on $BiVO_4$-ZnO[116]. The scavenger experiment investigated the effect of active species on the photocatalytic removal of ciprofloxacin. Sacrificial reagents such as isopropyl alcohol-0.1 mmol in 100 mL for OH**.**, triethanolamine-1 mmol in 100 mL for h+, benzoquinone(BQ)-0.1 mmol in 100 mL (for O_2**.-**) and ethanol-50 mL in 100 mL (for e−) were used to trap the active species involved in the degradation. The h+ plays a major role in the removal of ciprofloxacin because the removal rate was

reduced to a maximum by the addition of triethanolamine. The removal rate is also affected by BQ, so superoxide radicals also play a role in the removal of ciprofloxacin, but not as effectively as h+. As shown in fig.6, in the first step of ciprofloxacin decomposition, defluoridation and decarboxylation occurred and intermediates were produced (I, II). Then the hydroxyl radical attacks these intermediates and intermediate III is produced. Further oxidation was carried out and the piperazine ring of ciprofloxacin was completely destroyed to form the quinolone derivative (D1). In addition, the primary intermediates react with the hydroxyl radical and led to the cleavage of the quinolone ring and the formation of oxygenated aliphatic compounds. Finally, these aliphatic byproducts are mineralized to CO_2 and H_2O .The removal rate in 60 minutes for 10 mg/L ciprofloxacin is exposed to a visible light source ($\lambda < 400$ nm) and uses a tungsten lamp (150 mW/ cm−2) and the photocatalyst concentration is 0.3g/L. For the pure ZnO photocatalyst is 63.3%, for pure $BiVO_4$ photocatalyst 55.6%, for $BiVO_4$-ZnO photocatalyst 80.3% and finally for rGO- $BiVO_4$-ZnO 98.4%. The rGO structure resulted in an 18.1% increase in antibiotic removal rate compared to the $BiVO_4$-ZnO photocatalyst alone[115].

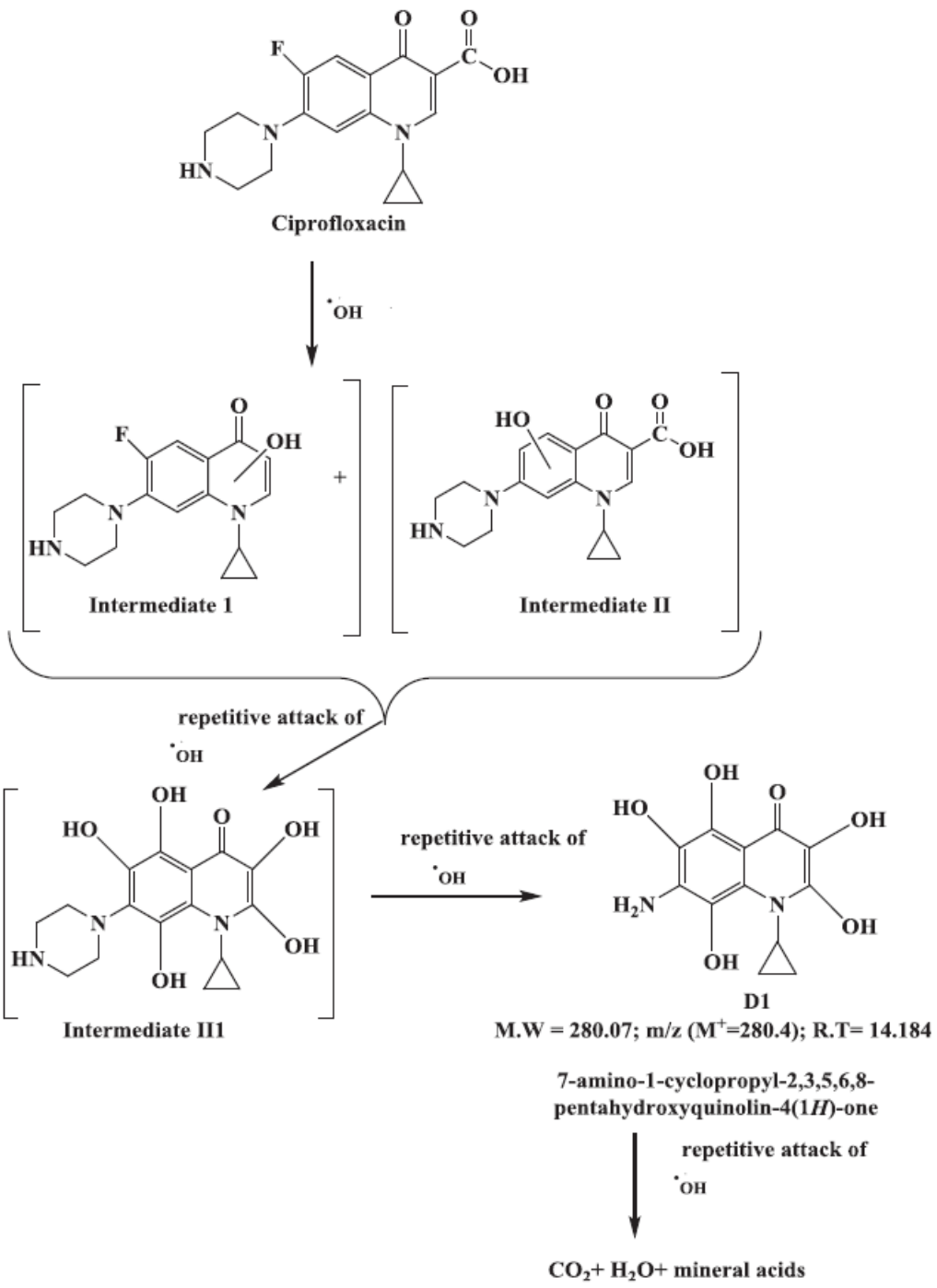

Fig.6- Photocatalytic mechanism of removal of antibiotic ciprofloxacin and intermediates formed in the photocatalytic reaction[115].

Equation 25 is a Pseudo-first-order apparent rate constant for the kinetic modeling of photocatalytic antibiotic removal reaction. Although the photocatalytic reaction of antibiotics is very complex, a

pseudo-first-order reaction is used to approximate and calculate the rate constant. where C_t is the concentration at time t, C_0 is the concentration at the initial time, and K_{app} is the rate constant. The apparent first-order rate constant normalized to the concentration of the photocatalyst for the rGO-$BiVO_4$-ZnO photocatalyst is 0.2143 min-1.g-1.L[115].

$$\ln\frac{C_t}{C_0} = -K_{app}t + b \qquad 25$$

Pu et al. [117] used Cu-TiO_2/GO photocatalyst to remove tetracycline hydrochloride. The synthesis method of TiO_2/GO photocatalyst is hydrothermal and the synthesis method of Cu-TiO_2/GO photocatalyst is impregnation. Adsorbed Cu in the center of TiO_2 are used to prevent electron-hole recombination. Copper with a reduction potential of 0.16V (Cu^{2+}/Cu^{+}) and 0.52v(Cu^{2+}/Cu) is a suitable modifier for GO/ TiO_2 photocatalyst[117,118]. The adsorption capacity of TiO_2 is greatly increased by the addition of Cu and GO. The specific surface area of TiO_2/GO is larger than that of TiO_2 alone due to the high specific surface area of GO. The regular hexagonal structure consisting of sp2 hybrid orbitals between C atoms is a characteristic of GO. The adsorption rate of TC on Cu-TiO_2/GO is enhanced due to the π-π interaction between GO and the four aromatic rings of TC. Photocatalyst performance increases from pH 3 to 7 and decreases from 7 to 11, which is due to the surface charges of the photocatalyst. Tetracycline has acidic and alkaline groups and the amount of removal depends on the electrostatic repulsion forces between tetracycline and the photocatalyst. As shown in fig.7 increasing the initial concentration of tetracycline leads to a decrease in photocatalytic activity because it leads to the active sites located on the surface of nanoparticles are not enough to remove high amounts of tetracycline and its intermediates. As shown in fig.8 also, a large amount of catalyst increases the active sites but prevents the absorption of UV light. Unlike TiO_2, GO/ TiO_2 and GO/ TiO_2/Cu has better performance in the visible light range. The absorption of GO/ TiO_2 is slightly better than GO/ TiO_2/Cu due to its darker color. The scavenger experiment investigated the effect of active species on the photocatalytic removal of tetracycline hydrochloride. Isopropanol (IPA),

benzoquinone (BQ), and EDTA-2Na were used to investigate the effects of ●OH radicals, ●O_2 –, and photogenerated h+ species on the photocatalytic removal of tetracycline hydrochloride antibiotic, respectively. The order of effect of active species was observed as $\bullet O_2^-$ > h^+ > •OH for both TiO_2/GO and Cu-TiO_2/GO photocatalysts. For TiO_2/GO photocatalyst, the role of •OH was 62.6% removal rate and for Cu- TiO_2/GO photocatalyst, the removal rate was 10.8%, which is due to the reactions taking place in the surface phase and the stronger adsorption of tetracycline on the catalyst surface. However, due to the higher production of $\bullet O_2^-$ and h^+ in the Cu- TiO_2/GO photocatalyst compared to TiO_2/GO, the removal rate of tetracycline hydrochloride is higher with the Cu- TiO_2/GO photocatalyst than with TiO_2/GO. The removal rate in UV light with a 300 W mercury lamp (λ > 400 nm)and 20 mg/L antibiotic for pure TiO_2 photocatalyst and GO/ TiO_2 photocatalyst in 60 minutes is about 92%, while this rate for TiO_2/Cu and GO/ TiO_2/Cu photocatalyst are about 95% and 99.8%, respectively. The increase removal amount with the addition of GO is about 4.8% compared to the TiO_2/Cu photocatalyst. The amount of energy consumed per gram of antibiotic removed for the Cu-TiO_2/GO photocatalyst in the optimal state is 450.9 kWh/g, which is a high amount of energy and requires a suitable reactor design to minimize energy consumption. The apparent rate constant normalized to the weight of the photocatalyst for the GO/ TiO_2/Cu photocatalyst is 0.185 min-1.g-1.L[119].

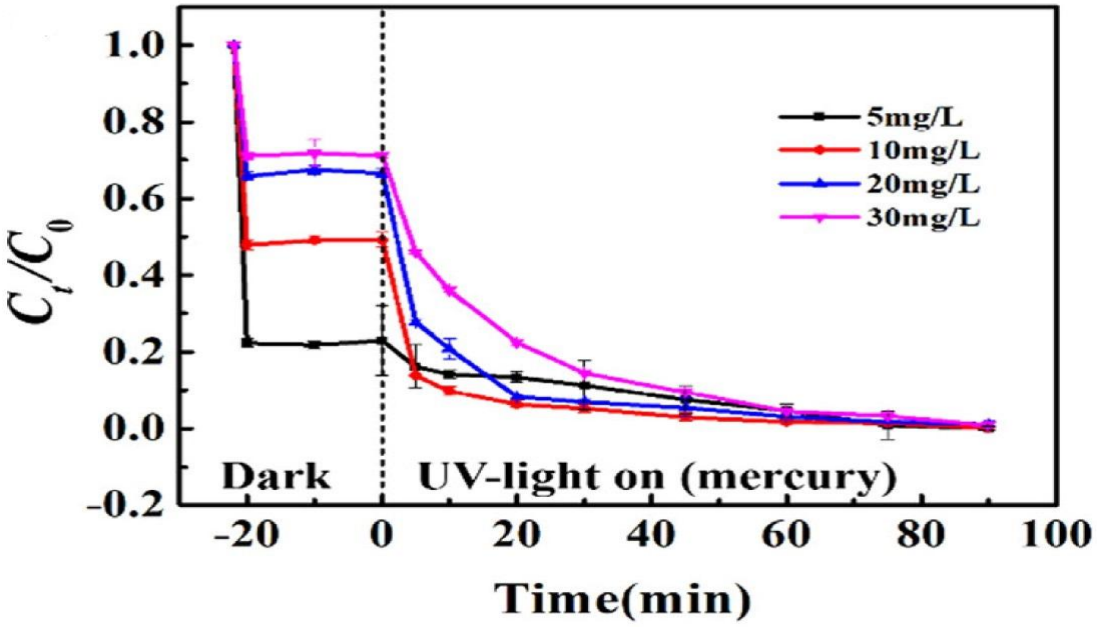

Fig.7- Photocatalytic removal of tetracycline at different initial concentrations of tetracycline in the dark and in the presence of UV light [119].

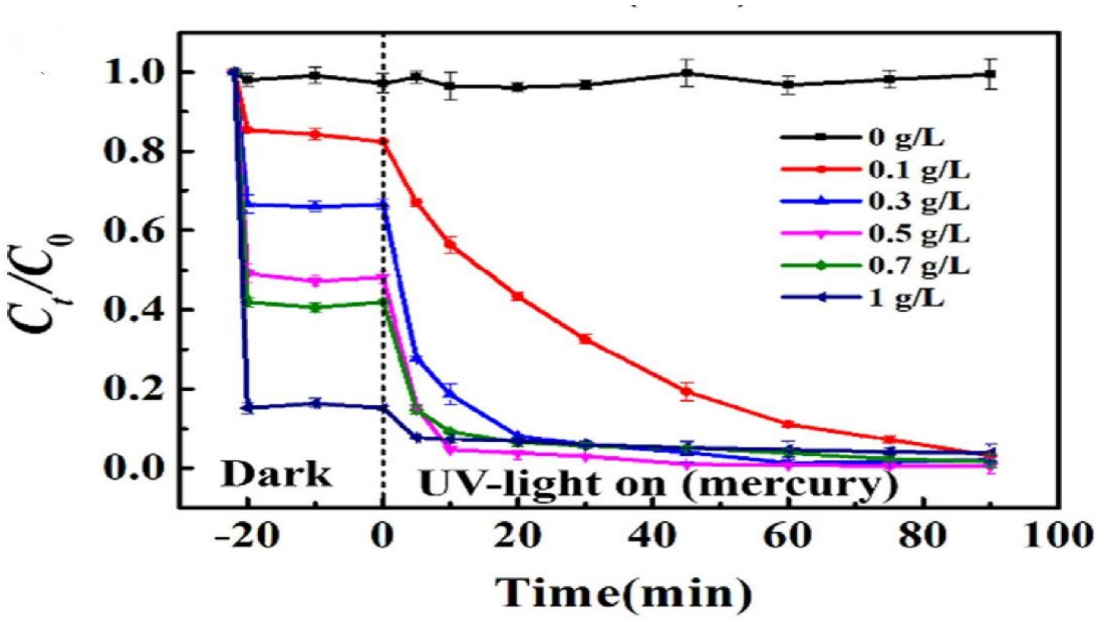

Fig.8- Photocatalytic removal of tetracycline at different catalytic dosages in the dark and in the presence of UV light [119].

Guo et al. [120] used a graphene-based TiO_2&Ag photocatalyst to remove chloramphenicol. TiO_2 has very good electrochemical and photocatalytic properties. However, due to its high band gap and fast electron-hole recombination, it is limited. Doping TiO_2 with silver leads to changes in the surface properties by increasing the produced electron-hole separation and leading to a broadening of the wavelength response. Doping with graphene or graphene oxide can improve the charge separation in TiO_2. Graphene oxide is a new nanomaterial that has features such as high specific surface area, high electronic properties and fast charge transfer. Graphene oxide as a support deposit TiO_2 and silver on its surface. The role of GO as a substrate for the distribution of silver and TiO_2 nanoparticles, which increases the contact of bacteria with nanoparticles and consequently increases the photocatalytic effect. The aim is to investigate the effect of the photocatalyst on ARB and ARGs, and the presence of the antibiotic Chloramphenicol is actually due to the effect of the presence of the antibiotic in the solution to investigate the efficiency of the photocatalyst in killing ARB and transferring ARGs. The

Survival rate of antibiotic-resistant bacteria for 5 mg/L chloramphenicol with light source (500W Xenon lamp) with 50 mg/L TiO_2/Ag/GO photocatalyst in 60 min is 86.2%. The article reports the Survival rate of antibiotic-resistant bacteria the TiO_2/Ag photocatalyst for comparison, but graphene oxide in the TiO_2/Ag photocatalyst structure is effective in the Survival rate of antibiotic-resistant bacteria [120]. Kumar et al. [121] used Carbon quantum dots/RGO/S@C_3N_4 /B@C_3N_4 (CRSB) photocatalyst for chloramphenicol removal. The S@C_3N_4 /B@C_3N_4(SB) junction structure uses the self-assembly method. The carbon material acts as an electron acceptor and generates current through electron-hole re-reduction. It is used in the visible region; however, the limitations of activated carbon nitride graphite, insufficient sunlight, as well as the replacement of carriers lead to the weakening of catalytic activities. Therefore, to solve it, metals and non-metals, and other doping compounds will be. The use of RGO is due to its high electron mobility, conductivity, and stability, as well as the creation of active sites for pollutant absorption, and acts as a catalyst support and electron mediator. Quantum carbon has high conversion characteristics, and the simulation of visible light activity with electron transfer becomes photo-induced electron transfer. It also expands the absorption spectrum. The use of S and B as electron donors and acceptors is to reduce electron-hole recombination. The specific surface area of the graphene carbon nitride photocatalyst is 44.2 m^2/g, while it is 124.2m^2/g for the doped photocatalyst. Also, the size and volume of graphene carbon nitride are less than those of the doped photocatalyst, which leads to an increase in active sites and better absorption of pollutants, resulting in photocatalytic activity. The band gap of carbon nitride graphene is 2.7ev, while it is 2.05ev for the doped photocatalyst. The good performance of the photocatalyst is due to the high absorption and specific surface area and increased activity in the visible light range of RGO, reducing the electron-hole recombination and increasing the charge transfer of RGO and CQDs. The addition of RGO to the B@CN and S@CN structures leads to an increase in the specific surface area, which leads to greater absorption of chloramphenicol for the photocatalytic reaction. RGO and CQDs are effective in electron transport because they act as electron sinks, electron sources in visible light, and transfer agents. Although the specific surface area increases with the addition of RGO, excessive addition hinders the photoabsorption of the junction and the rate decreases sharply. RGO and CQDs lead to an increase in

electron flow and a decrease in electron-hole recombination. The Fermi level of RGO at -0.08 eV helps it to act as an electron well. The generated electrons may accumulate on the RGO surface, in addition to migrating to the CB surfaces. As a result, more reactive oxygen species are produced. In fact, RGO acts as an electron well/mediator due to its high electron conductivity and mobility in its planar structure - reduced recombination and easy electron diffusion. PZC for the doped photocatalyst is 6.5 and the maximum amount of removal occurs at pH=6-7. In completely acidic and basic conditions, the pollutant and the catalyst have the same charge and electrostatic repulsion forces lead to low catalyst activity. In addition, this highly acidic property leads to the dissolution of the catalyst in the acid. Also, in completely alkaline conditions, the hydroxyl ion competes with the drug for absorption. The scavenger experiment investigated the effect of active species on the photocatalytic removal of chloramphenicol. The basis of the role of electrons, holes, and active oxygen species generated by irradiation, namely hydroxyl radical (●OH), superoxide radical anion (●O_2 −). Isopropanol, benzoquinone (BQ), and EDTA were used to investigate the effect of ●OH radicals, ●O_2–, and photogenerated h+ species on the photocatalytic removal of chloramphenicol antibiotic, respectively. The removal rate of chloramphenicol was significantly reduced by the addition of BQ, indicating that ●O_2– species plays an important role in the removal of chloramphenicol antibiotic. Electron scavenging also leads to a decrease in chloramphenicol degradation because they play an important role in the production of superoxide radicals. However, hydroxyl radicals are still active in the degradation. Therefore, further investigation is needed by ESR measurements and thermodynamic feasibility of radical formation, possible charge flow and junction properties. The removal rates of chloramphenicol at a concentration of 10 mg/L in 90 min in visible light radiation with 300 W Xe lamp (with 450mW.cm^{-2} intensity), 0.3g/L photocatalyst for the single photocatalyst g−C_3N_4, B@g− C_3N_4, S@g− C_3N_4 and CRSB(40% S@g− C_3N_4 in SB+8%RGO) are 44.4, 54.1, 60.3 and 99.1, respectively in visible light for solar light the removal rate of CRSB is 92.4 in 120 min, so adding 8% RGO to the photocatalyst helped increase the adsorption rate by 45% and 38.8%, respectively, compared to the B@g−C_3N_4 and S@g−C_3N_4 photocatalysts. The reason for the reduced removal rate in the presence of sunlight is due to the lower intensity of sunlight and its broader

spectrum. The apparent rate constant normalized to the weight of the photocatalyst for the CRSB photocatalyst is 0.27 min-1.g-1.L in visible light and 0.1707 min-1.g-1.L in solar light in 60 min [121]. Wang et al. [122] used Fe-Ag_3VO_4/GO photocatalyst to remove the antibiotic chloramphenicol. The synthesis method is precipitation method. Ag_3VO_4 has extensive properties in photocatalysts, medicine, lithium batteries and sensors. But the limitation of this photocatalyst is its fast electron-hole recombination. By doping with Go, the electron from the Ag_3VO_4 the valence band is excited by visible light and goes to Go, and the structure of the Go ring absorbs the chloramphenicol molecule well. Also, the precursor of iron, which is $FeCl_3$, reacts with chlorine ion and superoxide ion. and chlorine radical is created, which chlorine radical or ClO^- through electrophilic substitution reactions lead to improvement of the elimination process The ring structure of GO leads to the effective adsorption of chloramphenicol molecules on the surface of the Fe-Ag_3VO_4 photocatalyst. The removal rate of chloramphenicol with an initial concentration of 20 mg/L and 300W Xenon lamp covered with a UV filter (λ>420 nm) in time of 60 minutes is about 70% for Fe-Ag_3VO_4 /Go, while it is less than this value for the Ag_3VO_4 only photocatalyst[122]. Sodeinde et al. [123] used a reduced graphene oxide-zinc oxide nanocomposite (rGO-ZnO) photocatalyst for the removal of chloramphenicol. The synthesis method is the Solvothermal method .The photocatalytic interaction of 12.5g/L rGO-ZnO nanocomposite with UV radiation using a UVP Compact lamp (4 W, 230 V, λ = 254 nm) for 40 minutes. As shown in Fig 9, the presence of H_2O_2 leads to electron transfer from the valence band to the conduction band in the ZnO nanocomposite semiconductor and electron-hole generation. The reduced graphene oxide facilitates the reduction of the initial band gap and also improves the rapid charge transfer and free hydroxyl radical generation due to the interaction of OH- ions with the positive holes valence band of the ZnO photocatalyst. The conduction band electron reacts with O_2 and forms a superoxide radical. The superoxide radical reacts with water and produces the hydroxyl radical, which reacts with chloramphenicol and produces water, carbon dioxide, and nitrate and nitrite as byproducts. The addition of graphene oxide to the ZnO photocatalyst leads to a significant increase in the photodegradation process of chloramphenicol, reducing the band gap and preventing

electron-hole recombination and surface photo corrosion. Graphene oxide leads to an increase in the specific surface area of the photocatalyst to 722 m^2/g, which leads to the adsorption of more molecules of chloramphenicol and is effective in the removal rate. The removal rate for 1000mg/L chloramphenicol with the ZnO photocatalyst alone in 100 minutes is 56%, but for the rGO-ZnO photocatalyst, it is 90.8%. The removal rate increased by 34.8% with the presence of rGO. Also, for real livestock wastewater, it is 90.2%. Fig.9 shows the mechanism of antibiotic removal. The apparent rate constant of the rGO-ZnO photocatalyst is $K_{app} = 0.002 min^{-1}.g^{-1}.L$ [123].

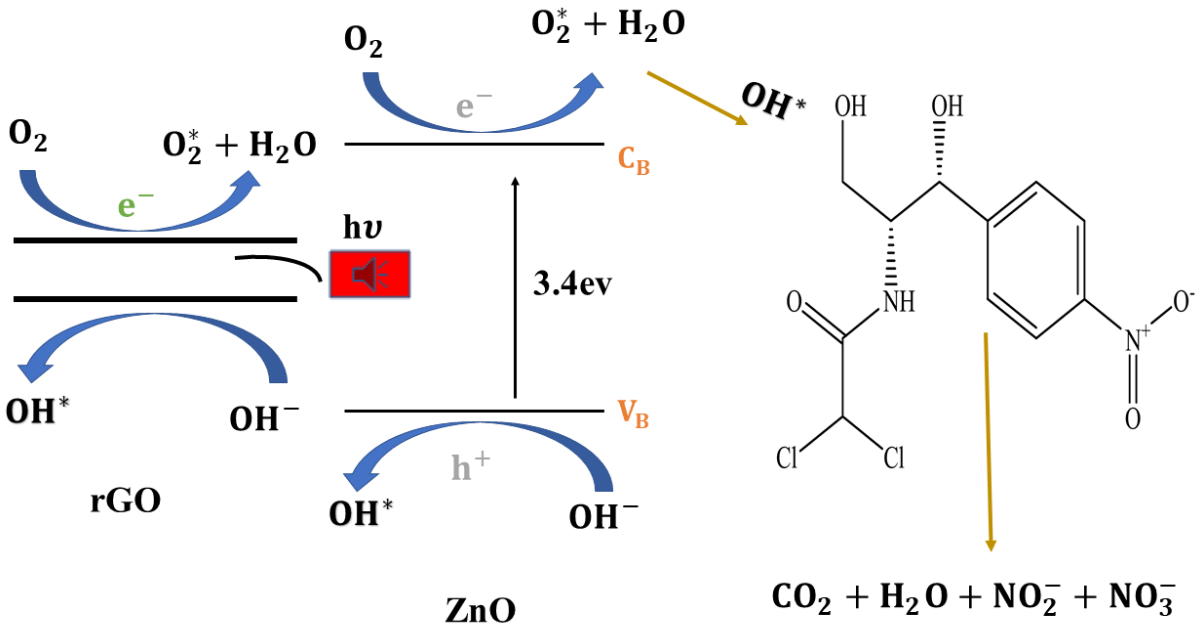

Fig.9-mechanism of photocatalytic degradation of chloramphenicol with rGO-ZnO nanocomposite and converted into simpler molecules [124].

4-1-1-EVALUATING THE CLAIM OF RGO AS AN ELECTRON SINK

Separation of charge carriers and electron-hole currents is essential in investigating the performance of photocatalytic processes. This can be investigated using Nyquist plots obtained from electrochemical impedance spectroscopy (EIS). As current passes through the photocatalyst, its resistance to the passage

of current is measured, which is called impedance, and if the electron transfer in the photocatalyst is high, the impedance decreases. As shown in fig10(a), an increase/decrease or change in electrochemical impedance indicates that there are changes in the properties of the photocatalyst interface. The arc radius represents the electron resistance. Doping S or B helps to reduce the interface resistance of the photocatalyst and leads to an increase in the electron transfer improvement. The radius for the reduced graphene oxide layers modified S@g-C_3N_4/B@ g-C_3N_4 structure has the lowest value, indicating the lowest resistance and the highest electron transfer compared to the single and S@g-C_3N_4/B@ g-C_3N_4 photocatalysts. In the time-current diagrams, the photocatalysts S@g-$C_3N_4$and B@ g-C_3N_4 show a weak photocurrent intensity due to the high electron-hole recombination, while for the reduced graphene oxide layers modified S@g-C_3N_4/B@ g-C_3N_4 photocatalyst, the photocurrent is high due to the presence of CQDs and RGO. As shown in fig10(b), also, the photoluminescence (PL) intensity for the g-C_3N_4 photocatalyst is the highest value, and respectively, g-C_3N_4 > S@ g-C_3N_4 > B@ g-C_3N_4 > SB- 40 > CRSB. The impurity levels created by S and B doping act as electron-hole separation centers. Electrons are transferred from the conduction band of B@ g-C_3N_4 to CQD and holes are transferred from the valence band of S@ g-C_3N_4, thus, the photoluminescence intensity for CRSB decreases. The electron-hole recombination for CRSB is the lowest and is also confirmed by EIS[125]. The PL spectra of ZnO, $BiVO_4$ and rGO-$BiVO_4$-ZnO show that the intensity of ZnO and $BiVO_4$ photocatalysts is higher compared to rGO-$BiVO_4$-ZnO photocatalyst. The lower intensity of rGO-$BiVO_4$-ZnO photocatalyst indicates the reduction of electron-hole recombination with the addition of rGO[115].

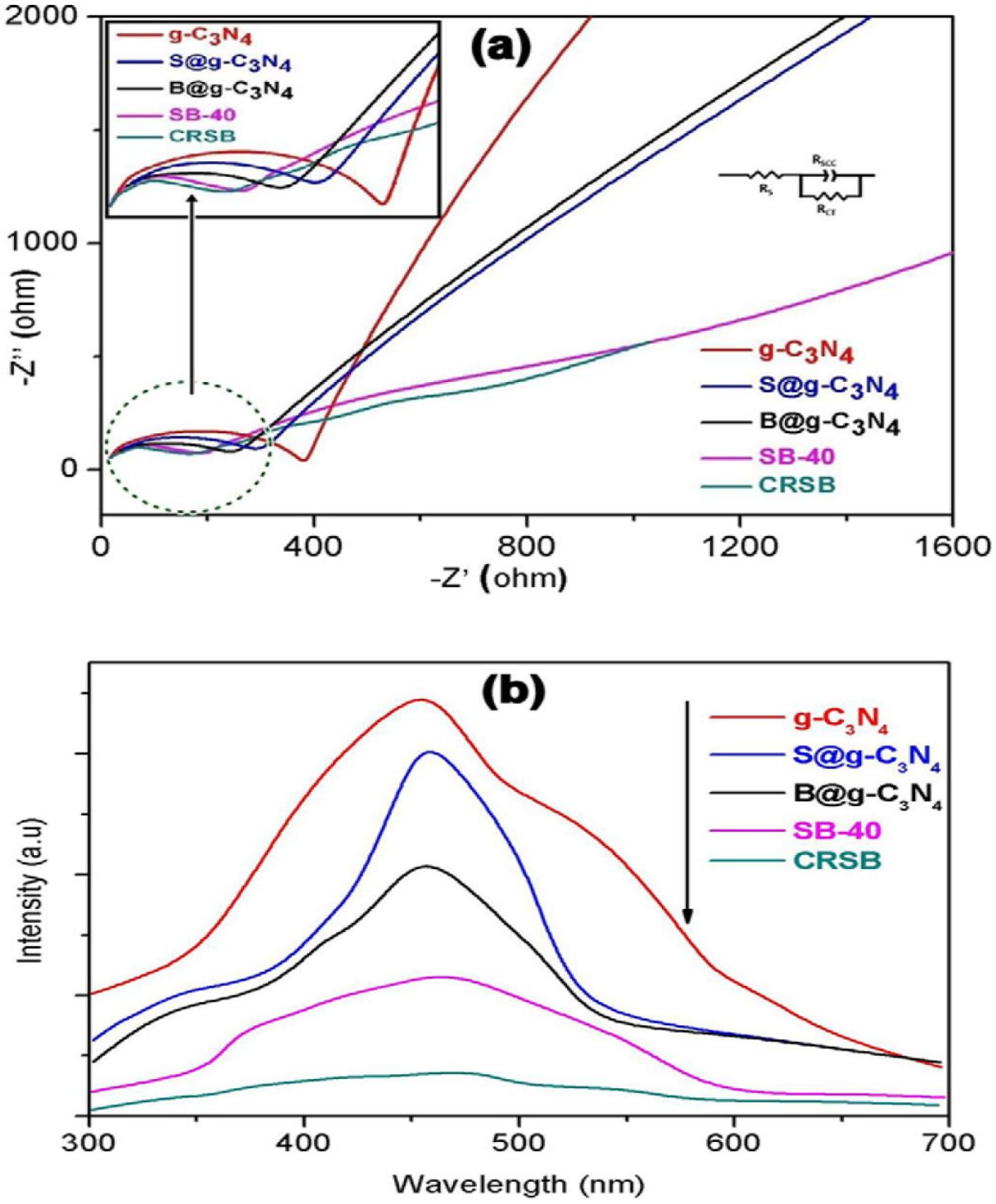

Fig.10- a) EIS Nyquist plots. b) Photoluminescence spectra for different photocatalysts[125].

4-1-2-COMPARATIVE EVALUATION OF GRAPHENE CONTRIBUTION IN PHOTOCATALYTIC SYSTEMS

Although graphene-based materials are frequently credited with exceptional photocatalytic enhancement, a closer comparison between systems with and without graphene reveals a more nuanced picture. Several studies in this section provide a clear basis for evaluating how much graphene actually contributes, and under what conditions its effect becomes decisive.

A representative example is the ternary rGO–$BiVO_4$–ZnO composite, in which the photocatalytic activity rises from 63.3% for ZnO to 80.3% for $BiVO_4$–ZnO, and ultimately to 98.4% when rGO is incorporated [115]. The roughly 18% improvement introduced by rGO is significant, yet the stepwise increase also shows that proper semiconductor coupling already contributes substantially to charge separation before graphene is added. In contrast, the Cu–TiO_2/GO system displays a more modest enhancement: TiO_2 removes 92%, Cu–TiO_2 removes 95%, and Cu–TiO_2/GO reaches 99.8% [119]. Here graphene provides only a small incremental benefit, suggesting that when the semiconductor junction is already efficient, GO's electron-migration function may play a supporting rather than dominant role.

Other reports demonstrate situations where graphene exerts a much stronger influence. The rGO–ZnO composite achieves 90.8% removal, compared to 56% for bare ZnO [124], reflecting the combined effect of improved charge transport and higher surface affinity. A similar trend appears in the CRSB composite, which attains 99.1% degradation, sharply outperforming pristine g-C_3N_4 (44.4%) and its doped analogues (54.1% and 60.3%) [125]. These large jumps indicate systems in which graphene not only facilitates electron extraction but also mitigates structural limitations of the host photocatalyst. Graphene can also function primarily as a dispersion scaffold, as seen in the Ag– TiO_2/GO system, where improved nanoparticle distribution and surface contact contribute more than electronic effects alone [120].

Taken together, these comparisons demonstrate that the contribution of graphene is highly system-dependent. Its impact ranges from marginal (a few percent) to transformative (over 30%), depending on factors such as semiconductor band alignment, intrinsic recombination rate, defect

density, and graphene–particle interfacial contact. Thus, while graphene is unquestionably valuable in many antibiotic-degradation photocatalysts, its role is not universal or uniformly dominant. Critical assessment of each composite system remains essential to avoid overstating graphene's mechanistic contribution.

Table3-Removal of antibiotics drug with different graphene photocatalysts.

Photocatalyst	**Antibiotic**	**Targeted pollutant concentration**	**Irradiation time**	**Optimized photocatalyst condition**	**Degradation**	**Reference**
RGO-ZnO-$BiVO_4$	ciprofloxacin	10mg/L	60 min	Visible light(($\lambda < 400$ nm) tungsten lamp (150 mW/ cm−2) hydrothermal method 0.3g/L catalyst Optimum pH is 7 $K_{app} = 0.2143\ min^{-1}.g^{-1}.L$	98.4%	[115]
Cu-TiO_2 /GO	tetracycline	20mg	90min	UV light with a 300 W mercury lamp ($\lambda > 400$ nm) TiO_2 /GO Synthesized by hydrothermal method, Cu-TiO_2 /GO	99.8%	[119]

				Synthesized by impregnation methods 0.2g/L catalyst is optimum PH=5 is optimum $K_{app} = 0.185 min^{-1}.g^{-1}.L$ 84.5% TOC in 360 min		
TiO_2/Ag/GO	chloramphenicol	5mg/L	60min	light source (500W Xenon lamp) 50 mg/L TiO_2/Ag/GO pH=7	86.2%	[126]
CQD//RGO/S@ C_3N_4/B@C_3N_4	Chloramphenicol	10mg/L	90min-visible light	visible and solar 300 W Xe lamp (with 450mW.cm^{-2} intensity) Self-assembly method 0.3g/L catalyst 8 % RGO is optimum $K_{app} =$ in $0.27 min^{-1}.g^{-1}.L$ 60 min in distilled water 84% TOC in 360min	99.1%	[125]

	chloramphenicol		120min Natural solar light	$K_{app} = 0.1707 min^{-1}.g^{-1}.L$ in 60 min in distilled water 70% TOC in 360 min	92.4%	
			90min visible light	$K_{app} = 0.207 min^{-1}.g^{-1}.L$ in 60 min in municipal tap water	82%	
Fe-Ag_3VO_4/Go	chloramphenicol	20mg/L	60min	Visible light 300W Xenon lamp covered with a UV filter (λ>420 nm) Precipitation method	70%	[127]
rGO-ZnO nanocomposite	chloramphenicol	1000mg/L	100min	uv light UVP Compact lamp (4 W, 230 V, λ = 254 nm) for 40 minutes Solvothermal synthesis 12.5g/L rGO-ZnO $K_{app} = 0.002 min^{-1}.g^{-1}.L$ distilled water	90.8%	[124]
				veterinary effluent	90.2%	

5- SEMICONDUCTOR HETEROJUNCTION PHOTOCATALYSTS

Table 5 summarizes the optimal concentrations of different antibiotics with different photocatalytic heterojunction structures. An effective method to reduce electron-hole recombination in heterogeneous photocatalysis is to couple it with another semiconductor with a different band gap. A semiconductor coupled with another semiconductor with a different band gap is called a heterojunction[102,128]. In general, semiconductors with different band structures, which can lead to particular band alignment[129]. A heterojunction structure is a region where two semiconductors with the same crystal structure are in contact with each other[130]. The band edges of these two semiconductors do not align with each other, so a band offset is developed at the heterojunction interface[102]. Semiconductor heterojunctions with appropriate band edge positions lead to increased visible light absorption and efficient electron-hole separation[131].

5-1- INTERFACE ENGINEERING PRINCIPLES

The photocatalytic performance of semiconductor systems is strongly governed by how efficiently photo-generated carriers are managed at solid–solid and solid–liquid interfaces. Interfacial engineering therefore represents a central design lever, enabling simultaneous control over light harvesting, interfacial charge separation/migration and surface redox reactions. In the context of antibiotic degradation, recent work has demonstrated that augmenting light absorption, improving charge separation, and strengthening interface interactions are key, synergistic strategies to construct high-efficiency photocatalysts [44,47]. Conceptually, junction interfaces can be classified as homogeneous or heterogeneous. Homogeneous junction interfaces are formed within a single compound, typically by constructing phase or facet junctions; these architectures create internal migration pathways for electrons and holes without introducing a secondary phase [43,47]. In practice, however, the synthetic complexity and cost of well-defined homojunctions often limit their deployment, prompting substantial interest in heterogeneous junction interfaces [42,48]. Heterojunction architectures—including Schottky, plasmonic, Z-scheme, and p–n configurations—have been widely explored as interfacial engineering platforms [41,47]. In such hybrid nanocomposite

systems, intimate surface and interface contacts are deliberately created to accelerate the spatial separation and transport of photoinduced carriers. For example, efficient 2D/2D and 3D/2D configurations provide large, coherent interfacial areas coupled with well-matched band structures, which together yield effective inter-surface contact, higher electron–hole separation, and improved overall photo absorption [41,42,47]. Representative systems such as $Bi_4Ti_3O_{12}$ /I-BiOCl and CdS-based composites anchored on carbonaceous hosts or oxide scaffolds clearly show that perfect or strong interface interactions enhance the generation and transfer of photo-excited carriers, reduce recombination, and translate into higher degradation rates for antibiotics like ciprofloxacin and tetracycline [42,48]. Similar conclusions have been drawn for direct Z-scheme constructions—for instance $CuInS_2/Bi_2WO_6$—where an intimate interface contact not only stabilizes the junction but also enforces a Z-scheme charge-transfer pathway. This configuration preserves strong redox potentials on the respective components, leading to markedly improved separation of photo-generated electrons and holes and superior photocatalytic activity in Fenton-assisted antibiotic degradation [42,43]. Even in earlier heterogeneous systems such as anatase TiO_2 /Co_3O_4 nanocomposites, the formation of a heterojunction has been shown to induce photon-driven oxidative pathways for antibiotic removal, underscoring the generality of the interface-engineering concept [41–43].

Beyond geometric contact, chemical bonding at the interface is crucial for dictating carrier dynamics. Covalent or strongly chemisorbed connections between different components can provide energetically favorable channels for directional charge transfer. An illustrative example is the Bi nanodots/Bi_3NbO_7 system, where covalent interactions between Bi nanodots and the Bi–O layers of Bi_3NbO_7 nanosheets markedly accelerate charge separation and interfacial carrier transfer [41,42,132]. The resulting improvement in interfacial kinetics enhances the activation of dissolved molecular oxygen to reactive oxygen species (ROS), especially superoxide radicals ($O_2^{\cdot -}$) and singlet oxygen ($^1O_2$), which in turn significantly boosts photocatalytic degradation efficiency [43,44,47]. Similar “strong interface interaction” effects have been reported for CdS/SnO_2 and CdS/carbon composites, where lattice

mismatch or intimate anchoring improves interfacial contact, speeds up charge migration, and suppresses radiative and non-radiative recombination pathways [42,43,133].

Interfacial performance is further tunable through defect and dopant engineering at or near the junction. Defects such as vacancies and heteroatom dopants play dual roles in photocatalysis, acting as trapping centers for carriers and simultaneously modulating the electronic structure and light-absorption profile [43,44,48]. Appropriately engineered shallow traps can extend carrier diffusion lengths and facilitate interfacial transfer, whereas deep traps tend to behave as recombination centers, reducing activity if not carefully controlled. Consequently, elaborated strategies based on vacancy construction and elemental doping have been proposed to exploit the beneficial aspects of defects while minimizing their detrimental effects [41,48]. Vacancies, in particular, are attractive because they alter the catalyst composition without introducing foreign species and allow fine tuning of the band structure by adjusting defect type and concentration; however, excessive vacancy densities can generate too many recombination centers, while insufficient densities are ineffective [41,42]. On the dopant side, the $Bi_4Ti_3O_{12}$ /I-BiOCl 2D/2D heterojunction provides a clear example where I^- doping, in conjunction with an efficient interfacial contact and band alignment, significantly improves visible-light absorption and accelerates inter-surface charge transfer, resulting in enhanced photocatalytic degradation of fluoroquinolone antibiotics [41,42,48]. Analogous concepts have been used in graphene-based systems, where controlled introduction of structural defects and heteroatom doping adjust conductivity and local electronic structure, thereby impacting the collection and transport of carriers at graphene/semiconductor interfaces [42–44].

Although interfacial charge-transfer behavior is often investigated through dedicated characterization techniques, trends in photocatalytic activity, reactive oxygen species (ROS) generation, and catalyst stability also provide meaningful insight into the effectiveness of charge separation and transport at engineered interfaces. In practice, interface-engineered photocatalysts are evaluated using a combination of steady-state and time-resolved methods that probe recombination dynamics and carrier

mobility, including photoluminescence (PL) quenching, transient photocurrent response, electrochemical impedance spectroscopy (EIS), and electron spin resonance (ESR) for identifying reactive radical species [41–43]. For example, the substantial enhancements in tetracycline and tetracycline-hydrochloride degradation achieved by 3D/2D heterostructures and direct Z-scheme architectures—together with their improved structural stability and reusability [41,42]—are typically correlated with reduced interfacial charge-transfer resistance, increased photocurrent response, and suppressed PL emission, all indicative of more efficient carrier separation and utilization at well-engineered interfaces. Moreover, even in systems governed partly by gas–liquid boundary-layer dynamics (e.g., sonolysis or UV–H_2O_2 advanced oxidation), the interplay between interfacial reaction zones and bulk-solution processes underscore the broader principle that optimizing interfacial transport and reaction environments is essential for maximizing radical-mediated pollutant degradation [42,43,47]. Overall, the integration of interface bonding design, defect/dopant engineering, and controlled interfacial charge-transfer pathways provide a coherent and unified framework for constructing next-generation photocatalysts with high efficiency and robustness toward antibiotic removal.

5-2- P-N-TYPE HETEROJUNCTION

The construction of a p-n heterojunction provides advantages, including high adsorption capacity, efficient collection and separation of charge carriers, longer life of the photogenerated electron-hole pair and fast charge transfer to the catalyst. As shown in fig.11, when n-type and p-type semiconductors are in contact, a space charge region is created at the interface due to the penetration of e^- and h^+, which leads to the production of a valence and conduction band that the e^- and h^+ move to the opposite direction. Light radiation in the p-n heterojunction with an energy higher than the Band gap of the catalyst causes rapid separation of photoelectron-hole pairs generated by the internal electric field. This electric field directs the electrons to the CB of the n-type semiconductor and h^+ to the VB of the p-type semiconductor[102].

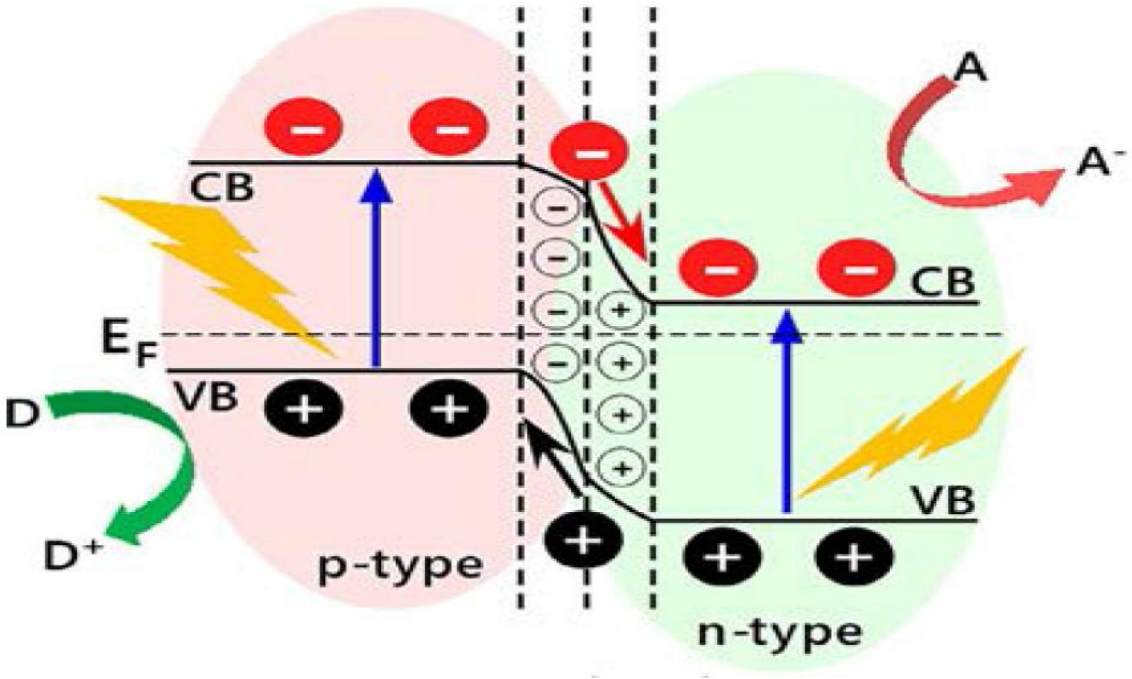

Fig.11- Schematic figure of p-n-type heterojunction and how oxidation and reduction occur and how charge is separated (adopted from [102]).

Cui Laia, et al. [134] used a CuS/$BiVO_4$ (0 4 0) binary p-n heterojunction photocatalyst for the removal of the antibiotic Ciprofloxacin. The synthesis method of $BiVO_4$ photocatalyst is a precipitation method and the synthesis method of CuS/$BiVO_4$ is probably wet chemical deposition depending on the type of synthesis. The Bi orbital (6S) is combined with the O orbital(2p), leading to a change in the valence band and, as a result, a reduction in the Band Gap. $BiVO_4$ has a limited Band Gap (2.4ev), so it has great absorption in the visible region. Fig.12 shows the mechanism of photocatalytic degradation of ciprofloxacin using CuS/$BiVO_4$ photocatalyst. The conduction band of the CuS photocatalyst (-0.32ev) is more negative than the conduction band of the $BiVO_4$ photocatalyst (+0.45ev). Therefore, the electron excited from the conduction band of CuS goes to $BiVO_4$ and the hole produced in the valence band of $BiVO_4$ goes to the valence band of CuS, as a result, it has led to the separation of production charge carriers. $BiVO_4$ The conduction band potential is more positive than O_2/O_2^- Reduction potential, also CuS valence band potential, is more negative than ($OH^{\cdot}/H_2O$), so the electron produced in the conduction band of $BiVO_4$ is not trapped to O_2^- radical and also hole. It is not able to react to produce hydroxide radicals from water. Therefore, the hole on the surface is used as the active species

for the removal process. The $CuS/BiVO_4$ heterojunction structure leads to an increase in the visible light range and an expansion of the optical band. The $CuS/BiVO_4$ heterojunction structure also has a pronounced red shift compared to $BiVO_4$. This structure leads to improved effective separation of generated charge carriers as well as more active sites and a large surface area. The removal rate in a 300W Xe lamp with a 420 nm cutoff filter, 1g/L photocatalyst, and 10mg/L ciprofloxacin for pure CuS photocatalyst is 8.1%. The removal rate with the pure $BiVO_4$ photocatalyst is 54.1%, while the removal rate for the $CuS/BiVO_4$ photocatalyst with a mass ratio of 7% reaches 86.7%. $K_{app} = 0.02151 min^{-1}.g^{-1}$. L is the apparent rate for the $CuS/BiVO_4$ photocatalyst with a mass ratio of 7%[135].

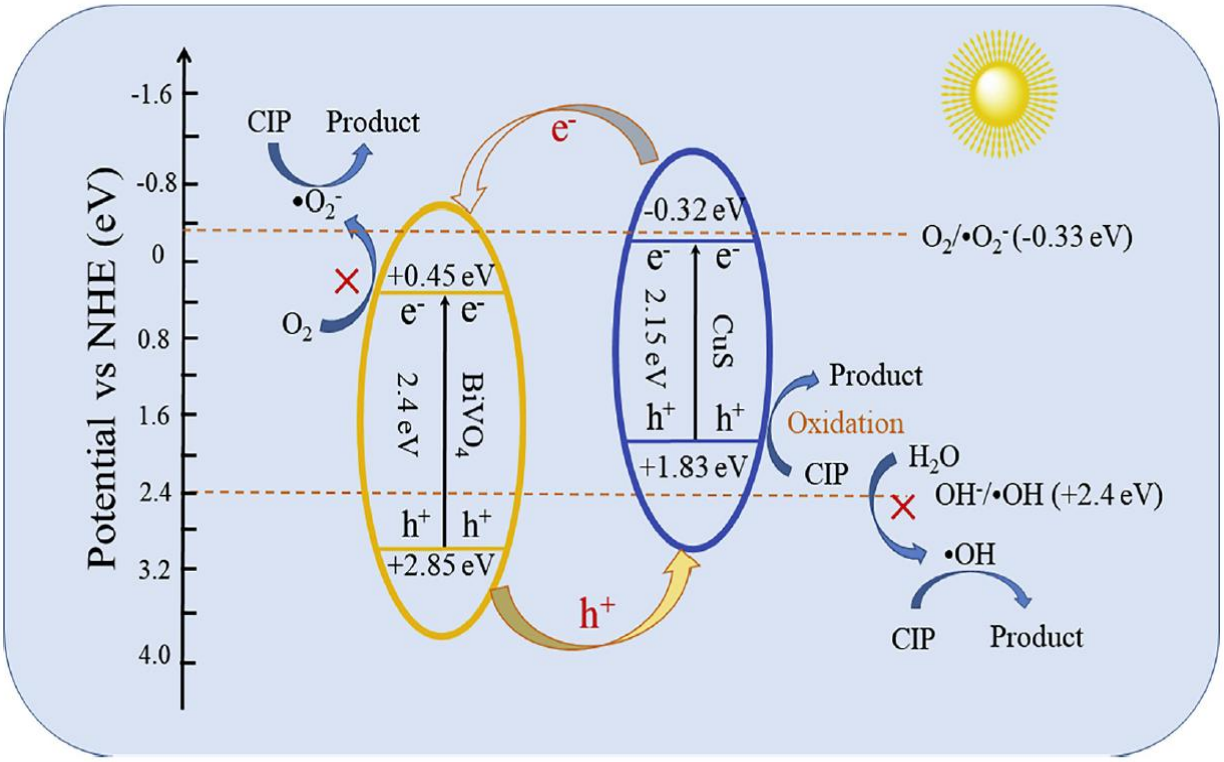

Fig.12- mechanism of photocatalytic degradation of Ciprofloxacin with $CuS/BiVO_4$ in the presence of sunlight and the production of reactive species [134].

Cui et al. [136] used $Cu_2O–TiO_2$ photocatalyst for the removal of tetracycline. The synthesis method of TiO_2–Pal photocatalyst is sol–gel, and the synthesis method of $Cu_2O–TiO_2$ –Pal photocatalyst is liquid-phase reduction. To overcome this problem, doping, depositing noble metals and combining semiconductors. Dispersing p-type semiconductors such as CuO and Co_3O_4 on the surface of an n-type semiconductor such as

TiO_2 leads to an increase in the electron-hole separation activity and an increase in the catalytic activity compared to the semiconductor only in the visible range. Palygorskite, a non-metallic mineral, has a high absorption capacity for organic compounds, is inexpensive, has stable physical and chemical properties, and is non-toxic. It is used as support here. In addition to increasing the antibiotic adsorption capacity, Pal in the Cu_2O-TiO_2-Pal photocatalyst structure is also effective in the degradation process. Palygorskite improves the light utilization in the photocatalyst due to its light-scattering property. The Cu_2O photocatalyst leads to a decrease in the band gap and an increase in the absorption of visible light[136]. Fig.13 shows the proposed mechanism for the removal of tetracycline under sunlight. When the photocatalyst is exposed to light, tetracycline is photocatalytically decomposed by the Cu_2O – TiO_2 p-n heterojunction, which leads to the transfer of electrons from the conduction band of Cu_2O to the conduction band of TiO_2 due to the fact that the conduction band of Cu_2O is more negative compared to TiO_2. In addition, the valence band of TiO_2 is more anodic than that of Cu_2O, which leads to hole transfer from the valence band of TiO_2 to the valence band of Cu_2O. Therefore, the electron-holes are effectively separated to minimize the energy, which leads to increased photocatalytic activity. The excited electrons from Cu_2O can generate OH radicals by absorbing O_2 molecules adsorbed on the photocatalyst surface. Also, the holes generated (h+) from TiO_2 lead to the generation of •OH radicals by reacting with OH^- and H_2O. •OH radicals play a key role in the removal of tetracycline. In this research, the removal rate under simulated solar light using a 500WXe lamp for tetracycline removal with 30mg/L and 1g/L photocatalyst in 240minutes in the presence of pure palygorskite is about 56%, in the presence of palygorskite doped with TiO_2, it is about 63%, while with palygorskite-supported Cu_2O–TiO_2 composite, the removal rate reaches 88.81%. The $K_{app} = 0.0129 min^{-1}.g^{-1}.L$ is apparent rate constant of the palygorskite-supported Cu_2O–TiO_2 photocatalyst[137].

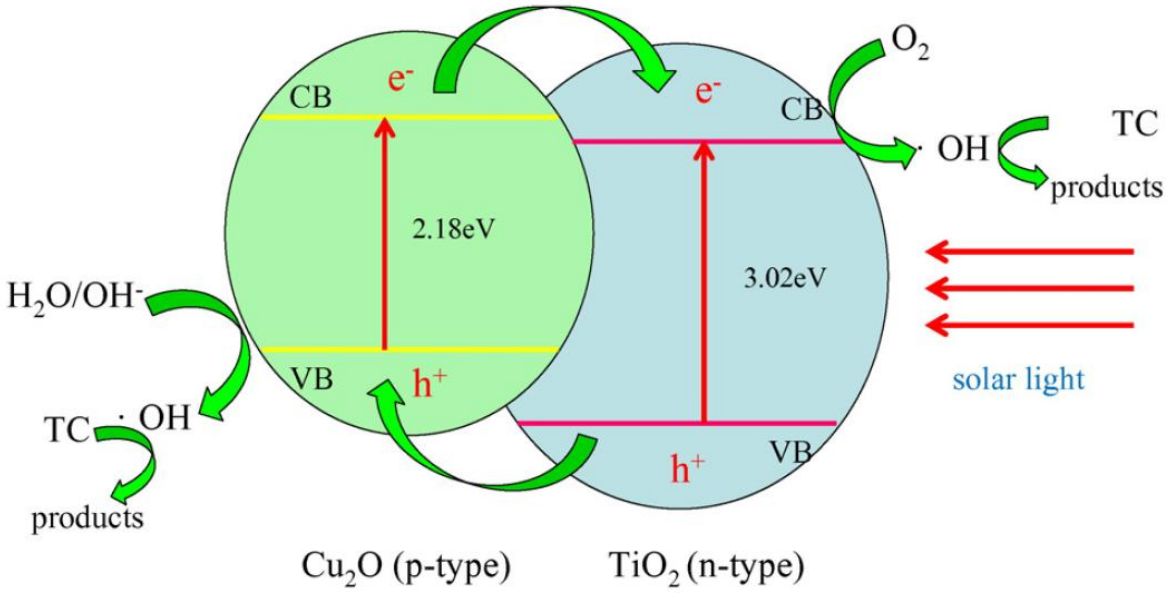

Fig.13- mechanism for the removal of tetracycline under sunlight with $Cu_2O - TiO_2$ in the presence of Solar Light[137].

Shen et al. [138] used $Cu_2O/Bi_2O_2CO_3$/PEO nanofibers photocatalyst to remove chloramphenicol. The synthesis method of $Cu_2O/Bi_2O_2CO_3$/PEO photocatalyst is the Chemical Precipitation Method, but the article does not directly mention it. $Bi_2O_2CO_3$ photocatalyst has a good performance in removing antibiotics, but its high electron-hole recombination, high band gap, and inactivation in the visible light range have led to its limitations. To overcome these limitations, Doping is the best solution for this problem. Cu_2O photocatalyst, which has a limited band gap, is activated in the visible light range. Despite the good photocatalytic activity of Cu_2O, it has limitations such as easy aggregation and is easy to scatter. To overcome these limitations, Cu_2O is combined with other polymers. Composite nanofibers have important applications, such as removing antibiotics. Due to the small diameter of the fibers, they have high flexibility for surface modification and restoration. Unlike the $Bi_2O_2CO_3$ photocatalyst, the $Cu_2O/Bi_2O_2CO_3$ photocatalyst has higher absorption in the visible range. As shown in fig.14, when $Bi_2O_2CO_3$ N-type photocatalyst forms a p-n heterojunction with $Bi_2O_2CO_3$ p-type photocatalyst, electrons are transferred from Cu_2O to $Bi_2O_2CO_3$ and holes from $Bi_2O_2CO_3$ to Cu_2O. Therefore, p-n heterojunction, the n-type photocatalyst is positively charged and Cu_2O p-type

photocatalyst has a negative charge. In the presence of this internal field, electron-hole recombination decreases due to the redistribution of electrons and holes on the surface. Chloramphenicol efficiently with radical O_2-, which is generated by electrons from the conduction band $Bi_2O_2CO_3$ by O_2**.** Adsorbed reacts. In addition, Cu_2O nanoparticles also shortened the distance of light charge transfer from the interior to the surface. Therefore, the photocatalytic activity increases. The removal rate of the antibiotic chloramphenicol with an initial concentration of 20 mg/L in 30 minutes using PEO is about 25% and 300 W Xe lamp equipped with a 420 nm cut off filter with visible light, for the $Bi_2O_2CO_3$/PEO photocatalyst the removal rate is about 84%, and for the PEO-based Cu_2O/ $Bi_2O_2CO_3$photocatalyst with a mass ratio of Cu_2O to $Bi_2O_2CO_3$ of 3%, it is about 98.2%. In this paper, instead of adding a pure amount of photocatalyst to the solution, a piece of membrane with a specific surface area was used, but since the mass or density of the membrane was not reported, it is not possible to calculate the apparent velocity normalized to the photocatalyst concentration; therefore, the $K_{app} = 0.1339 min^{-1}$ is first-order apparent velocity constant [138].

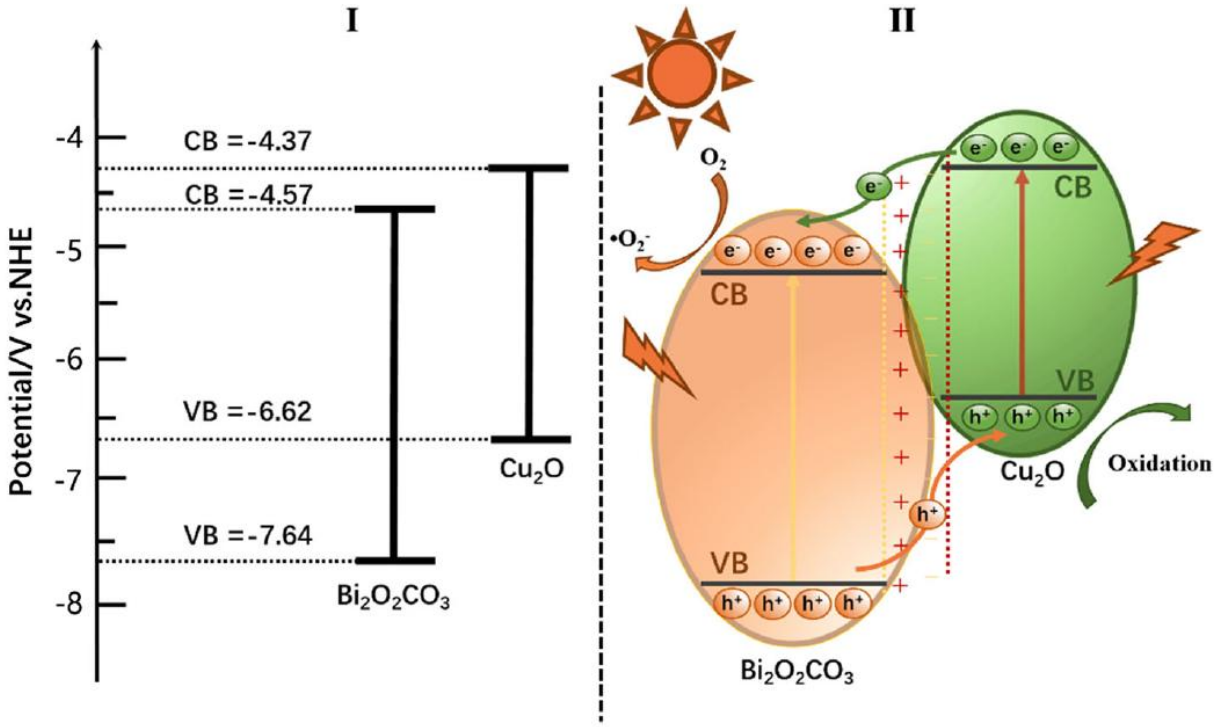

Fig.14-Schematic of Cu_2O/ $Bi_2O_2CO_3$ p–n heterojunctionand and the valence band and conduction band of the Cu_2O and $Bi_2O_2CO_3$photocatalysts[139].

Kim et al. [140] used ZnO/MoS_2 composites as photocatalysts to remove ciprofloxacin. The ZnO/MoS_2 photocatalyst synthesis method is hydrothermal. To overcome the limitation of ZnO, the best solution is to dope with another semiconductor to create composites or heterojunctions. MoS_2 under visible light is activated and its absorption capacity is improved in visible light. MoS_2 is a p-type semiconductor and ZnO is an n-type. The lowest photoluminescence intensity is related to the MZ-30 photoluminescence heterojunction structure, which has the lowest electron-hole recombination and the highest charge separation efficiency. When light is irradiated to MoS_2/ZnO, electron-hole pairs are generated. Due to the negative potential of ZnO, electrons generated in the CB band of ZnO are transferred to the CB band of MoS_2, which leads to electron-hole separation and charge facilitation. The electrons in the CB in MoS_2 react with oxygen to produce superoxide radicals, and the holes in the VB react with water molecules to produce hydroxyl radicals. The removal rate of the antibiotic ciprofloxacin with an initial concentration of 16.57mg/L, UV light with a 250 W metal halide lamp and 0.5g/L photocatalyst in 120 min with ZnO photocatalyst is 43%, while for 30 wt% MoS_2 it is 89% for 50 mg of photocatalyst, but for 200mg of photocatalyst it is 98.18%. For the ZnO/MoS_2 heterojunction photocatalyst, it results in a 46% increase compared to the ZnO photocatalyst. In Fig.15, the effect of the amount of catalyst on the rate constant of the photocatalytic reaction has been investigated in the values of 100 mg, 150 mg, 200 mg and 250 mg, and the rate constants were obtained as 0.022min^{-1}, as 0.025min^{-1}, as 0.032min^{-1} and as 0.026min^{-1} respectively. For different photocatalyst concentrations (100, 150, 200, and 250 mg), the removal percentage of ciprofloxacin was 91.12%, 94.06%, 96.18%, and 92.10%, respectively. As shown in Fig 15, by increasing the amount of catalyst from 100 mg to 150 mg, the rate constant increases. But by increasing the amount of catalyst from 200 mg to 250 mg, the rate constant has decreased, which is because the turbidity of the solution has increased at high amounts of catalyst, leading to the accumulation of particles and the effect of light

screening. The $K_{app} = 0.038 min^{-1}.g^{-1}.L$ is the apparent rate constant for the ZnO/MoS_2 photocatalyst with 30wt% MoS_2[140].

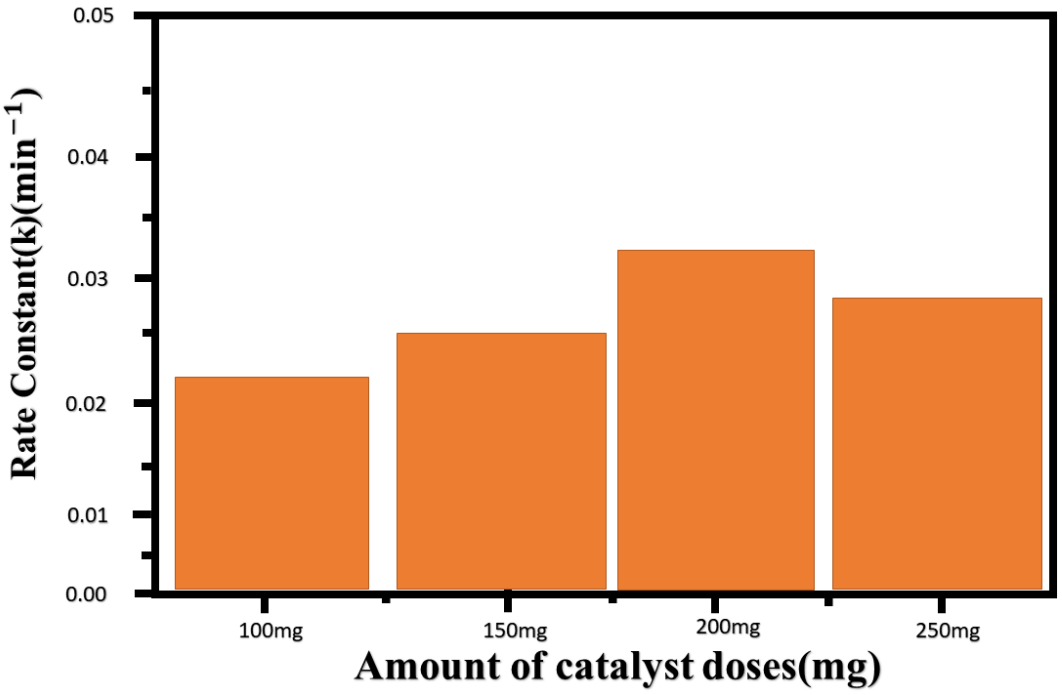

Fig.15- The effect of different amounts of photocatalyst on the apparent first-order rate constant of the reaction[141].

Qiua et al. [142] used ZnO-Ag_2O/porousg-C_3N_4composite for the removal of ciprofloxacin. The synthesis method of ZnO-Ag_2O/porous g-C_3N_4 photocatalyst is the calcination and hydrothermal method. The use of silver and silver oxide is considered due to their high solubility, larger ionic particle size, and minimal energy orbital. Ag_2O is used to overcome the large band gap of ZnO due to its limited band gap (1.3ev). To overcome the fast electron-hole recombination, g-C_3N_4 is used, which has excellent photocatalytic activity in the sunlight range with a band gap of 2.7ev and leads to separation and improved charge transfer and thus increases photocatalytic activity. The hole produced in the valence band of ZnO is easily transferred to the valence band of Ag_2O, but the electron produced in the conduction band of ZnO is due to its negative potential compared to Ag_2O is hardly transferred to the conduction band of Ag_2O. When the Ag_2O /ZnO/ g-

C_3N_4photocatalyst is activated in the visible light range, the electrons produced from the conduction band of Ag_2O is transferred to the conduction band of g-C_3N_4 and then to ZnO. As a result, the trapped oxygen becomes the radical anion superoxide produced and prevents electron-hole recombination. The hole produced from the valence band of ZnO to the valence band of and then to the valence band of Ag_2O Ciprofloxacin. The electron-hole recombination is inhibited by the interface between the Ag_2O and ZnO phases. The band gaps of ZnO, ZnO/Ag_2O and ZnO-Ag_2O/p-g-C_3N_4 are about 3.35, 2.83 and 2.60 eV, respectively, which leads to improved light absorption. The excited electrons in the zinc cations migrate to oxygen atoms and finally to C_3N_4, forming ZnO-pg$-C_3N_4$, which can lead to the improvement of ZnO excitation and consequently reduce the required energy. The low intensity of the ZnO-Ag_2O/pg-C_3N_4 photocatalyst in photoluminescence due to the combination of semiconductors indicates a higher separation rate of photoinduced charge carriers. The electrons generated in the conduction band of Ag_2O are transferred to the porous g-C_3N_4 sheets and finally to ZnO, producing superoxide radical anions ($\bullet O_2^-$) as the electrons are trapped by O_2. These events lead to the reduction of electron-hole recombination and consequently produce more •OH and $\bullet O_2^-$, which efficiently decompose organic pollutants because they are strong oxidants. Ciprofloxacin removal rate in 48 minutes and with an initial concentration of 20 mg/L, visible light with a tungsten lamp equipped with an ultraviolet cut filter to provide visible light with ≥420 nm and 0.5g/L photocatalyst using ZnO, porous g-C_3N_4, Ag_2O, ZnO-Ag_2O and ZnO-Ag_2O / porous g-C_3N_4photocatalysts under visible light are 8.2, 25.4, 42.3, 69.4, and 97.4%, respectively. The $K_{app} = 0.114 min^{-1}. g^{-1}. L$ *is* apparent rate constant for the ZnO-Ag_2O / porous g-C_3N_4 photocatalyst[142].

5-3-NON P-N-TYPE HETEROJUNCTION

As shown in fig.16, if the conduction band and valence band of a semiconductor (narrow band gap) are respectively lower and higher than the conduction and valence bands of the other semiconductor (wider band gap), then it is called band offset type I (symmetric). In the case of band offset type II(staggered), both the conduction and the valence bands of a semiconductor are higher than the bands of another

semiconductor. There is another type of heterojunction in which there is no overlap between the band gaps of the two semiconductors, and therefore it is called a type III (broken) offset band. Among the three different types of heterojunctions, the type II interface is suitable for visible light photocatalysis because with light radiation the narrow band gap semiconductor will be excited in which the electron and hole is generated and the created electron easily migrates to the conduction band of the wide band gap semiconductor, resulting in effective charge separation[102,143]. One of the disadvantages of type-II heterojunctions is that the reduction and oxidation reactions are carried out on semiconductors with lower reduction and oxidation potentials, respectively, thus greatly suppressing their redox ability[129]. Electron-hole separation efficiency at p-n heterojunction photocatalysts due to synergy between the internal electric field and band alignment is faster than type II[129].

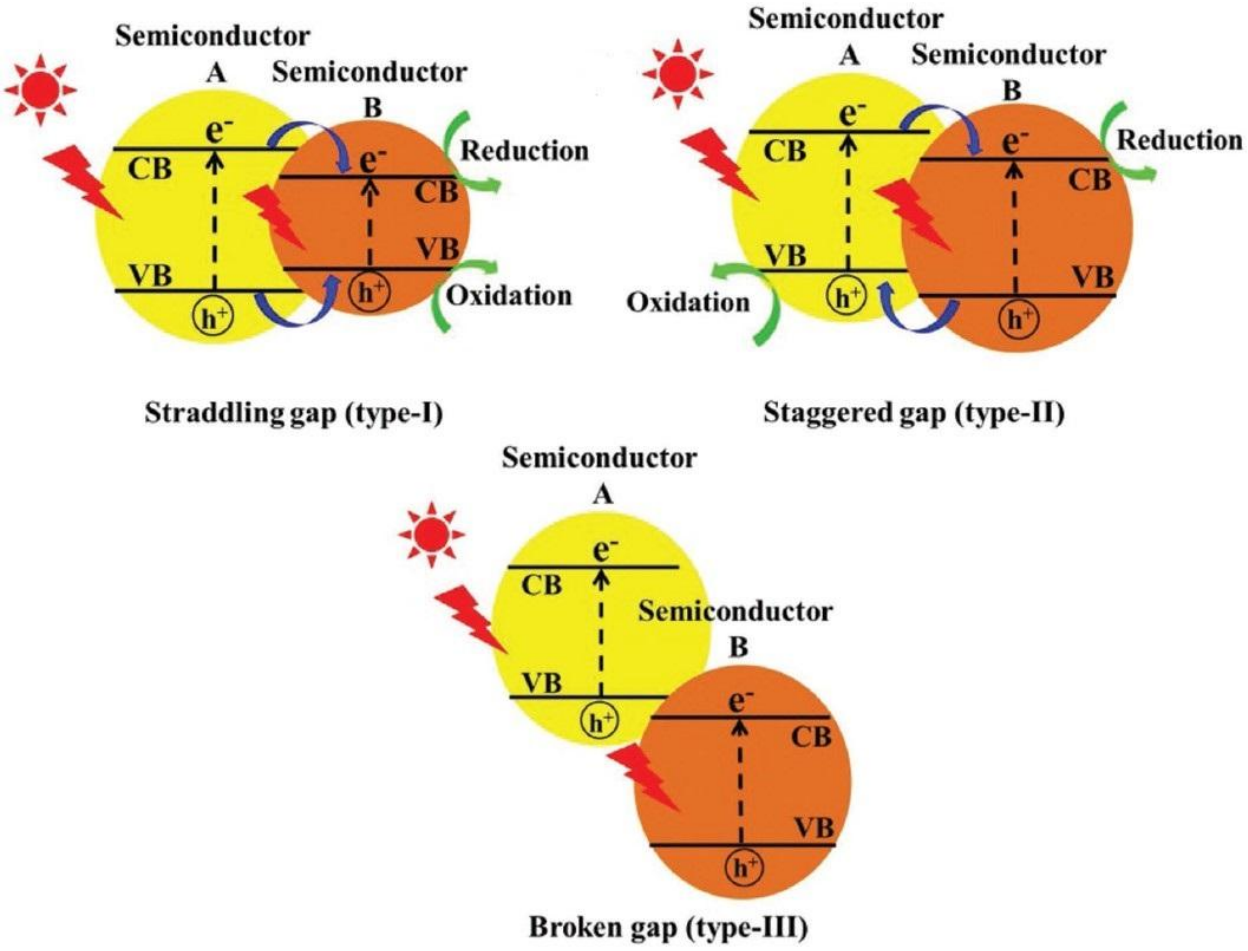

Fig.16- Schematic figure of non non-p-n-type heterojunction[129].

Mengelizadeh et al. [144] used a g-C_3N_4/Fe_2O_3 photocatalyst with a Type II heterojunction structure to remove ciprofloxacin. The synthesis method of g-C_3N_4photocatalyst is thermal condensation, and the synthesis method of g-C_3N_4/Fe_2O_3 nanocomposite photocatalyst is the calcination method. Considering the limitations of g-C_3N_4 photocatalyst, the solution is pairing with other semiconductors, including Fe_2O_3, which is an environmentally friendly photocatalyst that has attracted attention due to its abundance, high chemical stability, excellent electrical conductivity, and easy preparation. As shown in Fig17, both g-C_3N_4 and Fe_2O_3 photocatalysts are excited to produce electron-holes when the photocatalyst is irradiated by UV light. The valence band of Fe_2O_3 is more positive than g-C_3N_4 and the conduction band of g-C_3N_4 is more negative than Fe_2O_3, so the electrons in the conduction band of g-C_3N_4 are transferred to the conduction band of Fe_2O_3 to produce O_2•-. The hole in the valence band of Fe_2O_3 is transferred to the valence band of g-C_3N_4 to degrade ciprofloxacin and produce •OH. Finally, the electron-hole recombination decreases and the photolysis activity of ciprofloxacin adsorbed on the photocatalyst surface increases. In this research, hydroxyl radical and hole play an important role in the elimination of ciprofloxacin. Due to the reduction of electron-hole recombination, the generation of more reactive species, and the efficient coupling of two semiconductors, the energy consumption for photocatalyst activation is low. The removal rate of ciprofloxacin did not change after 5 repeated uses, so the stability of the g-C_3N_4/Fe_2O_3 photocatalyst is excellent .The removal rates for ciprofloxacin with an initial concentration of 25 mg/L and 60 min and 0.3g/L photocatalyst using UV alone with mercury lamp (photolysis), g-C_3N_4/Fe_2O_3 in the dark (absorption) and g-C_3N_4/Fe_2O_3 + UV (photocatalysis) are about 20%, about 69.35% and about 100%, respectively. The $K_{app} = 0.31 min^{-1}.g^{-1}.L$ is apparent rate constant for the g-C_3N_4/Fe_2O_3 photocatalyst[144].

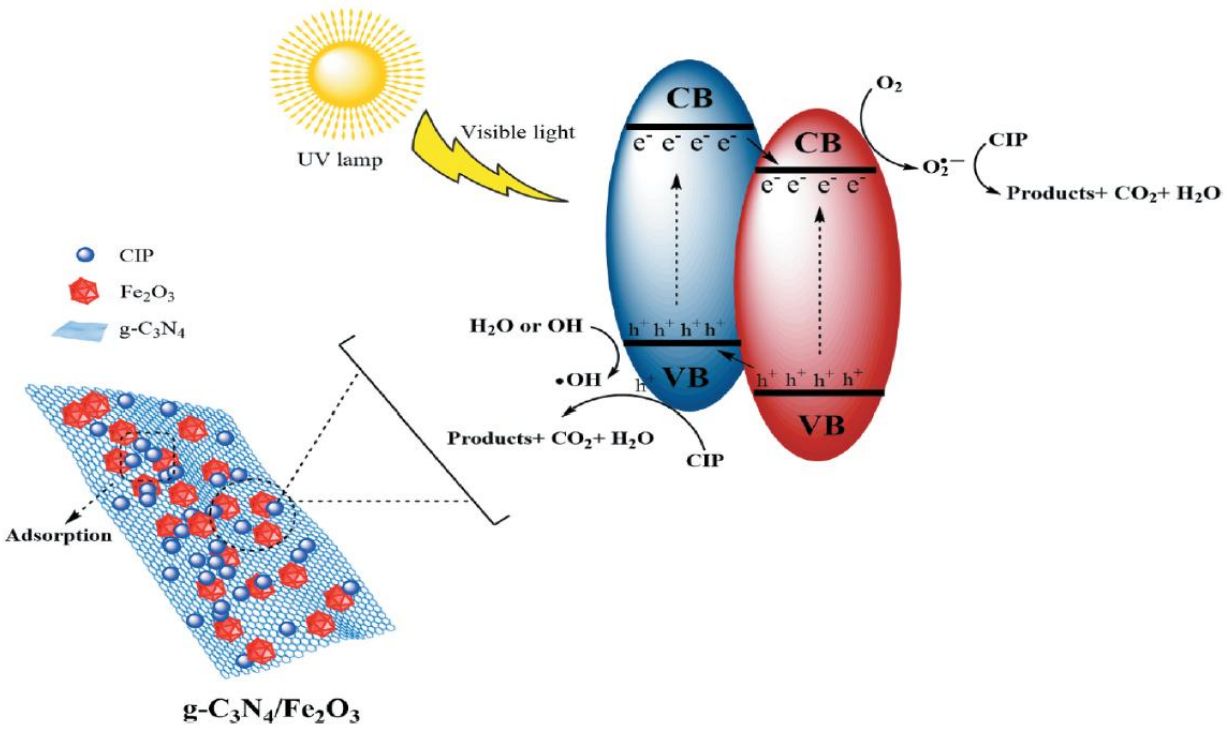

Fig.17-mechanism for the photodegradation of ciprofloxacin on the surface of g-C_3N_4/Fe_2O[145].

Yang et al. [146] used a type II heterojunction ZnS/BiOBr photocatalyst for the removal of tetracycline. The synthesis method of ZnS/BiOBr photocatalyst is a one-step, facile hydrothermal method. Combining two semiconducting structures is an effective strategy for charge separation in the photocatalyst. Therefore, the use of ZnS photocatalyst is optimal for designing a combined photocatalyst. When ZnS / BiOBr is subjected to sunlight, the electrons are excited in the Valence band of BiOBr to the conduction band and create in hole in the valence band. These electrons reach the ZnS surface and combine with a hole in the valence band of ZnS. The electron in ZnS is more negative than EO_2/ $O_2^{\bullet-}$(-0.33 ev) and reacts with O_2 to form a $O_2^{\bullet-}$. A hole in the valence band of BiOBr directly oxidizes tetracycline; as a result, the recombination of the electron-hole decreases and the photocatalytic activity increases. Removal rate in 25 minutes for pure BiOBr is about 70%, while for ZnS /BiOBr with 2.5wt% of ZnS, it is 82%. The $K_{app} = 0.1311 min^{-1}.g^{-1}.L$ is the apparent rate constant for the ZnS /BiOBr photocatalyst[146]. Zhou et al. [147] in doxycycline removal, g-C_3N_4 thin layer @ CeO_2 core-shell composite photocatalyst used. The synthesis method of photocatalyst Nano-sized g-C_3N_4 thin layer @ CeO_2 sphere is a simple

hydrothermal and in situ synthesis method. The photocatalyst with a limited band gap, which has more absorption in the visible region, has been considered. Metal oxides such as CeO_2 (2.8ev), MoO_3 (2.9ev), Bi_2O_3(2.3-2.8ev), CuO(1.2ev) and Fe_2O_3 (2.1ev) are the semiconductors of interest in the removal of pollutants. Also, g-C_3N_4 photocatalyst is a metal-free organic polymer that has a band gap limited to 2.7ev, which is easily activated in the visible region and also has high stability. However, the electron-hole recombination leads to a decrease in the performance of the photocatalyst. Therefore, the g-C_3N_4 photocatalyst must be modified. CeO_2 is widely used in the reduction of CO, CO_2 and NO_x as well as the removal of organic pollutants, have been taken into consideration. Despite the limited band gap and non-toxicity, it has poor photocatalytic performance due to weak electron-hole separation. However, the combination of these two photocatalysts leads to improvement. It becomes a photocatalyst. Photoluminescence spectra of g-C_3N_4@ CeO_2 photocatalyst with mass ratios of g-C_3N_4 to CeO_2 5% have the lowest peak intensity, as a result of which electron-hole recombination is low and the photocatalytic activity is increased. After the g-C_3N_4@ CeO_2 photocatalyst is activated, electrons and holes are generated. The electrons in the conduction band of the g-C_3N_4 photocatalyst is transferred to the conduction band of the CeO_2 photocatalyst, and $\cdot O_2^-$ radicals are generated from the reaction of electrons and oxygen. At the same time, the holes in the valence band of CeO_2 are partially transferred to the valence band of g-C_3N_4. The transfer of electrons and holes between g-$C_3N_4$and CeO_2 leads to the reduction of electron-hole recombination. The electrons and $\cdot O_2^-$ radicals react with H_2O_2 and lead to the decomposition of the antibiotic. The removal rate of doxycycline antibiotic with an initial concentration of 10 mg/L, with visible light, with a 150W Xeon lamp with a 420 nm filter in 60 min and 0.5 g/L for CeO_2, g-C_3N_4 and 5% g-C_3N_4@ CeO_2 photocatalysts is 14.8%, 18.3% and 19.3%, respectively. By adding 100 µL H_2O_2, the removal rate for these photocatalysts becomes 66.7%, 71.7% and 84%, respectively. The two photocatalysts g-C_3N_4 and CeO_2 have an increase of 12.3% and 17.3% compared to the heterojunction structure, respectively. The $K_{app} = 0.0655 min^{-1}.g^{-1}.L$ is apparent rate constant for the 5% g-C_3N_4@ CeO_2 photocatalyst[147]. In equations 26-32, after the g-

C_3N_4@ CeO_2 photocatalyst is activated by light, electrons and holes are produced. The electrons are separated and transferred to g-C_3N_4 and the holes are transferred to CeO_2. The electrons react with oxygen to produce superoxide radical, and also react with hydrogen peroxide to produce hydroxide ion and hydroxide radical. The superoxide radical reacts with hydrogen peroxide to produce hydroxide radical and positive H. The superoxide radical reacts with holes and the hydroxide radical reacts with the antibiotic doxycycline to finally produce water and carbon dioxide[148].

$$g - C_3H_4@CeO_2 + h\upsilon \rightarrow g - C_3H_4(e^- + h^+)@CeO_2(e^- + h^+) \quad 26$$

$$g - C_3H_4(e^- + h^+)@CeO_2(e^- + h^+) \rightarrow g - C_3H_4(h^+ + h^+)@CeO_2(e^- + e^-) \quad 27$$

$$e^- + O_2 \rightarrow O^{-\cdot}{}_2 \quad 28$$

$$e^- + H_2O_2 \rightarrow OH^{\cdot} + OH^- \quad 29$$

$$O^{-\cdot}{}_2 + H_2O_2 \rightarrow OH^{\cdot} + OH^{\cdot} + O_2 \quad 30$$

$$h^+ + H_2O \rightarrow OH^{\cdot} + H^+ \quad 31$$

$$O^{-\cdot}{}_2 + h^+ + OH^{\cdot} + DOX \rightarrow \text{products} + H_2O + CO_2 \quad 32$$

Li et al. [149] used Fe_3O_4/CdS/g-C_3N_4 photocatalyst to remove the antibiotic ciprofloxacin. The synthesis method of Fe_3O_4 photocatalyst is the co-precipitation method, the synthesis method of

Fe_3O_4/CdS photocatalyst is liquid chemistry, and the synthesis method of Fe_3O_4/CdS/g-C_3N_4 photocatalyst is monodispersion. CdS photocatalyst has a limited band gap of 2.4ev, and its absorption spectrum is very close to the spectrum of the sun, so the combination of these two photocatalysts leads to a reduction of electron-hole recombination and improves charge transfer. Magnetic separation is a convenient method to remove and recycle photocatalysts using an external magnetic field, Fe_3O_4 has been used for this purpose. One of the characteristics of the ideal photocatalyst is to maintain efficiency during its reuse. The heterojunction structure in Fe_3O_4/CdS/g-C_3N_4 (FCN) is of Z-scheme type, which leads to effective charge separation and makes full use of visible light. The two photocatalysts g-C_3N_4 and CdS are activated by visible light, and the electrons generated move rapidly to the CdS surface, and superoxide radicals (·O_2-) are produced in the adsorbed solution. The holes in the VB of CdS react with water molecules to form a hydroxyl radical (·OH). Superoxide radicals (·O_2-), in addition to being converted into hydroxyl radicals (·OH), can directly eliminate ciprofloxacin. The key role in the degradation of CPFX in water is actually the strong oxidation potential of hydroxyl radicals (·OH), thus accelerating the degradation. The role of Fe_3O_4 in the FCN structure is mainly used to magnetize the photocatalyst and load nanomaterials. In this way, the photocatalyst is separated into a suspension, and as a result, the problem of photocatalyst recovery is solved and it does not cause secondary pollution. The removal rate of Fe_3O_4/CdS/ g-C_3N_4 photocatalyst with 15 wt% g-C_3N_4 for an initial concentration of 20 mg/L, visible light with 250-W xenon lamp, 0.5g/L photocatalyst and a time of 180 minutes is 81%. The $K_{app} = 0.044 min^{-1}.g^{-1}.L$ is apparent rate constant for the Fe_3O_4/CdS/ g-C_3N_4 photocatalyst[149]. Liu et al. [150] used Carbon dots(CDs)/g-C_3N_4/ZnO nanocomposite for tetracycline removal. The synthesis method of g-C_3N_4/ZnO photocatalyst is a chemical deposition method, the synthesis method of CDs is an electrochemical method, and the synthesis method of CDs /g-C_3N_4/ZnO photocatalyst is a facile impregnation-thermal method. ZnO photocatalyst is characterized by outstanding optical and electrical properties, cheapness, high biological safety, compatibility with the environment and good degradation ability to remove organic pollutants in the presence of UV light. But due to the high band

gap in visible light, which includes about 43% of sunlight, it is not activated, which has led to its limitation. To overcome this problem, doping it with metals, non-metals and semiconductors. One of these photocatalysts is graphite carbon nitride, which has high photocatalytic activity. Although ZnO/ g-C_3N_4 photocatalyst is an excellent photocatalyst, one of its limitations is not being activated in visible light. To solve this problem, doping with Noble metals such as silver leads to increased absorption in the visible region as well as electron-hole separation. However, the use of noble metals along with two other photocatalysts leads to increased costs and limits their industrial application. CDs, a new type are one of nano carbon, which have a low price, high solubility in water, and also lead to an increase in the absorption range. To investigate the role of CDs in the photocatalytic structure of g-C_3N_4/ZnO, the quantum yield was investigated, which uses the method of measuring changes in luminescence quantum yield through Stern-Volmer plots. The photoluminescence of CDs under excitation at 485 nm is significantly reduced in the presence of an electron acceptor (2,4-dinitrotoluene (0.9 V vs. NHE)) and an electron donor (DEA, 0.88 V vs. NHE). The results indicate that CDs act as both acceptors and electron donors, leading to increased charge separation and improved photocatalytic activity. It leads to its easy transfer to the photocatalyst surface .ZnO/ g-C_3N_4 photocatalyst is an excellent photocatalyst, one of its limitations is not being activated in visible light. CDs, a new type of nanocarbons, have a low price, high solubility in water, and also lead to an increase in the absorption range. As a donor and acts as an electron acceptor, it leads to its easy transfer to the photocatalyst surface. The ZnO photocatalyst cannot be excited by visible light, so visible light only activates the g-C_3N_4 photocatalyst (2.7 eV). Since the conduction band potential of the g-C_3N_4 photocatalyst (1.12 eV vs. NHE) is more negative than that of the ZnO photocatalyst (0.5 eV vs. NHE), electrons in the conduction band of the g-C_3N_4 photocatalyst is directly transferred to the photocatalyst, creating holes in the valence band of the g-C_3N_4 photocatalyst. The electrons in the conduction band of the ZnO photocatalyst react with dissolved oxygen in water to form O_2 radicals because the conduction band potential of the ZnO photocatalyst (0.5 eV vs. NHE) is more negative than the standard redox potential E(O_2/O_2-) (0.33 eV vs. NHE).

When CDs are adsorbed on the g-C_3N_4/ZnO nanocomposite facilitates two tasks. CDs help the heterojunction structure to have a broader visible spectrum absorption and better stimulate g-C_3N_4/ZnO to form electrons. On the other hand, CDs act as electron donors and acceptors, allowing electrons to be easily transferred to the g-C_3N_4/ZnO surface, and the excess electrons on the CZ30 can also be transferred to CDs, which facilitates the separation of the electron pairs. Further improves the electron-hole. It can also be transferred to CDs, which further improves the separation of electron-hole pairs. The holes generated in the valence band of g-C_3N_4 (EVB = +1.40 eV vs. NHE) are not successful in oxidizing hydroxyl groups to OH radicals (E (OH/OH•) = +1.99 eV vs. NHE) of g-C_3N_4. OH radicals are produced from O_2 radicals by the photochemical reaction. The removal rate in visible light with 18 mW/cm^2, xenon lamp (λ>420 nm), 0.5g/L photocatalyst in 10mg/L tetracycline in 60 minutes in the presence of pure ZnO photocatalyst is about 8%, this rate is about 28% for g-C_3N_4 photocatalyst. The amount of removal in the presence of CDs/ ZnO/ g-C_3N_4nanocomposite, which is with mass ratio of g-C_3N_4/ZnO: 30%wt and CDs4%wt(CZ) are 100%.The $K_{app} = 0.164 \text{min}^{-1}.\text{g}^{-1}.\text{L}$ is apparent rate constant for the CDs/ ZnO/ g-C_3N_4 photocatalyst with an optimal amount of a mass ratio of g-C_3N_4/ZnO: 30%wt and CDs4%wt(CZ)[150]. Wang et al. [151] used CuO/ $CuFe_2O_4$ / g-C_3N_4 photocatalyst to remove tetracycline. The synthesis method of CuO/ $CuFe_2O_4$ / g-C_3N_4 photocatalysts is the calcination method. CuO is a P-type photocatalyst with a limited band gap of 1.2 eV, which has properties such as non-toxicity, low cost, and ideal electrochemical and optical properties. $CuFe_2O_4$ is an n-type photocatalyst that has relatively high stability and forms a p-n heterojunction with CuO with excellent photocatalytic properties. However, these metal oxide semiconductors tend to aggregate; as a result, the reaction sites to remove antibiotics are significantly reduced. Carbon-based nanostructures are often used as a substrate for the uniform dispersion of semiconductors, thereby creating sufficient reaction sites for photodegradation. The use of CuO/ $CuFe_2O_4$ / g-C_3N_4 (CCCN) photocatalyst is effective in removing tetracycline. In general, the activation of persulfate (PS) leads to the production of oxidizing substances, including hydroxyl radical (OH) and sulfate radical (SO_4). On the other hand,

the Cu(I) and Fe (II) ions in the surface lattice of the $CuO/CuFe_2O_4/g\text{-}C_3N_4$ could also lead to the activation of PS with the generation of $SO_4^{\bullet -}$ .Fig.18 shows the mechanism of tetracycline after photocatalyst activation in reactions 33-41. The photoinduced electrons react with PS to produce $SO_4\bullet-$ (Equation (34)), which prevents electron-hole recombination. Electrons can also react with dissolved oxygen (O_2) in the solution to produce $O_2\bullet-$ (equation (35)). In addition, Cu(I) and Fe (II) ions present in the CCCN surface network lead to PS activation by producing $SO_4\bullet -$ (equations (36)- (37). The standard oxidation-reduction potentials of $O_2/ O_2\bullet -$, Cu(II)/Cu(I) and Fe(III)/Fe(II) ions are −0.33, 0.16 and 0.77 V vs. the normal hydrogen electrode (NHE), respectively. Fe(III) and Cu(II) are reduced to Fe(II) and Cu(I), respectively, by $O_2\bullet -$ (equations (38)-((39)). The generation of •OH radicals is used through the oxidation of H_2O with $SO_4\bullet-$ (equation (40)). The removal rate in 10 mg/L tetracycline in simulated sunlight with a 300 W xenon lamp,0.1g/L photocatalyst in 30 minutes for pure $g\text{-}C_3N_4$ photocatalyst is 5%, this rate is 51% for $g\text{-}C_3N_4$ +PS photocatalyst. $CuO/ CuFe_2O_4$ removal rate is 31%, while for $CuO/ CuFe_2O_4$ +PS, this rate is 44%. Finally, for $CuO/ CuFe_2O_4$ / $g\text{-}C_3N_4$ with ratio of CuO, $CuFe_2O_4$and $g\text{-}C_3N_4$ as 1.4:1.0:19.0 this amount is 32% and for $CuO/ CuFe_2O_4$ / $g\text{-}C_3N_4$ +PS this amount is 99%.The $K_{app} = 1.3 min^{-1}.g^{-1}.L$ is apparent rate constant for the $CuO/ CuFe_2O_4$ / $g\text{-}C_3N_4$ +PS with ratio of CuO, $CuFe_2O_4$and $g\text{-}C_3N_4$ as 1.4:1.0:19.0 photocatalyst[151].

$$\mathbf{CCCN} \xrightarrow{h\nu} \mathbf{h^+ + e^-} \quad (33)$$

$$\mathbf{S_2O_8^{2-} + e^- \rightarrow SO_4^{\cdot -} + SO_4^{2-}} \quad (34)$$

$$\mathbf{O_2 + e^- \rightarrow O_2^{-\cdot}} \quad (35)$$

$$\mathbf{Cu(I) + S_2O_8^{2-} \rightarrow Cu(II) + SO_4^{\cdot -} + SO_4^{2-}} \quad (36)$$

$$Fe(II) + S_2O_8^{2-} \rightarrow Fe(III\ ) + SO_4^{\cdot -} + SO_4^{2-} \quad (37)$$

$$Cu(II\ ) + O_2^{\cdot -} \rightarrow Cu(I\ ) + O_2 \quad (38)$$

$$Fe(III\ ) + O_2^{\cdot -} \rightarrow Fe(II) + O_2 \quad (39)$$

$$H_2O + SO_4^{\cdot -} \rightarrow H^+ + OH^{\cdot} + SO_4^{2-} \quad (40)$$

$$OH^{\cdot}/SO_4^{\cdot -}/h^+ + \text{tetracycline} \rightarrow \text{intermediates} \rightarrow CO_2 + H_2O \quad (41)$$

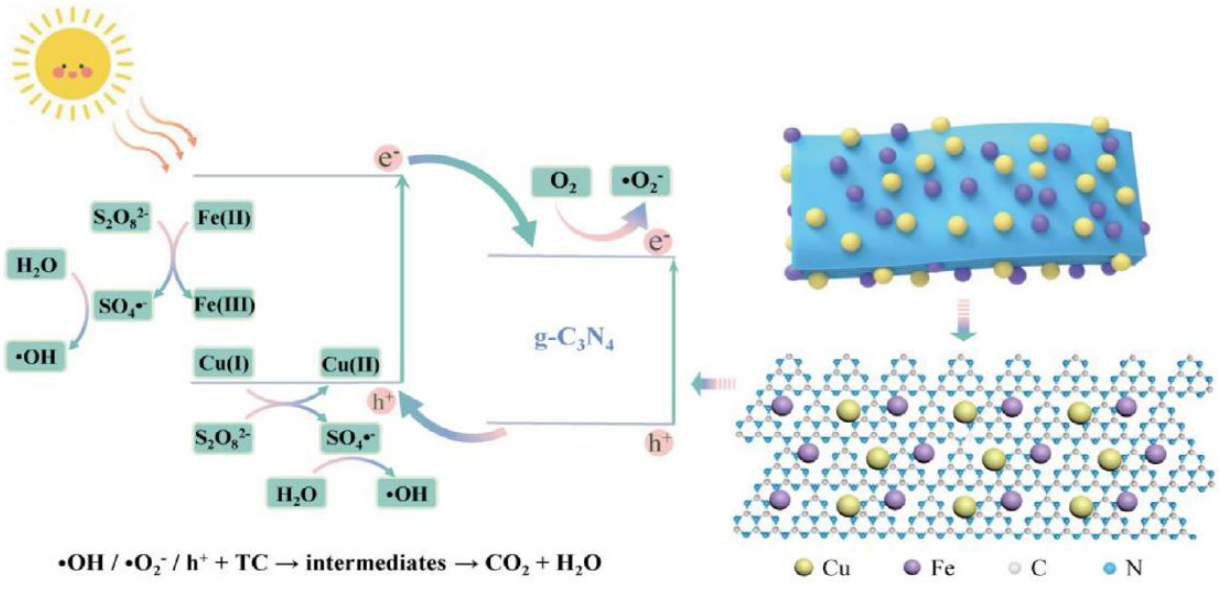

Fig.18- Mechanism of photocatalytic removal of tetracycline[152].

5-4- Z-SCHEME HETEROJUNCTION

All types of heterojunction photocatalysts are effective for increasing electron-hole separation. But oxidation and reduction processes occur in semiconductors with lower oxidation-reduction potentials, the redox ability of photocatalysts is sacrificed. To solve this problem and maximize the redox potential of the heterojunction system, Z-Scheme Heterojunctions are used[129,153]. According to equations 42-43 and as shown in Fig.19, a photocatalytic system with Z design is composed of two different semiconductors, photocatalyst I (PS I) and photocatalyst II (PS II) and an acceptor/donor (A/D) pair. PS I and PS II are in physical contact. During the photocatalytic reaction, the photogenerated electrons move from the conduction band of PS II to the valence band of PS I through a pair of A/D redox reactions.

$$A + e^- \rightarrow D \qquad 42$$

$$D + h^+ \rightarrow A \qquad 43$$

A is reduced into D by reaction with the photogenerated electron produced from the conduction band of PS II, and D is oxidized to A by holes created from VB. As electrons accumulate on PS I with further reduction potential, and holes accumulate on the PS II with higher oxidation potential, this leads to spatial separation of electron-hole pairs and optimal redox ability [129].

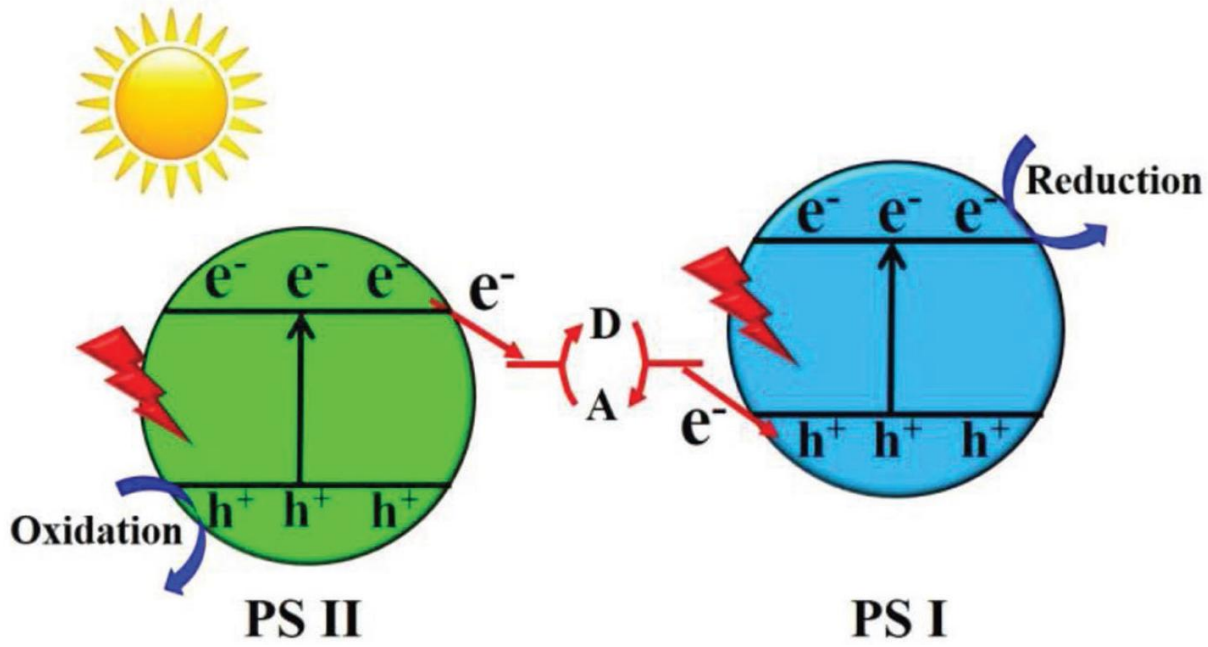

Fig.19- Schematic figure of Z-Scheme heterojunction[129].

Hernández-Uresti et al. [154] used WO_3/ g-C_3N_4 photocatalyst for the removal of ciprofloxacin. The synthesis method of WO_3/ g-C_3N_4 photocatalyst is a sonochemical process. WO_3 It is a semiconductor that shows absorption in the visible region of the sun's spectrum and can be used in various applications. However, Photocatalytic activity is limited due to the edge of its conduction band being lower than the position of single electron reduction of oxygen[154]. The conduction band and valence band for the g-C_3N_4 photocatalyst are estimated to be -1.22 eV and 1.58 eV, respectively, which are in agreement with reality. Also, for WO_3 photocatalyst, these values are 0.70 eV and 3.28 eV, respectively. When WO_3/ g-C_3N_4 is exposed to visible light, both semiconductors are excited and electron-holes are generated. In addition, the recombination between electrons in the conduction band of WO_3 and the hole in the valence band of g-C_3N_4 is performed due to the internal electric field generated between the two semiconductors, flexion of the edge of the band and the Coulomb interaction. As shown in fig.20, it reduces the recombination of electrons in g-C_3N_4 and a hole in WO_3. As a result, a Z-scheme heterojunction is obtained, which allows efficient spatial separation, increasing the photocatalytic activity[155]. To overcome these problems, g-C_3N_4 has been used. The WO_3/ g-C_3N_4 heterojunction structure leads to reduced electron-hole recombination and thus increased formation of reactive oxygen

species. Photogenerated holes in WO_3 and reduced electron recombination in g-C_3N_4. As a result, the heterogeneous Z-junction leads to effective spatial separation of generated charge carriers and leads to reduced electron-hole recombination and improved photocatalytic performance. Direct antibiotic removal is a feature of the holes generated by WO_3/ g-C_3N_4. The visible light with 35-W Xe lamp (6000 K) with a radiation intensity of 1380 μW·cm^2 ,1g/L photocatalyst and 10mg/L. Using only g-C_3N_4 photocatalyst, 60% removal is in 4 hours. Using WO_3 leads to only 19% removal. But using 5% WO_3 along with g-C_3N_4, It leads to 100% removal in 4 hours. The $K_{app} = 0.0256 min^{-1}.g^{-1}.L$ is apparent rate constant for the 5% WO_3/ g-C_3N_4 photocatalyst [155].

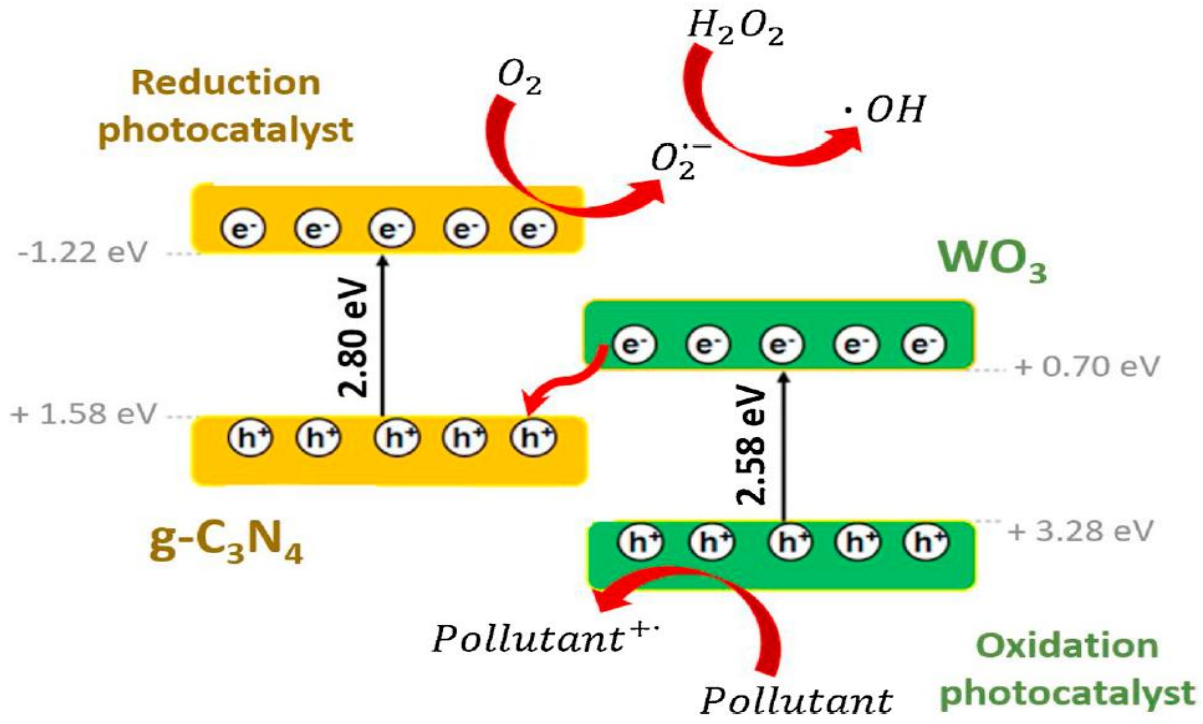

Fig.20- Schematic figure Z-scheme heterojunction WO_3/ g-C_3N_4 photocatalyst[155].

Wolski et al. [156] used a CeO_2/ZnO photocatalyst to remove the antibiotic ciprofloxacin. The synthesis method of CeO_2/ZnO photocatalyst is a facile coprecipitation method. Research shows that the photocatalytic activity of ZnO is improved by forming heterojunctions with other semiconductor materials. Research shows that the main component that plays the role of antibiotic absorption in

CeO_2/ZnO nanocomposite is ZnO. The interaction between ZnO and CeO_2 improves the formation of defect sites in the structure of metal oxides. The lower ability of the CeO_2/ZnO photocatalyst to adsorb Due to the lower adsorption of CeO_2, is related to the lower oxidation potential of the hole created in the valence band of CeO_2. Based on the position of the estimated band edges, it can be concluded that the electrons are transferred from the conduction band of CeO_2 to the conduction band of ZnO and the holes are transferred from the valence band of ZnO to the valence band of CeO_2. Such a transition leads to the accumulation of holes in CeO_2 and photo-excited electrons in ZnO, which leads to the effective separation of charge carriers. Photooxidation of antibiotic molecules by positive holes occurs on the surface of ceria particles, where the holes are accumulated, so the effective adsorption of ciprofloxacin molecules on the ceria surface is necessary to start the removal. Fig.21 shows two different mechanisms. Due to the lower absorption of CeO_2, Z-scheme heterojunction(B) is better than the Type II(A) heterojunction in removing ciprofloxacin. Removal of ciprofloxacin using CeO_2/ZnO photocatalyst proceeds from two parallel paths. Path 1: in which the path is dominant and in which the piperazine moiety of ciprofloxacin molecules is selectively oxidized by h^+, path 2: in which both the fluoroquinolone and piperazine moieties of the antibiotic were degraded. In path 2, the presence of both h^+ and hydroxyl radicals ($HO^{\cdot}$) is necessary. The ability to absorb CIP molecules for ZnO is much higher than that of CeO_2, and the hole in the valence band of ZnO has a stronger oxidizing potential than that of CeO_2. Therefore, the performance of the Z heterojunction structure is better than that of the II heterojunction structure. Ciprofloxacin removal with 15 mg/ L, 200 W Hg-Xe lamp equipped with a UV filter and 0.25g/L photocatalyst in 60 min using CeO_2 pure photocatalyst is about 13%, using ZnO pure photocatalyst, this amount is about 38%, while with ZnO photocatalyst with an optimal amount of 8wt% CeO_2, the removal rate reaches 63%. The $K_{app} = 0.052 min^{-1}.g^{-1}.L$ is apparent rate constant for the CeO_2/ZnO photocatalyst with an optimal amount of 40 wt% CeO_2 [156].

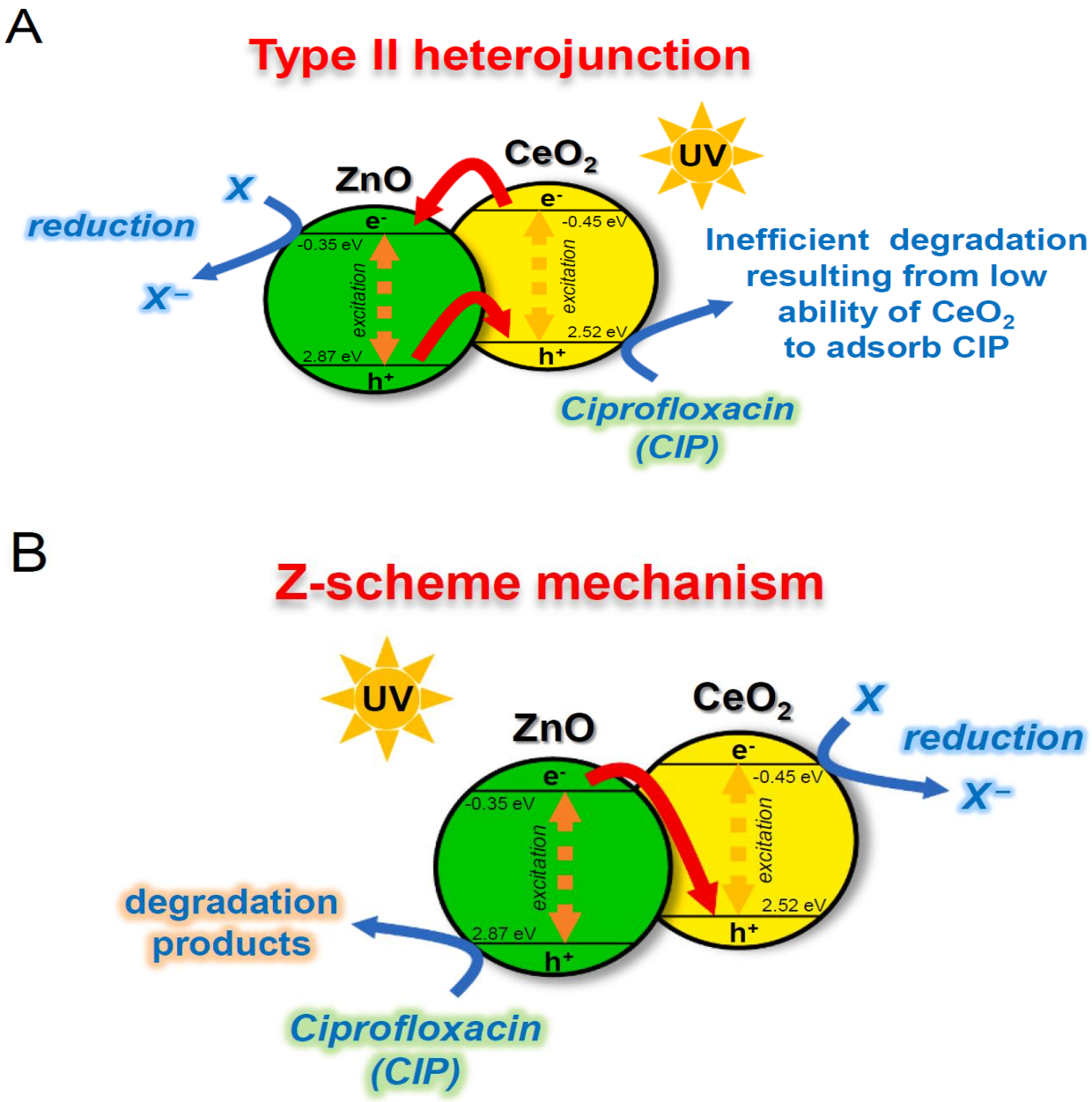

Fig.21- Mechanism of ciprofloxacin degradation over CeO_2/ZnO nanocomposites[157].

Du et al. [158] used a Z-scheme ZnO/Ag/Ag_3PO_4 photocatalyst for the removal of ciprofloxacin. The synthesis method of ZnO/Ag/Ag_3PO_4 photocatalyst is a simple precipitation deposition method and photoreduction technology. Ag_3PO_4 photocatalyst has photocatalyst activity and high quantum efficiency due to a limited band gap of 2.4ev. But due to poor stability and high cost, its use on a large scale is limited. ZnO photocatalyst combined with Ag_3PO_4 photocatalyst and leads to a reduction of electron-hole recombination and an increase in photocatalyst performance. Noble metals such as Ag lead to the expansion of the absorption range

and it also leads to the acceleration of charge transfer. Ag leads to rapid electron-hole transfer to ZnO and Ag_3PO_4. The addition of silver leads to a red shift and also increases the absorption of light in the visible region, which is related to the surface plasmon effect (SPR) of Ag. In this research $O_2^{-\cdot}$ the main species in elimination is ciprofloxacin. According in equations 44-52, after the ZnO/Ag/Ag_3PO_4 photocatalyst is activated by light, the electrons generated in the Ag_3PO_4 conduction band is transferred to Ag nanoparticles because the Fermi level of Ag_3PO_4 is lower than that of metallic Ag. The holes in the valence band of ZnO are transferred to the Ag surface and recombine with the electrons. Between Ag_3PO_4 and the ZnO photocatalyst, the silver nanoparticles act as a charge transfer bridge, which leads to a decrease in the photocatalytic efficiency due to recombination. The electrons in the Ag_3PO_4 conduction band cannot produce $O_2^{-\cdot}$ from O_2 because the reduction potential of $O_2/O_2^{-\cdot}$ (0.33 eV) is lower than the Ag_3PO_4 conduction band edge. The electrons can only react with ZnO and produce $O_2^{-\cdot}$ to oxidize organic pollutants. The valence band holes of Ag_3PO_4 can combine with H_2O and OH- because the valence band potential of Ag_3PO_4 is higher than that of O_2/H_2O and OH-/•OH. The ZnO/Ag/Ag_3PO_4 heterojunction structure plays an important role in carrier separation. The specific surface area of pure Ag_3PO_4 is 9.59 m2/g, which is 11.2 m2/g for the heterojunction structure, leading to an increase in the specific surface area. The amount of removal with 10 mg/L ciprofloxacin in 120 minutes in visible light with the 300 W xenon lamp with a wavelength of less than 420 nm and 0.5g/L photocatalyst, pure Ag_3PO_4 and pure ZnO is 56.1% and 29.8%, respectively. This amount of ZnO combined with Ag_3PO_4 reaches 77.5% and finally, with the doping of silver to this composition and ZnO/$Ag_3PO_4 wt\%: 0.6/1$, the removal rate reaches 87.1%. For the ZnO/Ag/Ag_3PO_4 photocatalyst, the energy consumption per gram of ciprofloxacin antibiotic removed is 688.86 kWh/g, which requires further attention to reduce it and optimize the photocatalytic reaction of ciprofloxacin antibiotic removal. The $K_{app} = 0.02886 min^{-1}.g^{-1}.L$ is the apparent rate constant with an optimal amount of ZnO/$Ag_3PO_4 wt\%: 0.6/1$for the Ag/ZnO/Ag_3PO_4 photocatalyst[158].

$$Ag_3PO_4 + hv \rightarrow Ag_3PO_4(e^- + h^+) \quad (44)$$

$$ZnO + hv \rightarrow ZnO(e^- + h^+) \quad (45)$$

$$Ag_3PO_4(e^-) \rightarrow Ag(e^-) \quad (46)$$

$$ZnO(h^+) \rightarrow Ag(h^+) \quad (47)$$

$$ZnO(e^-) + O_2 \rightarrow O_2^{-\cdot} \quad (48)$$

$$O_2 + 2H^+ + 2e^- \rightarrow H_2O_2 \quad (49)$$

$$Ag_3PO_4(h^+) + H_2O/OH^- \rightarrow OH^{\cdot} \quad (50)$$

$$H_2O_2 + hv \rightarrow 2OH^{\cdot} \quad (51)$$

$$O_2^{-\cdot} + h^+ + OH^{\cdot} + \text{Ciprofloxacin} \rightarrow \text{Degradation} \quad (52)$$

Pham et al. [159] used the Z-scheme AgI/N–TiO_2 photocatalyst for the removal of tetracycline. In this research, doping nitrogen with TiO_2 leads to a decrease in the band gap from 3.2ev to 2.7ev[160,161]. In the meantime, AgI has a band gap of 2.8ev and combines with other photocatalysts and leading to increased charge separation and adsorption capacity. The intensity of the photoluminescence peaks for the Z-scheme

AgI/N– TiO_2 photocatalyst is reduced, which proves that the heterojunction structure is effective in electron-hole separation. The N– TiO_2 photocatalyst has a large absorption in the visible range compared to TiO_2 alone, and the visible absorption edge of the N-TiO_2 photocatalyst is about 430 nm. The AgI/N–TiO_2 photocatalyst is a highly stable photocatalyst during the removal process of the antibiotic tetracycline, and the photocatalyst properties are similar to those of the recycled photocatalyst. AgI and N– TiO_2 photocatalysts have narrow band gaps and according to equations 53-58, after the photocatalysts are activated in the visible light range, electrons are transferred from the valence band to the conduction band and holes are generated in the valence band. The electrons transferred in the conduction band of N– TiO_2 easily move to the valence band of AgI to assume these h+ there. These transfers minimize electron-hole recombination and the absorption rate is much higher than that of single N-TiO_2 or AgI[159]. After the photocatalyst – TiO_2 is activated, electrons and holes are produced. The holes react with the antibiotic Tetracycline and are converted into simpler substances. The holes also react with water and produce hydroxide radical and hydrogen ion. The electrons react with oxygen and produce superoxide radical. The superoxide radical reacts with Tetracycline and is converted into simpler substances, also the superoxide radical reacts with water and produces hydroxide ion and hydroxide radical and oxygen[159].

$$\text{photocatalysts} \xrightarrow{\text{Visible light}} e^- + h^+ \quad (53)$$

$$h^+ + \text{Tetracycline} \rightarrow \text{Decomposition products} \quad (54)$$

$$h^+ + H_2O \rightarrow H^+ + OH^{\cdot} \quad (55)$$

$$e^- + O_2 \rightarrow O_2^{-\cdot} \quad (56)$$

$$O_2^{-\cdot} + \text{Tetracycline} \rightarrow \text{Decomposition products} \quad (57)$$

$$O_2^{-\cdot} + H_2O \rightarrow OH^{\cdot} + OH^{-} + \frac{1}{2}O_2 \quad (58)$$

The Total Organic Carbon (TOC) for the Z-scheme AgI/N–TiO_2photocatalyst with an initial concentration of 10 mg/L, visible light with 30 W DUHALLED, 0.5 g/L photocatalyst and a time of 105 minutes is about 73%, indicating that 73% of the compounds have been converted to minerals or lighter organic products. The article does not mention the rate of antibiotic removal and only states that the heterojunction structure was successful in the removal rate[159]. Zhang et al. [162] used Cu_2O/Bi_2S_3 photocatalyst to remove the antibiotic tetracycline. The synthesis method of Cu_2O/Bi_2S_3 photocatalyst is a simple hydrothermal method. Bi_2O_3 is a photocatalyst with a limited band gap of 1.3ev, which has good absorption in the entire visible region. Cu_2O is a photocatalyst with a cubic structure and P-type photocatalyst with a band gap of 2.2ev. photoelectrons are eliminated by the intense adsorption of molecular oxygen, Therefore, the level of electron-hole recombination is minimized, which leads to an increase in photocatalytic activity. The Cu_2O photocatalyst is activated in the wavelength range of 600 nm, while the Cu_2O/Bi_2S_3 photocatalyst has strong absorption in the visible light range of 40 to 80 nm. As a result, the formation of heterogeneous bonds adjusts the band gap and forms electron-hole pairs on the catalyst surface, which has a good effect on improving the photocatalytic performance. The Cu_2O/Bi_2O_3 photocatalyst produces electrons and holes after being activated by light. The electrons are transferred from the valence band of the Bi_2O_3 photocatalyst to the conduction band. The electrons in the conduction band cannot convert O_2 to the $^{\bullet}O_2^-$ radical because the potential of the Bi_2O_3 conduction band is more positive than the potential of the $O_2/^{\bullet}O_2^-$ (0.33 V vs. NHE). The electrons on the Bi_2O_3 conduction band are transferred to the valence band of the Cu_2O photocatalyst, and then convert oxygen to the $^{\bullet}O_2^-$ radical.

The Cu_2O photocatalyst has a more negative potential and also a part of the holes are related to the valence band of the Bi_2S_3 photocatalyst. The electron-hole generation is more characteristic of the heterogeneous structure. Therefore, the heterojunction structure cannot be p-n and the heterojunction structure are Z-type. In the photocatalytic antibiotic removal process, the $^{\bullet}OH$ species is practically ineffective in the removal rate, and the two species, $^{\bullet}O_2^-$ and h+, affect the photocatalytic reaction, with $^{\bullet}O_2^-$ playing the largest role. The removal rate for 20 mg/L of tetracycline in visible light with 200 W high-pressure mercury lamp in and 0.5g/L photocatalyst in 60 minutes with pure Cu_2O photocatalyst is about 72%, the removal rate with Bi_2O_3photocatalyst is about 79%. The removal rate with Cu_2O/Bi_2O_3 and 10wt% Cu_2O is 95.23. The $K_{app} = 0.088 min^{-1}.g^{-1}.L$ is apparent rate constant with an optimal amount of 10wt% Cu_2O for the Cu_2O/Bi_2S_3 photocatalyst[162]. Lu et al. [163] used a dual Z-Scheme AgI/ $ZnIn_2S_4/BiVO_4$ heterojunction photocatalyst for the removal of tetracycline. The synthesis method of AgI/ $ZnIn_2S_4/BiVO_4$ photocatalyst is hydrothermal method. Heterojunction is the simplest and most effective method to improve photocatalyst performance. $ZnIn_2S_4$ photocatalyst is a limited bandgap photocatalyst that has excellent photochemical conversion and chemical and physical stability. The $ZnIn_2S_4$ photocatalyst has a negative valence band, which is suitable for photocatalysts with a positive conduction band to form a Z-scheme heterojunction, which leads to improved separation of produced charges and retain the prominent redox potential. AgI is a light-sensitive material with a band gap of 2.8, which has photocatalytic performance, but its large particle size and poor stability have limited its use. To solve this limitation, a triple combination of photocatalysts $AgI/ZnIn_2S_4/BiVO_4$ dual Z -scheme is used, which leads to improved charge separation[163]. As shown in fig.22 and equations 59-63, In the type II photocatalytic mechanism(a), the photoinduced electrons move from the conduction band of $ZnIn_2S_4$ to the conduction band of AgI and then to the conduction band of $BiVO_4$. The hole created in the valence band of $BiVO_4$ is transferred to the valence band of AgI and then to the valence band of $BiVO_4$. The conduction band of $BiVO_4$ (0.32 V) is more positive than $O_2/•O_2^-$ (-0.33 V) and the valence band of $ZnIn_2S_4$ is more negative than OH–/ •OH (2.40 V) [164]. $AgI/ZnIn_2S_4/BiVO_4$ photocatalyst

follows the heterojunction of the Z scheme(b), the photoelectrons on the conduction band of AgI and $ZnIn_2S_4$ move to the valence band of $ZnIn_2S_4$ and $BiVO_4$, respectively. Simultaneously leaving the hole from the valence band of $BiVO_4$ (2.76 V) and the electron from the conduction band of $ZnIn_2S_4$ (-0.54 V), $\bullet O_2^-$ and •OH were produced in the photocatalysis reaction. Therefore, $\bullet O_2^-$ and •OH are the main species of the reaction, and the hole directly participates in the reaction and removes tetracycline. This photocatalyst structure, with the results the active species is compatible and improves charge separation. Compared to a type II heterojunction, Z-scheme heterojunction maintains an outstanding redox potential[164]. h+, $\bullet O_2^-$ and OH species were among the effective species in the photocatalytic removal process of tetracycline, and the most effective was $\bullet O_2^-$. The removal rate of 20 mg/L tetracycline in visible light with 300 W Xenon lamp(λ> 420 nm), 0.6g/L photocatalyst in 120 minutes in the presence of pure $BiVO_4$, AgI and $ZnIn_2S_4$ photocatalysts is 60.21%, 42.11% and 54.19%, respectively. While the removal rate for Z-scheme $AgI/ZnIn_2S_4/BiVO_4$ with a molar ratio of Bi to Ag:1:1 reaches 91.44%. The $K_{app} = 0.0353 min^{-1}.g^{-1}.L$ is apparent rate constant with an optimal amount of 10wt% Cu_2O for the Cu_2O/Bi_2S_3 photocatalyst [164].

$$AgI/\ ZnIn_2S_4/\ BiVO_4 \ + hv \rightarrow AgI(e^- + h^+)/\ ZnIn_2S_4(e^- + h^+)/\ BiVO_4(e^- + h^+) \quad (59)$$

$$AgI(e^- + h^+)/\ ZnIn_2S_4(e^- + h^+)/\ BiVO_4(e^- + h^+) \rightarrow AgI/\ ZnIn_2S_4(e^-)/\ BiVO_4(h^+) \quad (60)$$

$$e^- + O_2 \rightarrow O_2^{-\cdot} \quad (61)$$

$$h^+ + OH^- \rightarrow OH^{\cdot} \quad (62)$$

$$h^+/O_2^{-\cdot}/OH^{\cdot} + \text{tetracycline} \rightarrow \text{degradation products} \quad (63)$$

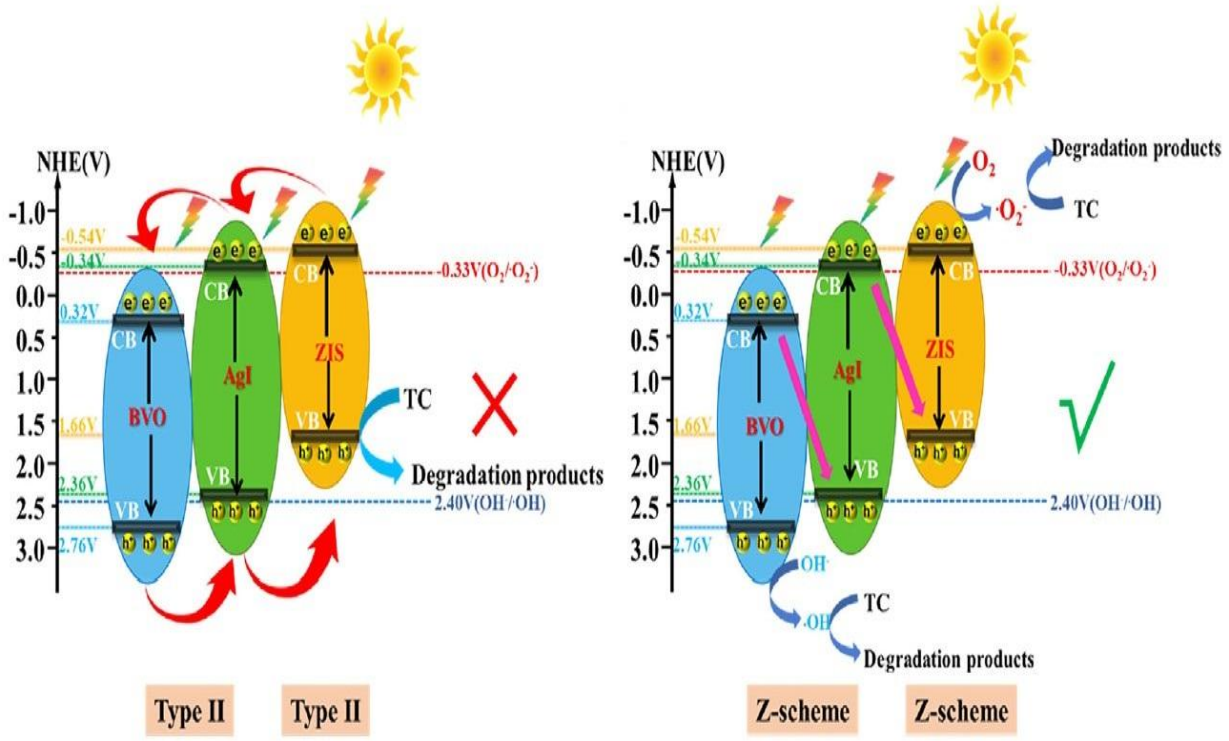

Fig.22- photocatalytic mechanism of tetracycline with AgI/$ZnIn_2S_4$/$BiVO_4$ heterojunction[164].

Liang et al. [165] used a $Bi_{12}O_{17}Cl_2$/Ag/ $AgMO_2$ Z-scheme system photocatalyst to remove the antibiotic tetracycline. The synthesis method of $Bi_{12}O_{17}Cl_2$/ $AgMO_2$ photocatalyst is in situ deposition-precipitation method and the synthesis method of $Bi_{12}O_{17}Cl_2$/Ag/ $AgMO_2$ photocatalyst is ultrasound (US)-assisted ethanol reduction method. Delafossite oxide, $AgMO_2$ (M=Fe,Co, Ni, Cr) has attracted a lot of attention. Meanwhile, $AgFeO_2$ It is easily activated in visible light due to its limited band gap. Also, due to its non-toxicity and compatibility with the environment, it has led to increased attention to this photocatalyst. Easy aggregation, poor use of sunlight, fast electron-hole recombination, and slow electron transfer have led to the limitations of this photocatalyst. $Bi_{12}O_{17}Cl_2$((BOC)) nanosheets as a substrate effectively suppressed the aggregation of $AgMO_2$(AFO) nanoparticles, which leads to an increase in the specific surface area and thus leads to an increase in the active sites for tetracycline molecules. The z-shaped system leads to strong charge separation and utilization of the powerful electrons and holes. According to equations 64-69, upon activation of the Z-scheme $Bi_{12}O_{17}Cl_2/AgMO_2$ photocatalyst, an electron-hole pair is generated. The

electrons in the conduction band of AFO were transferred to the electron shuttle intermediates (Ag nanoparticles) and the holes in the valence band of BOC photocatalyst were recombined. The electrons in the conduction band of BOC photocatalyst are able to react with oxygen and produce O_2 radical, which can react with surface-adsorbed H_2 to produce OH radicals or directly oxidize TC molecules. The holes generated in the valence band of AFO can directly contribute to the removal of TC. Also, the role of Ag nanoparticles leads to the excitation of surface electrons, increasing the interfacial electron migration and light absorption ability of the photocatalysts. The removal rate of 40 mg L^{-1} tetracycline in visible light, 0.5g/L photocatalyst in 60 minutes for pure $AgMO_2$ photocatalyst is 46.8%, this rate for pure $Bi_{12}O_{17}Cl_2$ photocatalyst is 53.9%. The removal rate for Ag/ $AgMO_2$ is 62%. The removal rate for $Bi_{12}O_{17}Cl_2/AgMO_2$ with a mass ratio of 20% is 77.3%. Finally, for $Bi_{12}O_{17}Cl_2/Ag/AgFeO_2$ with a mass ratio of $Bi_{12}O_{17}Cl_2/AgMO_2$: 20% it is 94.1%[166]. As shown in TEM images in Fig23, the Fig23 a shape corresponds to $AgMO_2$ photocatalyst, Fig23 b corresponds to $Bi_{12}O_{17}Cl_2$ and Fig23c corresponds to photocatalyst $Bi_{12}O_{17}Cl_2/Ag/AgFeO_2$ with a mass ratio of $Bi_{12}O_{17}Cl_2/AgMO_2$: 20% .TEM images confirm that the shape of $AgMO_2$ photocatalyst is spherical nanoparticles, while for photocatalyst $Bi_{12}O_{17}Cl_2$was stacked nanosheets. It is also clear from Fig23d that the addition of $Bi_{12}O_{17}Cl_2$ photocatalyst leads to the reduction of $AgMO_2$ agglomeration. The $K_{app} = 0.07738 min^{-1}.g^{-1}.L$ is apparent rate constant with an optimal amount of a mass ratio of$Bi_{12}O_{17}Cl_2/AgMO_2$: 20% for the $Bi_{12}O_{17}Cl_2/Ag/AgFeO_2$ photocatalyst[165].

$$AgFeO_2 + hv \rightarrow AgFeO_2(h^+/e^-) \quad (64)$$

$$Bi_{12}O_{17}Cl_2 + hv \rightarrow Bi_{12}O_{17}Cl_2(h^+/e^-) \quad (65)$$

$$Ag^0 + hv \rightarrow Ag^0(e^-)(\text{surface plasmon resonance}) \quad (66)$$

$$e^-(Bi_{12}O_{17}Cl_2) + O_2 \rightarrow O_2^{-\cdot} \quad (67)$$

$$O_2^{-\cdot}(Bi_{12}O_{17}Cl_2) + H^+ \rightarrow OH^{\cdot} \quad (68)$$

$$h^+/OH^{\cdot}/O_2^{-\cdot} + \text{tetracycline} \rightarrow \text{degraded products} \quad (69)$$

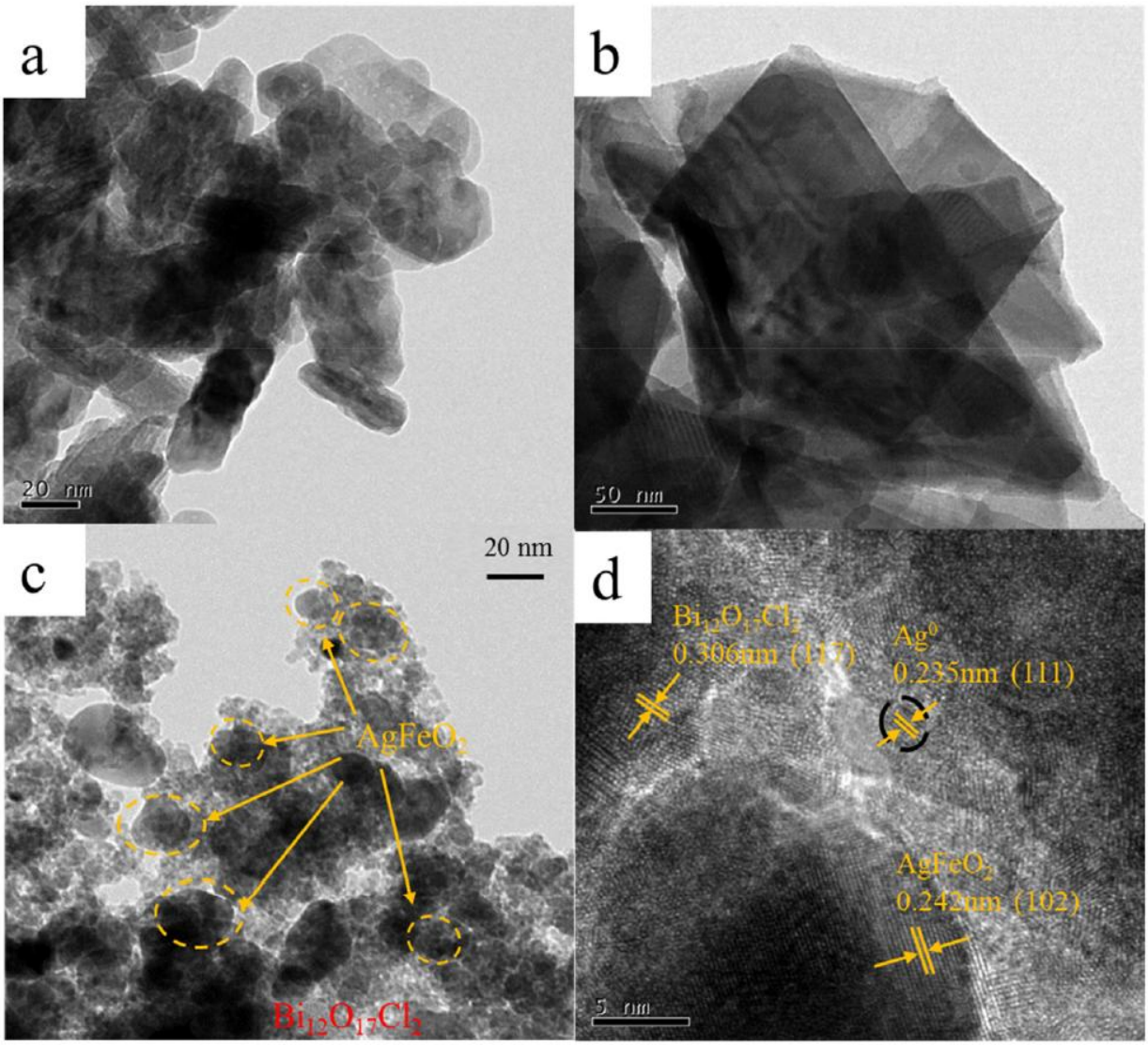

Fig.23- (a, b, c) TEM images of $AgFeO_2$, $Bi_{12}O_{17}Cl_2$ and 20- $Bi_{12}O_{17}Cl_2$/Ag/$AgFeO_2$, respectively; (d) HRTEM image of 20- $Bi_{12}O_{17}Cl_2$/Ag/ $AgFeO_2$[165].

Manikandan et al. [167] used WO_3@ g-C_3N_4 @MWCNT photocatalyst for the removal of tetracycline. The synthesis method of bulk g-C_3N_4 photocatalyst is a thermal condensation process, the synthesis method of WO_3 photocatalyst is a low-temperature hydrothermal process, and the synthesis method of WO_3@ g-C_3N_4 @MWCNT composites photocatalyst is a self-assembling method. g-C_3N_4 has a band gap of 2.7 eV, and its semiconductor nature is metal-free. WO_3 has a moving band structure, higher carrier mobility and narrow bandgap energy. Along with the higher VB potential at 3.2 eV, it has been noticed. Therefore, it exhibits stronger oxidizing properties. Unfortunately, the reduction ability is

lower due to the position of the conduction band at 0.4 eV, leading to the accumulation of charge from the valence band, so the rate of electron-hole recombination increases. MWCNT has a sp2 hybridization structure, so by combining it with a semiconductor nanostructure, excellent charge transfer with defects smooths the Schottky barrier. Also, due to their higher conductivity, they can act as an electron sink. Therefore, electron-hole recombination is reduced. MWCNT leads to an increase in the absorption in the visible region as well as the absorption intensity of the WO_3@ g-C_3N_4 @MWCNT photocatalyst and is effective in narrowing the band gap of the photocatalyst and producing more charge carriers. WO_3@ g-C_3N_4 @MWCNT photocatalyst generates electrons and holes after being activated by light. The electrons generated in the conduction band of WO_3 are transferred to the valence band of g-C_3N_4. The conduction band level of WO_3 is the same as the valence band of g-C_3N_4, so the holes generated by the g-C_3N_4 photocatalyst recombine with the electrons generated by the WO_3 photocatalyst, and simultaneously, the electrons in the conduction band of the g-C_3N_4 photocatalyst participate in the antibiotic removal process. The holes in the valence band of the WO_3 photocatalyst contribute to the oxidation of the pollutant. The presence of MWCNT, due to its negative work function (-4.95 eV vs. vacuum), traps electrons in the conduction band of WO_3, thus allowing electrons to be easily transported and preventing electron-hole recombination. MWCNT acts as a bridge for charge transfer and separation between the g-C_3N_4 photocatalyst and WO_3.The removal rate in visible light with halogen lamp 500 W, 420 nm, 0.2g/L photocatalyst in 20 mg/L of tetracycline in 120 minutes in the presence of pure WO_3 photocatalyst is 41.03%, this rate is 59.23% and 79.54% for WO_3@ g-C_3N_4 photocatalyst and WO_3@ g-C_3N_4 @MWCNT photocatalyst, respectively. The $K_{app} = 0.0861 min^{-1}.g^{-1}$. L is apparent rate constant for the WO_3@ g-C_3N_4 @MWCNT photocatalyst[167]. Lu et al. [168] used Ag_3PO_4/AgBr/g-C_3N_4 photocatalyst with dual Z-scheme heterojunction for the removal of tetracycline. The synthesis method of Ag_3PO_4, AgBr and g-C_3N_4 photocatalysts are facile chemical deposition method. Photocatalyst Ag_3PO_4 It is an excellent photocatalyst in the removal of organic pollutants in the presence of visible light. Silver halides are light-sensitive materials and lead to an increase in

photocatalytic activity and also lead to an increase in adsorption capacity in the visible region. In fig24(a), for three photocatalysts g-C_3N_4, AgBr and Ag_3PO_4 two mechanisms of conventional and Z heterojunction are proposed. In Figure 24a, the electrons produced in the conduction band of g-C_3N_4 are transferred to the conduction band of AgBr and then to the conduction band of Ag_3PO_4, and the holes produced in the valence band of Ag_3PO_4 are transferred to the valence band of AgBr and finally to the valence band of g-C_3N_4. As a result, electrons and holes accumulate on Ag_3PO_4 and g-C_3N_4, respectively. Neither the electrons in Ag_3PO_4 nor the holes in g-C_3N_4 are capable of producing reactive species such as $O_2^{-\cdot}$ and $OH^{\cdot}$ because the conduction band of Ag_3PO_4 is more positive than $O_2/O_2^{-\cdot}$ (−0.046 e). The g-C_3N_4 valence band is more negative than the $H_2O/OH^{\cdot}$ potential (2.72 eV). Therefore, $O_2^{-\cdot}$ and $OH^{\cdot}$ radicals cannot be produced in a conventional heterojunction, and this mechanism is ineffective with these photocatalysts. In Fig24(b) in the z mechanism, Ag^+ in Ag_3PO_4 and AgBr photocatalysts is reduced to metallic Ag, which is used as an electron transfer mediator to facilitate electron-hole recombination. In the z mechanism, Ag^+ in Ag_3PO_4 and AgBr photocatalysts is reduced to metallic Ag, which is used as an electron transfer mediator to facilitate electron-hole recombination. The electron produced in the conduction band of AgBr is transferred to the metallic Ag and combines with the holes produced in the valence band of g-C_3N_4, in addition, the electrons in the conduction band of Ag_3PO_4 recombine with the holes in the valence band of AgBr through the metallic Ag, which leads to effective electron-hole separation. The electrons in the g-C_3N_4 conduction band is not more positive than the potential of O_2 to $O_2^{-\cdot}$ and the holes in the valence band of Ag_3PO_4 are not more negative than the potential of H_2O to $OH^{\cdot}$. As a result, $O_2^{-\cdot}$ and $OH^{\cdot}$ are produced and this mechanism is effective in removing tetracycline. The removal rate 40mg/L tetracycline in visible light with 300 W Xe lamp with 160 mW.cm^{-2} , 0.5g/L photocatalyst in 25 minutes in the presence of pure Ag_3PO_4 photocatalyst is about 62%, for Ag_3PO_4/0.6AgBr is about 70% while this rate reaches 80.2% in the presence of Ag_3PO_4/AgBr/ g-C_3N_4 photocatalyst with a mass ratio of g-C_3N_4 to Ag_3PO_4 : 20%.The K_{app} =

$0.24 \text{min}^{-1}.\text{g}^{-1}$. L is apparent rate constant photocatalyst with an optimal amount of a mass ratio of g-C_3N_4 to Ag_3PO_4 : 20% for the Ag_3PO_4/AgBr/ g-C_3N_4 photocatalyst[168].

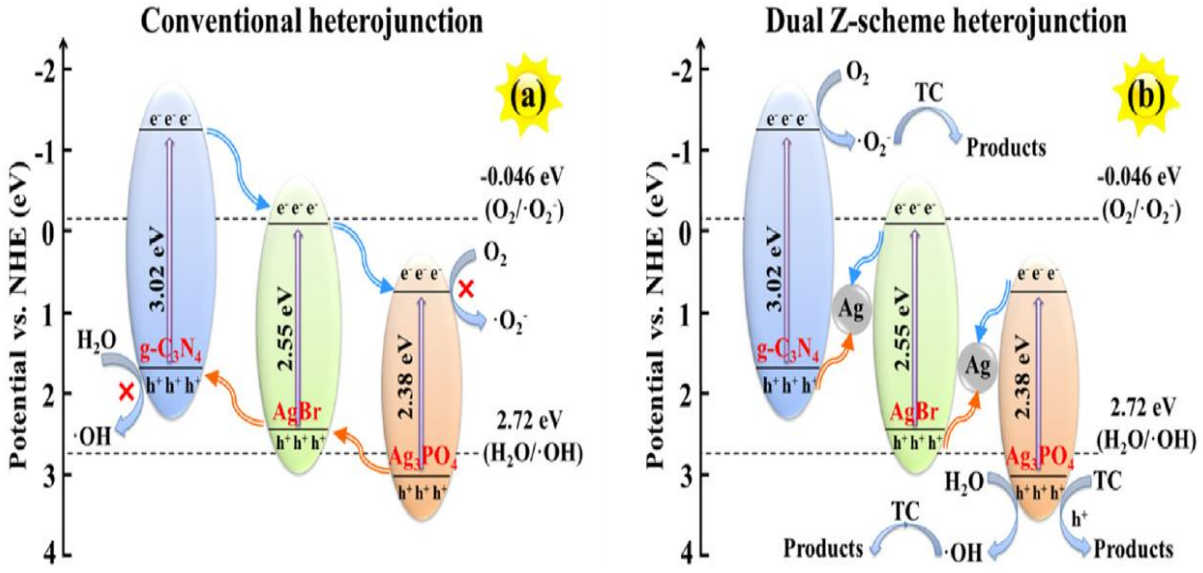

Fig.24- Photocatalytic mechanism of Ag_3PO_4/AgBr-g-C_3N_4: (a) conventional heterojunction; (b) dual Z-scheme heterojunction[169].

Malinga et al. [170]. used g-C_3N_4/Nb_2O_5 / HPEI/PES photocatalytic membrane for tetracycline removal. The synthesis method of g-C_3N_4/Nb_2O_5 / HPEI/PES photocatalysts is in-situ hydrothermal method. Niobium oxide photocatalyst (Nb_2O_5) is a photocatalyst with a bandgap of 3.2 eV, low toxicity, high acidity level, high specific surface area and excellent performance in removing organic pollutants, including antibiotics. To overcome this limitation, g-C_3N_4 with a band gap of 2.7 eV has been used in a heterojunction. Although absorption occurs in the visible region in this two-dimensional structure, the formation of this structure leads to the non-dispersion of Nb_2O_5 on the g-C_3N_4 layers. hyperbranched polyethyleneimine (HPEI) has amine groups as ligands for connecting nanoparticles, and its structure consists of shells that prevent the aggregation of nanoparticles and lead to improved photocatalytic activity. Polyethersulfone (PES) polymer matrix, due to its mechanical and chemical stability used as a photocatalytic membrane[171]. In fig25, the conduction band potential of

heterostructures (-0.67 ev) is lower than the reduction/oxidation potential of O_2/ O_2- (-0.35 ev), also valence band potential is more positive (2.5 ev) than the redox potential of H_2O/OH- (1.23 ev). When g-C_3N_4/Nb_2O_5 photocatalyst is activated by visible light, the electrons produced in the conduction band are transferred to O_2 molecules, and a superoxide radical is produced. The holes created in the valence band participate in the generation of hydroxyl radicals that increase the degradation of tetracycline over redox potentials. Since both g-C_3N_4/Nb_2O_5 are n-type semiconductors, the upward bending of the edges limits the recombination of g-C_3N_4 electrons with Nb_2O_5 holes, which is expected in a Z-scheme heterojunction. The presence of HPEI improves the removal rate due to the presence of holes that play the role of the catalytic site and are a favorable place for photocatalytic interaction with tetracycline. The suitable separation structure and strong absorption in the visible light range are the characteristics of the Z-scheme g-C_3N_4/Nb_2O_5 composite membrane photocatalyst. The membrane is also effective in visible light absorption and charge separation efficiency. The removal rate in 5mg/L tetracycline in 50 W visible light**,** 180minutes the presence of pristine PES is 68%, while the removal rate in 0.3% g-C_3N_4/ Nb_2O_5/HPEI in pristine PES is 88%. In this article, the photocatalyst is on a polymer membrane and since it is not soluble, the photocatalyst concentration in milligrams per liter is not available, so it is not possible to calculate the normalized apparent rate. The $K_{app} = 4.5 \times 10^{-4} min^{-1}$ is apparent rate constant with an optimal amount of 0.3% g-C_3N_4 for the g-C_3N_4/ Nb_2O_5/HPEI in pristine photocatalyst[170].

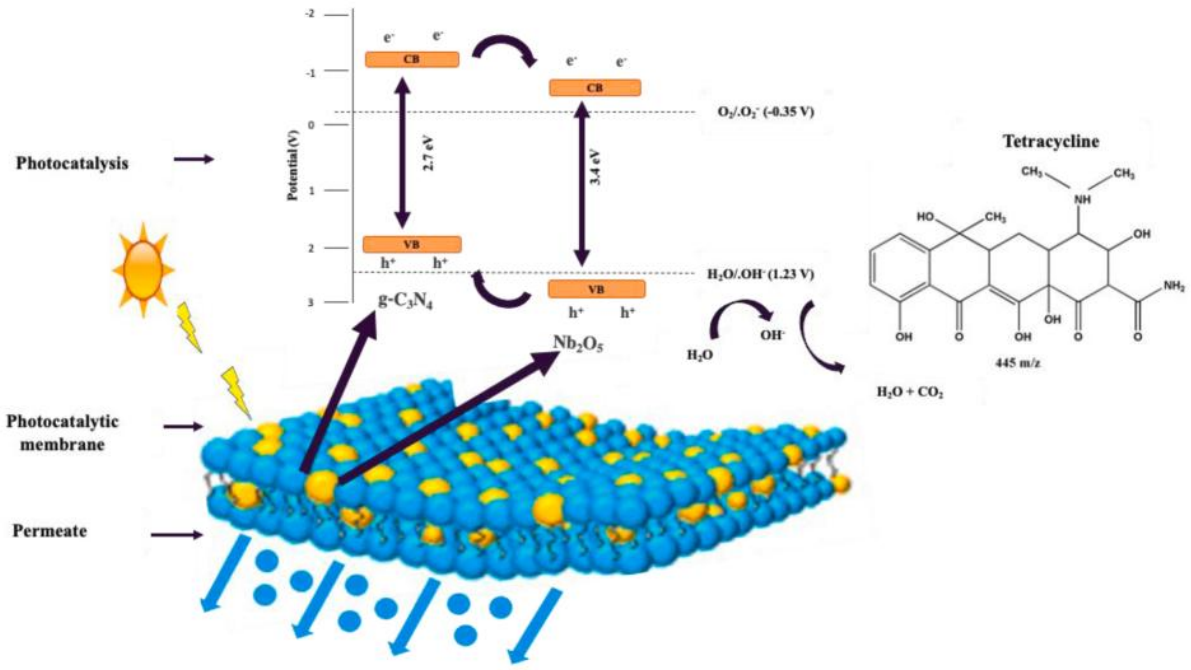

Fig.25- photocatalytic degradation of tetracycline[170].

Kai Yan et al. [172] used a Z-scheme composite of TiO_2 nanorod/g-C_3N_4 nanosheet photocatalyst for the removal of ciprofloxacin. considering that TiO_2 photocatalyst is non-toxic, stable and cheap[173–175], but its weak response in the range of visible light and electron-hole recombination has led to the limitation of this method[176–178]. TiO_2 nanorod has a high dimension ratio. The use of graphene carbon nitride as the reason for the limited Band Gap, its high thermal and chemical stability and its good performance in removing organic pollutants have been considered. Doping the TiO_2 photocatalyst with graphene carbon nitride has led to the widening of the visible light range and better electron-hole separation[179–182]. This photocatalyst shows a shorter penetration path and a freer path for charge transfer. The advantages of electron conservation and one-way transfer are very clear for charge transfer, so it prevents electron-hole recombination and increases separation and charge transfer. The optimum pH is 6.3 and at pH less than 6.3, due to electrostatic forces between the drug and the photocatalyst, preventing the removal of the drug. Also, at a pH greater than 6.3, due to the electrostatic attraction between the drug and the photocatalyst leads to an increase in the photocatalytic activity. The electrostatic repulsion between the drug and the photocatalyst intensifies with increasing pH, resulting in a reduction in the amount of removal. Compared with TiO_2, the TiO_2 nanorod/g-C_3N_4 nanosheet photocatalyst shifts towards the 450–500 nm red wavelength range and is able to be activated by visible

light and shows significant additional absorption in the 450 nm region. The composites with different amounts of g-C_3N_4 show significant additional absorption in the 450 nm region. After the activation of the g-C_3N_4 / TiO_2 photocatalyst in equations 70-77, the holes formed in the TiO_2 photocatalyst is transferred to the g-C_3N_4 photocatalyst and the electrons generated from the g-$C_3N_4$are transferred to TiO_2. The valence band of the g-C_3N_4 (+1.54 eV) is lower than the standard redox potentials of **.**OH/OH- and OH/H_2O, which are +1.99 eV and +2.38 eV, respectively. As a result, the holes of the g-C_3N_4 photocatalyst are unable to produce **.**OH from the oxidation process of OH- and H_2O in the conventional heterojunction structure. h+ and **.**OH plays a role in the removal of antibiotics **.**OH is most likely formed through the oxidation of OH- and H_2O by h+ in the E_{VB} of the TiO_2 nanorods (+2.94 eV). Therefore, the heterojunction structure is Z. In fact, in the Z-scheme structure, unlike the conventional heterojunction, holes remain in TiO_2, which have a higher potential (+2.94 eV) and can easily generate active species (such as ·OH) [172]. The electrons present in the g-C_3N_4 photocatalyst react with oxygen to form the radical O_2**-.** , and the holes in TiO_2 react with water molecules to produce **.**OH. Finally, these active species are converted into CO_2, H_2O, F^-, and NO_3^-[172].

$$TiO_2 \text{ nanorod/ g-}C_3N_4 + h\nu \rightarrow TiO_2 \text{ nanorod } (h^+, e^-)/ \text{ g-}C_3N_4\ (h^+, e^-) \quad (70)$$

$$TiO_2 \text{ nanorod } (h^+, e^-)/ \text{ g-}C_3N_4\ (h^+, e^-) \rightarrow TiO_2 \text{ nanorod } (h^+) + \text{g-}C_3N_4\ (e^-) \quad (71)$$

$$\text{g-}C_3N_4\ (e^-) + O_2 \rightarrow \cdot O_2^- \quad (72)$$

$$\cdot O_2^- + 2H^+ \rightarrow H_2O_2 \quad (73)$$

$$H_2O_2 + g\text{-}C_3N_4\ (e^-) \rightarrow \cdot OH + OH^- \quad (74)$$

$$H_2O + TiO_2\ \text{nanorod}\ (h^+) \rightarrow \cdot OH + H^+ \quad (75)$$

$$OH^- + TiO_2\ \text{nanorod}\ (h^+) \rightarrow \cdot OH \quad (76)$$

$$h^+/\cdot OH/\cdot O_2^- + CIP \rightarrow \text{Intermediates} \rightarrow CO_2 + H_2O + F^- + NO_3^- \quad (77)$$

The removal rate of 6.63mg/L ciprofloxacin in visible light with a 500W Xenon lamp, 0.2g/L photocatalyst in 120 min for g-C_3N_4 photocatalyst was about 30%, for TiO_2 photocatalyst powder about 68%, and for TiO_2 nanorod-CN (mass ratio of g-C_3N_4 %, 30 wt%) about 92%. The $K_{app} = 0.183 \text{min}^{-1}.\text{g}^{-1}$. L is apparent rate constant with 30 wt% mass ratio of g-C_3N_4 for the TiO_2 nanorod/g-C_3N_4 photocatalyst[172]. Hu et al. [183] used the SnS_2@$ZnIn_2S_4$@kaolinite photocatalyst to remove the antibiotic tetracycline hydrochloride. The synthesis method of SnS_2@$ZnIn_2S_4$@kaolinite photocatalysts is the hydrothermal method. $ZnIn_2S_4$ photocatalyst is a ternary metal sulfide semiconductor that is activated due to the suitable band gap in the visible light range. Tin disulfide (SnS_2) has a band gap of 2.35 eV, which is capable of absorbing visible light. This photocatalyst is non-toxic, cheap, and has visible light responsiveness. This photocatalyst is only susceptible to photo-corrosion and has the problem of electron-hole separation. SnS_2@$ZnIn_2S_4$ heterojunction leads to charge separation and improved photocatalytic activity. To improve the recyclability and performance of photocatalysts, natural non-metallic minerals are often used as carriers to disperse photocatalysts, due to their wide availability, low cost, synergistic effect, and ease of recovery. Kaolinite ($Al_2Si_2O_5(OH_4)$) is an abundant mineral that contains the aluminosilicate structure is a layer which facilitates the dispersion of nanocatalysts to achieve better performance. As shown in fig.26, after the

SnS_2@$ZnIn_2S_4$ @kaolinite photocatalyst is activated by visible light, the electrons generated in the conduction band of the $ZnIn_2S_4$ photocatalyst recombine with the holes in the valence band of the SnS2 photocatalyst, resulting in the holes in the valence band of the $ZnIn_2S_4$ photocatalyst and the electrons in SnS_2 being separated. The electron potential in the conduction band of SnS_2 is 0.43 eV (vs. NHE) because it is more negative than the O_2/•O_2- potential (0.33 eV vs. NHE), it is able to generate the •O_2 radical from oxygen, which reacts directly with tetracycline hydrochloride. Also, some electrons attack tetracycline hydrochloride. The holes in the valence band of $ZnIn_2S_4$ have a potential of 2.07 eV and are able to oxidize oxygen to O_2/$1O_2$ (1.88 eV vs. NHE).$1O_2$ is able to oxidize tetracycline hydrochloride to intermediates and CO_2 and H_2O. The removal rate in 40 mg/L of tetracycline hydrochloride in visible light with 300 W xenon lamp with a 420 nm cut-off filter, 0.2g/L photocatalyst in 60 minutes for pure kaolinite is 2.24%, this rate is about 18% for pure SnS_2 photocatalyst, while it is about 43% for pure $ZnIn_2S_4$ photocatalyst, and finally for SnS_2@ $ZnIn_2S_4$@kaolinite photocatalyst with SnS_2/ $ZnIn_2S_4$ wt%: 0.75:1, The removal rate is 88.23%. The $K_{app} = 0.1155 min^{-1}.g^{-1}.L$ is apparent rate constant with mass ratio of SnS_2/ $ZnIn_2S_4$ wt%: 0.75:1 for the SnS_2@$ZnIn_2S_4$ @kaolinite photocatalyst[183].

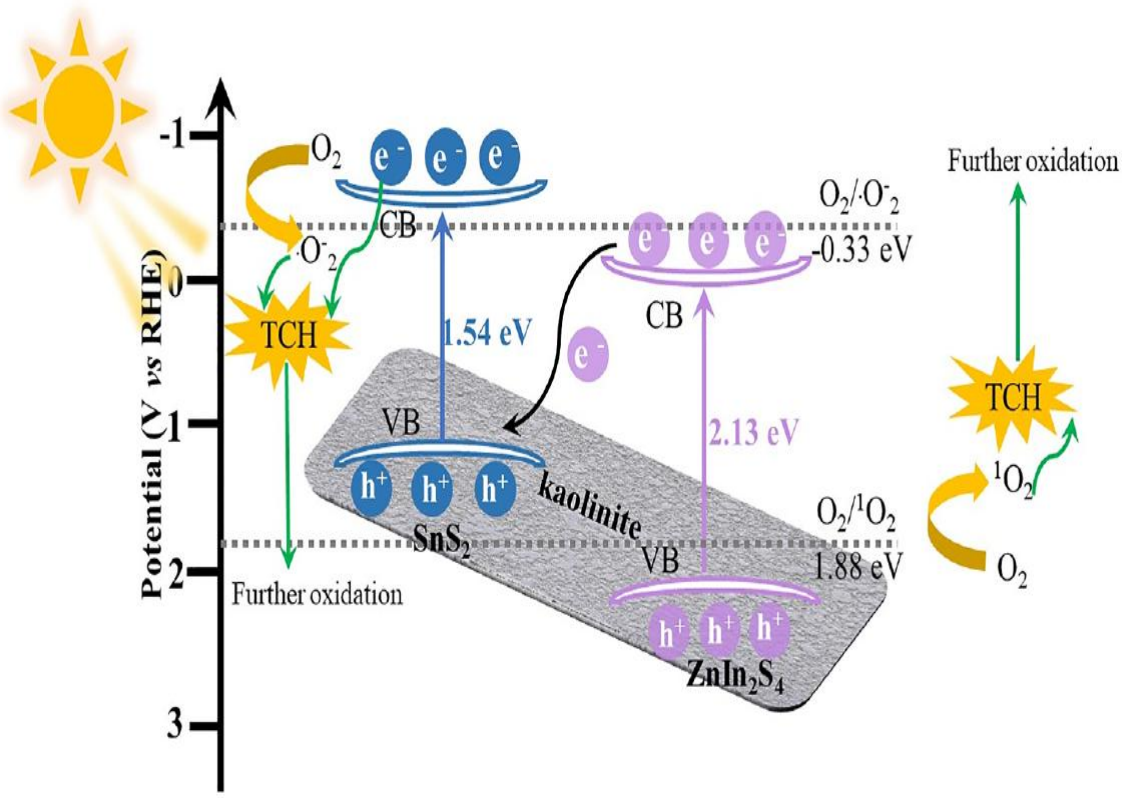

Fig.26-Photocatalytic mechanism of SnS_2@$ZnIn_2S_4$ @kaolinite heterojunction structure for the removal of tetracycline hydrochloride[184].

Tian et al. [185] used the Z-scheme 2D/3D g-C_3N_4@ZnO photocatalyst for the removal of the antibiotic cephalexin. The synthesis method of g-C_3N_4@ZnO photocatalyst is a thermal atomic layer deposition method. As a polymer semiconductor, g-C_3N_4has a limited band gap of 2.7ev, and it has relatively high photocatalyst activity and stability. This polymer is easily compatible with other catalysts. The aggregation of nanoparticles is one of the disadvantages of g-C_3N_4 photocatalyst[186]. The use of ZnO, which is an n-type inorganic semiconductor with high quantum efficiency, low cost, and environmental compatibility[185,187]. When the ZnO layer on the surface of g-C_3N_4 is placed, leading to an increase in the specific surface area of the catalyst, an increase in photocatalytic activity through a decrease in aggregation and an increase in oxidation potential. It also leads to an increase in the active sites for antibiotic absorption and higher zeta potential of the surface Z-scheme g-C_3N_4@ZnO leads to an increase in the attraction between the photocatalyst and the drug,

and as a result, the molecules are easily absorbed[185]. After the Z-scheme 2D/3D g-C_3N_4@ZnO photocatalyst is activated by light, electrons are transferred from the valence band of g-$C_3N_4$and ZnO to the conduction band of the photocatalysts, resulting in holes remaining in the valence band. The valence band potential of the photocatalysts (1.58 V) and ZnO (2.64 V) is 2.27 V, which is between the potentials of the two photocatalysts. Therefore, it is natural that OH radicals are generated on the valence band of the ZnO photocatalyst through the oxidation of water by holes (Equation 2), but cannot be generated on the valence band of g-C_3N_4. Due to the more negative CB edge potential of g-C_3N_4 (−1.17 V) compared to the standard O2/$-O_2$**.** redox potential (−0.33 V), O_2 is converted to $-O_2$**.** only in the conduction band of the g-C_3N_4 photocatalyst. The electron-hole transfer generated by light does not follow the traditional double charge law. Electrons in the conduction band of ZnO photocatalyst are transferred by the potential difference (1.64 V) as the driving force of the valence band of g-C_3N_4 photocatalyst, and electrons remain in the conduction band of g-C_3N_4 and holes in the valence band of ZnO photocatalyst (Equation (78)). As a result, the 2D/3D g-C_3N_4@ZnO is determined as a Z-type photocatalyst. The holes in the valence band of ZnO can react with cephalexin directly (Equation (79)) or react with water to produce active species OH (Equation (80)). The electron in the conduction band of g-C_3N_4 reacts with oxygen to form $-O_2$**.** radicals (Equation (81)). With further reaction between $-O_2$**.** and e−,·OH is also produced (equations (82) and (83)). The ·OH and $-O_2$**.** radicals that were formed later also contributed to the decomposition of cephalexin (equations (84) and (85)) [185].

$$g - C_3N_4@ZnO + hv \rightarrow h^+(ZnO) + e^-(g - C_3N_4) \quad (78)$$

$$h^+(ZnO) + \text{cephalexin} \rightarrow \text{products} \quad (79)$$

$$h^+(ZnO) + H_2O \rightarrow OH^{\cdot} + H^+ \quad (80)$$

$$e^{-}(g-C_3N_4)+O_2 \rightarrow O_2^{-\cdot} \quad (81)$$

$$O_2^{-\cdot}+e^{-}+2H^{+} \rightarrow H_2O_2 \quad (82)$$

$$H_2O_2+e^{-} \rightarrow OH^{\cdot}+OH^{-} \quad (83)$$

$$O_2^{-\cdot}+\text{cephalexin} \rightarrow \text{products} \quad (84)$$

$$OH^{\cdot}+\text{cephalexin} \rightarrow \text{products} \quad (85)$$

The removal rates of the antibiotic cephalexin with initial concentrations of 10 mg/L and in solar light with Xenon lamp (300 W), 0.3g/L photocatalyst in 60 minutes without photocatalyst, g-C_3N_4, ZnO and g-C_3N_4@ZnO are 5.8%, 58.4%, 45.3% and 98.9%, respectively. The apparent rate constant for the g-C_3N_4@ZnO photocatalyst is $K_{app} = 0.245 min^{-1}.g^{-1}.L$. The g-$C_3N_4$@ZnO structure leads to an increase in removal rate of 53.6% and 40.5% compared to ZnO and g-C_3N_4 photocatalysts, respectively[185]. Ding et al. [188] used a magnetic dual Z-scheme $BiVO_4$/ g-C_3N_4/$NiFe_2O_4$ photocatalyst for the removal of ofloxacin. $BiVO_4$/ g-C_3N_4/$NiFe_2O_4$ photocatalyst has been used in the removal of ofloxacin. $BiVO_4$ has been considered due to its ineffectiveness, non-toxicity and band gap of 2.4ev. However, due to fast electron and hole recombination, weak quantum function and weak response in the visible light range, its use has been limited. Among the different photocatalysts, g-C_3N_4 a semiconductor is a suitable option to be combined with $BiVO_4$ due to its high specific surface area, suitable chemical performance and suitable electronic structure of the band. Reusing the photocatalyst and recovering it on a nanoscale in aqueous environments

becomes a challenge and prevents it from being used on a large scale. To solve this problem, magnetic Fe_3O_4 It is used together with a catalyst. and reducing the performance of the photocatalyst. $NiFe_2O_4$ It is an attractive magnetic material with a band gap of 1.7ev and has a very good response in the visible light range and does not have the limitations of Fe_3O_4. After the $BiVO_4$/ g-C_3N_4/$NiFe_2O_4$ photocatalyst was activated by light in a conventional heterojunction structure, electrons in the conduction band of g-C_3N_4 and $NiFe_2O_4$ were transferred to $BiVO_4$, while holes were transferred in the opposite direction to the valence band. The electrons were unable to generate O_2- radicals from oxygen because the conduction band potential of $BiVO_4$ (+0.46 eV) was lower than the O_2/•O_2- redox potential (-0.33 eV). The oxidation-reduction potential of •OH/H_2O (+2.27 eV) as well as •OH/$OH-$ (+1.99 eV) is lower than the valence band potential of g-C_3N_4 (+1.60 eV) and $NiFe_2O_4$ (+1.07 eV), which leads to insufficient capacity of the professions in producing •OH. Therefore, the conventional heterojunction structure is unable to produce •OH and •O_2-. After activation, the electrons in the conduction band of $BiVO_4$ and the holes in the valence band of g-C_3N_4 and $NiFe_2O_4$ occurred in a direct double Z-pattern. The migration speed of electrons is higher than that of holes. As a result, the holes in the valence band of $BiVO_4$ and the electrons in the conduction band of g-C_3N_4 and $NiFe_2O_4$ can provide effective separation under the assumption of a direct Z-pattern structure. The oxidation-reduction potential of •OH /H_2O and •OH/$OH-$ of the valence band of $BiVO_4$ photocatalyst (+2.87 eV) is higher than that of holes to produce •OH. The O_2/•O_2- redox potential has a higher position compared to the conduction band electrons of g-C_3N_4 (-1.14 eV) and $NiFe_2O_4$ (-0.57 eV), which leads to the generation of •O_2- radicals from oxygen and can even be further oxidized by holes to $1O_2$. The Z-design heterojunction resulted in better charge separation and stronger oxidation and reduction capacity. The removal rates of the antibiotic ofloxacin with an initial concentration of 10 mg/L in visible light with 300 W Xenon lamp with the filter ($\lambda >$ 420 nm),1g/L photocatalyst for $NiFe_2O_4$ and g-C_3N_4 photocatalysts in 60 min are 9% and 28%, respectively. For pure $BiVO_4$, the removal rate is 70% in 30 min. For the $BiVO_4$/ g-C_3N_4/$NiFe_2O_4$ photocatalyst with a mass fraction of 5% g-C_3N_4 in $BiVO_4$/g- C_3N_4, it is 93.8% in 20 min. The

$K_{app} = 0.1353 min^{-1}.g^{-1}.L$ is the apparent rate constant for the $BiVO_4$/ g-C_3N_4/$NiFe_2O_4$ photocatalyst[188]. Wang et al. [189] used a direct Z-scheme g-C_3N_4/CdS photocatalyst to remove the antibiotic erythromycin. The synthesis method of Bulk g-C_3N_4 photocatalyst is thermal polymerization method, the synthesis method of CdS nanorods photocatalyst is solvothermal method, and the synthesis method of g-C_3N_4/CdS photocatalyst is chemisorption and self-assembly method. g-C_3N_4 photocatalyst despite having a limited band gap of 2.7ev, which is easily activated in the visible light range. It has chemical and thermal stability and unique electronic properties, but the the low specific surface area and fast electron-hole recombination and the weak quantum efficiency has led to the limitation of the use of this photocatalyst. Therefore, a photocatalyst is needed that, in addition to preventing electron-hole recombination, also leads to an increase in the absorption limit. CdS having a limited band gap of 2.4ev leads to an increase in the amount of absorption in the visible region. Due to its instability, the S^{2-} ion easily produces oxide with the created hole, so the electron-hole recombination leads to the weakening of the photocatalyst performance. Also, the rapid transfer of the hole created in the valence band effectively prevents optical corrosion and stabilizes the photocatalyst. Fortunately, by comparing the valence band of CdS and g-C_3N_4 photocatalysts, it is clear that these two photocatalysts have a good overlap, on the other hand, The heterogeneous structure leads to the rapid separation of the generated electron-hole and, as a result, leads to an increase in the photocatalytic performance. The combination of these two photocatalysts leads to the improvement of the photocatalytic performance of both photocatalysts. Since CdS and g-C_3N_4 photocatalysts have narrow band gaps; upon activation by light, electrons and holes are generated. The holes generated in the valence band of the g-C_3N_4 photocatalyst are doubly recombined with electrons generated in the conduction band of the CdS photocatalyst. The electrons generated in the conduction band of the g-C_3N_4 photocatalyst have a more negative potential (-1.12 eV) than the standard O_2/$\cdot O_2^-$ redox potential (-0.33 V vs. NHE) and are prone to react with oxygen and produce $\cdot O_2^-$ radicals. The valence band of CdS photocatalyst (1.94 eV) is lower compared to the $\cdot OH/H_2O$ potential (2.68 eV vs. NHE). As a

result, the holes generated in the valence band of CdS photocatalyst cannot react with H_2O to produce **.**OH, but can react with antibiotics to produce carbon dioxide, water, and other small inorganic molecules. The ultrathin nanosheet structure of g-C_3N_4 reduces the distance of the generated carriers to the interface, which leads to reduced electron-hole recombination. The removal rates of erythromycin antibiotic with an initial concentration of 50 mg/L, visible light with a 35W Xenon lamp, a stable wavelength of 300–2500 nm, 0.5g/L photocatalyst and a time of 60 min for g-C_3N_4, CdS, and g-C_3N_4/CdS photocatalysts with nominal mass ratios of g-C_3N_4/CdS 3:1 are 49.09%, 55.12%, and 81.02% at pH 5, respectively. The g-C_3N_4/CdS heterojunction structure increases removal rates of 31.93% and 25.9% compared to g-C_3N_4 and CdS photocatalysts, respectively. The $K_{app} = 0.056 min^{-1}.g^{-1}.L$ is the apparent rate constant with mass ratios of g-C_3N_4/CdS 3:1 for the g-C_3N_4/CdS photocatalyst[189].

While numerous heterojunction photocatalysts have been described as operating through Z-scheme charge-transfer pathways, establishing the true direction of electron–hole migration remains a non-trivial task and requires careful interpretation of experimental evidence. Several characterization strategies have therefore been employed to probe this mechanism, although each provides only partial insight. Electron paramagnetic resonance (EPR) using spin-trapping agents such as 5,5-dimethyl-1-pyrroline-N-oxide (DMPO) is widely used to identify reactive oxygen species including $\cdot O_2^-$ and ·OH [190–192]. In many reported Z-scheme systems, the simultaneous formation of strong oxidation and reduction radicals is interpreted as indirect evidence that highly oxidative holes and strongly reducing electrons are preserved on different components of the heterostructure. Nevertheless, radical detection alone cannot unequivocally confirm a Z-scheme pathway, since similar species may also arise in type-II heterojunctions or through secondary interfacial reactions. In situ irradiation X-ray photoelectron spectroscopy (XPS) provides complementary information by monitoring light-induced shifts in binding energies, which can reveal charge redistribution between coupled semiconductors. However, the surface sensitivity of XPS and the vacuum environment of the measurement may limit its ability to fully represent photocatalytic processes occurring at solid–liquid interfaces [191,193,194]. Photodeposition experiments, in which noble metal ions are selectively reduced at electron-rich sites, have also been employed to map reduction

centers and infer charge-transfer routes. Yet the deposition process can be affected by surface defects, adsorption behavior, and kinetic factors that complicate mechanistic interpretation. Consequently, convincing identification of Z-scheme photocatalysis typically relies on the combined analysis of these techniques together with band-structure evaluation and photocatalytic performance trends, rather than on any single experimental method alone [193,195].

5-5-METAL/SEMICONDUCTOR SCHOTTKY JUNCTION

As shown in fig.27, the loading of metal nanoparticles on the surface of semiconductor nanoparticles is called heterojunction between metal and semiconductor, which leads to the removal of limitations such as: reduction of carrier recombination by increasing charge separation, covering a wide range of light ranges, increasing selectivity towards the destruction of specific pollutants and acting as a trapping center to increase carrier life[196].

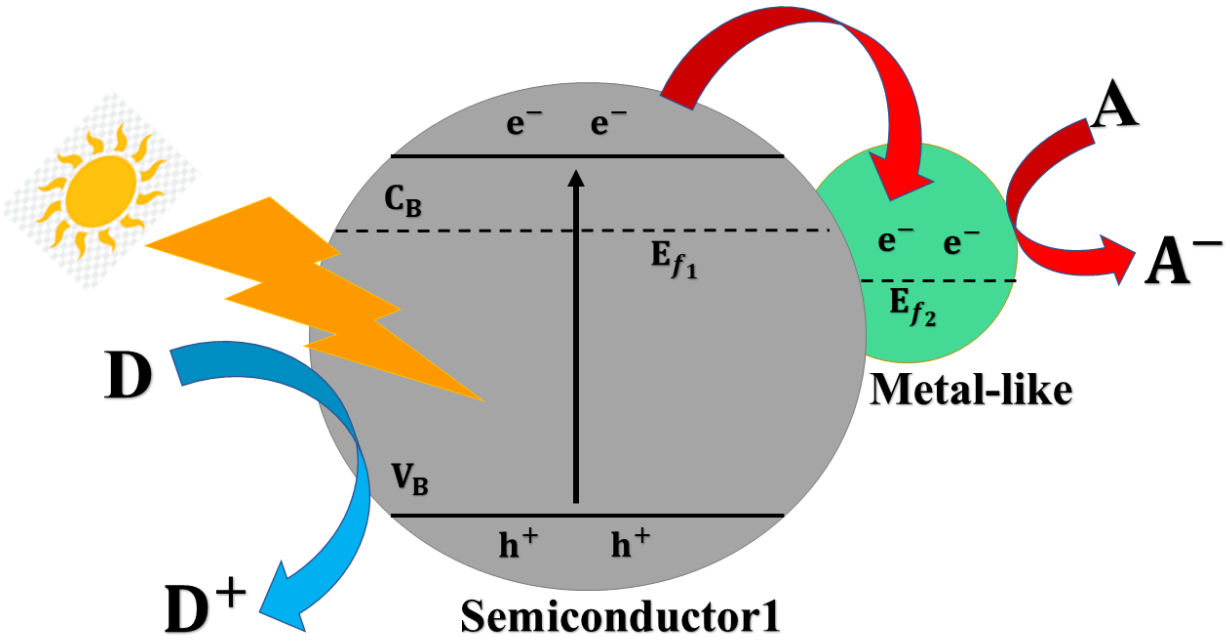

Fig.27- Schematic figure of Schottky junction [130].

5-6-INTEGRATING HETEROJUNCTION STRUCTURE WITH GRAPHENE-BASED CONDUCTIVE NETWORKS

Zhu, Guo et al. [197] used BiOI/ZnO/rGO photocatalyst to remove chloramphenicol. The synthesis method is a simple one-step hydrothermal. Zinc oxide photocatalyst with a band gap of 3.37 eV and a higher exciton binding energy (60 meV) and ease of fabrication in various forms has been considered in the removal of antibiotics, but due to the rapid charge recombination and the settled band structures, its application is limited. The improvement of charge carrier density, increase in optical current conductivity and effective electron-hole separation can be mentioned as the effect of rGO on BiOI/ZnO photocatalyst. Also, rGO prevents the aggregation of BiOI and ZnO. The presence of rGO reduces light reflection and helps to enhance light absorption. However, the excessive use of rGO leads to excessive graphene aggregation, which reduces the efficiency of the photocatalyst. In fact, the excessive presence of rGO occupies the active sites of ZnO and prevents sufficient light from reaching the photocatalyst [197]. Zinc oxide photocatalyst with a band gap of 3.37 eV and a higher exciton binding energy (60 meV) and ease of fabrication in various forms has been considered in the removal of antibiotics, but due to the rapid charge recombination and the settled band structures, its application is limited. The combination of p-type BiOI photocatalyst with n-type ZnO photocatalyst, which forms a p-n heterojunction structure, which leads to the creation of an internal electric field and electron-hole separation and continuous surface charge transfer, and the performance of BiOI/ZnO photocatalyst from ZnO and BiOI is as follows The main role of graphene in this composition is not only to inhibit the accumulation, improve the specific surface area and the possibility of effective absorption of pollutants, but also to delocalize the photogenerated electrons via its π network and finally delay the recombination rate of the carrier. The carrier density of BiOI/ZnO/rGO with a mass fraction of rGO of 5 is approximately doubled compared to BiOI/ZnO, indicating that the electron density is increased in the presence of graphene oxide. The BiOI/ZnO/rGO photocatalyst has a red shift after the addition of GO, which is due to the reduction in light reflection and the improvement in light absorption. Electrons

in the ZnO photocatalyst are transferred to the BiOI photocatalyst, leading to the accumulation of negative charge on the BiOI particle. Holes are transferred from the BiOI photocatalyst to the ZnO photocatalyst, creating a positive region in the ZnO. After charge separation, an electrostatic field directed by ZnO to BiOI is generated, so that electrons generated by visible light irradiation flow from the conduction band of BiOI to ZnO, leaving holes in the valence band. The conduction band potential is more reducing than the potential of the O_2 species (O_2 / O_2**.**, -0.28 eV), while the valence band potential of BiOI/ZnO/rGO is more oxidizing than the potential of the OH species (**.**OH/H_2O, +2.27 eV). As a result, electrons and holes easily convert H_2O and O_2 to OH ·, **.**O_2. Compared to the conduction band of BiOI/ZnO, the potential of rGO (rGO/rGO·, -0.08 eV) has a smaller decrease, enabling rGO to effectively receive photoactivated electrons from the BiOI/ZnO heterojunction. The removal rate of chloramphenicol with an initial concentration of 10 mg/L in 300 W Xenon lamp as the visible light source without any cutting filter and a reaction time of 180 min with 0.5g/L BiOI/ZnO/rGO photocatalyst is about 31%, about 72%, about 78%, and about 90% for BiOI, ZnO, BiOI/ZnO, and BiOI/ZnO/5%wt rGO (BZG5) photocatalysts, respectively. The apparent rate constant of the BZG5 photocatalyst is $K_{app} = 0.0306 min^{-1}.g^{-1}.$L. In summary, it can be said that the heterojunction structure helps in charge separation by creating an electric field, and the graphene structure as an adsorbent leads to an increase in the specific surface area[198]. Nguyen et al[199] used WO_3/AgI heterojunction photocatalyst decorated on rGO to remove the antibiotic amoxicillin. Amoxicillin is a beta-lactam antibiotic. After the photocatalyst is activated by visible light, electrons in WO_3 and AgI photocatalysts are transferred from the valence band to the conduction band, leaving holes in the valence band. The electrons in the conduction band react with oxygen to produce superoxide radicals(**.**O_2-). **.**O_2- reacts with water to produce hydroxyl radical (•OH), which is used to remove amoxicillin. The holes also react with water to produce hydroxyl radical (•OH) or directly react with the antibiotic amoxicillin. Compared with single photocatalysts, in WO_3/AgI photocatalyst, due to the Z scheme heterojunction, the electron in the conduction band of WO_3 photocatalyst recombines

with the holes in AgI photocatalyst, which leads to the reduction of electron-hole recombination. Therefore, the Z scheme heterojunction structure leads to the creation of significant holes and electrons in the valence band of WO_3 photocatalyst and in the conduction band of AgI photocatalyst, respectively. As a result, these charges have a high oxidation-reduction ability for the photocatalyst reaction compared with single WO_3 and AgI photocatalysts. The rGO structure in WO_3/AgI photocatalyst, as an electron transfer medium, leads to the efficient transfer of electrons from the conduction band of WO_3 photocatalyst to the valence band of AgI photocatalyst due to the folded three-dimensional π-conjugated structure, leading to the improvement of charge separation. Also, rGO leads to an increase of 71.39 m2/g of the specific surface area of rGO/ WO_3/AgI photocatalyst compared to WO_3/AgI photocatalyst. The removal rates under visible light with a 30W LED lamp and 0.5g/L photocatalyst with an initial concentration of 20mg/L of amoxicillin antibiotic in 240 min for WO_3, AgI, WO_3/AgI and rGO/WO_3/AgI photocatalysts are 36.4%, 41.1%, about 65% and. 86.1%, respectively. Therefore, rGO leads to an increase in the removal rate of about 21.1%. For the rGO/WO_3/AgI photocatalyst, the energy consumption per gram of amoxicillin antibiotic removed is 348.43 kWh/g, which requires optimizing the energy required for the photocatalytic removal of amoxicillin antibiotic .The apparent pseudo-first-order rate constant is $K_{app} = 0.0212 min^{-1}.g^{-1}.L$ for rGO/WO_3/AgI photocatalysts[199].

5-7- EVALUATING THE CLAIM TYPES OF HETEROJUNCTION STRUCTURES

In Fig.28. A and B, the Mott–Schottky diagram, which is an electrochemical method used to analyze semiconductors and determine the type of semiconductor, is shown. The slope of the Cu_2O photocatalyst is negative according to the Mott–Schottky analysis, indicating that the photocatalyst is p-type, while the slope of the $Bi_2O_2CO_3$ photocatalyst is positive according to the Mott–Schottky analysis, indicating that the photocatalyst is n-type. In addition, the flat band potential (VFB) of the Cu_2O photocatalyst and the $Bi_2O_2CO_3$ photocatalyst are 1.92 V and 0.27 V, respectively. The valence band for p-type semiconductors is about 0.2 volts lower than VFB, while the conduction band for n-

type semiconductors is about -0.2 volts more negative than VFB. Thus, V_{CB} for $Bi_2O_2CO_3$ and V_{VB} for Cu_2O are calculated to be −4.57 eV and −6.62 eV, respectively[139].

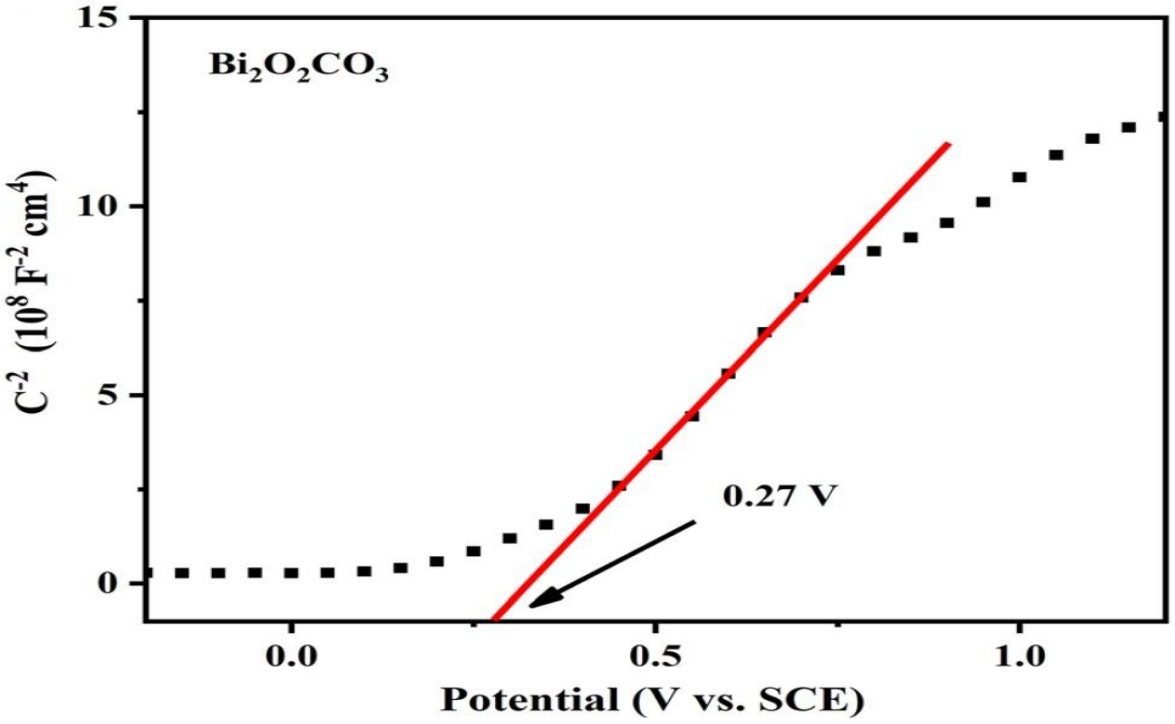

a)

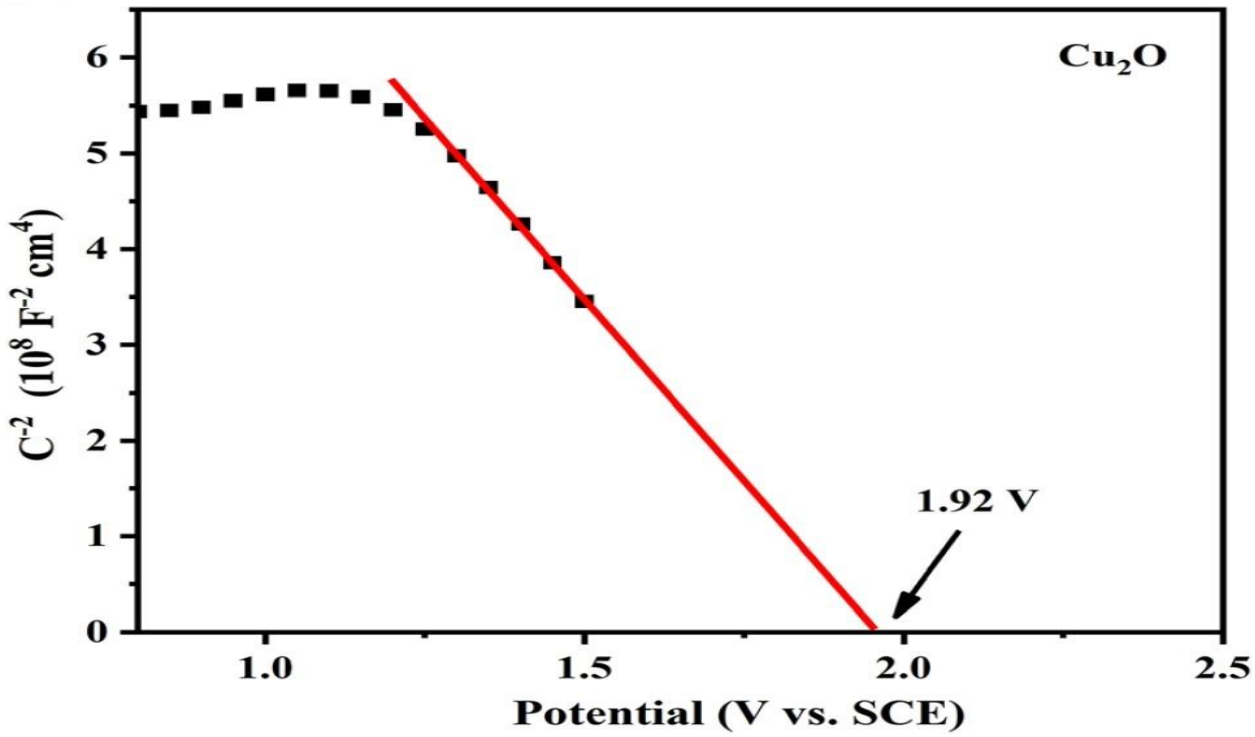

b)

Fig.28- Mott–Schottky curve for photocatalysts (a) $Bi_2O_2CO_3$ and (b) Cu_2O[139].

Also, according to the Photoluminescence spectra (PL) curve, the Cu_2O/ $Bi_2O_2CO_3$photocatalyst has a much lower intensity than that of $Bi_2O_2CO_3$, which indicates that the electron-hole recombination of the Cu_2O/ $Bi_2O_2CO_3$ photocatalyst is reduced compared to the $Bi_2O_2CO_3$ photocatalyst. The highest separation efficiency corresponds to a mass ratio of Cu_2O to $Bi_2O_2CO_3$ (wt%) :3(C3B). Using photocurrent response and electrochemical impedance spectroscopy (EIS), the improvement of charge separation and electron transport in the Cu_2O/ $Bi_2O_2CO_3$ photocatalyst was confirmed. The longest photoelectric carrier lifetime and effective separation of electron-hole pairs were found for the C3B photocatalyst, which had the highest photocurrent density. Also, EIS Nyquist plots show that the higher rate of surface reactions and the lowest charge transport resistance were found for the C3B photocatalyst. These analyses prove that the p–n heterojunction shape between Cu_2O and $Bi_2O_2CO_3$ improved the charge transport and enhanced the photocatalyst performance[139]. For the MoS_2/ZnO photocatalyst with 30 wt% of MoS_2(MZ-30), the current density is 3.5 μA.cm-2 while for the ZnO only photocatalyst, this value is 1.58μA.cm-2. Therefore, the MZ-30 photocatalyst has the highest photocurrent, which leads to increased charge generation and separation of electrons and reduced electron-hole recombination. The photoluminescence (PL) spectrum confirms the results regarding the photocurrent. It shows that the lowest intensity is associated with the MZ-30 photocatalyst, which has the highest electron-hole separation efficiency[141]. The article states that the type of heterojunction structure is p-n by analyzing the formation of the internal electric field, photoelectrochemical measurements, electrochemical impedance spectroscopy (EIS), and Mott–Schottky diagram[198]. According to the energy band arrangement and photocurrent tests, electrochemical impedance spectroscopy (EIS), photoluminescence (PL) spectroscopy, and the proposed mechanism, the heterojunction structure is a p-n heterojunction[134,137,200].The conduction band position of the g-C_3N_4 photocatalyst (−1.12 eV vs. NHE) is more negative than that of the ZnO photocatalyst (−0.5 eV). As a result, the photogenerated electrons in the conduction band of the g-C_3N_4 photocatalyst are directly

transferred to the ZnO photocatalyst, but the holes remain in the g-C_3N_4 photocatalyst, which confirms the type II heterojunction structure. The photoluminescence (PL) spectra show that the fluorescent intensity is greatly reduced in the CZ30-CDs4 photocatalyst compared to the g-C_3N_4, g-C_3N_4/ZnO(CZ) photocatalyst, indicating that the introduction of CDs into the CZ heterojunction structure leads to faster electron transfer in the CZ-CDs structure. Also, the charge transfer between the two photocatalysts ZnO and g-C_3N_4 is confirmed by electrochemical impedance spectroscopy (EIS) and photocurrent (PC) experiments. Higher photocurrents lead to increased photocatalytic activity and effective separation of photogenerated charges. Scavenger test shows that after the addition of BQ and EDTA-2Na, the photocatalytic degradation efficiency decreases by 10.2% and 87.3%, respectively, with oxygen being the main reaction species while h^+ plays a minor role in the removal reaction of tetracycline antibiotic. When isopropanol is added to the solution, the reduction in removal is 42%, indicating that the OH radical is the secondary species. This pattern is exactly consistent with the type II mechanism, because the electrons in ZnO react with oxygen to produce $^{\bullet}O_2^-$, while the holes in the g-C_3N_4 photocatalyst do not have enough potential to directly convert water molecules to $^{\bullet}OH$, and the secondary $^{\bullet}OH$ is formed from $^{\bullet}O_2^-$[201]. Considering the arrangement of energy bands and the proposed scavenger test and mechanism, the heterojunction structure is a type II heterojunction [145,148,202,203]. The paper does not perform any of the key experiments to distinguish Type-II and Z-scheme (such as Mott-Schottky, XPS before and after photocatalysis, or electron-mediated tracking) and does not report the positions of the energy bands quantitatively. Also, the system studied is not a pure photocatalytic system but a hybrid photocatalyst/persulfate (PS) system. Therefore, the main active species (such as $SO_4^{\bullet-}$ and •OH are mainly produced from the activation of persulfate by electrons or Cu(I)/Fe(II) ions and may not be related to the charge separation in a heterojunction. Therefore, the type of heterojunction cannot be precisely determined. But it is probably a Type II heterojunction[152]. The paper did not directly determine the type of heterojunction using the Mott–Schottky test, but rather by analyzing tests such as CB ZnO is higher than CB CeO_2 and VB ZnO is more positive than VB CeO_2

(ZnO: CB = −0.35 eV, VB = +2.87 eV CeO_2: CB = −0.45 eV, VB = +2.52 eV), and the decrease in PL intensity (which confirms effective charge separation), LC-MS data indicate that oxidation occurs on ZnO in the degradation of the antibiotic. As shown in fig.29, in the scavenger test, the presence of 2-propanol in the reaction medium reduces the degradation of the antibiotic ciprofloxacin, indicating that hydroxyl radicals are effective but not the determining factor in the removal of the antibiotic. By adding EDTA-Na_2, a very sharp decrease in the rate constant of the h^+ scavenger is observed; in fact, the EDTA-Na_2 molecules react with the hole and no hole remains to react with the antibiotic ciprofloxacin and the reaction stops. Different ROS scavengers showed that hydroxyl radicals participate in the removal of the antibiotic, but the main reaction species are positive holes in the valence band of metal oxides. Since the positive holes react directly with the antibiotic, it can be said that the destruction of the antibiotic on the surface of the photocatalyst is a local surface reaction. According to LC-MS studies, ZnO is the main component in the CeO_2/ZnO photocatalyst for the removal of the antibiotic ciprofloxacin. In other words, the destruction of the antibiotic in the CeO_2/ZnO photocatalyst starts using the existing holes in the valence band of the ZnO photocatalyst and does not start in the holes accumulated in the valence band of ceria. According to the type II heterogeneous mechanism, the photooxidation of ciprofloxacin molecules should occur by h^+ on the surface of ceria particles where the holes accumulate. Therefore, effective adsorption of the antibiotic on the ceria surface is necessary, but according to the absorption graphs, the adsorption of ciprofloxacin by ceria is low and the photocatalytic activity is also limited. Therefore, considering this evidence, it is claimed that the heterojunction structure cannot be type II. ZnO shows a greater ability to adsorb ciprofloxacin molecules and the holes in the valence band of ZnO have a stronger oxidizing ability than the holes in the valence band of CeO_2. It can be claimed that the heterojunction structure is Z-scheme, which is consistent with the performed analyses[157].

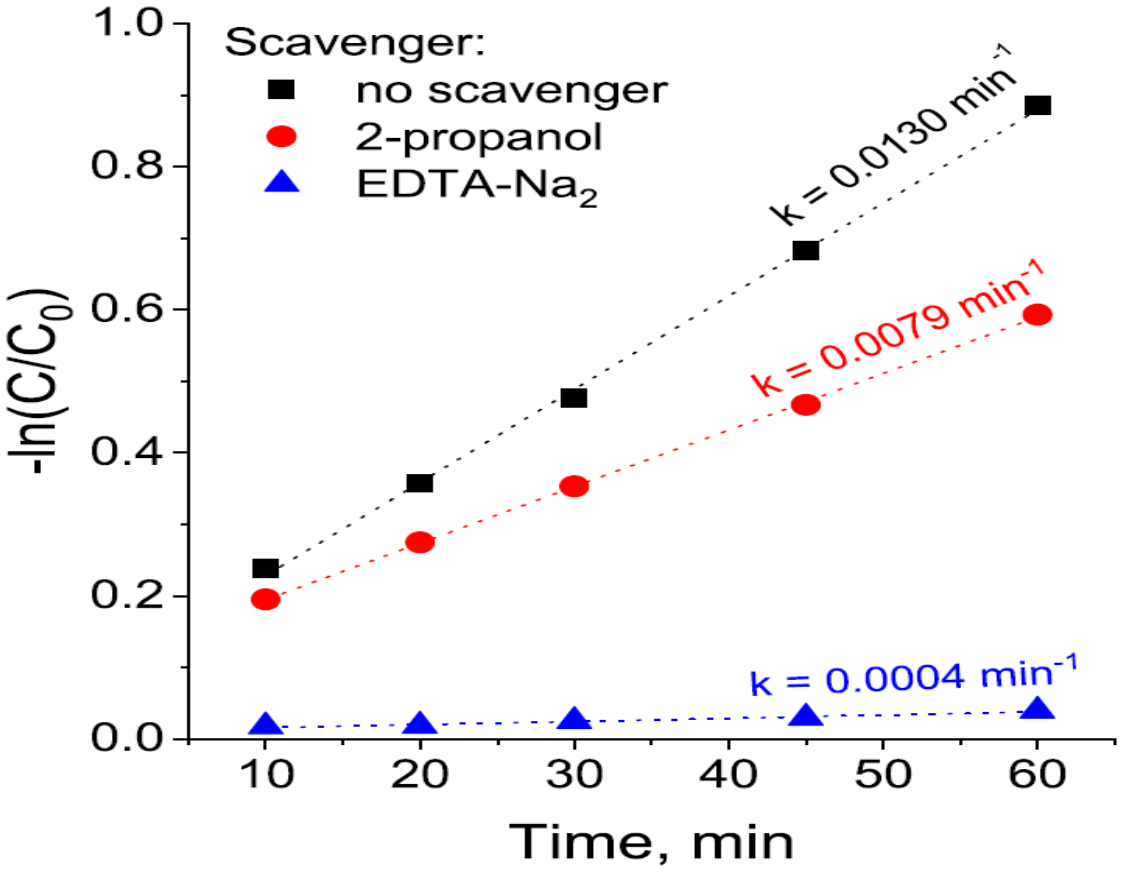

Fig.29-The effect of scavengers on the removal of the antibiotic ciprofloxacin by CeO_2/ZnO photocatalyst with 40% Wt CeO_2 under the following conditions: *Reaction conditions:* catalyst loading: 0.25g.L^{-1} (or other, if indicated), 100 mL of CIP aqueous solution (15 mg.L^{-1}, pH = 3.2), concentration of ROS scavengers: 10 mmol.L^{-1}, stirring rate: 1000 rpm, temperature: 30 ◦C[157].

To investigate the heterojunction structure of the Cu_2O / Bi_2S_3 photocatalyst, the flat-band potentials of Cu_2O and Bi_2S_3 were studied using an electrochemical workstation. As shown in Fig. 30, the Mott-Schottky (M-S) diagram is shown in fig 30a and 30b for both photocatalysts. After plotting the intersections on the horizontal axis of the curves, the negative slope and n-type semiconductor are identified for the Cu_2O photocatalyst, and the positive slope and p-type semiconductor are identified for the Bi2S3 photocatalyst. In addition, the U_{fb} of the Cu_2O and Bi_2S_3 photocatalysts are 0.125 V (vs. standard hydrogen electrode (SCE)) and -0.43 V, respectively, which are 0.37 V (vs. NHE) and -0.185 V (vs. NHE), respectively. Also, in general, the flat band potential of a p-type semiconductor is 0.1 to 0.3 volts higher than the conduction band potential, while the conduction band potential of an n-type

semiconductor is 0.1 to 0.3 volts lower than the flat band potential. Using the flat band potential from the Mott–Schottky data, the CB and VB have been calculated. CB of Bi_2S_3 is −0.285 eV, VB of Cu_2O is +0.47 eV, VB of Bi_2S_3 is +1.015 eV and CB of Cu_2O is −1.73 eV. This is consistent with the Z-scheme heterojunction mechanism. In the scavenger test, three sacrificial agents, IPA, BQ and EDTA-2Na, were added to the solution to investigate the effects of free radical species ($^{\bullet}OH$), superoxide anions ($^{\bullet}O_2^-$) and light-generated impurities (h^+) on the removal of tetracycline. After adding IPA to the solution, the removal rate decreased from 95.23% to 90.77% for the Cu_2O / Bi_2S_3 photocatalyst with 10%wt Cu_2O, while the addition of BQEDTA-2Na and BQ resulted in a decrease in the removal rate from 95.23% to 44.61% and 6.15%, respectively. The results indicate that h^+ and $^{\bullet}O_2^-$ are the active species in the photocatalytic reaction of tetracycline removal, with $^{\bullet}O_2^-$ being the key species and $^{\bullet}OH$ being almost ineffective. According to the position of the energy bands calculated from the Mott Schottky data, the conduction band electrons of the Bi_2S_3 photocatalyst are not able to convert O_2 to $^{\bullet}O_2^-$ (because CB of Bi_2S_3 = −0.285 eV is higher than $E°(O_2/^{\bullet}O_2^-)$ = −0.33 eV). Therefore, to produce $^{\bullet}O_2^-$, the electrons must be in the conduction band of Cu_2O, which occurs when the electrons of the conduction band of the Bi_2S_3 photocatalyst are transferred to the valence band of the Cu_2O photocatalyst and recombine with the holes there, which is the Z-scheme mechanism[204].

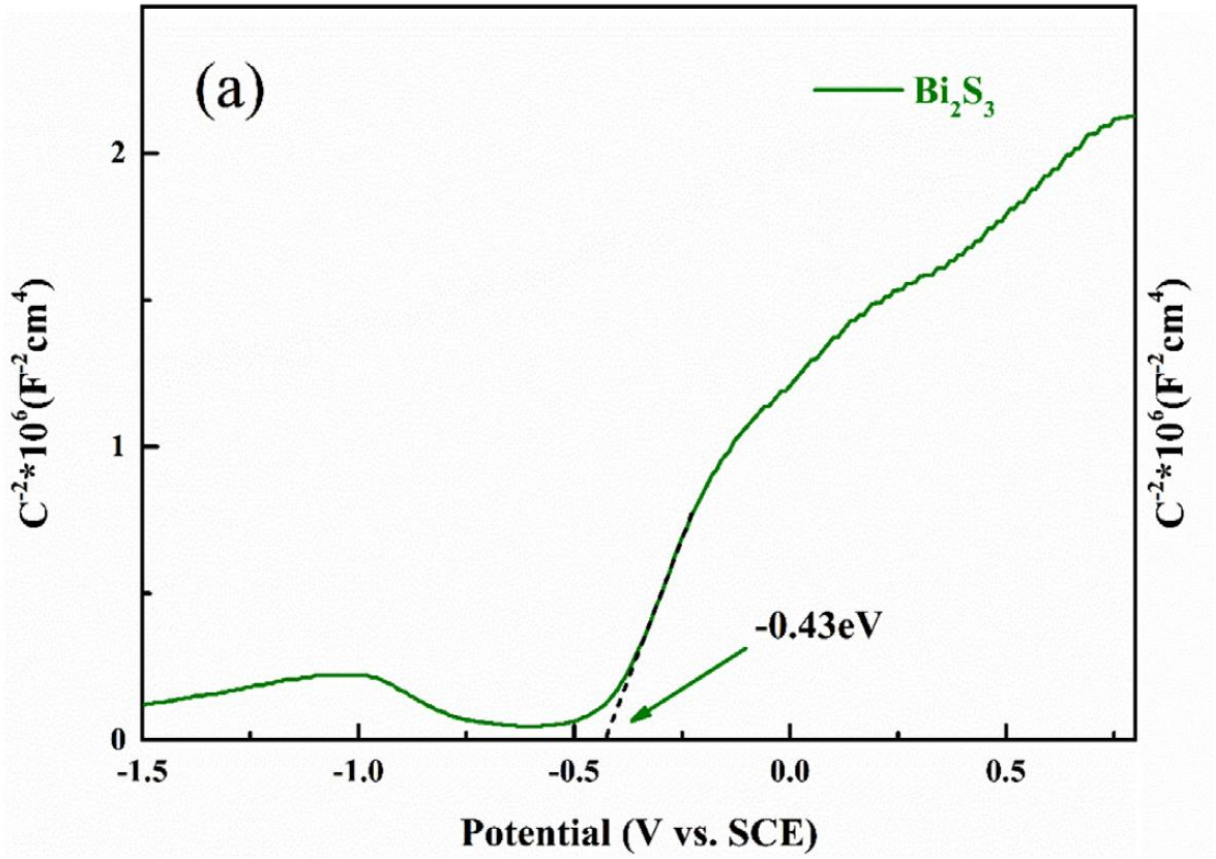
(a)
Bi2S3
2
1
0
C-2*10^6(F-2cm4)
C-2*10^6(F-2cm4)
-0.43eV
-1.5
-1.0
-0.5
0.0
0.5
Potential (V vs. SCE)

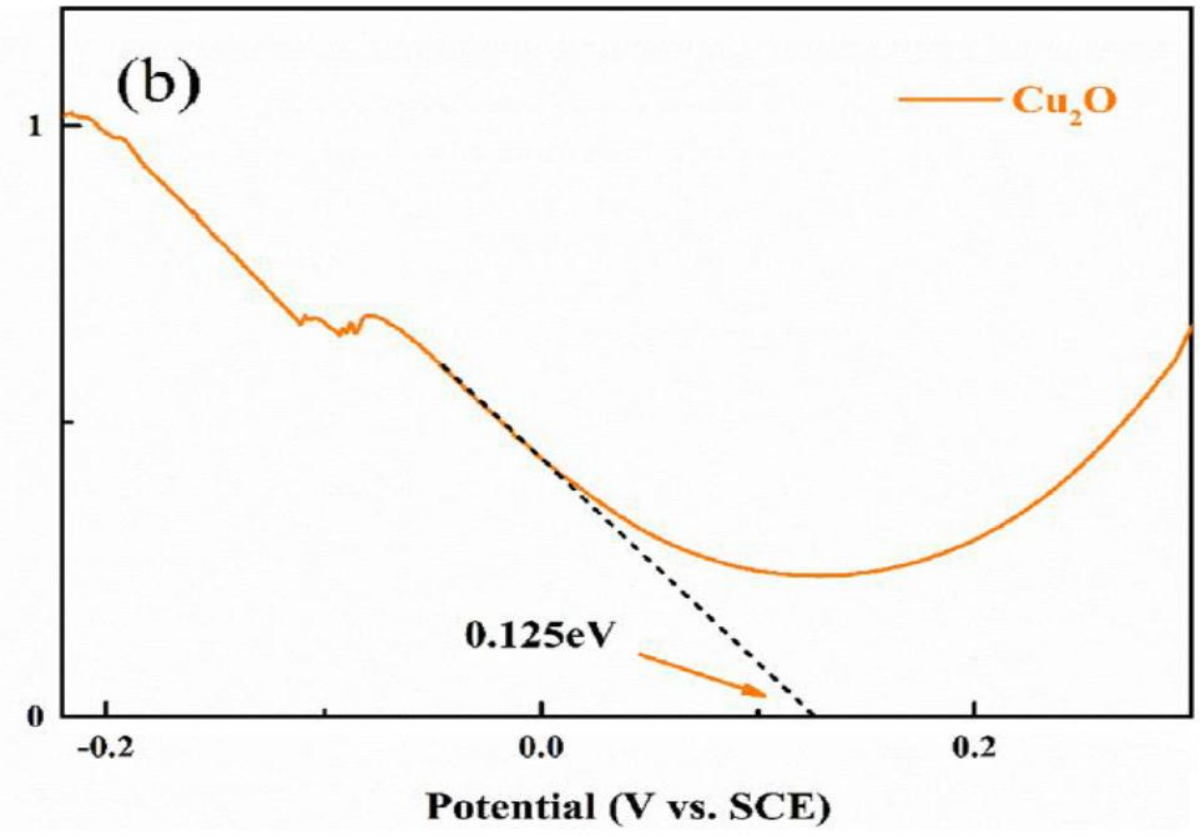
(b)
Cu2O
1
0
0.125eV
-0.2
0.0
0.2
Potential (V vs. SCE)

Fig.30- Mott-Schottky diagram for photocatalyst a) Bi_2S_3 and b) for photocatalyst Cu_2O[204][91].

For the AgI/ $ZnIn_2S_4$/$BiVO_4$ photocatalyst, similar to the Cu_2O / Bi_2S_3 photocatalyst, the paper proves with indirect methods, such as scavenger, ESR, conduction and valence band calculations, that the structure is a dual Z-scheme, but it does not use direct methods, such as a dual Z-scheme[164]. The paper first investigated the positions of the VBs and CBs of the $Bi1_2O_{17}Cl_2$ (BOC) and $AgFeO_2$ (AFO) photocatalysts and then calculated the flat band potentials of AFO and BOC through the Mott–Schottky diagrams. Both AFO and BOC have typical n-type semiconductor characteristics because the slope of the linear potential curves is positive 1/C2. Therefore, the heterojunction structure cannot be p-n. Also, their flat potentials were measured as −0.7 V and +0.29 V with respect to NHE, respectively. The positions of the conduction bands and valence bands were also determined as CB of AFO is +0.19 V, VB of AFO is +2.04 V, CB of BOC is −0.8 V and VB of BOC is +1.43 V. In the scavenger test, benzoquinone (BQ, a typical superoxide radical scavenger) was used, and only 11.1% tetracycline removal was achieved. It can be concluded that O_2 plays a key role in the removal rate. The heterojunction structure is not type-II, because the electrons in the conduction band of AFO (0.19 V) are not able to reduce oxygen to $\bullet O_2^-$ due to the lower potential than ($O_2/\bullet O_2^-$ = −0.33 V). In contrast, in the Z-scheme heterojunction structure, the excited electrons of the AFO conduction band were transferred to the electron shuttle intermediates (Ag nanoparticles) and subsequently recombined with the equivalent holes generated on the VB of BOC. As a result, the high-energy electrons remain in the BOC conduction band (−0.8 V) and are able to produce $\bullet O_2^-$, which is fully consistent with the scavenger and ESR data and the band position of the photocatalysts. So, it can be said that the heterojunction structure is Z-scheme[165]. In the Mott-Schottky test, the slopes of the three photocatalysts Ag_3PO_4, AgBr and g-C_3N_4 were positive, indicating that they are n-type semiconductors. Therefore, the heterojunction structure cannot be p-n. According to these graphs, the flat band potentials for g-C_3N_4, Ag_3PO_4 and AgBr are -1.49, -0.27 and 0.44, respectively. The valence band potentials of g-C_3N_4, Ag_3PO_4 and AgBr photocatalysts are 1.77, 2.52 and 3.06 eV. Three

scavengers, isopropanol (IPA), (BQ) and $Na_2C_2O_4$, were investigated to determine the effect of $^{\bullet}OH$, h+ and $\bullet O_2^-$ on the removal rate of tetracycline respectively. The removal rate was significantly reduced by adding BQ or $Na_2C_2O_4$ compared to the absence of adsorbent, but the removal of tetracycline was slightly inhibited by adding IPA. Therefore, $^{\bullet}OH$ has little effect on the removal rate of tetracycline, but h+ and $\bullet O_2^-$ species have a significant effect on the removal of tetracycline. The Ag_3PO_4/AgBr-20% g-C_3N_4 composite has a higher photocurrent density than the single photocatalysts. Also, the Ag_3PO_4/AgBr-20% g-C_3N_4 photocatalyst had the smallest arc radius, which indicates the lowest charge migration resistance and the best separation of e− and h+ pairs. The presence of (Ag^0) acts through electron transfer between $Ag_3PO_4$and AgBr as well as AgBr and g-C_3N_4. Therefore, the Ag_3PO_4/AgBr/ g-C_3N_4 photocatalyst is not a Type-II heterojunction structure and the dual Z-scheme structure can be justified according to the analyses[169]. By analyzing the position of energy bands, scavenger and ESR experiments, and electrochemical data, the paper rejects the Type-II heterojunction structure and for the photocatalyst, due to the absence of a metal intermediate, charge transfer occurs through direct contact between the two semiconductors, which is the definition of the Z-scheme direct heterojunction structure[172,184,185,205,206].The paper logically proves that the heterojunction structure is Z-scheme using scavenger tests, PL data, EIS, photocurrent, and energy band position calculations[155,164,207–209]. The paper refers to the band positions (CB = −0.67 V and VB = +2.5 V vs. NHE) and does not refer to key experiments such as scavenger, ESR, Mott-Schottky, or in-situ XPS. Since both semiconductors are n-type, the upward bending of the edges limits the recombination of electrons from g-$C_3N_4$with Nb_2O_5 holes, which is expected in a Z-scheme heterojunction. However, staggered gap alignment is a feature of type II heterojunctions that is effective in electron and hole separation[170]. Since antibiotics have complex structures and are mostly toxic, the need for an efficient method to remove antibiotics is increasingly felt. As shown in Table 5, the most common method to increase the performance of photocatalysts and prevent electron-hole recombination and activation in the visible light range is doping. Although doping leads to an increase in the specific surface area, a decrease in

the band gap in nonmetals mainly by raising the valence band and in metals by creating impurity levels within the energy gap, a decrease in electron-hole recombination, due to the high cost of some metals such as noble metals, pollution caused by the release of some metals into the environment and aggregation of nanoparticles which leads to a decrease in photocatalytic activity. Therefore, the use of dopants has recently been reconsidered[14,210,211]. In the type II heterojunction structure, photogenerated electrons are transferred from the conduction band of photocatalyst A to the conduction band of photocatalyst B, while holes migrate from the valence band of B to the valence band of A, which leads to electron-hole separation and thus increases the lifetime of charge carriers, but electrons accumulate in the conduction band of photocatalyst B (with lower energy) and holes in the valence band of photocatalyst A (with higher energy), which leads to a decrease in the reduction and oxidation potentials and the overall efficiency of redox reactions. However, the Z-scheme heterojunction structure provides a stronger redox potential due to the highest energy charge carriers. The low-energy holes in the valence band of the semiconductor combine with the low-energy electrons in the conduction band of the semiconductor, while the high-energy electrons and high-energy holes remain to carry out the reduction and oxidation reactions. The heterojunction structures of traditional Z-scheme systems, due to the use of soluble redox couples, have an unstable redox environment in the liquid phase, which affects the photocatalytic performance. Also, if the photocatalysts are poorly selected or the Fermi levels are not aligned properly, a sufficient potential difference is not created for effective charge separation. This misalignment of the conduction and valence bands is the main reason for the lack of a significant redox potential gradient in some Z-scheme systems. In the p-n heterojunction structure, at the interface between the p-type and n-type regions, there is a depletion region due to the diffusion of charge carriers, which allows for efficient charge separation, but it is difficult to select photocatalysts that are p-type and n-type[14,60,212–215]. Among the Z-scheme structures (first, second and third generation) that have attracted much attention in antibiotic removal, the third generation has better performance in antibiotic removal because it solves the problems of the first and second

generations, such as instability and backward reaction[212]. Table 4 summarizes the advantages and disadvantages of different heterojunction structures.

Table4-Comparison of different heterojunction structures and doping[14,60,212,213,216,217].

Structure type	Advantages	Disadvantages
Type II heterojunctions	Effective separation of electron-hole pairs, increasing electron lifetime	Reducing the redox potential of the entire system, Complex synthesis
Z-scheme heterojunction	electrons with high reduction ability and holes with high oxidation ability and provides a continuous redox cycle, efficient utilization of light energy	poor stability and backward reaction, require liquid phases, Complex synthesis, No significant oxidation-reduction potential gradient
p-n heterojunction	strong internal electric field, depletion region due to the diffusion of charge carriers	Limitations in the selection of n-type and p-type photocatalysts, Complex synthesis
Doping	increasing specific surface area, Simplicity in synthesis, increasing light absorption, improving charge mobility, reducing band gap, creating	The high cost of some dopants, such as noble metals, Pollution caused by metals and non-metals in the

	more active sites, reducing photogenerated electron-hole recombination, promoting charge carrier generation	environment, and Aggregation of nanoparticles

6- INVESTIGATING THE ENVIRONMENTAL EFFECTS OF GRAPHENE-BASED PHOTOCATALYSTS AND HETEROJUNCTION STRUCTURES IN THE REMOVAL OF ANTIBIOTICS

Given that environmental issues have received great attention, the photocatalytic degradation of antibiotics is no exception to this rule, and this section examines the environmental issues related to the removal of antibiotics using photocatalytic structures with graphene and heterojunctions.

6-1-INVESTIGATION OF BACTERIAL ANTIBIOTIC RESISTANCE IN PHOTOCATALYTIC ANTIBIOTIC REMOVAL

Guo et al. [126] used the TiO_2/Ag/GO photocatalyst to investigate the effect on ARB. To investigate ARB inactivation, the bacterial strains E. coli HB101 (resistant to kanamycin, tetracycline, and ampicillin), E. coli HB10663 (resistant to tetracycline and gentamicin), and E. coli HB10667 (resistant to streptomycin) were used. Bactericidal activity of TiO_2/Ag/GO under simulated sunlight irradiation on the survival rate of ARB under different concentrations of TiO_2/Ag/GO has been investigated. The survival rate shows a decreasing trend with increasing photocatalyst concentration. When exposed to sunlight without the presence of photocatalyst, the survival rate of E. coli HB10667 and E. coli HB10663 reached 92.7% and 96.5%, respectively, which was a slight decrease, while the reduction of E. coli HB101 reached less than 80%, indicating that different bacteria have different tolerances to sunlight. The photocatalyst at a concentration of 10 mg/L and above has significant inactivation activity for E. coli HB101, while this is not the case for E. coli HB10663 and E. coli HB10667. With the

addition of 10 mg/L of TiO_2/Ag/GO, the survival rate of E. coli HB101 is 63.4%, while to achieve the same level of inactivation, 80 mg/L and 100 mg/L of TiO_2/Ag/GO photocatalyst should be added to the E. coli HB10667 and E. coli HB10663 solutions, respectively. The survival rates of E. coli HB101, E. coli HB10667 and E. coli HB10663 were reduced by 59.1%, 43.4% and 12.2%, respectively, with the addition of 100 mg/L of TiO_2/Ag/GO. The observed sequence of bacterial survival rates regardless of the increase in photocatalyst is (E. coli HB101<E. coli HB10667<E. coli HB10663). Fig.31(a) investigates the role of the antibiotic chloramphenicol (CAP) in the ARB inactivation process a) in the absence of photocatalyst and b) in the presence of photocatalyst with a bacterial concentration of 10^8CFU (Colony Forming Units)/mL. The Fig.31(a) shows that the effect of chloramphenicol has little effect on ARB survival. The survival rate of bacteria remains high with increasing contact time. Different concentrations of the antibiotic chloramphenicol have little effect on ARB survival because after one hour of reaction, the survival rate of bacteria with different concentrations of chloramphenicol (5, 10, 20 mg/L) is 86.2%, 86.1% and 83.4%, respectively. In Fig.31(b), the survival of ARB changes drastically by adding photocatalyst to the solution at a concentration of 50mg/L TiO_2/Ag/GO. The lowest bactericidal activity corresponds to a concentration of 20 mg/L of clonidine[126].

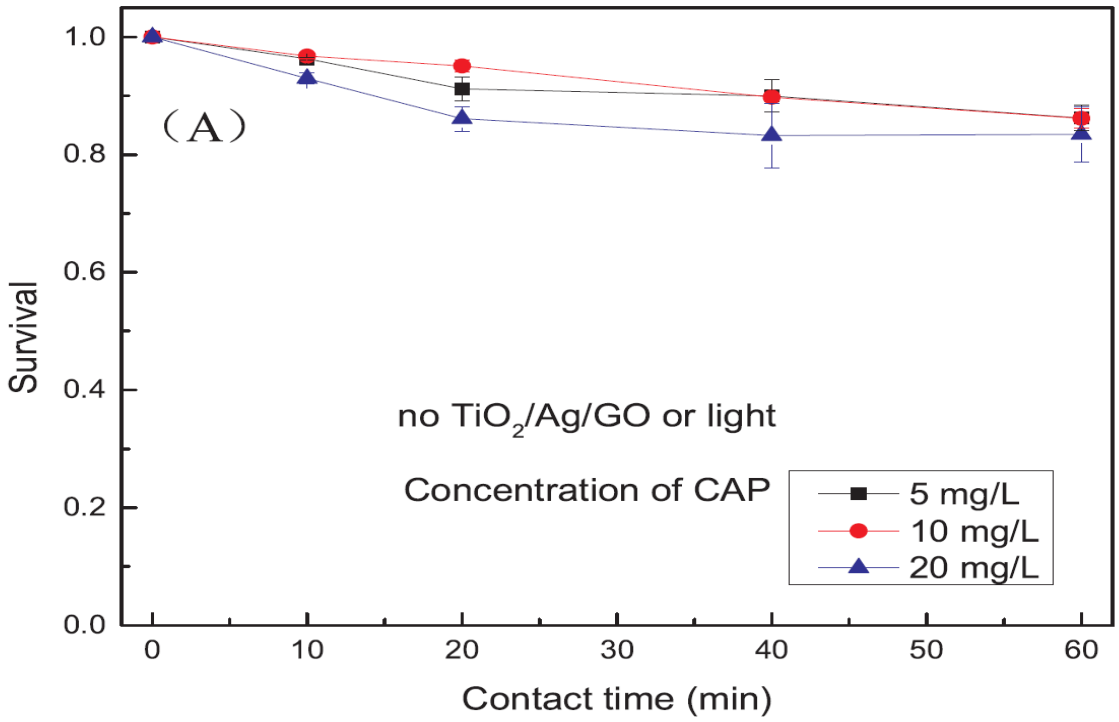

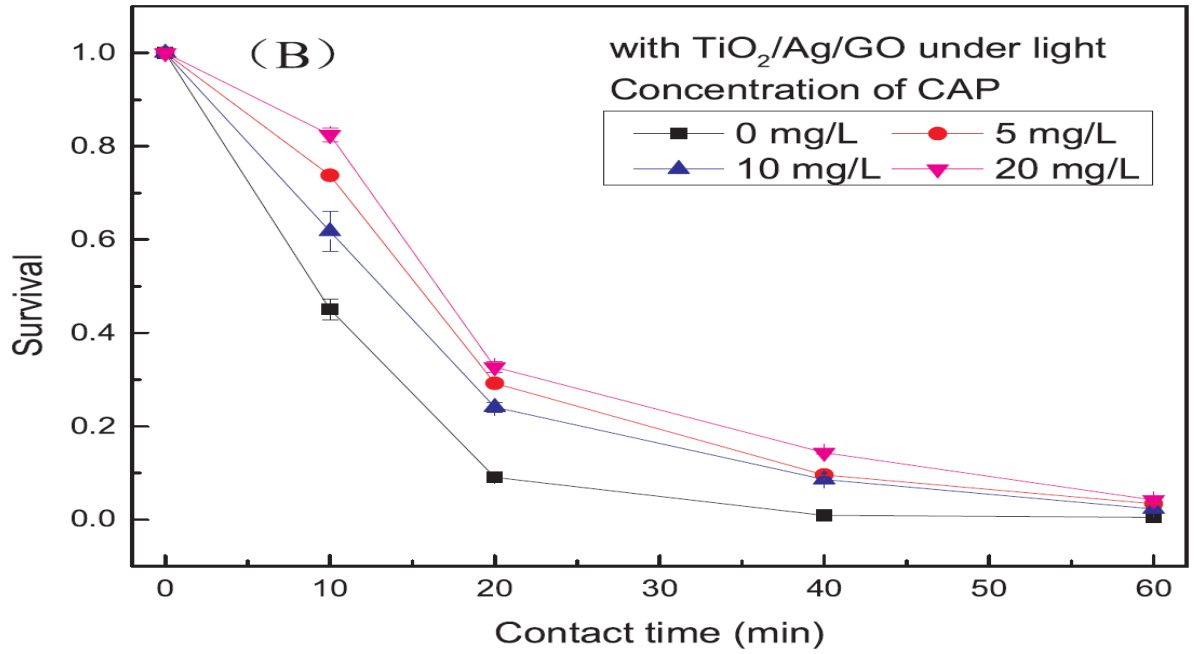

Fig.31-ARB levels with different concentrations of the antibiotic chloramphenicol A) without the presence of photocatalyst, depending on the contact time with a bacterial concentration of 10^8 CFU/mL B) in the presence of 50mg/L TiO_2/Ag/GO photocatalyst[126].

Shen et al[139] evaluated the performance of the synthesized photocatalyst in antibacterial experiments. PEO and $Bi_2O_2CO_3$/PEO did not show any antibacterial activity against Escherichia coli and Staphylococcus aureus. However, the Cu_2O / $Bi_2O_2CO_3$/PEO photocatalyst showed antibacterial activity against both bacteria. The antibacterial activity was directly proportional to the amount of Cu_2O in the nanocomposite. Due to the ability of Cu_2O to penetrate through the cell wall or outer membrane of bacteria and bind to DNA, thereby blocking the cell proliferation process, it is used against pathogens. Therefore, the Cu_2O / $Bi_2O_2CO_3$PEO photocatalyst is an attractive option for the treatment of wastewater contaminated with both organic pollutants and pathogenic microorganisms. Also, the inhibition rate for Escherichia coli was up to 81.5% and for Staphylococcus aureus was up to 75.6%, indicating that the Cu_2O / $Bi_2O_2CO_3$/PEO photocatalyst performed well in reducing bacterial growth[139]. Manikandan et al. [208] investigated the antibacterial performance of the synthesized photocatalyst in the experiments. The WO_3/g-C_3N_4/MWCNT photocatalyst was investigated on two clinical isolates, namely Bacillus subtilis and Klebsiella pneumonae, by the agar disk diffusion method.

Advanced oxidation process is an efficient method for converting toxic pollutants into non-toxic substances. While the microorganism carries a negative charge, the oxide semiconductor carries positive charges, in which electrostatic attraction occurs between them, where the oxidation reaction caused by the metal oxide can kill the microorganism. Therefore, the WO_3/g-C_3N_4/MWCNT photocatalyst is not only highly effective in degrading the antibiotic tetracycline but also has significant antibacterial activity against gram-negative bacteria under visible light[208]. One of the research gaps in the photocatalytic removal of antibiotics literature is the attention to ARB and ARG, and their study alongside antibiotic removal.

6-2-INVESTIGATION OF THE USE OF REAL WASTEWATER IN THE PHOTOCATALYTIC REMOVAL OF ANTIBIOTICS

Kumar et al. [125] investigated the removal of the antibiotic chloramphenicol from CRSB photocatalyst in the presence of visible light for 90 minutes in municipal tap water and the removal rate reached about 82%, which is about 17.1% less than distilled water in laboratory conditions, and the apparent pseudo-first-order rate constant is also $K_{app} = 0.207 \text{min}^{-1}.\text{g}^{-1}.\text{L}$. No studies have been conducted for municipal tap water in the presence of sunlight[125]. Wang et al. [124] used a 0.1g rGO-ZnO photocatalyst to remove the antibiotic chloramphenicol with an initial concentration of 1000mg/L in 100 minutes. In veterinary effluent in the presence of UV light, the removal rate was 90.2%, which was 0.6% lower than the experimental conditions, indicating good performance of the photocatalyst. The reason for this is the use of auxiliary oxidant H_2O_2, the very high surface area of the photocatalyst (722 m2/ g) and the use of rGO and its protective role against the toxicity of the ZnO photocatalyst and the prevention of photocorrosion of the surface, and [124]. Tian et al[185] used 0.3g g-C_3N_4@ZnO photocatalyst to remove the antibiotic cephalexin with an initial concentration of 10 mg/L in 60 min. From the sludge collected from municipal wastewater in the presence of simulated sunlight, the removal rate was 92.7%, which was 6.2% lower than that under laboratory conditions, indicating good

performance of the photocatalyst[185]. One of the research gaps in the photocatalytic removal of antibiotics literature is the attention to the removal rate of antibiotics in real wastewater and the effort to improve the performance of photocatalysts on an industrial scale.

6-3-MINERALIZATION AND TOXICITY ASSESSMENT

The purpose of examining Total Organic Carbon (TOC) is to completely destroy the antibiotic by converting it to CO_2 and H_2O, because the antibiotic may be completely removed but converted into intermediates that are harmful to the environment. Therefore, TOC is an important parameter in environmental issues. Shengyan Pu et al. [119] investigated the TOC for Cu-TiO_2/GO photocatalyst. The antibiotic tetracycline hydrochloride with an initial concentration of 20mg/L, 0.3g/L photocatalyst concentration in 90 min and UV–visible light with intensity of 300 W has a 100% removal rate. However, the TOC is 84.5% in 360 min. For TiO_2 and TiO_2/GO photocatalysts, the TOC is also lower than that of tetracycline hydrochloride degradation. The reduction in TOC in the removal of tetracycline hydrochloride antibiotic compared to antibiotic removal is because the removal generally starts from some specific structures (C-N-C) [119]. Kumar et al. [125] investigated the TOC of the photocatalyst Carbon quantum dots/RGO/S@C_3N_4/B@C_3N_4(CRSB). The antibiotic chloramphenicol, with an initial concentration of 10mg/L, 0.3g/L photocatalyst concentration at 360 min and Xe lamp (with 450mWcm−2 intensity), showed a TOC of 84% and 70% under visible and solar light, respectively. Kumar et al. [125] evaluated the toxicity of the antibiotic chloramphenicol with the CRSB photocatalyst on PBL cells using the MTT assay. The purpose of investigating the toxicity of photocatalytic removal of antibiotics is to determine whether the removal process has harmful or lethal effects on living organisms (such as cells, bacteria, fish, or even humans). The MTT assay is a tetrazolium salt (pale yellow) and is reduced to formazan (dark blue) by mitochondrial dehydrogenases. Fig.32(a) shows the percentage cell viability in untreated cells, ConA (concanavalin A) as a positive control, and photocatalyst-treated water obtained after CMP degradation. The cell viability for untreated cells was 85.2% and for ConA (95.1%), which are high values. For cells treated with the mineralized products

of the antibiotic chloramphenicol, the cell viability was still 84.4%, indicating mineralization of non-toxic products. The treated water did not affect the viability of blood cells and mitochondrial function. Fig.32((b), (c), and (d)) shows Digital images of treated PBL cells, where no increase in dead cell debris is observed for cells treated with degradation products. Also, CRSB photocatalyst is a stable metal-free photocatalyst with high removal rate and mineralization performance[125].

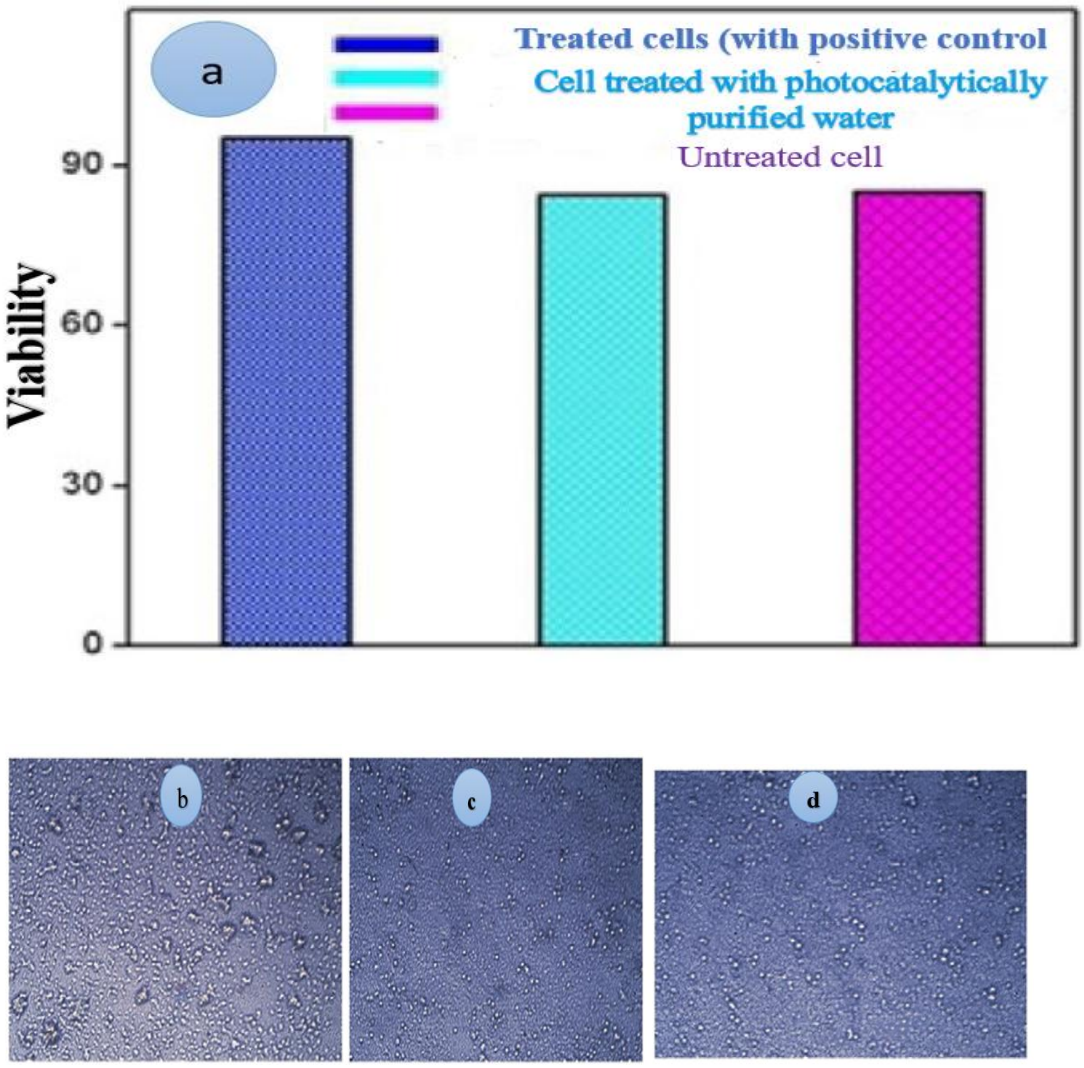

Fig.32-a) Cytotoxicity of Chloramphenicol degradation of products with CRSB photocatalyst (treated water sample) under visible light b) Human peripheral blood lymphocytes (PBL) treated with Con A (positive control-an immunomodulatory drug) c) Untreated PBL cells d) PBL cells treated with water containing Chloramphenicol degradation products (adopted from [125]).

Shen et al. [139] investigated the toxicity of the photocatalyst $Cu_2O/Bi_2O_2CO_3$/PEO nanofibers under the conditions of 20 mg/L of the antibiotic chloramphenicol in a 300 W Xe lamp equipped with a 420 nm cut-off filter with visible light. After exposing the test solution for 24 h using cytotoxicity assay (CCK-8) and fibroblast cells (L-929), it was shown that during the photocatalytic degradation process of chloramphenicol, some intermediate products, such as dehydrochloramphenicol and nitrosamine chloramphenicol, can increase the toxicity of the solution. In fact, between 90 and 120 minutes of the process, the toxicity increased significantly and the cell viability reached less than 70%[139]. Mengelizadeh et al. [145]investigated the parameters of TOC, COD and BOD to evaluate the degree of mineralization during the photocatalytic removal process of the antibiotic ciprofloxacin (CIP). In this study, the mineralization rate of 25 mg/L CIP was evaluated under operating conditions including pH of 7, 0.3 g/L of g-C_3N_4/Fe_2O_3 and UV intensity of 36 W. With increasing irradiation time from 10 to 60 min, TOC increased from 18.68% to 93.86%. The amount of oxygen required for the complete oxidation of organic matter and some chemicals in water is called Chemical Oxygen Demand (COD). The COD value increased from 16.74% to 94.93% with increasing irradiation time from 10 to 60 min. The amount of oxygen that microbes need to decompose organic matter in water is called Biochemical Oxygen Demand (BOD). It increased from 24.48% to 75.49% with increasing irradiation time from 10 to 60 minutes. Also, with increasing irradiation time from 10 to 60 minutes, the BOD/COD ratio increased from 0.12 to 0.66, which indicates that the CIP antibiotic removal process has been completed into degradable compounds. The optical density (OD) of E. coli and E. fecalis bacteria was used to investigate the toxicity of the solution treated with the g-C_3N_4/Fe_2O_3-based photocatalytic process. The OD values in the untreated solution for E. fecalis and E. coli ranged from 0 to 1.09 and 0 to 0.96, respectively, between times 1 to 24 hours. When the solution was treated with the g-C_3N_4/Fe_2O_3 /UV process, the OD increased significantly compared to the initial solution, indicating that the CIP antibiotic was efficiently degraded into non-toxic substances[145]. Wolski et al. [157] investigated the TOC and mineralization parameters for the photocatalytic removal process of the antibiotic

ciprofloxacin (CIP). The initial concentration of CIP was 15 mg/L, CIP was evaluated under operating conditions of pH = 3.2, CeO_2/ZnO dosage of 0.5 and UV intensity. According to Fig33, the TOC value decreased from about 9 mg/L to about 0.7 mg/L in 360 min, which is a reduction of about 92.2%. Mineralization actually means the complete conversion of organic compounds into inorganic end products such as CO_2, H_2O and inorganic ions (NH_4+, NO_3-, F-). Mineralization is about 92% in 360 min[157].

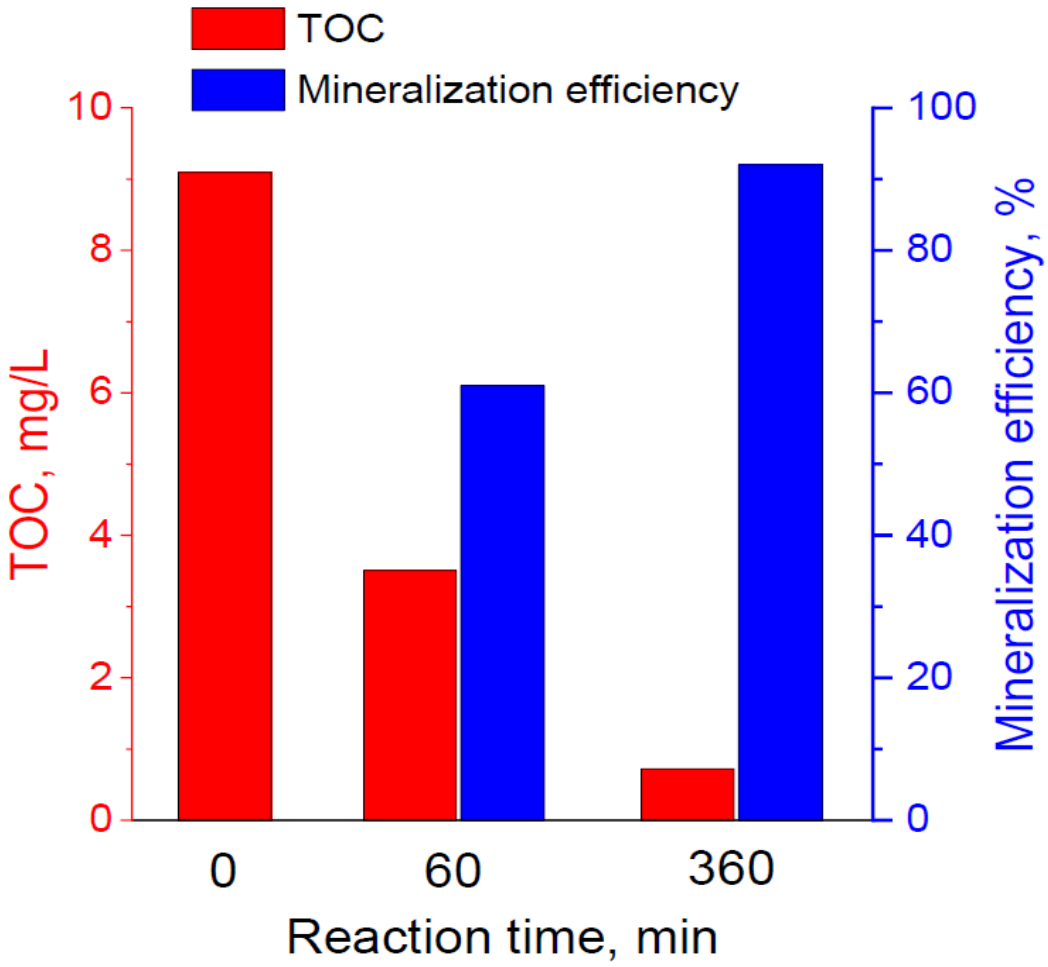

Figure.33 - Investigation of TOC and mineralization of the antibiotic ciprofloxacin in the presence of CeO_2/ZnO photocatalyst[157].

Lu et al. [164] investigated the TOC parameter for the photocatalytic removal process of tetracycline(TC) antibiotic. In this study, the initial concentration of 20 mg/L, TC under the operating

conditions of 300 W Xenon lamp AgI/$ZnIn_2S_4$/$BiVO_4$((AZB)) was evaluated under visible light. The COD and TOC removal efficiencies for AZB photocatalyst with molar ratios of Bi to Ag 1:1 were 64.89% and 57.85%, respectively, which were lower than the photocatalytic properties. The reason for the low COD and TOC for TC antibiotic is that the antibiotic was not completely decomposed and the intermediates still existed[164]. Wang et al. [152] investigated the COD parameter for the photocatalytic removal process of tetracycline hydrochloride antibiotic (TC). In this study, the initial concentration of 20 mg/L, TC was evaluated under the operating conditions of a 300 W xenon lamp under simulated sunlight with 0.1 g/L CuO/$CuFe_2O_4$/g-C_3N_4 ((CCCN)). The COD removal efficiency for the photocatalysts CCCN, g-C_3N_4 and $CuFe_2O_4$/g-C_3N_4 was 48%, 35% and 39%, respectively. After adding PS, the COD was 74%, 47% and 54%, respectively. Therefore, the addition of PS led to an increase in the COD efficiency[152]. Hu et al. [184] investigated the TOC parameter for the photocatalytic removal of the antibiotic tetracycline hydrochloride (TCH). In this study, the initial concentration of 40 mg/L, TCH under the operating conditions of 300 W xenon lamp SnS_2@$ZnIn_2S_4$@kaolinite ((SZK)) was evaluated to be 0.2g/L photocatalyst under visible light. The TOC removal efficiency for the SZK photocatalyst with weight ratios of SnS_2@$ZnIn_2S_4$:0.75:1 showed a TCH removal rate of 88.23% in 60 min, while the TOC removal efficiency was 55.86%. Mineralization was not completely completed and the materials were still present[184]. Tian et al. [185] investigated the TOC parameter for the photocatalytic removal process of antibiotic cephalexin. In this study, the initial concentration of 10 mg/L, cephalexin under the operating conditions of a 300 W xenon lamp (300 W) with g-C_3N_4@ZnO was evaluated to be 0.3g/L under solar light. The TOC removal rate of cephalexin solution for g-C_3N_4, ZnO and g-C_3N_4@ZnO photocatalysts was 34.2%, 25.6% and 72.8% in 60 min, respectively[185]. Wang et al. [205] investigated the TOC parameter for the photocatalytic removal process of the antibiotic ofloxacin. In this study, the initial concentration of 10 mg/L ofloxacin was evaluated at 1g/L under the operating conditions of 300 W Xenon lamp $BiVO_4$/g-C_3N_4/$NiFe_2O_4$ under visible light. The TOC removal rate of ofloxacin solution for the $BiVO_4$/g-C_3N_4/$NiFe_2O_4$

photocatalyst was 28.2% and 40.5% at 60 and 120 min, respectively[205]. As the goal of removing antibiotics from wastewater is to preserve the environment and prevent the spread of disease, it is necessary to pay attention to TOD, COD and BOD because antibiotics may be converted by the photocatalyst into intermediates that are even more dangerous than the antibiotics themselves. Therefore, their investigation is essential in the photocatalytic removal of antibiotics and is considered a research gap.

6-4-INVESTIGATING THE CHANGE IN ANTIBIOTIC REMOVAL RATE BY REUSING THE PHOTOCATALYST

One of the effective parameters in the photocatalytic removal of antibiotics is the reuse of photocatalysts in reactions, which leads to cost reduction and enables their use on an industrial scale. Raja et al. [115] used the RGO-$BiVO_4$-ZnO photocatalyst at a concentration of 0.3 g/L to remove 10 mg/L of the antibiotic ciprofloxacin in 60 min under visible light. The rGO-$BiVO_4$-ZnO photocatalyst did not significantly degrade after 6 times of use in the photocatalytic reaction and was reusable[115]. Pu et al. [119] used Cu-TiO_2/GO photocatalyst with a concentration of 0.3 g/L to remove 20 mg/L of tetracycline hydrochloride antibiotic in 90 min under UV light. After 5 times of use of Cu-TiO_2/GO photocatalyst in the photocatalytic reaction, the removal rate decreased from 99.8% to 98.5%, which was a 1.3% decrease after 5 times of use of the photocatalyst, indicating a very good performance of the photocatalyst[119]. Kumar et al. [125] used the photocatalyst reduced graphene oxide layers modified S@g-C_3N_4/B@g-C_3N_4 (CRSB) to remove the antibiotic chloramphenicol. After 5 times of using the photocatalyst, there is no significant decrease in the removal rate[125]. Sodeinde et al. [124] used rGO-ZnO photocatalyst with a concentration of 2.5 g/L to remove 1000 mg/L of the antibiotic chloramphenicol in 40 min under UV light. After 4 times of use of the rGO-ZnO photocatalyst in the photocatalytic reaction, the removal rate decreased from 87% to 68%, which was a 19% decrease after 4 times of use of the photocatalyst, indicating the relative stability of the photocatalyst[124]. Cui et al. [137] used palygorskite (Pal)-supported Cu_2O–TiO_2 photocatalyst with a concentration of 1 g/L to

remove 30 mg/L of tetracycline hydrochloride antibiotic in 240 min under solar light source. After 3 times of photocatalytic reaction, the photocatalyst Cu_2O–TiO_2–Pal photocatalyst showed that the photocatalytic degradation rate without light exposure and the adsorption rate were 81.45%, 78.42%, and 73.88% in the first, second, and third cycles, respectively. The physical adsorption in the dark was 7.36%, which was not combined with the photocatalytic degradation, and the recovery rate of photocatalytic degradation was investigated[137]. Shen et al. [139] used a photocatalyst $Cu_2O/Bi_2O_2CO_3$/PEO nanofibers with a mass ratio of Cu_2O to $Bi_2O_2CO_3$ of 3% to remove the antibiotic chloramphenicol. After using the photocatalyst 4 times, the removal rate of photodegradation remained at a similar level, indicating that the photocatalyst is stable[139]. Mengelizadeh et al. [145] used g-C_3N_4/Fe_2O_3 photocatalyst with a concentration of 0.3 g/L to remove 25 mg/L of the antibiotic ciprofloxacin in 60 min under UV light. After 8 cycles of g-C_3N_4/Fe_2O_3 photocatalyst, the removal efficiency in the fifth and eighth cycles was 98.21% to 91.58%, respectively. This decrease is probably due to the saturation of the active sites of the photocatalyst and the decrease in the amount of photocatalyst during the recovery process[145] . Li et al. [203] used a 0.5 g/L Fe_3O_4/CdS/g-C_3N_4 photocatalyst to remove the antibiotic 20 mg/L ciprofloxacin.in visible light. the Fe_3O_4/ CdS /15 wt% g-C_3N_4photocatalyst is reduced by about 4.8% after three test cycles in 330 min, which indicates a very good performance of this photocatalyst[203]. Du et al. [207] used a ZnO/Ag/Ag_3PO_4 photocatalyst with a concentration of 0.5g/L to remove 10 mg/L of the antibiotic ciprofloxacin in 120 min under visible light. The photocatalyst ZnO/Ag/Ag_3PO_4 wt%:0.6/1 After 4 times of use in the photocatalytic reaction, the removal rate decreased from 90.1% to 75%, which shows the good stability of the photocatalyst[207]. Zhang et al. [204] used Cu_2O/Bi_2S_3 photocatalyst with a concentration of 0.5 g/L to remove 20 mg/L of tetracycline antibiotics in 60 min under visible light. The Cu_2O/Bi_2S_3 photocatalyst with 10 wt% Cu_2O after 4 times of photocatalytic reaction, the removal rate decreased from 95.23% to 92.8%. The decrease in the removal rate may be due to the adsorption of organic pollutants on the surface of the material, and a small part of it was not completely washed away. Also,

the p-n heterojunction was not formed and the high photocarrier separation efficiency was not damaged in the degradation process[204]. Lu et al. [148] used AgI/ $ZnIn_2S_4$/$BiVO_4$(AZB) photocatalyst with a concentration of 0.6g/L to remove 20 mg/L tetracycline, an antibiotic, in 120 min under visible light. The AZB photocatalyst, with a molar ratio of Bi to Ag: 1:1, after 10 cycles of photocatalytic reaction, the removal rate decreased from 91.44% to 82.16%. The reduction in the removal rate was about 9% in the 10th cycle. The formation of heterogeneous bonding of the AZB composite effectively inhibited the photocorrosion phenomenon of the catalyst, and the photocatalyst had excellent recovery performance[164]. After using the photocatalyst 4 times, the photocatalyst still had a high performance in removing antibiotics[148]. Manikandan et al. [208] used WO_3/P- g-C_3N_4 -MWCNT photocatalyst for the removal of tetracycline antibiotic. The photocatalyst did not show much decrease in removal rate after 3 times of recovery[208]. Liu et al. [201] used a CDs/g-C_3N_4/ZnO photocatalyst with a mass ratio of g-C_3N_4/ZnO: 30%wt and CDs4%wt(CZ) for the removal of the antibiotic tetracycline. The photocatalyst showed complete stability during repeated experiments after 10 times of recovery, although the degradation efficiency decreased slightly[201]. Lu et al. [169] used Ag_3PO_4/AgBr/g-C_3N_4 photocatalyst to remove the antibiotic tetracycline. The photocatalyst showed relatively good stability after 5 recycling cycles, which may be due to the photocorrosion of Ag+[169]. Wang et al. [152] used CuO/$CuFe_2O_4$ /g-C_3N_4 photocatalyst for the removal of the antibiotic tetracycline hydrochloride. The photocatalyst achieved a removal rate of 93.50% after 4 recycling cycles, which was a very good performance. This decrease was due to the possible blocking of the active site by organic intermediates decomposed by tetracycline hydrochloride[152]. Hu et al. [97] used the photocatalyst SnS_2@$ZnIn_2S_4$@kaolinite (SZK) with a mass ratio of SnS_2/ $ZnIn_2S_4$ wt%: 0.75:1 to remove the antibiotic tetracycline hydrochloride. The photocatalyst was reduced by 6.86% after 3 times of recovery, which showed very good performance. Also, the catalyst deposition performance was excellent and it could be deposited rapidly in a short time [97] . Tian et al. [185] used g-C_3N_4@ZnO photocatalyst for the removal of the antibiotic cephalexin. The photocatalyst decreased by 1.9% after

5 times of recovery, which may be due to the mass loss during the regeneration of g-C_3N_4@ZnO. Therefore, the photocatalyst showed excellent performance after 5 times of removal[185]. Ding et al. [205] used $BiVO_4$/g-C_3N_4/$NiFe_2O_4$ photocatalyst to remove the antibiotic ofloxacin. The photocatalyst decreased from 94% to 89% after 5 times of recovery, indicating very good stability of the photocatalyst[205]. Zhu, Guo, et al. [198] used a BiOI/ZnO/rGO photocatalyst with 5%wt rGO to remove the antibiotic chloramphenicol. The photocatalyst was recycled four times, and the removal rate remained above 95% even after the fourth time[198].

6-5-LIMITATIONS OF THE USE OF PHOTOCATALYSTS AND THEIR ENVIRONMENTAL CHALLENGES

In addition to the limitations of photocatalysts themselves, they also pose challenges for the environment. Although semiconductor photocatalysts have shown effective performance in the removal of antibiotics, they have limitations, such as catalyst stability, because many photocatalysts that are exposed to long-term light undergo photocorrosion or structural degradation, and the photocatalytic performance decreases. Most photocatalysts are activated by UV light and have poor performance in visible light. Due to poor charge transfer and inefficient separation, the low quantum efficiency of photocatalysts is low. Some effective photocatalysts use rare and expensive materials, which limit their application on an industrial scale. Due to variable environmental conditions, such as reactor size and maintenance, scaling from laboratory to industrial scale has become a serious challenge. Electron-hole recombination is also a fundamental limitation of photocatalysts[218]. When treating wastewater with photocatalysts, photocatalyst nanoparticles may remain in the water. The assessment of toxicity and risks to human health should be investigated. If the photocatalyst nanoparticles are lipophilic, they tend to remain in the food chain and eventually reach our digestive system, posing a direct threat to humans. Metals like silver, lead, mercury, arsenic and cadmium nanoparticles photocatalysts have adverse effects on human health due to their high toxicity, carcinogenic properties and potential damage to organs such as the liver, heart, eyes, and skin. Although

carbon-based photocatalysts such as carbon nanotubes have lower toxicity, they require a costly ultrafast centrifugation process to purify them from wastewater; otherwise, secondary pollution will occur and increase toxicity to aquatic life and humans. Separation of photocatalyst nanoparticles after wastewater treatment is a major challenge. The high surface area of photocatalysts leads to strong interactions with water molecules, complicating the separation process. Also, due to the attraction between photocatalytic nanoparticles molecules, their tendency to aggregate increases and their resistance to sedimentation or filtration removal methods increases. If photocatalysts contain surface charges, they create electrostatic interactions with water molecules. Photocatalytic nanoparticles are often lightweight and float in water, making their separation by gravity-based methods difficult[219]. Photocatalysts released into aquatic environments can cause toxic effects, the consequences of which for aquatic species and humans are unknown; however, they pose a risk through entry into the food chain[220]. Various parameters such as environmental conditions, crystalline phase, presence of surface coating, size of nanoparticles, Active surface area, chemical composition and shape affect toxicity[221,222].

Table5-Removal of antibiotics with different photocatalysts with heterojunction

Photocatalyst	**Antibiotics**	**Targeted pollutant concentration**	**Irradiation time**	**Optimized photocatalyst condition**	**Degradation**	**Reference**
$CuS/BiVO_4$	ciproflo xacin	10mg/L	90min	Visible light 300W Xe lamp Precipitation method for $BiVO_4$ 1g/L catalyst 7%CuS is optimum $K_{app} = 0.02151 \text{min}^{-1}.g^{-1}$	86.7%	[134]
WO_3	ciproflo xacin	10mg/L	4h	Visible light sonochemical process	19%	[155]
$g\text{-}C_3H_4$	ciproflo xacin	10mg/L	4h	Visible light sonochemical process	60%	
WO_3/ $g\text{-}C_3H_4$	ciproflo xacin	10mg/L	4h	Visible light	100%	

				sonochemical process 35-W Xe lamp 1g/L catalyst %5Wt WO_3 is optimum $K_{app} = 0.02561 min^{-1}.g^{-1}$		
ZnO-Ag_2O/porous g-C_3N_4	ciproflo xacin	20mg/L	48min	Visible light tungsten lamp calcination and hydrothermal method 0.5g/L catalyst $K_{app} = 0.114 min^{-1}.g^{-1}.L$	97.4%	[200]
Z-scheme ZnO/Ag/Ag_3PO_4	ciproflo xacin	10mg/L	60min	Visible light 300 W xenon lamp simple precipitation deposition method and and photoreduction technology 0.5g/L catalyst a mass ratio of ZnO to Ag_3PO_4 is 0.6:1 is optimum $K_{app} = 0.02886 min^{-1}.g^{-1}$	87.1%	[207]
Fe_3O_4/CdS/g-C_3N_4	ciproflo xacin	20mg/L	330min	Visible light 250-W xenon lamp Fe_3O_4 Synthesized by co-precipitation method, Fe_3O_4/CdS Synthesized by liquid chemistry, Fe_3O_4/CdS/g-C_3N_4 Synthesized by monodispersion 0.5 g/L catalyst 15%wt g-C_3N_4 is optimum $K_{app} = 0.044 min^{-1}.g^{-1}.L$	81%	[203]
CeO_2/ZnO nanocomposites	ciproflo xacin	15mg/L	60min	UV light 200 W Hg-Xe lamp simple co-precipitation method 0.25 g/L catalyst 8%Wt is CeO_2 is optimum pH=3.2 with 40% Wt CeO_2, K_{app} is $K_{app} = 0.052 min^{-1}.g^{-1}.L$ 92.2%TOC in 360min with 0.5g/L catalyst	63%	[157]

MoS_2/ZnO composites	ciproflo xacin	16.57mg/L	120min	Visible light 250 W metal halide lamp hydrothermal method Optimum catalyst doses:0.2g 30%wt is MoS_2 is optimum with 0.5g/L photocatalyst K_{app} is $K_{app} = 0.038 min^{-1}.g^{-1}.L$	96.18%	[141]
Haematite (Fe_2O_3) loaded on graphitic carbon nitride (g-C_3N_4)	ciproflo xacin	25 mg/L	60min	UV light mercury lamp calcination method 0.3g/L catalyst $K_{app} = 0.31 min^{-1}.g^{-1}.L$ 93.86% TOC in 60min 94.93% COD in 60 min 75.49% BOD in 60min	100%	[145]
g-C_3N_4/TiO_2nanorod	ciproflo xacin	6.63mg/L	60min	Visible light 500WXenon lamp 30% g-C_3N_4 is optimum PH=6.3 is optimum $K_{app} = 0.183 min^{-1}.g^{-1}.L$	93.4%	[172]
Z-scheme AgI/N–TiO_2	tetracycl ine	10mg/L	105min	decomposition: visible light 30 W DUHALLED 0.5g/L photocatalyst Optimum AgI/N-TiO_2 molar ratio:30%	73%	[159]
palygorskite-supported Cu_2O–TiO_2 composite	tetracycl ine	30mg/L	240min	Solar light 500WXe lamp palygorskite- TiO_2 Synthesized by sol–gel method, palygorskite-supported Cu_2O–TiO_2 composite Synthesized by liquid-phase reduction method 1g/L catalyst is optimum PH=8.7 is optimum $K_{app} = 0.0129 min^{-1}.g^{-1}.$	88.81%	[137]
ZnS/BiOBr	tetracycl ine	-	25min	sunlight	82%	[202]

				one-step facile hydrothermal method 2.5wt%ZnS is optimum K_{app} $= 0.1311 \text{min}^{-1}.g^{-1}.L$		
Cu_2O/Bi_2O_3	tetracycline	20mg/L	60min	Visible light 200 W high-pressure mercury lamp simple hydrothermal method 0.5g/L catalyst is optimum 10%wt Cu_2O is optimum K_{app} $= 0.088 min^{-1}.g^{-1}.L$	95.23%	[204]
$AgI/ZnIn_2S_4/BiVO_4$	tetracycline	20 mg/L	120min	Visible light 300 W Xenon lamp(λ> 420 nm) hydrothermal method and in-situ precipitation method 0.6g/L photocatalyst molar ratios of Bi to Ag:1:1 is optimum $K_{app} = 0.0353 \text{min}^{-1}.g^{-1}.L$ 57.85% TOC 64.89% COD	91.44%	[164]
$Bi_{12}O_{17}Cl_2/Ag/AgFeO_2$ Z-scheme photocatalysts	tetracycline	40mg/L	60min	Visible light $Bi_{12}O_{17}Cl_2/AgFeO_2$:in-situ deposition-precipitation method $Bi_{12}O_{17}Cl_2/Ag/AgFeO_2$: ultrasound (US)-assisted ethanol reduction method 0.5g/L catalyst 20%wt $Bi_{12}O_{17}Cl_2$ is optimum pH=3.8 is optimum K_{app} $= 0.07738 min^{-1}.g^{-1}$	94.1%	[165]
bifunctional direct Z-scheme WO_3@g-C_3N_4@MWCNT ternary nanocomposites	tetracycline	20 mg/L	120min	Visible light Halogen lamp 500 W, 420 nm Self assembling method 0.2g/L catalyst in pH=7, The removal rate is79.54% in pH=10 The removal rate is 86% K_{app} $= 0.0861 min^{-1}.g^{-1}.$	79.54%	[208]

CDs/g-C_3N_4/ZnO (CZ)nanocomposite	tetracycline	10mg/L	30min	Visible light 18 mW/cm_2, xenon lamp($\lambda > 420nm$) facile impregnation-thermal method mass ratio of g-C_3N_4/ZnO: 30%wt and CDs4%wt are optimum is $K_{app} = 0.164\text{min}^{-1}.g^{-1}.\text{L}$	100%	[201]
Ag_3PO_4/AgBr/g-C_3N_4	tetracycline	40mg/L	25min	visible light 300 W Xe lamp with 160 mW.cm^{-2} facile chemical deposition method 0.5g/L a mass ratio of g-c_3N_4 to Ag_3PO_4 20% is optimum The optimum pH is 7 $K_{app} = 0.24\text{min}^{-1}.g^{-1}.L$	80.2%	[169]
nanostructured g-C_3N_4/Nb_2O_5/HPEI/PES photocatalytic membrane	tetracycline	5mg/L	200min	Visible light visible light source (250 W) in-situ hydrothermal method 0.3%g-C_3N_4/Nb_2O_5/HPEI is optimum pH=10 is optimum $K_{app} = 4.5 \times 10^{-4}\text{min}^{-1}$	88%	[170]
CuO/$CuFe_2O_4$ / g-C_3N_4+PS	tetracycline	20 mg/L	30min	simulated sunlight 300 W xenon lamp ratio of CuO, $CuFe_2O_4$and g-C_3N_4 as 1.4:1:19 pH=3 and 0.2 g/L photocatalyst +PS=1mmol/L is optimum $K_{app} = 1.3\text{min}^{-1}.\text{g}^{-1}.L$ in 0.1g/L photocatalyst +PS,74% COD	99%	[152]
SnS_2@ $ZnIn_2S_4$@kaolinite	tetracycline	40mg/L	60min	Visible light 300 W xenon lamp with a 420 nm cut-off filter hydrothermal method. 0.2g/L Wt%SnS_2/$ZnIn_2S_4$: 0.75:1 is optimum $K_{app} = 0.1155\text{min}^{-1}.g^{-1}.L$	88.23%	[184]

				55.86% TOC in 60min		
$Cu_2O/Bi_2O_2CO_3$/PEO nanofibers	chloramphenicol	20mg/L	30min	Visible light 300 W Xe lamp mass ratio of Cu_2O to $Bi_2O_2CO_3$:3 is Optimum $K_{app} = 0.1339 min^{-1}$	98.2%	[139]
Z-scheme g-C_3N_4@ZnO	Cephalexin	10mg/L	60min	Sunlight Xenon lamp (300 W) thermal atomic layer deposition 0.3g/L The optimum PH is 6.3 $K_{app} = 0.245 min^{-1}.g^{-1}.L$ distilled water 72.8%TOC in 60min	98.9%	[185]
				Sewage from municipal wastewater treatment plant	92.7%	
g-C_3N_4 thin layer @ CeO_2	doxycycline	10mg/L	60min	Visible light 150W Xeon lamp simple hydrothermal and in situ synthesis 0.5g/L catalyst 5% g-C_3N_4/ CeO_2 is optimum $K_{app} = 0.0655 min^{-1}.g^{-1}.$	84%	[148]
g-C_3N_4/ $NiFe_2O_4$/ $BiVO_4$	ofloxacin	10 mg/L	20min	Visible light 300 W Xenon lamp (λ > with the filter 420 nm) 1g/L catalyst 5% wt g-C_3N_4 in $BiVO_4$/ g-C_3N_4 is optimum Optimum PH is 9 $K_{app} = 0.1353 min^{-1}.g^{-1}.$ 40.5%TOC in 120min	93.8%	[205]
Z-scheme g-C_3N_4/CdS	erythromycin	50mg/L	60min	Visible light The 35W Xenon lamp a stable wavelength of 300–2500 nm chemisorption and self-assembly method 0.5g/L Optimum is mass CN/CS:3/1 PH=5 is optimum	81.02%	[206]

7-

				$K_{app} = 0.056 min^{-1}.g^{-1}.L$		
BiOI/ZnO/rG	Ochloramphenicol	10mg/L	180min	Visible light 300 W Xenon lamp simple one −step hydrothermal 0.5g/L BiOI/ZnO/rGO rGO with a mass fraction of 5% is optimum $K_{app} = 0.0306 min^{-1}.g^{-1}.$	90%	[198]
WO_3/ AgI/rGO	amoxicillin	20mg/L	180min	Visible light 30W LED lamp 0.5g/L catalyst $K_{app} = 0.0212 min^{-1}.g^{-1}.$	86.1%	[209]

OPERATING PARAMETERS AFFECTING PHOTOCATALYTIC REMOVAL OF ANTIBIOTICS

Although the choice of photocatalyst type and its synthesis method are important in the photocatalytic removal of antibiotics, operational conditions such as initial antibiotic concentration, amount of photocatalyst, environmental pH, and light source are effective in the removal rate. pH plays a very important role in the photocatalytic removal of antibiotics because pH changes affect the concentration of H^+ and OH^- ions, which have a direct effect on reactive species h^+, hydroxyl radicals($OH^{\cdot}$), and superoxide radicals($O_2^{-\cdot}$)[223]. Therefore, pH affects the valence and conduction band positions, aggregation, surface energy, photocatalyst charge, and photocatalyst size. So, the optimal pH value has a better performance in antibiotic removal rate [224]. Raja et al. [115] used rGO- $BiVO_4$-ZnO photocatalyst to remove the antibiotic (CIP)ciprofloxacin. With increasing pH from 3 to 7, the CIP removal rate increases and then decreases after pH 7. The CIP removal rates at pH 3, 5, 7, 9 and 11 are 54%, 71.1%, 97.8%, 92.4% and 80.5% after 60 min in the presence of visible light, respectively. The removal rate is optimal at pH 7. The zero point charge(ZPC) of rGO- $BiVO_4$-ZnO photocatalyst, calculated by potentiometric titration, is 7.3, which is lower than that of ZnO photocatalyst. The surface

charge density of the photocatalyst is negative when the pH is higher than the ZPC. This affects the adsorption of CIP, which is anionic at pH levels higher than 7. Therefore, the CIP removal rate is low at pH 3 and 11[115]. Mengelizadeh et al. [145] used a g-C_3N_4/Fe_2O_3 photocatalyst to remove ciprofloxacin (CIP). At a g-C_3N_4/Fe_2O_3 dose of 0.3 g/L, an initial CIP concentration of 25 mg/L, an irradiation intensity of 36 W, and a time of 60 min, the effect of pH on CIP degradation was investigated. In completely alkaline (pH = 11) and completely acidic (pH = 3) conditions, the CIP removal rates were 52.67% and 51.73%, respectively. While at pH 7, it gave complete CIP removal. The pH_{zpc} for the g-C_3N_4/Fe_2O_3 photocatalyst was 5.9 and the pKa of CIP was between 6.16 and 8.23. Therefore, CIP was in anionic form at pH > 8.23, in zwitterionic form at pH 6.16-8.23, and in cationic form at pH < 6.16. In strongly acidic and basic pHs, CIP and the g-C_3N_4/Fe_2O_3 photocatalyst have very similar surface charges, so adsorption on the photocatalyst surface is limited. At pH greater than 8, the photocatalyst surface is covered with OH-Fe complex and fills the holes created in the photocatalyst by OH^- ions[145]. Wang et al. [152] used CuO/ $CuFe_2O_4$/g-C_3N_4(CCCN) photocatalyst to remove tetracycline (TC). The change of pH affects the generation of free radicals. To adjust the solution, 0.1 mol/L sulfuric acid or sodium hydroxide was added to the solution. At pH 3, 9 and 11, the removal rate decreased to 81.5%, 60.0% and 21.8%, respectively. The decrease in TC removal rate is due to the increase of electrostatic repulsion between persulfate and CCCN with increasing pH, which significantly reduces the generation of $SO_4^{\bullet-}$ [152]. A high initial antibiotic concentration means that more active sites on the photocatalyst surface are required for the antibiotic molecules, while the active sites are limited. In addition, with increasing antibiotic concentration, more by-products and intermediates are produced that compete with the antibiotic molecules for the limited active sites. As the concentration increases and the solution becomes more concentrated, the passage of the solution decreases, resulting in the photons reaching the photocatalyst surface being slower, so fewer photons reach the photocatalyst surface and fewer reactive species are produced. Also, some antibiotics absorb photons and prevent them from reaching the photocatalyst. Therefore, the optimal initial antibiotic

concentration has a better performance in antibiotic removal rate[225,226]. Mengelizadeh et al. [145] used a g-C_3N_4/Fe_2O_3 photocatalyst to remove (CIP)ciprofloxacin. At a g-C_3N_4/Fe_2O_3 dose of 0.3 g/L, radiation intensity of 36 W, pH 7, and time of 60 min, the effect of CIP concentration on CIP degradation was investigated. The CIP removal rate decreased from 100% to 84.79% with an increase in the initial CIP concentration from 10 to 50 mg/L. The decrease in removal rate was probably due to the reduction in the path length of the incoming photons into the solution and the occupation of the active sites of the nanocomposite. Also, the reason for the decrease in removal rate at high concentrations under constant reaction conditions is that since the reaction rate is constant, the amount of active species produced is limited and is sufficient to remove large amounts of CIP[145]. Zhang et al. [204] used Cu_2O/Bi_2S_3 photocatalyst to remove the antibiotic (TC) tetracycline. With 50 mg of Cu_2O/Bi_2S_3 photocatalyst, the photocatalytic removal of TC with different concentrations from 5 to 40 mg/L was investigated. The TC removal was complete in 40 min when the concentration was low. When the concentration was increased to 20 mg/L, the TC removal rate could reach about 95%. When the concentration was increased to 30 mg/L, the removal rate reached 75% in 60 min. Finally, at 40 mg/L TC, the removal rate reached 60%. A certain amount of photocatalyst was able to produce limited active species, which was not sufficient for high TC concentrations[204]. Increasing the amount of photocatalyst leads to the creation of more active sites that participate in the photocatalytic reactions of the antibiotic. However, increasing the amount of photocatalyst beyond the optimal amount leads to the aggregation of the photocatalysts, resulting in a decrease in the number of active sites and turbidity of the solution, resulting in a decrease in the removal rate of the antibiotic Therefore, the optimal photocatalyst amount has better performance in antibiotic removal rate[225,227]. Raja et al. [115] used rGO- $BiVO_4$-ZnO photocatalyst to remove the antibiotic (CIP)ciprofloxacin(CIP). For rGO- $BiVO_4$-ZnO photocatalyst with 10, 20, 30 and 40 mg photocatalyst, the removal percentages are 83.9%, 88%, 98.4% and 96.4% in 60 min, respectively. Therefore, the optimum photocatalyst loading is 30 mg. The decrease in CIP removal rate for 40 mg loading is due to the reflection of light by the photocatalyst

particles[115]. Zhang et al. [204] used Cu_2O/Bi_2S_3 photocatalyst to remove the antibiotic tetracycline (TC). At a concentration of 20 mg/L TC, the degradation rate increased from 50% to 85% with increasing the amount of photocatalyst from 10 mg to 30 mg. If the amount of photocatalyst increased from 30 mg, the removal rate decreased due to insufficient light transmission and increased turbidity of the suspension[204]. The wavelength and intensity of light have a direct effect on the rate of removal of antibiotics in the presence of light because photocatalysts are sensitive to the wavelength of light and its intensity. With increasing light intensity, the number of photons increases and more charge carriers are produced for the photocatalytic oxidation reactions of antibiotics. The wavelength and intensity of light must also be optimal because if the wavelength is greater than the optimal wavelength, no reaction occurs because the photon is not absorbed. If the wavelength is less than the optimal value, too much energy may damage the photocatalyst structure. Also, high light intensity leads to electron-hole recombination and low intensity leads to a slow photocatalytic reaction of antibiotic degradation [225]. Mengelizadeh et al. [145] used a g-C_3N_4/Fe_2O_3 photocatalyst to remove (CIP)ciprofloxacin. At a g-C_3N_4/Fe_2O_3 dose of 0.3 g/L, an initial CIP concentration of 25 mg/L, pH 7, and a time of 60 min, the effect of light intensity on CIP degradation was investigated. The CIP removal efficiency increased significantly from 78.19% to 100% with increasing light intensity from 8 to 36 W. The reason for this increase is probably due to the increased production of reactive species through water hydrolysis by UV alone and the photocatalyst surface[145].

7-1- INFLUENCE OF WATER MATRIX COMPONENTS

In realistic water environments, photocatalytic removal of antibiotics occurs in complex matrices containing natural organic matter (NOM), dissolved inorganic ions, and multiple coexisting pollutants. These constituents can substantially influence photocatalytic performance by modifying light absorption, reactive oxygen species (ROS) dynamics, adsorption equilibria, and charge-carrier utilization. Consequently, evaluating photocatalysts solely in simplified laboratory solutions may lead to misleading conclusions regarding their practical efficiency[228–230].

Natural organic matter is an unavoidable component of natural and engineered water bodies and therefore a critical variable when extrapolating photocatalytic antibiotic removal from idealized solutions to real matrices. A detailed kinetic and mechanistic study on tetracycline photolysis in the presence of humic-like surrogates (tannic acid and gallic acid) underscores the non-trivial, and partly counter-intuitive, role of NOM [231]. When these NOM analogues were introduced under UV irradiation, the overall disappearance of tetracycline became slower, even though the indirect, ROS-mediated routes were actually promoted. In other words, NOM simultaneously acts as a photosensitizer that opens additional reaction channels and as an inhibitor that suppresses the most efficient, direct excitation of the antibiotic [231,232]. This duality is precisely what many simplified studies fail to capture when they evaluate catalyst performance in NOM-free media and then generalize those trends to natural waters. Mechanistically, the work reveals that aromatic NOM components strongly compete with the antibiotic for incoming photons and thus attenuate direct photolysis. Spectroscopic analyses show that tannic and gallic acids exhibit humic-like fluorescence signals, which are quenched progressively as tetracycline concentration increases, indicating intimate interaction and excited-state quenching between the drug and the NOM matrix [231,233]. Such quenching is consistent with the formation of ground-state complexes and with deactivation of NOM triplet states that would otherwise participate in ROS generation. In parallel, however, excitation of these humic-like species gives rise to singlet oxygen and related reactive intermediates, which mediate an indirect oxidative attack on tetracycline [232,234]. The net observed outcome is therefore a redistribution: the contribution of NOM-sensitized pathways increases, but the suppression of direct absorption by the antibiotic dominates, leading to a lower apparent degradation rate. Importantly, despite this pronounced kinetic influence, NOM does not substantially alter the distribution of phototransformation products, indicating that it primarily modulates reaction rates rather than fundamentally changing degradation pathways [230,231].

In addition to NOM, dissolved inorganic ions present in natural and engineered waters can significantly modulate photocatalytic antibiotic degradation by interacting with reactive intermediates or affecting surface reactions. Studies on Bi_2O_3/Ti^{3+}-TiO_2 p–n heterojunctions for visible-light degradation of tetracyclines (TC, OTC, TCH) provide a representative example of such matrix effects [229]. Systematic tests with common cations (K^+, Na^+, Ca^{2+}) revealed negligible influence on tetracycline degradation, suggesting that these species mainly behave as background electrolytes under typical experimental conditions [229]. In contrast, the impact of anions is more pronounced and strongly species-dependent. The addition of Cl^- and NO_3^- at concentrations of 0.02–0.10 mol L^{-1} did not significantly inhibit tetracycline removal, indicating limited interaction with the dominant oxidative species responsible for degradation. However, the presence of SO_4^{2-} produced a measurable reduction in degradation efficiency, which was attributed to its role as a radical scavenger that competes with tetracycline for reactive oxygen species generated on the catalyst surface [229,232]. Experiments conducted in real water matrices such as tap, mineral, and river water further confirmed that mixed ionic compositions can introduce moderate inhibition through combined radical scavenging, competitive adsorption, and light-screening effects, although the photocatalytic system maintained overall activity [229]. These observations highlight that the influence of inorganic ions on antibiotic degradation is highly ion-specific and closely linked to the dominant reaction mechanism.

Beyond inorganic constituents, antibiotics in wastewater typically coexist with a wide range of additional organic and inorganic contaminants originating from industrial, agricultural, and municipal sources. Such pollutant mixtures can substantially influence photocatalytic reactions by altering charge-carrier dynamics and redistributing redox processes among different substrates. Evidence for this behavior is provided by mixed-pollutant photocatalytic systems involving Cr(VI) and nitrophenol derivatives, where simultaneous reduction and oxidation reactions occur on the catalyst surface. In these systems, photogenerated electrons are preferentially consumed in the reduction of Cr(VI) to Cr(III), while photogenerated holes or derived oxidative species participate in the degradation of

nitrophenol compounds. This complementary consumption of charge carriers suppresses electron–hole recombination and improves photocatalytic efficiency through more effective charge utilization [228,235]. The extent of this cooperative behavior strongly depends on catalyst architecture and interfacial charge-transfer pathways. For instance, oxygen-vacancy-rich Bi_2MoO_6 coupled with MIL-121 forms a heterostructured system that promotes spatial separation of photogenerated carriers, enabling parallel reduction and oxidation reactions during the simultaneous removal of Cr(VI) and 2-nitrophenol [235,236]. Similarly, engineered dual heterojunction systems such as Ag_2O–Ag_2CO_3 /g-C_3N_4 facilitate directional charge migration and interfacial electron transfer, supporting concurrent transformation of multiple pollutants through distinct oxidative and reductive pathways [237]. Nevertheless, pollutant coexistence does not always enhance performance. In many cases, different contaminants compete for adsorption sites, reactive oxygen species, or photogenerated charge carriers, which can suppress degradation efficiency. The overall outcome therefore depends on the relative redox potentials of the pollutants, their adsorption affinity toward the catalyst surface, and the kinetics of the competing reactions [235,238]. As a result, pollutant coexistence can either promote synergistic redox utilization or introduce competitive pathways that diminish photocatalytic activity, underscoring the importance of evaluating photocatalysts under realistic multi-component water matrices.

8- CONCLUSION

Environmental challenges are increasing and becoming more complex day by day. One of the most important policies in developed countries is to pay attention to environmental issues of industries. There are various pollutants in the environment, including noise pollutants, air pollutants, and pollutants in wastewater. Among the various pollutants in wastewater, heavy metals, pesticides, toxins, and drugs can be mentioned. The consumption of drugs is increasing due to advances in medical fields and population growth, and this trend is expected to continue. Among drugs, antibiotics deserve special attention due to their different applications in animal husbandry and the human sector. Drug pollutants

have complex structures and conventional methods increase in complexity due to the presence of different antibiotics in water. Among the different methods for removing antibiotics, the most common is photocatalyst, which leads to the conversion of antibiotics into simpler substances, water and carbon dioxide. The use of different graphene structures alongside other photocatalysts leads to an increase in the specific surface area and, consequently, an increase in antibiotic removal. Graphene has played an effective role in the photocatalytic removal of antibiotics.

The graphene structure provides effective charge separation and improves the photocatalyst performance. The addition of rGO to the $BiVO_4$-ZnO structure leads to an 18.1% increase in the removal of ciprofloxacin with an initial concentration of 10 mg/L in 60 min in the presence of visible light. In the Cu-TiO_2 structure, the presence of GO leads to a 4.8% increase in the removal of 20 mg/L antibiotic tetracycline hydrochloride in 90 min in the presence of UV light. Also, the energy consumption per gram of antibiotic removed is 450.9 kWh/g, which is a high number on a laboratory scale. The addition of rGO to the ZnO photocatalyst leads to a 34.8% increase in the removal of 1000 mg/L of chloramphenicol in 100 min in the presence of UV light. The addition of 8% rGO in the S@g-C_3N_4/B@g-C_3N_4 structure leads to an improvement in the photocatalytic performance of 45% and 38.8% compared to B@ g-C_3N_4 and S@ g-C_3N_4, respectively, in the presence of visible light and in 90 min for 10 mg/L chloramphenicol.

The heterojunction structure with different energy band positions leads to effective electron-hole separation and broadening of light absorption and enhancement of redox potential. In p-n heterojunction structure for Cu_2O/$Bi_2O_2CO_3$/PEO photocatalyst, it leads to 14.2% increase over $Bi_2O_2CO_3$/PEO photocatalyst for removal of 20 mg/L Ciprofloxacin in 30 min under visible light. In removal of 20 mg/L Ciprofloxacin in 48 min under visible light, ZnO-Ag_2O/porous g-C_3N_4 photocatalyst has effective removal performance compared to single photocatalysts. Compared to single ZnO photocatalyst, ZnO/MoS_2 heterojunction structure leads to 46% increase in performance of 16.57 mg/L Ciprofloxacin in UV light.

In the type II heterojunction structure, compared to the g-C_3N_4 photocatalyst, the heterojunction structure leads to a 72% increase in the removal of tetracycline antibiotic 10 mg/L in the presence of visible light and a time of 60 min. In the CuO/ $CuFe_2O_4$ / g-C_3N_4 +PS heterojunction structure, the heterojunction structure leads to a 48% increase compared to g-C_3N_4 +PS for tetracycline antibiotic 10 mg/L in the presence of sunlight in 30 min.

In the Z-scheme heterojunction structure, the Cu_2O/Bi_2O_3 heterojunction structure leads to a 23.23% increase compared to Cu_2O for the removal of 20 mg/L of tetracycline in 60 min in the presence of visible light. The heterojunction structure of $Bi_{12}O_{17}Cl_2$/Ag/$AgFeO_2$ leads to a 32.1% increase compared to Ag/$AgMO_2$ leading to the removal of 40 mg/L of tetracycline in the presence of visible light in 60 min.

The simultaneous combination of the heterojunction structure and the graphene structure leads to a significant increase in the removal rate of the antibiotic. In the photocatalytic structure of BiOI/ZnO/rGO, the removal rate of the BiOI/ZnO photocatalyst increases by 6% in the removal of 10 mg/L of chloramphenicol in 180 min in the presence of visible light compared to the ZnO photocatalyst, while in the heterojunction structure of BiOI/ZnO with 5%wt rGO, the removal rate increases by 12% compared to BiOI/ZnO. The removal rate of 20mg/L of amoxicillin in the presence of visible light and in 240 min for WO_3/AgI photocatalyst leads to an increase of 28.6% compared to WO_3 photocatalyst, while adding rGO to the WO_3/AgI structure leads to an increase of 21.1% compared to WO_3/AgI.

8-1-FUTURE DIRECTIONS

- **Development of advanced photocatalyst architectures:**

Future research should focus on designing novel photocatalytic structures such as MOFs, covalent organic frameworks (COFs), and multifunctional nanocomposites with enhanced visible-light activity, high stability, and large specific surface areas to improve antibiotic degradation efficiency[239,240].

- **Integration of machine learning in photocatalyst discovery:**

Machine learning techniques can accelerate the identification of optimal photocatalyst compositions by screening large materials databases and predicting the most promising structures, synthesis routes, and operational conditions for antibiotic removal.

- **Optimization of Operational Parameters and Reactor Design:**

Further research is required to optimize operational conditions such as pH, photocatalyst dosage, light intensity, and pollutant concentration. In addition, the development of efficient photoreactor designs is essential for improving degradation performance and enabling large-scale treatment applications [241].

- **Coupling artificial intelligence with density functional theory (DFT):**

The integration of artificial intelligence with DFT calculations can significantly accelerate the discovery of new photocatalysts by rapidly predicting key material properties such as band structure, optical absorption, and structural stability, thereby enabling efficient screening of large numbers of candidate materials.

ACKNOWLEDGEMENT

FUNDING

Not applicable.

COMPETING INTERESTS

The authors have no relevant financial or non-financial interests to disclose.

AUTHOR CONTRIBUTIONS

Asghar Taghiloo, Milad Aalipour and Seyed Mohammad Matin Ahmadi: Investigation, Writing (Original draft preparation).

Afsanehsadat Larimi, Ali Akbar Asgharinezhad and Rui Tan: Supervision, Writing (Reviewing and Editing).

ETHICS APPROVAL AND CONSENT TO PARTICIPATE

Not applicable.

CONSENT FOR PUBLICATION

All listed authors have approved the manuscript before submission.

AVAILABILITY OF DATA AND MATERIALS

All data generated or analyzed during this study are included in this published article.

REFERENCES

[1] A. Asadi, A. Larimi, Z. Jiang, A. Naderifar, Modeling and simulation of photocatalytic CO2 reduction into methanol in a bubble slurry photoreactor, Chem. Eng. Sci. 263 (2022) 118078. https://doi.org/10.1016/J.CES.2022.118078.

[2] A. Rastgaran, H. Fatoorehchi, N. Khallaghi, A. Larimi, T.N. Borhani, Modelling of photocatalytic CO2 reduction into value-added products in a packed bed photoreactor using the ray tracing method, Carbon Capture Science & Technology (2023) 100118. https://doi.org/https://doi.org/10.1016/j.ccst.2023.100118.

[3] Z. Yang, S. Zhou, X. Feng, N. Wang, O. Ola, Y. Zhu, Recent Progress in Multifunctional Graphene-Based Nanocomposites for Photocatalysis and Electrocatalysis Application, Nanomaterials 13 (2023) 2028. https://doi.org/10.3390/nano13132028.

[4] A. Al Miad, P. Saikat, K. Alam, Nanoscale Advances Metal oxide-based photocatalysts for the e ffi cient degradation of organic pollutants for a sustainable environment : a review, (2024) 4781–4803. https://doi.org/10.1039/d4na00517a.

[5] M. Beshtar, S. Mohammad, M. Ahmadi, A. Akbar, A. Larimi, In-depth Review : Catalysis and process parameters in photocatalytic oxidative desulfurization of liquid transportation fuels, J. Clean. Prod. 508 (2025) 145462. https://doi.org/10.1016/j.jclepro.2025.145462.

[6] M.A. Ahmed, A.A. Mohamed, Recent progress in semiconductor/graphene photocatalysts: synthesis, photocatalytic applications, and challenges, RSC Adv. 13 (2023) 421–439. https://doi.org/10.1039/d2ra07225d.

[7] Z. Yang, S. Zhou, X. Feng, N. Wang, O. Ola, Y. Zhu, Recent Progress in Multifunctional Graphene-Based Nanocomposites for Photocatalysis and Electrocatalysis Application, Nanomaterials 13 (2023) 2028. https://doi.org/10.3390/nano13132028.

[8] J. Ma, Y. Chen, G. Zhou, H. Ge, H. Liu, Recent Advances in Photocatalytic Degradation of Tetracycline Antibiotics, Catalysts 14 (2024) 762. https://doi.org/10.3390/catal14110762.

[9] A. Al Miad, P. Saikat, K. Alam, Nanoscale Advances Metal oxide-based photocatalysts for the e ffi cient degradation of organic pollutants for a sustainable environment : a review, (2024) 4781–4803. https://doi.org/10.1039/d4na00517a.

[10] M. Osanloo, F. Khorasheh, A. Larimi, Journal of Water Process Engineering Development of a novel Z - scheme TiO 2 / CuBi 2 O 4 @ GO with enhanced performance for the photocatalytic degradation of metronidazole, Journal of Water Process Engineering 72 (2025) 107641. https://doi.org/10.1016/j.jwpe.2025.107641.

[11] M.A. Ahmed, A.A. Mohamed, Recent progress in semiconductor/graphene photocatalysts: synthesis, photocatalytic applications, and challenges, RSC Adv. 13 (2023) 421–439. https://doi.org/10.1039/d2ra07225d.

[12] X. Wang, J. Zhang, H. Wang, M. Liang, Q. Wang, F. Chen, Revealing the Role of Defect in 3D Graphene-Based Photocatalytic Composite for Ef fi cient Elimination of Antibiotic and Heavy Metal Combined Pollution, (2024) 1–11. https://doi.org/10.1002/eem2.12616.

[13] K.M. Mohamed, J.J. Benitto, J.J. Vijaya, M. Bououdina, Recent Advances in ZnO-Based Nanostructures for the Photocatalytic Degradation of Hazardous, Non-Biodegradable Medicines, Crystals (Basel). 13 (2023) 329. https://doi.org/10.3390/cryst13020329.

[14] J. Ma, Y. Chen, G. Zhou, H. Ge, H. Liu, Recent Advances in Photocatalytic Degradation of Tetracycline Antibiotics, Catalysts 14 (2024) 762. https://doi.org/10.3390/catal14110762.

[15] X. Wang, J. Zhang, H. Wang, M. Liang, Q. Wang, F. Chen, Revealing the Role of Defect in 3D Graphene-Based Photocatalytic Composite for Ef fi cient Elimination of Antibiotic and Heavy Metal Combined Pollution, (2024) 1–11. https://doi.org/10.1002/eem2.12616.

[16] K.M. Mohamed, J.J. Benitto, J.J. Vijaya, M. Bououdina, Recent Advances in ZnO-Based Nanostructures for the Photocatalytic Degradation of Hazardous, Non-Biodegradable Medicines, Crystals (Basel). 13 (2023) 329. https://doi.org/10.3390/cryst13020329.

[17] J. Sengupta, C.M. Hussain, Advanced Graphene-Based Technologies for Antibiotic Removal from Wastewater: A Review (2016–2024), C (Basel). 10 (2024) 92. https://doi.org/10.3390/c10040092.

[18] E.Y. Klein, I. Impalli, S. Poleon, P. Denoel, M. Cipriano, T.P. Van Boeckel, S. Pecetta, D.E. Bloom, A. Nandi, Global trends in antibiotic consumption during 2016–2023 and future projections through 2030, Proceedings of the National Academy of Sciences 121 (2024) 1–9. https://doi.org/10.1073/pnas.2411919121.

[19] J. Sengupta, C.M. Hussain, Advanced Graphene-Based Technologies for Antibiotic Removal from Wastewater: A Review (2016–2024), C (Basel). 10 (2024) 92. https://doi.org/10.3390/c10040092.

[20] A. Chauhan, R. Kumar, P. Raizada, S. Thakur, V.H. Nguyen, A. Singh, Q. Van Le, P. Singh, A. Sudhaik, Novel hydrogen-bonded organic framework (HOF) for highly efficient photocatalysis: From structural designs to multifunctional applications, Coord. Chem. Rev. 535 (2025). https://doi.org/10.1016/j.ccr.2025.216634.

[21] S. Sharma, P. Dhull, R. Kumar, A. Sudhaik, P. Raizada, Q. Van Le, A.A. Parwaz Khan, P. Singh, T. Kamal, K.A. Alzahrani, Recent updates on a Cs3Bi2Br9-based heterojunction photocatalyst for selective CO2 conversion into (CO/CH4) products, Journal of Industrial and Engineering Chemistry 148 (2025). https://doi.org/10.1016/j.jiec.2025.01.029.

[22] A. Chauhan, R. Kumar, S. Devi, Sonu, P. Raizada, P. Singh, V.K. Ponnusamy, A. Sudhaik, A.K. Mishra, R. Selvasembian, Recent advances on Co3O4-based nanostructure photocatalysis: Structure, synthesis, modification strategies, and applications, Surfaces and Interfaces 54 (2024). https://doi.org/10.1016/j.surfin.2024.105152.

[23] M.A. Ahmed, A.A. Mohamed, Recent progress in semiconductor/graphene photocatalysts: synthesis, photocatalytic applications, and challenges, RSC Adv. 13 (2022). https://doi.org/10.1039/d2ra07225d.

[24] R. Kumar, M. Malhotra, A. Sudhaik, P. Raizada, X.C. Luu, A.A. Parwaz Khan, S. Thakur, T. Ahamad, V.H. Nguyen, P. Singh, Unlocking the non-covalent electrostatic engineering of photocatalysts: From molecular interactions to multifield tuning strategies toward enhanced charge dynamics, Advanced Powder Materials 4 (2025). https://doi.org/10.1016/j.apmate.2025.100338.

[25] R. Kumar, A. Sudhaik, A.A. Pawaz Khan, V.H. Nguyen, A. Singh, P. Singh, S. Thakur, P. Raizada, Designing tandem S-scheme photo-catalytic systems: Mechanistic insights, characterization techniques, and applications, Wuli Huaxue Xuebao/ Acta Physico - Chimica Sinica 41 (2025). https://doi.org/10.1016/j.actphy.2025.100150.

[26] A. Sudhaik, P. Raizada, P. Shandilya, D.Y. Jeong, J.H. Lim, P. Singh, Review on fabrication of graphitic carbon nitride based efficient nanocomposites for photodegradation of aqueous phase organic pollutants, Journal of Industrial and Engineering Chemistry 67 (2018). https://doi.org/10.1016/j.jiec.2018.07.007.

[27] A. Rana, S. Sonu, A. Sudhaik, R. Kumar, A. Chawla, P. Raizada, V. Chaudhary, T. Ahamad, S. Kaya, N. Kumar, K.P. Katin, C.M. Hussain, P. Singh, Tailoring dual S-Scheme based g-C3N4/ZnO/TiO2 ternary

photocatalytic system immobilized on floating cork for environmental remediation, J. Taiwan Inst. Chem. Eng. 168 (2025). https://doi.org/10.1016/j.jtice.2024.105914.

[28] A. Sudhaik, R. Kumar, S. Sharma, A. Sharma, S. Devi, P. Raizada, Q. Van Le, T. Ahamad, V.H. Nguyen, P. Singh, Structural design of dual Z-scheme GCN/CdO/CaFe2O4 ternary heterojunction with high visible light activity: Photocatalytic performance and mechanism in the degradation of Congo red dye, Inorg. Chem. Commun. 172 (2025). https://doi.org/10.1016/j.inoche.2024.113697.

[29] R. Kumar, A. Sudhaik, D. Kumar, R. Devi, E. Devi, A. Chawla, P. Raizada, C.M. Hussain, T. Ahamad, P. Singh, Synergistic photocatalytic activity of Bi2O3/g-C3N4/ZnO ternary heterojunction with dual Z-scheme charge transfer towards textile dye degradation, Journal of Industrial and Engineering Chemistry 144 (2025). https://doi.org/10.1016/j.jiec.2024.10.002.

[30] A. Sudhaik, R. Kumar, P. Raizada, T. Ahamad, S. Kaya, N.T.T. Nguyen, K.P. Katin, N. Kumar, V. Puri, V.H. Nguyen, P. Singh, Manipulating the charge transfer pathway in a dual Z-scheme BiOBr/g-C3N4/V2O5-Al2O3 heterojunction toward efficient degradation of textile dyes, J. Taiwan Inst. Chem. Eng. 178 (2026). https://doi.org/10.1016/j.jtice.2025.106373.

[31] A. Chauhan, A.A.P. Khan, A. Sudhaik, R. Kumar, K.P. Katin, S. Kaya, P. Raizada, P. Singh, N. Azum, K.A. Alzahrani, Fabrication of a dual Z-scheme Ag3PO4/g-C3N4/Bi2MoO6 ternary nanocomposite for effective degradation of methylene blue dye, J. Solgel Sci. Technol. 112 (2024). https://doi.org/10.1007/S10971-024-06556-W.

[32] I.J. Budiarso, V.A. Dabur, R. Rachmantyo, H. Judawisastra, C. Hu, A. Wibowo, Carbon nitride- and graphene-based materials for the photocatalytic degradation of emerging water pollutants, Mater. Adv. 5 (2024) 2668–2688. https://doi.org/10.1039/D3MA01078C.

[33] Y. Bai, D. Hao, S. Feng, L. Lu, Q. Wang, A magnetically reusable Ce-MOF/GO/Fe 3 O 4 composite for effective photocatalytic degradation of chlortetracycline, Physical Chemistry Chemical Physics 26 (2024) 3832–3841. https://doi.org/10.1039/D3CP04499H.

[34] A. Larimi, F. Khorasheh, Carbonaceous supports decorated with Pt e TiO 2 nanoparticles using electrostatic self-assembly method as a highly visible-light active photocatalyst for CO 2 photoreduction, Renew. Energy 145 (2020) 1862–1869. https://doi.org/10.1016/j.renene.2019.07.105.

[35] A. Larimi, Carbonaceous Supports Decorated with Pt-TiO_2 Nanoparticles Using Electrostatic Self-Assembly Method As a Highly Visible Light Active Photocatalyst for CO_2 Photoreduction, in: 2018 AIChE Annual Meeting, AIChE, 2018.

[36] Ahmadi, S. M. M.; Taghiloo, A.; Asgharinezhad, A. A.; Larimi, A. Next-Generation Photocatalysts for Hydrogen Production : Innovations , Challenges , and Future Perspectives. 2026. https://doi.org/10.1021/acs.energyfuels.6c00604.

[37] M. Beshtar, F. Khorasheh, A. Larimi, A. Akbar Asgharinezhad, Photocatalytic oxidative desulfurization of model fuel using iron-molybdenum nanocatalyst based on cerium oxide (FeyMox/CeO2) under visible light, Fuel 360 (2024) 130549. https://doi.org/https://doi.org/10.1016/j.fuel.2023.130549.

[38] M. Beshtar, A. Larimi, A.A. Asgharinezhad, F. Khorasheh, Ultra-deep Photocatalytic Oxidative Desulfurization of Model Fuel Using Ti-UiO-66(Zr) Metal–Organic Framework, Catal. Letters (2023). https://doi.org/10.1007/s10562-023-04506-9.

[39] M. Beshtar, A. Akbar Asgharinezhad, A. Larimi, Ultra-deep photocatalytic oxidative desulfurization of liquid fuels by Ti@CeO2/ZnO nanophotocatalyst under visible light and mild operating conditions,

Journal of Industrial and Engineering Chemistry (2024). https://doi.org/https://doi.org/10.1016/j.jiec.2024.01.017.

[40] Y. Ahmed, K.R. Dutta, P. Akhtar, A. Hossen, J. Alam, O.A. Alharbi, H. Almohamadi, A.W. Mohammad, Emerging strategies in the sustainable removal of antibiotics using semiconductor-based photocatalysts, (2025) 264–285. https://doi.org/10.3762/bjnano.16.21.

[41] X. Yang, Z. Chen, W. Zhao, C. Liu, X. Qian, M. Zhang, G. Wei, E. Khan, Y. Hau Ng, Y. Sik Ok, Recent advances in photodegradation of antibiotic residues in water, Chemical Engineering Journal 405 (2021). https://doi.org/10.1016/j.cej.2020.126806.

[42] K. Rokesh, M. Sakar, T.O. Do, Emerging hybrid nanocomposite photocatalysts for the degradation of antibiotics: Insights into their designs and mechanisms, Nanomaterials 11 (2021). https://doi.org/10.3390/nano11030572.

[43] A.K. Potbhare, S.K.T. Aziz, M.M. Ayyub, A. Kahate, R. Madankar, S. Wankar, A. Dutta, A. Abdala, S.H. Mohmood, R. Adhikari, R.G. Chaudhary, Bioinspired graphene-based metal oxide nanocomposites for photocatalytic and electrochemical performances: an updated review, Nanoscale Adv. 6 (2024). https://doi.org/10.1039/d3na01071f.

[44] J. Sengupta, C.M. Hussain, Advanced Graphene-Based Technologies for Antibiotic Removal from Wastewater: A Review (2016–2024), C-Journal of Carbon Research 10 (2024). https://doi.org/10.3390/c10040092.

[45] P.P. Singh, G. Pandey, Y. Murti, J. Gairola, S. Mahajan, H. Kandhari, S. Tivari, V. Srivastava, Light-driven photocatalysis as an effective tool for degradation of antibiotics, RSC Adv. 14 (2024). https://doi.org/10.1039/d4ra03431g.

[46] S. Shurbaji, P.T. Huong, T.M. Altahtamouni, Review on the visible light photocatalysis for the decomposition of ciprofloxacin, norfloxacin, tetracyclines, and sulfonamides antibiotics in wastewater, Catalysts 11 (2021). https://doi.org/10.3390/catal11040437.

[47] P.K. Pandis, C. Kalogirou, E. Kanellou, C. Vaitsis, M.G. Savvidou, G. Sourkouni, A.A. Zorpas, C. Argirusis, Key Points of Advanced Oxidation Processes (AOPs) for Wastewater, Organic Pollutants and Pharmaceutical Waste Treatment: A Mini Review, ChemEngineering 6 (2022). https://doi.org/10.3390/chemengineering6010008.

[48] Z. Yang, S. Zhou, X. Feng, N. Wang, O. Ola, Y. Zhu, Recent Progress in Multifunctional Graphene-Based Nanocomposites for Photocatalysis and Electrocatalysis Application, Nanomaterials 13 (2023). https://doi.org/10.3390/nano13132028.

[49] L. Zhu, X. Lin, Z. Di, F. Cheng, J. Xu, Occurrence, Risks, and Removal Methods of Antibiotics in Urban Wastewater Treatment Systems: A Review, Water (Switzerland) 16 (2024). https://doi.org/10.3390/w16233428.

[50] D. Kanakaraju, B.D. Glass, P.S. Goh, Advanced oxidation process-mediated removal of pharmaceuticals from water: a review of recent advances, Environmental Science and Pollution Research 32 (2025). https://doi.org/10.1007/s11356-025-36547-5.

[51] Y. Wang, C. Zhou, J. Wu, J. Niu, Insights into the electrochemical degradation of sulfamethoxazole and its metabolite by Ti/SnO2-Sb/Er-PbO2 anode, Chinese Chemical Letters 31 (2020). https://doi.org/10.1016/j.cclet.2020.03.073.

[52] P.K. Thai, L.X. Ky, V.N. Binh, P.H. Nhung, P.T. Nhan, N.Q. Hieu, N.T.T. Dang, N.K.B. Tam, N.T.K. Anh, Occurrence of antibiotic residues and antibiotic-resistant bacteria in effluents of pharmaceutical manufacturers and other sources around Hanoi, Vietnam, Science of the Total Environment 645 (2018). https://doi.org/10.1016/j.scitotenv.2018.07.126.

[53] P. Karaolia, I. Michael-Kordatou, E. Hapeshi, C. Drosou, Y. Bertakis, D. Christofilos, G.S. Armatas, L. Sygellou, T. Schwartz, N.P. Xekoukoulotakis, D. Fatta-Kassinos, Removal of antibiotics, antibiotic-resistant bacteria and their associated genes by graphene-based TiO2 composite photocatalysts under solar radiation in urban wastewaters, Appl. Catal. B 224 (2018). https://doi.org/10.1016/j.apcatb.2017.11.020.

[54] Q. Wu, C.G. Pan, Y.H. Wang, S.K. Xiao, K.F. Yu, Antibiotics in a subtropical food web from the Beibu Gulf, South China: Occurrence, bioaccumulation and trophic transfer, Science of the Total Environment 751 (2021). https://doi.org/10.1016/j.scitotenv.2020.141718.

[55] V.P. Letswalo, L.N. Dlamini, S.P. Malinga, Efficient degradation of tetracycline using a nanostructured g-C3N4/Nb2O5/HPEI/PES photocatalytic membrane, Environmental Advances 10 (2022). https://doi.org/10.1016/j.envadv.2022.100322.

[56] Q. Yang, Y. Gao, J. Ke, P.L. Show, Y. Ge, Y. Liu, R. Guo, J. Chen, Antibiotics: An overview on the environmental occurrence, toxicity, degradation, and removal methods, Bioengineered 12 (2021). https://doi.org/10.1080/21655979.2021.1974657.

[57] Y. Li, J.G. Mahy, S.D. Lambert, Adsorption and Photo(electro)catalysis for Micropollutant Degradation at the Outlet of Wastewater Treatment Plants: Bibliometric Analysis and Challenges to Implementation, Processes 13 (2025). https://doi.org/10.3390/pr13061759.

[58] S. Chen, W. Zhang, J. Li, M. Yuan, J. Zhang, F. Xu, H. Xu, X. Zheng, L. Wang, Ecotoxicological effects of sulfonamides and fluoroquinolones and their removal by a green alga (Chlorella vulgaris) and a cyanobacterium (Chrysosporum ovalisporum), Environmental Pollution 263 (2020). https://doi.org/10.1016/j.envpol.2020.114554.

[59] K. Zhu, X. Li, Y. Chen, Y. Huang, Z. Yang, G. Guan, K. Yan, Recent advances on the spherical metal oxides for sustainable degradation of antibiotics, Coord. Chem. Rev. 510 (2024). https://doi.org/10.1016/j.ccr.2024.215813.

[60] Y. Ahmed, K.R. Dutta, P. Akhtar, A. Hossen, J. Alam, O.A. Alharbi, H. Almohamadi, A.W. Mohammad, Emerging strategies in the sustainable removal of antibiotics using semiconductor-based photocatalysts, (2025) 264–285. https://doi.org/10.3762/bjnano.16.21.

[61] M.A. Hanif, M. Touqeer, M. Usman, M. Zahid, Wastewater Treatment by Biological Processes, International Journal of Chemical and Biochemical Sciences 11 (2017) 5–19.

[62] J. Chen, Y.S. Liu, J.N. Zhang, Y.Q. Yang, L.X. Hu, Y.Y. Yang, J.L. Zhao, F.R. Chen, G.G. Ying, Removal of antibiotics from piggery wastewater by biological aerated filter system: Treatment efficiency and biodegradation kinetics, Bioresour. Technol. 238 (2017) 70–77. https://doi.org/10.1016/j.biortech.2017.04.023.

[63] N.H. Tran, H. Chen, M. Reinhard, F. Mao, K.Y.H. Gin, Occurrence and removal of multiple classes of antibiotics and antimicrobial agents in biological wastewater treatment processes, Water Res. 104 (2016) 461–472. https://doi.org/10.1016/j.watres.2016.08.040.

[64] L. Wu, Q. Wei, Y. Zhang, Y. Fan, M. Li, L. Rong, X. Xiao, X. Huang, X. Zou, Effects of antibiotics on enhanced biological phosphorus removal and its mechanisms, Science of the Total Environment 774 (2021). https://doi.org/10.1016/j.scitotenv.2021.145571.

[65] T. ting Zhu, Z. xian Su, W. xia Lai, Y. bin Zhang, Y. wen Liu, Insights into the fate and removal of antibiotics and antibiotic resistance genes using biological wastewater treatment technology, Science of the Total Environment 776 (2021) 145906. https://doi.org/10.1016/j.scitotenv.2021.145906.

[66] J.P. Ribeiro, N.C. Cruz, M.C. Neves, S.M. Rodrigues, L.A.C. Tarelho, M.I. Nunes, Granulated biomass fly ash coupled with fenton process for pulp and paper wastewater treatment, Environmental Pollution 317 (2023) 1–8. https://doi.org/10.1016/j.envpol.2022.120777.

[67] H. Shi, J. Ni, T. Zheng, X. Wang, C. Wu, Q. Wang, Remediation of wastewater contaminated by antibiotics. A review, Environ. Chem. Lett. 18 (2020) 345–360. https://doi.org/10.1007/s10311-019-00945-2.

[68] M. Grassi, G. Kaykioglu, V. Belgiorno, G. Lofrano, Removal of Emerging Contaminants from Water and Wastewater by Adsorption Process, in: G. Lofrano (Ed.), Emerging Compounds Removal from Wastewater, Springer Netherlands, Dordrecht, 2012: pp. 15–37. https://doi.org/10.1007/978-94-007-3916-1_2.

[69] F. Çeçen, Ö. Aktaş, Activated Carbon for Water and Wastewater Treatment: Integration of Adsorption and Biological Treatment, Wiley-VCH Verlag GmbH & Co. KGaA, 2011. https://doi.org/10.1002/9783527639441.

[70] H. Shi, J. Ni, T. Zheng, X. Wang, C. Wu, Q. Wang, Remediation of wastewater contaminated by antibiotics. A review, Environ. Chem. Lett. 18 (2020) 345–360. https://doi.org/10.1007/s10311-019-00945-2.

[71] L. El Azzouzi, S. El Aggadi, M. Ennouhi, A. Ennouari, O.K. Kabbaj, A. Zrineh, Removal of the Amoxicillin antibiotic from aqueous matrices by means of an adsorption process using Kaolinite clay, Sci. Afr. 18 (2022) e01390. https://doi.org/10.1016/j.sciaf.2022.e01390.

[72] M. Stylianou, A. Christou, C. Michael, A. Agapiou, P. Papanastasiou, D. Fatta-Kassinos, Adsorption and removal of seven antibiotic compounds present in water with the use of biochar derived from the pyrolysis of organic waste feedstocks, J. Environ. Chem. Eng. 9 (2021) 105868. https://doi.org/10.1016/j.jece.2021.105868.

[73] D. Kanakaraju, B.D. Glass, M. Oelgemöller, Advanced oxidation process-mediated removal of pharmaceuticals from water: A review, J. Environ. Manage. 219 (2018) 189–207. https://doi.org/10.1016/j.jenvman.2018.04.103.

[74] M. Osanloo, F. Khorasheh, A. Larimi, Fabrication of nano-dandelion magnetic TiO2/CuFe2O4 doped with silver as a highly visible-light-responsive photocatalyst for degradation of Naproxen and Rhodamine B, J. Mol. Liq. 407 (2024) 125242. https://doi.org/10.1016/j.molliq.2024.125242.

[75] F. Almomani, R. Bhosale, A. Kumar, M. Khraisheh, Potential use of solar photocatalytic oxidation in removing emerging pharmaceuticals from wastewater: A pilot plant study, Solar Energy 172 (2018) 128–140. https://doi.org/10.1016/j.solener.2018.07.041.

[76] D. Kanakaraju, B.D. Glass, M. Oelgemöller, Advanced oxidation process-mediated removal of pharmaceuticals from water: A review, J. Environ. Manage. 219 (2018) 189–207. https://doi.org/10.1016/j.jenvman.2018.04.103.

[77] H. Xia, C. Li, G. Yang, Z. Shi, C. Jin, W. He, J. Xu, G. Li, A review of microwave-assisted advanced oxidation processes for wastewater treatment, Chemosphere 287 (2022) 131981. https://doi.org/10.1016/j.chemosphere.2021.131981.

[78] A. Gil, L.A. Galeano, M.Á. Vicente, eds., Applications of Advanced Oxidation Processes (AOPs) in Drinking Water Treatment, Springer International Publishing, Cham, 2019. https://doi.org/10.1007/978-3-319-76882-3.

[79] I. Gültekin, N.H. Ince, Synthetic endocrine disruptors in the environment and water remediation by advanced oxidation processes, J. Environ. Manage. 85 (2007) 816–832. https://doi.org/10.1016/j.jenvman.2007.07.020.

[80] I. Gültekin, N.H. Ince, Synthetic endocrine disruptors in the environment and water remediation by advanced oxidation processes, J. Environ. Manage. 85 (2007) 816–832. https://doi.org/10.1016/j.jenvman.2007.07.020.

[81] C.J. Miller, S. Wadley, T.D. Waite, Fenton, photo-Fenton and Fenton-like processes, Water Intelligence Online 16 (2017) 297–332. https://doi.org/10.2166/9781780407197_0297.

[82] P.K. Pandis, C. Kalogirou, E. Kanellou, C. Vaitsis, M.G. Savvidou, G. Sourkouni, A.A. Zorpas, C. Argirusis, Key Points of Advanced Oxidation Processes (AOPs) for Wastewater, Organic Pollutants and Pharmaceutical Waste Treatment: A Mini Review, ChemEngineering 6 (2022) 8. https://doi.org/10.3390/chemengineering6010008.

[83] C.J. Miller, S. Wadley, T.D. Waite, Fenton, photo-Fenton and Fenton-like processes, Water Intelligence Online 16 (2017) 297–332. https://doi.org/10.2166/9781780407197_0297.

[84] A.M. Gorito, A.R. Lado, P. Rodrigues, M.F.R. Pereira, L. Guimar, C.M.R. Almeida, Antibiotics removal from aquaculture effluents by ozonation : chemical and toxicity descriptors, 218 (2022). https://doi.org/10.1016/j.watres.2022.118497.

[85] I.C. Iakovides, I. Michael-kordatou, N.F.F. Moreira, A.R. Ribeiro, T. Fernandes, Continuous ozonation of urban wastewater : Removal of antibiotics , antibiotic-resistant Escherichia coli and antibiotic resistance genes and phytotoxicity, Water Res. 159 (2019) 333–347. https://doi.org/10.1016/j.watres.2019.05.025.

[86] J.P. Ribeiro, N.C. Cruz, M.C. Neves, S.M. Rodrigues, L.A.C. Tarelho, M.I. Nunes, Granulated biomass fly ash coupled with fenton process for pulp and paper wastewater treatment, Environmental Pollution 317 (2023) 1–8. https://doi.org/10.1016/j.envpol.2022.120777.

[87] M.S. Mahtab, I.H. Farooqi, A. Khursheed, Zero Fenton sludge discharge: a review on reuse approach during wastewater treatment by the advanced oxidation process, International Journal of Environmental Science and Technology 19 (2022) 2265–2278. https://doi.org/10.1007/s13762-020-03121-0.

[88] D. Ma, H. Yi, C. Lai, X. Liu, X. Huo, Z. An, L. Li, Y. Fu, B. Li, M. Zhang, L. Qin, S. Liu, L. Yang, Critical review of advanced oxidation processes in organic wastewater treatment, Chemosphere 275 (2021) 130104. https://doi.org/10.1016/j.chemosphere.2021.130104.

[89] N. Serpone, Y.M. Artemev, V.K. Ryabchuk, A. V. Emeline, S. Horikoshi, Light-driven advanced oxidation processes in the disposal of emerging pharmaceutical contaminants in aqueous media: A brief review, Curr. Opin. Green Sustain. Chem. 6 (2017) 18–33. https://doi.org/10.1016/j.cogsc.2017.05.003.

[90] J. Zhong, B. Yang, F.Z. Gao, Q. Xiong, Y. Feng, Y. Li, J.N. Zhang, G.G. Ying, Performance and mechanism in degradation of typical antibiotics and antibiotic resistance genes by magnetic resin-mediated UV-Fenton process, Ecotoxicol. Environ. Saf. 227 (2021). https://doi.org/10.1016/j.ecoenv.2021.112908.

[91] Y. Jiang, J. Ran, K. Mao, X. Yang, L. Zhong, C. Yang, X. Feng, H. Zhang, Recent progress in Fenton/Fenton-like reactions for the removal of antibiotics in aqueous environments, Ecotoxicol. Environ. Saf. 236 (2022) 113464. https://doi.org/10.1016/j.ecoenv.2022.113464.

[92] M. Chamack, I. Madjid, S. Ali, A. Razavi, A. Morsali, A. Addad, A. Larimi, S. Szunerits, R. Boukherroub, Photocatalytic Performance of Perovskite and Metal − Organic Framework Hybrid Material for the Reduction of N 2 to Ammonia, (2022) 2–11. https://doi.org/10.1021/acs.inorgchem.1c03622.

[93] G.N. Nanosheets, Efficient Photocatalytic Degradation of Aqueous Atrazine over, (2023).

[94] C. Nannou, K.N. Maroulas, C. Tsamtzidou, K. Ladomenou, G.Z. Kyzas, A New Generation Material Graphene: Applications in Water Technology, Springer International Publishing, Cham, 2019. https://doi.org/10.1007/978-3-319-75484-0.

[95] K. Akbar, E. Moretti, A. Vomiero, Carbon Dots for Photocatalytic Degradation of Aqueous Pollutants : Recent Advancements, 2100532 (2021). https://doi.org/10.1002/adom.202100532.

[96] A. Larimi, F. Khorasheh, Carbonaceous supports decorated with Pt e TiO 2 nanoparticles using electrostatic self-assembly method as a highly visible-light active photocatalyst for CO 2 photoreduction, Renew. Energy 145 (2020) 1862–1869. https://doi.org/10.1016/j.renene.2019.07.105.

[97] F. Quddus, A. Shah, F.J. Iftikhar, N.S. Shah, A. Haleem, Environmentally Benign Nanoparticles for the Photocatalytic Degradation of Pharmaceutical Drugs, Catalysts 13 (2023) 511. https://doi.org/10.3390/catal13030511.

[98] C. Nannou, K.N. Maroulas, C. Tsamtzidou, K. Ladomenou, G.Z. Kyzas, A New Generation Material Graphene: Applications in Water Technology, Springer International Publishing, Cham, 2019. https://doi.org/10.1007/978-3-319-75484-0.

[99] A.M. Nasir, J. Jaafar, F. Aziz, N. Yusof, W.N.W. Salleh, A.F. Ismail, M. Aziz, A review on floating nanocomposite photocatalyst: Fabrication and applications for wastewater treatment, Journal of Water Process Engineering 36 (2020) 101300. https://doi.org/10.1016/j.jwpe.2020.101300.

[100] X. Bai, W. Chen, B. Wang, T. Sun, B. Wu, Y. Wang, Photocatalytic Degradation of Some Typical Antibiotics: Recent Advances and Future Outlooks, Int. J. Mol. Sci. 23 (2022). https://doi.org/10.3390/ijms23158130.

[101] A.K. Nayak, N.K. Sahu, Nanostructured Materials for Visible Light Photocatalysis, Elsevier, 2021.

[102] A.K. Nayak, N.K. Sahu, Nanostructured Materials for Visible Light Photocatalysis, Elsevier, 2021.

[103] M. fang Li, Y. guo Liu, G. ming Zeng, N. Liu, S. bo Liu, Graphene and graphene-based nanocomposites used for antibiotics removal in water treatment: A review, Chemosphere 226 (2019) 360–380. https://doi.org/10.1016/j.chemosphere.2019.03.117.

[104] Z. Masood, A. Ikhlaq, A. Akram, U.Y. Qazi, O.S. Rizvi, R. Javaid, A. Alazmi, M. Madkour, F. Qi, Application of Nanocatalysts in Advanced Oxidation Processes for Wastewater Purification: Challenges and Future Prospects, Catalysts 12 (2022) 1–23. https://doi.org/10.3390/catal12070741.

[105] C.N.R. Rao, A.K. Sood, Graphene, Wiley, 2012. https://doi.org/10.1002/9783527651122.

[106] S.C. Ray, Applications of Graphene and Graphene-Oxide Based Nanomaterials, Elsevier, 2015. https://doi.org/10.1016/C2014-0-02615-9.

[107] Mu. Naushad, ed., A New Generation Material Graphene: Applications in Water Technology, Springer, 2019.

[108] C.N.R. Rao, A.K. Sood, Graphene, Wiley, 2012. https://doi.org/10.1002/9783527651122.

[109] Z. Masood, A. Ikhlaq, A. Akram, U.Y. Qazi, O.S. Rizvi, R. Javaid, A. Alazmi, M. Madkour, F. Qi, Application of Nanocatalysts in Advanced Oxidation Processes for Wastewater Purification: Challenges and Future Prospects, Catalysts 12 (2022) 1–23. https://doi.org/10.3390/catal12070741.

[110] M. fang Li, Y. guo Liu, G. ming Zeng, N. Liu, S. bo Liu, Graphene and graphene-based nanocomposites used for antibiotics removal in water treatment: A review, Chemosphere 226 (2019) 360–380. https://doi.org/10.1016/j.chemosphere.2019.03.117.

[111] Mu. Naushad, ed., A New Generation Material Graphene: Applications in Water Technology, Springer, 2019.

[112] S.C. Ray, Applications of Graphene and Graphene-Oxide Based Nanomaterials, Elsevier, 2015. https://doi.org/10.1016/C2014-0-02615-9.

[113] M. Beshtar, A. Larimi, A. Akbar, Journal of Photochemistry & Photobiology , A : Chemistry Enhanced super-ultra-deep photocatalytic oxidative desulfurization by titanium-activated metal-organic frameworks nanophotocataltyst, J. Photochem. Photobiol. A Chem. 459 (2025) 116056. https://doi.org/10.1016/j.jphotochem.2024.116056.

[114] Y. Vasseghian, E. Dragoi, F. Almomani, V.T. Le, Graphene-based materials for metronidazole degradation: A comprehensive review, Chemosphere 286 (2022) 131727. https://doi.org/10.1016/j.chemosphere.2021.131727.

[115] A. Raja, P. Rajasekaran, K. Selvakumar, M. Arunpandian, K. Kaviyarasu, S. Asath Bahadur, M. Swaminathan, Visible active reduced graphene oxide-BiVO4-ZnO ternary photocatalyst for efficient removal of ciprofloxacin, Sep. Purif. Technol. 233 (2020). https://doi.org/10.1016/j.seppur.2019.115996.

[116] A. Raja, P. Rajasekaran, K. Selvakumar, M. Arunpandian, K. Kaviyarasu, S. Asath Bahadur, M. Swaminathan, Visible active reduced graphene oxide-BiVO4-ZnO ternary photocatalyst for efficient removal of ciprofloxacin, Sep. Purif. Technol. 233 (2020). https://doi.org/10.1016/j.seppur.2019.115996.

[117] S. Qian, S. Pu, Y. Zhang, P. Wang, Y. Bai, B. Lai, New insights on the enhanced non-hydroxyl radical contribution under copper promoted TiO2/GO for the photodegradation of tetracycline hydrochloride, J. Environ. Sci. (China) 100 (2021) 99–109. https://doi.org/10.1016/j.jes.2020.06.039.

[118] A. Ostovar, A. Larimi, Z. Jiang, M. Lotfi, C. Ghotbi, F. Khorasheh, Enhanced visible-light photocatalytic oxidative desulfurization of model fuel over Pt-decorated carbon-doped TiO 2 nanoparticles, Environmental Science and Pollution Research 31 (2024) 18188–18199. https://doi.org/10.1007/s11356-023-26597-y.

[119] S. Qian, S. Pu, Y. Zhang, P. Wang, Y. Bai, B. Lai, New insights on the enhanced non-hydroxyl radical contribution under copper promoted TiO2/GO for the photodegradation of tetracycline hydrochloride, J. Environ. Sci. (China) 100 (2021) 99–109. https://doi.org/10.1016/j.jes.2020.06.039.

[120] M.T. Guo, X.B. Tian, Impacts on antibiotic-resistant bacteria and their horizontal gene transfer by graphene-based TiO2&Ag composite photocatalysts under solar irradiation, J. Hazard. Mater. 380 (2019) 120877. https://doi.org/10.1016/j.jhazmat.2019.120877.

[121] A. Kumar, A. Kumari, G. Sharma, B. Du, M. Naushad, F.J. Stadler, Carbon quantum dots and reduced graphene oxide modified self-assembled S@C3N4/B@C3N4 metal-free nano-photocatalyst for high performance degradation of chloramphenicol, J. Mol. Liq. 300 (2020) 112356. https://doi.org/10.1016/j.molliq.2019.112356.

[122] Y. Ma, D. Wu, C. Liu, J. Guan, J. Lu, H. Wang, P. Huo, Y. Yan, Preparation of Fe-Ag3VO4/GO Composite Photocatalyst for Enhanced Photodegradation of Chloramphenicol, DEStech Transactions on Engineering and Technology Research (2018) 199–203. https://doi.org/10.12783/dtetr/icace2018/25515.

[123] K.O. Sodeinde, S.O. Olusanya, O.S. Lawal, M. Sriariyanun, A.A. Adediran, Enhanced adsorptional-photocatalytic degradation of chloramphenicol by reduced graphene oxide-zinc oxide nanocomposite, Sci. Rep. 12 (2022) 1–13. https://doi.org/10.1038/s41598-022-21266-5.

[124] K.O. Sodeinde, S.O. Olusanya, O.S. Lawal, M. Sriariyanun, A.A. Adediran, Enhanced adsorptional-photocatalytic degradation of chloramphenicol by reduced graphene oxide-zinc oxide nanocomposite, Sci. Rep. 12 (2022) 1–13. https://doi.org/10.1038/s41598-022-21266-5.

[125] A. Kumar, A. Kumari, G. Sharma, B. Du, M. Naushad, F.J. Stadler, Carbon quantum dots and reduced graphene oxide modified self-assembled S@C3N4/B@C3N4 metal-free nano-photocatalyst for high performance degradation of chloramphenicol, J. Mol. Liq. 300 (2020) 112356. https://doi.org/10.1016/j.molliq.2019.112356.

[126] M.T. Guo, X.B. Tian, Impacts on antibiotic-resistant bacteria and their horizontal gene transfer by graphene-based TiO2&Ag composite photocatalysts under solar irradiation, J. Hazard. Mater. 380 (2019) 120877. https://doi.org/10.1016/j.jhazmat.2019.120877.

[127] Y. Ma, D. Wu, C. Liu, J. Guan, J. Lu, H. Wang, P. Huo, Y. Yan, Preparation of Fe-Ag3VO4/GO Composite Photocatalyst for Enhanced Photodegradation of Chloramphenicol, DEStech Transactions on Engineering and Technology Research (2018) 199–203. https://doi.org/10.12783/dtetr/icace2018/25515.

[128] M. Ahmadi, S. Mehdi, A. Larimi, UV–vis light responsive Bi2WO6 nanosheet/TiO2 nanobelt heterojunction photo-catalyst for CO2 reduction, Catal. Commun. 179 (2023) 106681. https://doi.org/10.1016/j.catcom.2023.106681.

[129] J. Low, J. Yu, M. Jaroniec, S. Wageh, A.A. Al-Ghamdi, Heterojunction Photocatalysts, Advanced Materials 29 (2017) 1601694. https://doi.org/10.1002/adma.201601694.

[130] D. Ma, H. Yi, C. Lai, X. Liu, X. Huo, Z. An, L. Li, Y. Fu, B. Li, M. Zhang, L. Qin, S. Liu, L. Yang, Critical review of advanced oxidation processes in organic wastewater treatment, Chemosphere 275 (2021) 130104. https://doi.org/10.1016/j.chemosphere.2021.130104.

[131] M.M. Khan, D. Pradhan, Y. Sohn, Nanocomposites for visible light-induced photocatalysis, Springer International Publishing, 2017.

[132] K. Wang, Y. Li, G. Zhang, J. Li, X. Wu, 0D Bi nanodots/2D Bi3NbO7 nanosheets heterojunctions for efficient visible light photocatalytic degradation of antibiotics: Enhanced molecular oxygen activation and mechanism insight, Appl. Catal. B 240 (2019). https://doi.org/10.1016/j.apcatb.2018.08.063.

[133] L. Zhang, C.G. Niu, C. Liang, X.J. Wen, D.W. Huang, H. Guo, X.F. Zhao, G.M. Zeng, One-step in situ synthesis of CdS/SnO2 heterostructure with excellent photocatalytic performance for Cr(VI) reduction and tetracycline degradation, Chemical Engineering Journal 352 (2018). https://doi.org/10.1016/j.cej.2018.07.102.

[134] C. Lai, M. Zhang, B. Li, D. Huang, G. Zeng, L. Qin, X. Liu, H. Yi, M. Cheng, L. Li, Z. Chen, L. Chen, Fabrication of CuS/BiVO4 (0 4 0) binary heterojunction photocatalysts with enhanced photocatalytic activity for Ciprofloxacin degradation and mechanism insight, Chemical Engineering Journal 358 (2019) 891–902. https://doi.org/10.1016/j.cej.2018.10.072.

[135] C. Lai, M. Zhang, B. Li, D. Huang, G. Zeng, L. Qin, X. Liu, H. Yi, M. Cheng, L. Li, Z. Chen, L. Chen, Fabrication of CuS/BiVO4 (0 4 0) binary heterojunction photocatalysts with enhanced photocatalytic activity for Ciprofloxacin degradation and mechanism insight, Chemical Engineering Journal 358 (2019) 891–902. https://doi.org/10.1016/j.cej.2018.10.072.

[136] Y. Shi, Z. Yang, B. Wang, H. An, Z. Chen, H. Cui, Adsorption and photocatalytic degradation of tetracycline hydrochloride using a palygorskite-supported Cu2O-TiO2 composite, Appl. Clay Sci. 119 (2016) 311–320. https://doi.org/10.1016/j.clay.2015.10.033.

[137] Y. Shi, Z. Yang, B. Wang, H. An, Z. Chen, H. Cui, Adsorption and photocatalytic degradation of tetracycline hydrochloride using a palygorskite-supported Cu2O-TiO2 composite, Appl. Clay Sci. 119 (2016) 311–320. https://doi.org/10.1016/j.clay.2015.10.033.

[138] Q. Wang, S. Ji, Q. Xu, L. Shen, W. Shi, Preparation of PEO-based Cu2O/Bi2O2CO3 electrospun fibrous membrane toward enhanced photocatalytic degradation of chloramphenicol, J. Mater. Sci. 56 (2021) 4599–4614. https://doi.org/10.1007/s10853-020-05564-9.

[139] Q. Wang, S. Ji, Q. Xu, L. Shen, W. Shi, Preparation of PEO-based Cu2O/Bi2O2CO3 electrospun fibrous membrane toward enhanced photocatalytic degradation of chloramphenicol, J. Mater. Sci. 56 (2021) 4599–4614. https://doi.org/10.1007/s10853-020-05564-9.

[140] Y.M. Hunge, A.A. Yadav, S.W. Kang, S. Jun Lim, H. Kim, Visible light activated MoS2/ZnO composites for photocatalytic degradation of ciprofloxacin antibiotic and hydrogen production, J. Photochem. Photobiol. A Chem. 434 (2023) 114250. https://doi.org/10.1016/j.jphotochem.2022.114250.

[141] Y.M. Hunge, A.A. Yadav, S.W. Kang, S. Jun Lim, H. Kim, Visible light activated MoS2/ZnO composites for photocatalytic degradation of ciprofloxacin antibiotic and hydrogen production, J. Photochem. Photobiol. A Chem. 434 (2023) 114250. https://doi.org/10.1016/j.jphotochem.2022.114250.

[142] X. Rong, F. Qiu, Z. Jiang, J. Rong, J. Pan, T. Zhang, D. Yang, Preparation of ternary combined ZnO-Ag2O/porous g-C3N4 composite photocatalyst and enhanced visible-light photocatalytic activity for degradation of ciprofloxacin, Chemical Engineering Research and Design 111 (2016) 253–261. https://doi.org/10.1016/j.cherd.2016.05.010.

[143] M. Ja'fari, S.L. Ebrahimi, M.R. Khosravi-Nikou, Ultrasound-assisted oxidative desulfurization and denitrogenation of liquid hydrocarbon fuels: A critical review, Ultrason. Sonochem. 40 (2018) 955–968. https://doi.org/10.1016/j.ultsonch.2017.09.002.

[144] P. Rajiv, N. Mengelizadeh, G. McKay, D. Balarak, Photocatalytic degradation of ciprofloxacin with Fe2O3 nanoparticles loaded on graphitic carbon nitride: mineralisation, degradation mechanism and toxicity assessment, Int. J. Environ. Anal. Chem. 00 (2021) 1–15. https://doi.org/10.1080/03067319.2021.1890059.

[145] P. Rajiv, N. Mengelizadeh, G. McKay, D. Balarak, Photocatalytic degradation of ciprofloxacin with Fe2O3 nanoparticles loaded on graphitic carbon nitride: mineralisation, degradation mechanism and toxicity assessment, Int. J. Environ. Anal. Chem. 00 (2021) 1–15. https://doi.org/10.1080/03067319.2021.1890059.

[146] S. Yan, J. Yang, Y. Li, X. Jia, H. Song, One-step synthesis of ZnS/BiOBr photocatalyst to enhance photodegradation of tetracycline under full spectral irradiation, Mater. Lett. 276 (2020) 128232. https://doi.org/10.1016/j.matlet.2020.128232.

[147] W. Liu, J. Zhou, Z. Hu, Nano-sized g-C3N4 thin layer @ CeO2 sphere core-shell photocatalyst combined with H2O2 to degrade doxycycline in water under visible light irradiation, Sep. Purif. Technol. 227 (2019) 115665. https://doi.org/10.1016/j.seppur.2019.06.003.

[148] W. Liu, J. Zhou, Z. Hu, Nano-sized g-C3N4 thin layer @ CeO2 sphere core-shell photocatalyst combined with H2O2 to degrade doxycycline in water under visible light irradiation, Sep. Purif. Technol. 227 (2019) 115665. https://doi.org/10.1016/j.seppur.2019.06.003.

[149] N. Zhang, X. Li, Y. Wang, B. Zhu, J. Yang, Fabrication of magnetically recoverable Fe3O4/CdS/g-C3N4 photocatalysts for effective degradation of ciprofloxacin under visible light, Ceram. Int. 46 (2020) 20974–20984. https://doi.org/10.1016/j.ceramint.2020.05.158.

[150] F. Guo, W. Shi, W. Guan, H. Huang, Y. Liu, Carbon dots/g-C3N4/ZnO nanocomposite as efficient visible-light driven photocatalyst for tetracycline total degradation, Sep. Purif. Technol. 173 (2017) 295–303. https://doi.org/10.1016/j.seppur.2016.09.040.

[151] L. Wang, X. Ma, G. Huang, R. Lian, J. Huang, H. She, Q. Wang, Construction of ternary CuO/CuFe2O4/g-C3N4 composite and its enhanced photocatalytic degradation of tetracycline hydrochloride with persulfate under simulated sunlight, J. Environ. Sci. (China) 112 (2021) 59–70. https://doi.org/10.1016/j.jes.2021.04.026.

[152] L. Wang, X. Ma, G. Huang, R. Lian, J. Huang, H. She, Q. Wang, Construction of ternary CuO/CuFe2O4/g-C3N4 composite and its enhanced photocatalytic degradation of tetracycline hydrochloride with persulfate under simulated sunlight, J. Environ. Sci. (China) 112 (2021) 59–70. https://doi.org/10.1016/j.jes.2021.04.026.

[153] S. Salehian, A. Larimi, A. Akbar, N. Khallaghi, nanocomposite as a high-performance visible-light-active photocatalyst for ultra-deep oxidative desulfurization of liquid fuel, Surfaces and Interfaces 42 (2023) 103432. https://doi.org/10.1016/j.surfin.2023.103432.

[154] A.I. Navarro-Aguilar, S. Obregón, D. Sanchez-Martinez, D.B. Hernández-Uresti, An efficient and stable WO3/g-C3N4 photocatalyst for ciprofloxacin and orange G degradation, J. Photochem. Photobiol. A Chem. 384 (2019) 112010. https://doi.org/10.1016/j.jphotochem.2019.112010.

[155] A.I. Navarro-Aguilar, S. Obregón, D. Sanchez-Martinez, D.B. Hernández-Uresti, An efficient and stable WO3/g-C3N4 photocatalyst for ciprofloxacin and orange G degradation, J. Photochem. Photobiol. A Chem. 384 (2019) 112010. https://doi.org/10.1016/j.jphotochem.2019.112010.

[156] L. Wolski, K. Grzelak, M. Muńko, M. Frankowski, T. Grzyb, G. Nowaczyk, Insight into photocatalytic degradation of ciprofloxacin over CeO2/ZnO nanocomposites: Unravelling the synergy between the metal oxides and analysis of reaction pathways, Appl. Surf. Sci. 563 (2021). https://doi.org/10.1016/j.apsusc.2021.150338.

[157] L. Wolski, K. Grzelak, M. Muńko, M. Frankowski, T. Grzyb, G. Nowaczyk, Insight into photocatalytic degradation of ciprofloxacin over CeO2/ZnO nanocomposites: Unravelling the synergy between the

metal oxides and analysis of reaction pathways, Appl. Surf. Sci. 563 (2021). https://doi.org/10.1016/j.apsusc.2021.150338.

[158] C. Du, J. Song, S. Tan, L. Yang, G. Yu, H. Chen, L. Zhou, Z. Zhang, Y. Zhang, Y. Su, X. Wen, S. Wang, Facile synthesis of Z-scheme ZnO/Ag/Ag3PO4 composite photocatalysts with enhanced performance for the degradation of ciprofloxacin, Mater. Chem. Phys. 260 (2021) 124136. https://doi.org/10.1016/j.matchemphys.2020.124136.

[159] M.H. Thanh Tung, N.T. Dieu Cam, D. Van Thuan, P. Van Quan, C. Van Hoang, T.T. Thu Phuong, N.T. Lam, T.T. Tam, N.T. Phuong Le Chi, N.T. Lan, D.N. Thoại, T.D. Pham, Novel direct Z-scheme AgI/N–TiO2 photocatalyst for removal of polluted tetracycline under visible irradiation, Ceram. Int. 46 (2020) 6012–6021. https://doi.org/10.1016/j.ceramint.2019.11.058.

[160] M.H. Thanh Tung, N.T. Dieu Cam, D. Van Thuan, P. Van Quan, C. Van Hoang, T.T. Thu Phuong, N.T. Lam, T.T. Tam, N.T. Phuong Le Chi, N.T. Lan, D.N. Thoại, T.D. Pham, Novel direct Z-scheme AgI/N–TiO2 photocatalyst for removal of polluted tetracycline under visible irradiation, Ceram. Int. 46 (2020) 6012–6021. https://doi.org/10.1016/j.ceramint.2019.11.058.

[161] M. Abdollahi, A. Larimi, Z. Jiang, F. Khorasheh, C. Ghotbi, Photocatalytic oxidative desulfurization of model fuel over visible light-active Cu-impregnated carbon-doped TiO2, J. Clean. Prod. 380 (2022) 134968. https://doi.org/10.1016/j.jclepro.2022.134968.

[162] R. Zhang, Y. Li, W. Zhang, Y. Sheng, M. Wang, J. Liu, Y. Liu, C. Zhao, K. Zeng, Fabrication of Cu2O/Bi2S3 heterojunction photocatalysts with enhanced visible light photocatalytic mechanism and degradation pathways of tetracycline, J. Mol. Struct. (2020). https://doi.org/10.1016/j.molstruc.2020.129581.

[163] S. Wang, L. Zhao, L. Gao, D. Yang, S. Wen, W. Huang, Z. Sun, J. Guo, X. Jiang, C. Lu, Fabrication of ternary dual Z-Scheme AgI/ZnIn2S4/BiVO4 heterojunction photocatalyst with enhanced photocatalytic degradation of tetracycline under visible light, Arabian Journal of Chemistry 15 (2022) 104159. https://doi.org/10.1016/j.arabjc.2022.104159.

[164] S. Wang, L. Zhao, L. Gao, D. Yang, S. Wen, W. Huang, Z. Sun, J. Guo, X. Jiang, C. Lu, Fabrication of ternary dual Z-Scheme AgI/ZnIn2S4/BiVO4 heterojunction photocatalyst with enhanced photocatalytic degradation of tetracycline under visible light, Arabian Journal of Chemistry 15 (2022) 104159. https://doi.org/10.1016/j.arabjc.2022.104159.

[165] J. Guo, L. Jiang, J. Liang, W. Xu, H. Yu, J. Zhang, S. Ye, W. Xing, X. Yuan, Photocatalytic degradation of tetracycline antibiotics using delafossite silver ferrite-based Z-scheme photocatalyst: Pathways and mechanism insight, Chemosphere 270 (2021) 128651. https://doi.org/10.1016/j.chemosphere.2020.128651.

[166] J. Guo, L. Jiang, J. Liang, W. Xu, H. Yu, J. Zhang, S. Ye, W. Xing, X. Yuan, Photocatalytic degradation of tetracycline antibiotics using delafossite silver ferrite-based Z-scheme photocatalyst: Pathways and mechanism insight, Chemosphere 270 (2021) 128651. https://doi.org/10.1016/j.chemosphere.2020.128651.

[167] V.S. Manikandan, S. Harish, J. Archana, M. Navaneethan, Fabrication of novel hybrid Z-Scheme WO3@g-C3N4@MWCNT nanostructure for photocatalytic degradation of tetracycline and the evaluation of antimicrobial activity, Chemosphere 287 (2022) 132050. https://doi.org/10.1016/j.chemosphere.2021.132050.

[168] H. Yu, D. Wang, B. Zhao, Y. Lu, X. Wang, S. Zhu, W. Qin, M. Huo, Enhanced photocatalytic degradation of tetracycline under visible light by using a ternary photocatalyst of Ag3PO4/AgBr/g-C3N4 with dual

Z-scheme heterojunction, Sep. Purif. Technol. 237 (2020) 116365. https://doi.org/10.1016/j.seppur.2019.116365.

[169] H. Yu, D. Wang, B. Zhao, Y. Lu, X. Wang, S. Zhu, W. Qin, M. Huo, Enhanced photocatalytic degradation of tetracycline under visible light by using a ternary photocatalyst of Ag3PO4/AgBr/g-C3N4 with dual Z-scheme heterojunction, Sep. Purif. Technol. 237 (2020) 116365. https://doi.org/10.1016/j.seppur.2019.116365.

[170] V.P. Letswalo, L.N. Dlamini, S.P. Malinga, Efficient degradation of tetracycline using a nanostructured g-C3N4/Nb2O5/HPEI/PES photocatalytic membrane, Environmental Advances 10 (2022) 100322. https://doi.org/10.1016/j.envadv.2022.100322.

[171] V.P. Letswalo, L.N. Dlamini, S.P. Malinga, Efficient degradation of tetracycline using a nanostructured g-C3N4/Nb2O5/HPEI/PES photocatalytic membrane, Environmental Advances 10 (2022) 100322. https://doi.org/10.1016/j.envadv.2022.100322.

[172] K. Hu, R. Li, C. Ye, A. Wang, W. Wei, D. Hu, R. Qiu, K. Yan, Facile synthesis of Z-scheme composite of TiO2 nanorod/g-C3N4 nanosheet efficient for photocatalytic degradation of ciprofloxacin, J. Clean. Prod. 253 (2020). https://doi.org/10.1016/j.jclepro.2020.120055.

[173] M. Ahmadi, S. Mehdi, A. Larimi, International Journal of Hydrogen Energy Effective CO 2 photoreduction to methane over Bi 2 MoO 6 / Ni , N co-doped TiO 2 nano-photocatalyst, Int. J. Hydrogen Energy 56 (2024) 1309–1323. https://doi.org/10.1016/j.ijhydene.2023.12.291.

[174] M. Bahadorian, F.A. Roghabadi, V. Ahmadi, A. Larimi, Highly efficient photocatalytic conversion of CO2 to hydrocarbons using visible-active co-doped TiO2/ PDMS nanocomposite, Clean. Eng. Technol. (2026) 101147. https://doi.org/10.1016/j.clet.2026.101147.

[175] A. Larimi, Titanium-based nanophotocatalysts for CO2 conversion, in: Nanomaterials for Carbon Dioxide Capture and Conversion Technologies, Elsevier, 2023: pp. 153–180. https://doi.org/10.1016/B978-0-323-89851-5.00008-1.

[176] M. Ahmadi, S. Mehdi, A. Larimi, Highly active platinum decorated BiVO 4 nanosheet / TiO 2 nanobelt heterojunction for photocatalytic CO 2 reduction, Surfaces and Interfaces 45 (2024) 103908. https://doi.org/10.1016/j.surfin.2024.103908.

[177] M. Ahmadi, S.M. Alavi, A.A. Asgharinezhad, A. Haghighatzadeh, A. Larimi, Uniform sono-dispersed co-catalysts unlock superior CO_2 photoreduction on Bi_2MoO_6/TiO_2, Catal. Today 466 (2026) 115674. https://doi.org/10.1016/j.cattod.2025.115674.

[178] J. Chi, Z. Jiang, J. Yan, A. Larimi, Z. Wang, L. Wang, W. Shangguan, Recent advancements in bismuth vanadate photoanodes for photoelectrochemical water splitting, Mater. Today Chem. 26 (2022) 101060. https://doi.org/10.1016/J.MTCHEM.2022.101060.

[179] K. Hu, R. Li, C. Ye, A. Wang, W. Wei, D. Hu, R. Qiu, K. Yan, Facile synthesis of Z-scheme composite of TiO2 nanorod/g-C3N4 nanosheet efficient for photocatalytic degradation of ciprofloxacin, J. Clean. Prod. 253 (2020). https://doi.org/10.1016/j.jclepro.2020.120055.

[180] R. Nematollahi, C. Ghotbi, F. Khorasheh, A. Larimi, Ni-Bi co-doped TiO 2 as highly visible light response nano-photocatalyst for CO 2 photo-reduction in a batch photo-reactor, Journal of CO2 Utilization 41 (2020) 101289. https://doi.org/10.1016/j.jcou.2020.101289.

[181] M. Moradi, F. Khorasheh, A. Larimi, Pt nanoparticles decorated Bi-doped TiO2 as an efficient photocatalyst for CO2 photo-reduction into CH4, Solar Energy 211 (2020) 100–110. https://doi.org/https://doi.org/10.1016/j.solener.2020.09.054.

[182] M. Ahmadi, S. Mehdi Alavi, A. Larimi, Pt–Cu@Bi2MoO6/TiO2 Photocatalyst for CO2 Reduction, Inorg. Chem. 62 (2023) 20372–20389. https://doi.org/10.1021/acs.inorgchem.3c03372.

[183] Y. Li, B. Yu, Z. Hu, H. Wang, Construction of direct Z-scheme SnS2@ZnIn2S4@kaolinite heterostructure photocatalyst for efficient photocatalytic degradation of tetracycline hydrochloride, Chemical Engineering Journal 429 (2022) 132105. https://doi.org/10.1016/j.cej.2021.132105.

[184] Y. Li, B. Yu, Z. Hu, H. Wang, Construction of direct Z-scheme SnS2@ZnIn2S4@kaolinite heterostructure photocatalyst for efficient photocatalytic degradation of tetracycline hydrochloride, Chemical Engineering Journal 429 (2022) 132105. https://doi.org/10.1016/j.cej.2021.132105.

[185] N. Li, Y. Tian, J. Zhao, J. Zhang, W. Zuo, L. Kong, H. Cui, Z-scheme 2D / 3D g-C 3 N 4 @ ZnO with enhanced photocatalytic activity for cephalexin oxidation under solar light, Chemical Engineering Journal 352 (2018) 412–422. https://doi.org/10.1016/j.cej.2018.07.038.

[186] N. Li, Y. Tian, J. Zhao, J. Zhang, W. Zuo, L. Kong, H. Cui, Z-scheme 2D / 3D g-C 3 N 4 @ ZnO with enhanced photocatalytic activity for cephalexin oxidation under solar light, Chemical Engineering Journal 352 (2018) 412–422. https://doi.org/10.1016/j.cej.2018.07.038.

[187] S.M.M. Ahmadi, A. Larimi, A.A. Asgharinezhad, F. Khorasheh, C. Ghotbi, Inside- and Outside-Coated PANI and/or PIN-TiO 2 Nanotubes for Enhanced Photocatalytic Degradation of 4-Nitrophenol in Wastewater, ACS Omega 9 (2024) 51320–51336. https://doi.org/10.1021/acsomega.4c08137.

[188] G. Zhao, J. Ding, F. Zhou, X. Chen, L. Wei, Q. Gao, K. Wang, Q. Zhao, Construction of a visible-light-driven magnetic dual Z-scheme BiVO4/g-C3N4/NiFe2O4 photocatalyst for effective removal of ofloxacin: Mechanisms and degradation pathway, Chemical Engineering Journal 405 (2021) 126704. https://doi.org/10.1016/j.cej.2020.126704.

[189] G. Li, B. Wang, J. Zhang, R. Wang, H. Liu, Rational construction of a direct Z-scheme g-C 3 N 4 /CdS photocatalyst with enhanced visible light photocatalytic activity and degradation of erythromycin and tetracycline, Appl. Surf. Sci. 478 (2019) 1056–1064. https://doi.org/10.1016/j.apsusc.2019.02.035.

[190] Y. Jiang, K. Huang, W. Ling, X. Wei, Y. Wang, J. Wang, Investigation of the kinetics and reaction mechanism for photodegradation tetracycline antibiotics over sulfur-doped Bi2WO6-x/ZnIn2S4 direct Z-scheme heterojunction, Nanomaterials 11 (2021). https://doi.org/10.3390/nano11082123.

[191] Y. Wang, L. Ding, C. Liu, Y. Lu, Q. Wu, C. Wang, Q. Hu, 0D/2D/2D ZnFe2O4/Bi2O2CO3/BiOBr double Z-scheme heterojunctions for the removal of tetracycline antibiotics by permonosulfate activation: Photocatalytic and non-photocatalytic mechanisms, radical and non-radical pathways, Sep. Purif. Technol. 283 (2022). https://doi.org/10.1016/j.seppur.2021.120164.

[192] M. Yang, D. Ren, S. Sun, J. Cui, Q. Yang, Y. Luo, S. Liang, One-pot construction of unprecedented direct Z-scheme ZnS/GaOOH heterojunction for photodegradation of antibiotics, Appl. Surf. Sci. 576 (2022). https://doi.org/10.1016/j.apsusc.2021.151742.

[193] Y. Deng, L. Tang, G. Zeng, C. Feng, H. Dong, J. Wang, H. Feng, Y. Liu, Y. Zhou, Y. Pang, Plasmonic resonance excited dual Z-scheme BiVO4/Ag/Cu2O nanocomposite: Synthesis and mechanism for enhanced photocatalytic performance in recalcitrant antibiotic degradation, Environ. Sci. Nano 4 (2017). https://doi.org/10.1039/c7en00237h.

[194] N. Liu, P. Liu, Z. Du, Z. Zeng, Y. Zheng, C. Xue, J. Lu, Synergistic enhancement of charge separation and light absorption in a Z-scheme g-C3N4/Bi/BiPO4 photocatalyst for antibiotic degradation, Journal of Water Process Engineering 76 (2025). https://doi.org/10.1016/j.jwpe.2025.108214.

[195] M. Ren, Y. Ao, P. Wang, C. Wang, Construction of silver/graphitic-C3N4/bismuth tantalate Z-scheme photocatalyst with enhanced visible-light-driven performance for sulfamethoxazole degradation, Chemical Engineering Journal 378 (2019). https://doi.org/10.1016/j.cej.2019.122122.

[196] R.C. Pawar, C.S. Lee, Heterogeneous Nanocomposite-Photocatalysis for Water Purification, Elsevier, 2015. https://doi.org/10.1016/C2014-0-02650-0.

[197] Z. Zhu, F. Guo, A. Li, W. Xu, X. Zhang, Simple synthesis of BiOI/ZnO/rGO for efficient photocatalytic degradation of antibiotic chloramphenicol under visible light, J. Environ. Sci. (China) (2022). https://doi.org/10.1016/j.jes.2022.05.045.

[198] Z. Zhu, F. Guo, A. Li, W. Xu, X. Zhang, Simple synthesis of BiOI/ZnO/rGO for efficient photocatalytic degradation of antibiotic chloramphenicol under visible light, J. Environ. Sci. (China) (2022). https://doi.org/10.1016/j.jes.2022.05.045.

[199] M.H. Thanh Tung, T.T. Thu Phuong, N.T. Phuong Le Chi, D.M. The, N.T. Quoc, D.T. Khan, T.D. Pham, N.V. Khoa, T.T. Thu Hien, N.T. Dieu Cam, Novel amoxicillin degradation via photocatalysis of WO3/AgI heterojunction decorated on rGO, Ceram. Int. 49 (2023) 10881–10888. https://doi.org/10.1016/j.ceramint.2022.11.281.

[200] X. Rong, F. Qiu, Z. Jiang, J. Rong, J. Pan, T. Zhang, D. Yang, Preparation of ternary combined ZnO-Ag2O/porous g-C3N4 composite photocatalyst and enhanced visible-light photocatalytic activity for degradation of ciprofloxacin, Chemical Engineering Research and Design 111 (2016) 253–261. https://doi.org/10.1016/j.cherd.2016.05.010.

[201] F. Guo, W. Shi, W. Guan, H. Huang, Y. Liu, Carbon dots/g-C3N4/ZnO nanocomposite as efficient visible-light driven photocatalyst for tetracycline total degradation, Sep. Purif. Technol. 173 (2017) 295–303. https://doi.org/10.1016/j.seppur.2016.09.040.

[202] S. Yan, J. Yang, Y. Li, X. Jia, H. Song, One-step synthesis of ZnS/BiOBr photocatalyst to enhance photodegradation of tetracycline under full spectral irradiation, Mater. Lett. 276 (2020) 128232. https://doi.org/10.1016/j.matlet.2020.128232.

[203] N. Zhang, X. Li, Y. Wang, B. Zhu, J. Yang, Fabrication of magnetically recoverable Fe3O4/CdS/g-C3N4 photocatalysts for effective degradation of ciprofloxacin under visible light, Ceram. Int. 46 (2020) 20974–20984. https://doi.org/10.1016/j.ceramint.2020.05.158.

[204] R. Zhang, Y. Li, W. Zhang, Y. Sheng, M. Wang, J. Liu, Y. Liu, C. Zhao, K. Zeng, Fabrication of Cu2O/Bi2S3 heterojunction photocatalysts with enhanced visible light photocatalytic mechanism and degradation pathways of tetracycline, J. Mol. Struct. (2020). https://doi.org/10.1016/j.molstruc.2020.129581.

[205] G. Zhao, J. Ding, F. Zhou, X. Chen, L. Wei, Q. Gao, K. Wang, Q. Zhao, Construction of a visible-light-driven magnetic dual Z-scheme BiVO4/g-C3N4/NiFe2O4 photocatalyst for effective removal of ofloxacin: Mechanisms and degradation pathway, Chemical Engineering Journal 405 (2021) 126704. https://doi.org/10.1016/j.cej.2020.126704.

[206] G. Li, B. Wang, J. Zhang, R. Wang, H. Liu, Rational construction of a direct Z-scheme g-C 3 N 4 /CdS photocatalyst with enhanced visible light photocatalytic activity and degradation of erythromycin and tetracycline, Appl. Surf. Sci. 478 (2019) 1056–1064. https://doi.org/10.1016/j.apsusc.2019.02.035.

[207] C. Du, J. Song, S. Tan, L. Yang, G. Yu, H. Chen, L. Zhou, Z. Zhang, Y. Zhang, Y. Su, X. Wen, S. Wang, Facile synthesis of Z-scheme ZnO/Ag/Ag3PO4 composite photocatalysts with enhanced performance for the degradation of ciprofloxacin, Mater. Chem. Phys. 260 (2021) 124136. https://doi.org/10.1016/j.matchemphys.2020.124136.

[208] V.S. Manikandan, S. Harish, J. Archana, M. Navaneethan, Fabrication of novel hybrid Z-Scheme WO3@g-C3N4@MWCNT nanostructure for photocatalytic degradation of tetracycline and the evaluation of antimicrobial activity, Chemosphere 287 (2022) 132050. https://doi.org/10.1016/j.chemosphere.2021.132050.

[209] M.H. Thanh Tung, T.T. Thu Phuong, N.T. Phuong Le Chi, D.M. The, N.T. Quoc, D.T. Khan, T.D. Pham, N.V. Khoa, T.T. Thu Hien, N.T. Dieu Cam, Novel amoxicillin degradation via photocatalysis of WO3/AgI heterojunction decorated on rGO, Ceram. Int. 49 (2023) 10881–10888. https://doi.org/10.1016/j.ceramint.2022.11.281.

[210] K.I. John, G. Ho, D. Li, Recent progresses in synthesis and modification of g-C3N4 for improving visible-light-driven photocatalytic degradation of antibiotics, Water Science & Technology 89 (2024) 3047–3078. https://doi.org/10.2166/wst.2024.166.

[211] S. Shukla, H. Pandey, P. Singh, A.K. Tiwari, V. Baranwal, A.C. Pandey, Synergistic impact of photocatalyst and dopants on pharmaceutical-polluted waste water treatment: a review, Environmental Pollutants and Bioavailability 33 (2021) 347–364. https://doi.org/10.1080/26395940.2021.1987843.

[212] K.I. John, G. Ho, D. Li, Recent progresses in synthesis and modification of g-C3N4 for improving visible-light-driven photocatalytic degradation of antibiotics, Water Science & Technology 89 (2024) 3047–3078. https://doi.org/10.2166/wst.2024.166.

[213] S. Shukla, H. Pandey, P. Singh, A.K. Tiwari, V. Baranwal, A.C. Pandey, Synergistic impact of photocatalyst and dopants on pharmaceutical-polluted waste water treatment: a review, Environmental Pollutants and Bioavailability 33 (2021) 347–364. https://doi.org/10.1080/26395940.2021.1987843.

[214] T.L. Wakjira, A.B. Gemta, G.B. Kassahun, D.M. Andoshe, K. Tadele, Bismuth-Based Z-Scheme Heterojunction Photocatalysts for Remediation of Contaminated Water, ACS Omega 9 (2024) 8709–8729. https://doi.org/10.1021/acsomega.3c08939.

[215] X. He, T. Kai, P. Ding, Heterojunction photocatalysts for degradation of the tetracycline antibiotic: a review, 2021. https://doi.org/10.1007/s10311-021-01295-8.

[216] T.L. Wakjira, A.B. Gemta, G.B. Kassahun, D.M. Andoshe, K. Tadele, Bismuth-Based Z-Scheme Heterojunction Photocatalysts for Remediation of Contaminated Water, ACS Omega 9 (2024) 8709–8729. https://doi.org/10.1021/acsomega.3c08939.

[217] X. He, T. Kai, P. Ding, Heterojunction photocatalysts for degradation of the tetracycline antibiotic: a review, 2021. https://doi.org/10.1007/s10311-021-01295-8.

[218] M. Kumar, V.P. Singh, S.B. Bhat, R. Kumar, Environmental risks of textile dyes and photocatalytic materials for sustainable treatment: current status and future directions, Springer International Publishing, 2025. https://doi.org/10.1007/s44274-025-00337-0.

[219] S. Thakur, A. Ojha, S.K. Kansal, N.K. Gupta, H.C. Swart, J. Cho, A. Kuznetsov, S. Sun, J. Prakash, Advances in powder nano-photocatalysts as pollutant removal and as emerging contaminants in

water: Analysis of pros and cons on health and environment, Advanced Powder Materials 3 (2024) 100233. https://doi.org/10.1016/j.apmate.2024.100233.

[220] G. Lofrano, F. Ubaldi, L. Albarano, M. Carotenuto, V. Vaiano, F. Valeriani, G. Libralato, G. Gianfranceschi, I. Fratoddi, S. Meric, M. Guida, V. Romano Spica, Antimicrobial Effectiveness of Innovative Photocatalysts: A Review, Nanomaterials 12 (2022). https://doi.org/10.3390/nano12162831.

[221] S. Thakur, A. Ojha, S.K. Kansal, N.K. Gupta, H.C. Swart, J. Cho, A. Kuznetsov, S. Sun, J. Prakash, Advances in powder nano-photocatalysts as pollutant removal and as emerging contaminants in water: Analysis of pros and cons on health and environment, Advanced Powder Materials 3 (2024) 100233. https://doi.org/10.1016/j.apmate.2024.100233.

[222] R. Chandoliya, S. Sharma, V. Sharma, R. Joshi, I. Sivanesan, Titanium Dioxide Nanoparticle: A Comprehensive Review on Synthesis, Applications and Toxicity, Plants 13 (2024) 2964. https://doi.org/10.3390/plants13212964.

[223] A. Kutuzova, T. Dontsova, W. Kwapinski, Application of TiO2-Based Photocatalysts to Antibiotics Degradation: Cases of Sulfamethoxazole, Trimethoprim and Ciprofloxacin, Catalysts 11 (2021) 728. https://doi.org/10.3390/catal11060728.

[224] P. Pascariu, C. Gherasim, A. Airinei, Metal Oxide Nanostructures (MONs) as Photocatalysts for Ciprofloxacin Degradation, Int. J. Mol. Sci. 24 (2023) 9564. https://doi.org/10.3390/ijms24119564.

[225] A. Kutuzova, T. Dontsova, W. Kwapinski, Application of TiO2-Based Photocatalysts to Antibiotics Degradation: Cases of Sulfamethoxazole, Trimethoprim and Ciprofloxacin, Catalysts 11 (2021) 728. https://doi.org/10.3390/catal11060728.

[226] N. Zulfiqar, R. Nadeem, O.A. Musaimi, Photocatalytic Degradation of Antibiotics via Exploitation of a Magnetic Nanocomposite: A Green Nanotechnology Approach toward Drug-Contaminated Wastewater Reclamation, ACS Omega (2023). https://doi.org/10.1021/acsomega.3c08116.

[227] P. Pascariu, C. Gherasim, A. Airinei, Metal Oxide Nanostructures (MONs) as Photocatalysts for Ciprofloxacin Degradation, Int. J. Mol. Sci. 24 (2023) 9564. https://doi.org/10.3390/ijms24119564.

[228] H. Li, F. Deng, Y. Zheng, L. Hua, C. Qu, X. Luo, Visible-light-driven Z-scheme rGO/Bi2S3-BiOBr heterojunctions with tunable exposed BiOBr (102) facets for efficient synchronous photocatalytic degradation of 2-nitrophenol and Cr(vi) reduction, Environ. Sci. Nano 6 (2019). https://doi.org/10.1039/c9en00957d.

[229] T. Tang, Z. Yin, J. Chen, S. Zhang, W. Sheng, W. Wei, Y. Xiao, Q. Shi, S. Cao, Novel p-n heterojunction Bi2O3/Ti3+-TiO2 photocatalyst enables the complete removal of tetracyclines under visible light, Chemical Engineering Journal 417 (2021). https://doi.org/10.1016/j.cej.2020.128058.

[230] M. Sillanpää, M.C. Ncibi, A. Matilainen, Advanced oxidation processes for the removal of natural organic matter from drinking water sources: A comprehensive review, J. Environ. Manage. 208 (2018). https://doi.org/10.1016/j.jenvman.2017.12.009.

[231] C. Song, K.X. Zhang, X.J. Wang, S. Zhao, S.G. Wang, Effects of natural organic matter on the photolysis of tetracycline in aquatic environment: Kinetics and mechanism, Chemosphere 263 (2021). https://doi.org/10.1016/j.chemosphere.2020.128338.

[232] S. Jia, Z. Yang, K. Ren, Z. Tian, C. Dong, R. Ma, G. Yu, W. Yang, Removal of antibiotics from water in the coexistence of suspended particles and natural organic matters using amino-acid-modified-chitosan

flocculants: A combined experimental and theoretical study, J. Hazard. Mater. 317 (2016). https://doi.org/10.1016/j.jhazmat.2016.06.024.

[233] A. Fattahi, M.J. Arlos, L.M. Bragg, R. Liang, N. Zhou, M.R. Servos, Degradation of natural organic matter using Ag-P25 photocatalyst under continuous and periodic irradiation of 405 and 365 nm UV-LEDs, J. Environ. Chem. Eng. 9 (2021). https://doi.org/10.1016/j.jece.2020.104844.

[234] D.C.A. Gowland, N. Robertson, E. Chatzisymeon, Photocatalytic oxidation of natural organic matter in water, Water (Switzerland) 13 (2021). https://doi.org/10.3390/w13030288.

[235] J. Qiu, D. Dai, L. Zhang, G. Xia, J. Yao, Oxygen vacancy-rich Bi2MoO6 anchored on cuboid metal-organic frameworks for photocatalytic elimination of Cr(VI)/2-nitrophenol mixed pollutants, Sep. Purif. Technol. 301 (2022). https://doi.org/10.1016/j.seppur.2022.121990.

[236] M.E.M. Ali, E.A. Assirey, S.M. Abdel-Moniem, H.S. Ibrahim, Low temperature-calcined TiO2 for visible light assisted decontamination of 4-nitrophenol and hexavalent chromium from wastewater, Sci. Rep. 9 (2019). https://doi.org/10.1038/s41598-019-55912-2.

[237] C. Zhao, L. Xue, H. Shi, W. Chen, Y. Zhong, Y. Zhang, Y. Zhou, K. Huang, Simultaneous degradation of p-nitrophenol and reduction of Cr(VI) in one step using microwave atmospheric pressure plasma, Water Res. 212 (2022). https://doi.org/10.1016/j.watres.2022.118124.

[238] O.M. Bankole, K.I. Ojubola, O.S. Adanlawo, K.A. Oluwafemi, A.O. Adedapo, M.A. Adeyemo, S.E. Olaseni, N.A. Oladoja, E.J. Olivier, E.E. Ferg, A.S. Ogunlaja, Atmospheric CO2 mediated formation of Ag2O-Ag2CO3/g-C3N4 (p-n/n-n dual heterojunctions) with enhanced photoreduction of hexavalent chromium and nitrophenols, J. Photochem. Photobiol. A Chem. 427 (2022). https://doi.org/10.1016/j.jphotochem.2022.113800.

[239] X. Liu, X. Tian, H. Zhang, Y. Gan, H. Hao, Y. Luo, Z. Feng, Y. Qiao, Z. Jiang, X. Zhu, C. Wang, M. Larimi, Y. Zhao, C. Ye, R. Tan, J. Yang, Shifting from MOF powder: monoliths for efficient removal of hazardous substances, Rare Metals (2025). https://doi.org/10.1007/s12598-025-03519-0.

[240] K.-G. Liu, F. Bigdeli, A. Panjehpour, A. Larimi, A. Morsali, A. Dhakshinamoorthy, H. Garcia, Metal organic framework composites for reduction of CO2, Coord. Chem. Rev. 493 (2023) 215257. doi:10.1016/J.CCR.2023.215257.

[241] M. Ahmadi, S. Mehdi, A. Akbar, A. Haghighatzadeh, A. Larimi, Enhanced CO 2 photoreduction via synergistic tungsten – nitrogen co-doping and Bi 2 MoO 6 heterojunction engineering of TiO 2, Catal. Today. 468 (2026) 115728. doi:10.1016/j.cattod.2026.115728.